INVESTIGATING THE REGULATION OF COHESIN DYNAMICS DURING MEIOTIC PROPHASE IN *C. ELEGANS*

a thesis submitted for the degree of

Doctor of Philosophy

2014

OLIVER CRAWLEY

Imperial College London

MRC Clinical Sciences Centre

DECLARATION OF ORIGINALITY

I, hereby, declare that the work presented in this thesis is my own and has not been submitted in any form for another degree or diploma at any other university. Information derived from the published work of others has been acknowledged in the text and a list of references is given.

COPYRIGHT DECLARATION

The copyright of this thesis rests with the author and is made available under a Creative Commons Attribution Non-Commercial No Derivatives licence. Researchers are free to copy, distribute or transmit the thesis on the condition that they attribute it, that they do not use it for commercial purposes and that they do not alter, transform or build upon it. For any reuse or redistribution, researchers must make clear to others the licence terms of this work.

ACKNOWLEDGEMENTS

First and foremost I would like to thank my supervisor Fadri (Enrique Martinez-Perez) for his generous direction, discussion, encouragement and constructive criticism throughout my PhD. Secondly I want to thank the other members of our lab for their specific contributions to the project and the patient sharing of skills and knowledge. In particular I want to acknowledge Sarah Testori for her significant work as part of the WAPL-1 project, especially making the cohesin transgenes. I also hugely appreciated her willingness to share innumerable cups of tea (or occasional beers) and chat things over, including the project. I want to thank Nuria Ferrandiz-Diaz for her help with the embryo imaging, Westerns and her general kind support. Thanks also go to Consuelo Barroso for her various contributions and for her reliable help and optimism. I would like to also acknowledge Nicola Silva for his brutally honest opinions and humour. Thanks also to Daimona Kounde for her vital supply of snacks and sunny outlook. I am massively grateful to all my friends, family and housemates for being there to help me in various ways outside the lab. Most importantly I would like to thank my long-suffering, wonderful girlfriend Isabel Adrados. Her love, support and advice with everything has been essential to me over the last two years, I could not have made it without her. I also congratulate her for beating me to the PhD finish line!

ABSTRACT

The physical linking of sister chromatids after S-phase is known as sister chromatid cohesion (SCC) and is largely provided by the cohesin complex. The coordinated loss of SCC at anaphase onset is essential for correct chromosome segregation, a process mediated by proteolysis of the kleisin subunit of cohesin. In addition, during mitotic prophase of most organisms a large portion of cohesin is removed from chromosomes by a non-proteolytic pathway that depends on the conserved protein WAPL. Cohesin is also known to reload and SCC is re-established in response to DSBs after mitotic S-phase. During meiosis, SCC is similarly established during S-phase, but is then released in two steps during the sequential meiotic divisions. Also, unlike mitosis, multiple cohesin complexes with divergent functions exist in meiosis. Whether cohesin is dynamically associated with chromosomes during meiotic prophase and how this may be regulated was not known. Thus, the key aims of this project were to determine if WAPL mediates cohesin removal during meiotic prophase, and to find out if meiotic cohesin complexes display turnover on prophase chromosomes of the nematode *C. elegans*. Alternative meiosis-specific kleisins (REC-8, COH-3, and COH-4) define the different complexes present during worm meiosis. I show here that WAPL-1 limits the association of COH-3/4 complexes with meiotic prophase chromosomes, which severely limits their cohesive function. REC-8 complexes on the other hand are not affected much by WAPL-1. I show that loss of WAPL-1 affects the structure of axial elements and disrupts chromosome segregation and DSB repair. I also demonstrate by FRAP live imaging that there is significant turnover of cohesin on meiotic prophase chromosomes. Dynamic turnover of COH-3 is much greater that REC-8, as predicted by the different sensitivity to WAPL-1 of REC-8 and COH-3 cohesin complexes. These findings demonstrate that cohesin is actively removed and reloaded during meiotic prophase. Dysregulation of these processes could be relevant for human fertility, since SCC exhaustion over time is thought to contribute to the decline in fertility with increased maternal age.

TABLE OF CONTENTS

LIST OF FIGURES AND TABLES

LIST OF ABBREVIATIONS

AE	Axial element
APC	Anaphase promoting complex
ATP	Adenosine 5'-triphosphate
BSA	Bovine serum albumin
CE	Central element
CGC	Caenorhabditis Genetics Centre
cM	CentiMorgan
CO	Crossover
D-loop	displacement loop
DAPI	(4', 6-diamidino-2-phenylindole)
DNA	deoxyribonucleic acid
dHJ	Double Holliday junction
DSB	double stranded break
dsDNA	Double stranded DNA
dsRNA	Double stranded RNA
dpy	Dumpy
EMS	Ethylmethane sulphonate
EDTA	Ethylenediaminetetraacetic acid
FISH	Fluorescence in situ hybridization
FRAP	Fluorescence recovery after photobleaching
g	Grams
GFP	Green fluorescent protein
Gys	Grays
him/HIM	High incidence of males
hr	Hours
HR	Homologous recombination
IH	Inter-homologue
IS	Inter-sister
L4	Larval moult 4
l	Litres

LB	Lysogeny broth
LE	Lateral element
MI	Meiosis I
MII	Meiosis II
M9	Salt buffer
M	Molarity
min	Minutes
ml	Millitres
mm	Millimetre
mM	Millimolar
mRNA	Messenger RNA
MRX	Mre11-Rad50-Xrs2 complex
NCO	Non-crossover
NE	Nuclear envelope
ng	Nanogramme
NGM	Nematode growth media
NHEJ	Non-homologous end-joining
OP50	Attenuated E. coli strain
PBS	Phosphate buffered saline
PBST	Phosphate buffered saline Tween
PC	Pairing Centre
PCR	Polymerase chain reaction
PFA	Paraformaldehyde
rDNA	Ribosomal DNA
RNA	Ribonucleic acid
RNAi	RNA interference
ROI	Region of interest
rol	Roller
rpm	Revolutions per minute
RT	Room temperature
SC	Synaptonemal complex
SCC	Sister chromatid cohesion
sec	Seconds
s	Seconds

SD	Standard deviation
SEI	Single end invasion
SEM	Standard error of the mean
SMC	Structural maintenance of chromosomes
SNP	Single nucleotide polymorphism
ssDNA	Single stranded DNA
ssRNA	Single stranded RNA
TAE	Tris base, acetic acid and EDTA buffer
Tm	Melting temperature
TZ	Transition zone
unc	Uncoordinated
ZMM	Zip1-Zip2-Zip3-Zip4-Msh4-Msh5-Mer3 network
µg	Microgram
µl	Microlitres
µm	Micrometres
µM	Micromolar
°C	Degree centigrade

INTRODUCTION

1.1 Background

1.11 General background

The genome of eukaryotes is made up of several discrete linear entities called chromosomes, which are found in the nucleus of cells. These molecular chapters together provide the coded information to instruct the cell in all its processes and therefore must be passed down faithfully to daughter cells upon cell division. For most eukaryotes, chromosomes exist in homologous pairs making a diploid set, so that each genomic region has a duplicate copy in the genome. For each chromosome one copy is inherited from the mother, maternal, and the other from the father, paternal, and these two copies are referred to as homologous chromosomes or homologues. Homologues can differ in their exact sequence, which not only serves as back up for defective mutations but also allows for hugely increased variation that fuels evolution. An elegant, and highly ordered program of events has evolved to ensure that chromosomes are accurately copied and distributed to every daughter cell. In somatic cells a cell division program called mitosis produces daughter cells containing an exact copy of all chromosomes. During mitosis chromosomes are replicated to create two identical sister chromatids that are held together by sister chromatid cohesion (SCC), until anaphase. This cohesion is predominantly provided by a protein complex called cohesin whose regulated removal from chromosomes allows the coordinated segregation of sister chromatids at anaphase (Petronczki et al. 2003). The maternal and paternal chromosomes of every homologous pair independently segregate their two sister chromatids, forming diploid daughter cells with copies of both homologues. Defects in mitotic SCC and segregation can lead to the wrong number of chromosomes, known as aneuploidy, which is a significant factor in carcinogenesis (Barber et al. 2008b).

However, to produce offspring most eukaryote life depends on sexual reproduction, which poses different requirements on cell division. The mother and father must half their diploid set of chromosomes to produce haploid gametes before they are combined at fertilization. This halving in chromosome number is achieved during meiosis, the specialized cell division program that allows the separation of homologous chromosomes

during gamete formation. Meiosis ensures that the chromosome number of a species stays constant across generations, and also brings together different variants in the population, which is vital for evolution. During meiosis a single round of DNA replication is followed by two rounds of chromosome segregation, thereby producing haploid gametes (Figure 1). As in mitosis, replicated chromosomes are held together by cohesion during meiosis, but following meiotic S-phase homologues must find and pair up with each other. This process culminates with the formation of inter-homologue crossover events (COs) that, together with SCC, maintain the attachment of homologues to one another until anaphase I when the selective loss of cohesion segregates homologues (Klein et al. 1999; Buonomo et al. 2000). Loss of the remaining cohesion at the second meiotic division segregates sister chromatids. Although some of the core functions of cohesin during meiosis are known, many questions remain unanswered, particularly with regard to the regulation and dynamics of cohesin and SCC during the prolonged prophase that precedes the first meiotic division.

1.1.2 Clinical significance

Meiotic cohesin regulation is important medically because meiotic segregation defects are particularly common in humans, and cohesion plays such a fundamental role in segregation. This is most obviously evidenced by the relatively high rate of aneuploidies in babies where a small number of them are developmentally tolerated to develop to birth or beyond. Down syndrome (trisomy 21), Klinefelter (XXY) and Turner syndrome (X0) can all develop into adulthood but with various developmental, medical and fertility problems (Hassold and Jacobs 1984). Patau syndrome (trisomy 13) and Edwards syndrome (trisomy 18) have very serious developmental impacts with 80% and 92% of affected individuals dying in the first year respectively. Together 0.2% of all human newborn infants are estimated to have one of these five trisomies (Hassold and Jacobs 1984). Furthermore, XXX syndrome and XYY syndrome together make up 0.1% of newborns. Although both generally appear to develop normally into relatively fertile females and males respectively, there are various reports of increased behavioral, psychological and learning problems, as well as mild physical and reproductive anomalies (Visootsak and Graham 2009; Otter et al. 2010).

However, these live-born aneuploidies only represent a small fraction of the total meiotic segregation defects, because aneuploidies of all other chromosomes and often many of the

above aneuploidies result in developmental failure leading to spontaneous abortions (miscarriage) or occasionally stillbirths. It is estimated that as many as 35% of all spontaneous abortions are aneuploid in clinically recognized pregnancies (6 - 20 weeks). The limited data on stillbirths shows a 4% rate of aneuploidy. Amazingly, spontaneous abortions account for around 15% of all recognised pregnancies, therefore this means in total at least 5% of all recognised pregnancies are aneuploid (Hassold and Hunt 2001). This figure is very likely an underestimation because clinically recognized pregnancies do not account for the many conceptions from embryos that do not implant and spontaneous abortions that occur prior to 6-8 weeks. These are either unreported or not even detected. Data from *in vitro* fertilisation (IVF) suggests that the rate of human embryo aneuploidy may be as high as 30% and even higher with older maternal age (Jamieson et al. 1994; Franasiak et al. 2014). It is not fully understood why such high rates of chromosome non-disjunction would exist for such a fundamentally important process. However, it is known that the vast majority of these errors originate from human oocytes; over 90% of aneuploidies are thought to have a maternal origin, while sperm are aneuploid relatively rarely (Jacobs 1992; Hassold 1998). This is in a large part due to the phenomenon of prophase I arrest (dictyate arrest) that occurs in oogenesis but not spermatogenesis of mammals and birds (Mira 1998). There is evidence to suggest that a major cause for oocyte aneuploidy arises from defects in SCC (Caburet et al. 2014). These defects are thought to originate from the fact that cohesin must continually provide SCC during the prolonged prophase arrest that separates S-phase from the first meiotic division, a process that can last several decades in women (Nagaoka et al. 2012). Gradual degradation of cohesion correlates with reduced cohesion and premature loss of SCC. Along with age related decline in the various other cell components that facilitate segregation, this decline in SCC of arrested oocytes may explain why aneuploidy and infertility rise so dramatically with maternal age (Nybo Andersen et al. 2000). Furthermore, maternal age has itself been steadily rising in the UK and much of the developed world in the past few decades (Atlas of Health in Europe 2008; Jefferies 2008). Thus, understanding the mechanisms that regulate the association and dissociation of cohesin with chromosomes during meiosis, especially during meiotic prophase, has increasingly important implications for reproductive health.

1.1.3 *C. elegans* as a model organism

Ideally, the study of human meiosis would be most informative for our own health, however, the difficulty in obtaining samples, especially of human female meiosis, plus the lack of genetic manipulation means that several model organisms are regularly used to study this evolutionarily conserved process. These include: *Mus musculus* (mouse), *Saccharomyces cerevisiae* (budding yeast) *Saccharomyces pombe* (fission yeast), *Caenorabditis elegans* (*C. elegans*), *Drosophila Melanogaster* (*Drosophila*), and *Arabidopsis thaliana* (*Arabidopsis*). Each of these organisms provides particular advantages, such as relevance to human biology or ease of manipulation, while also having certain limitations. For many reasons *C. elegans* is a very useful system to investigate meiosis as it strikes a good balance between these features. *C. elegans* is a 1mm long nematode worm with a short life cycle, large brood size and relatively simple growth conditions. Importantly, worms are amenable to an extensive range of molecular, genomic, biochemical and cytological experimental approaches, making them a very powerful experimental organism. The *C. elegans* germ line not only makes up more than half the adult cells, but is also composed of syncytial nuclei arranged in a spatio-temporal gradient, such that a clear time-course of meiosis can be observed at any moment (Figure 2). Specific meiotic stages are easily identified not only by the position of a nucleus within the germ line, but also by the distinctive appearance of chromosomes at different stages. The transparency of its tissues, plus the relatively low chromosome number (6 pairs of homologues) also greatly facilitates investigation of intact meiotic nuclei by both immunofluorescence (IF) and live imaging. Furthermore, at late prophase I, *C. elegans* oocytes align in single file prior to fertilization, and observation of these oocytes allows the easy identification of defects in CO formation, cohesion and DNA repair.

Furthermore, *C. elegans* also provides an easy readout of segregation problems during the meiotic divisions. Sex is determined in this species by the number of X chromosomes; males have a single copy (X0), while hermaphrodites have two copies (XX). Young hermaphrodite germ lines undergo spermatogenesis storing the sperm in the spermatheca, they then switch to creating oocytes which are fertilized as they pass the spermatheca at the end of prophase I (Figure 2). Unless mated, hermaphrodites self fertilize producing more hermaphrodites with a low spontaneous incidence of males, <0.2% (Hodgkin et al. 1979). High meiotic non-disjunction of the X chromosomes will cause increased spontaneous proportion of male offspring. Non-disjunction of the

autosomes can also be assessed by levels of embryonic lethality, as most aneuploid oocytes are laid as eggs but go on to arrest during embryonic development.

The following introduction will initially outline the present understanding of the stages of meiosis and then focus on cohesion regulation during the cell cycle and some key questions regarding meiotic cohesin, making special note of consistencies and idiosyncrasies in *C. elegans*.

1.2 Meiotic progression

Meiosis is a complex and highly specialized version of cell division with many different steps that must be coordinated temporally and spatially for the correct sequence of events to occur. These various processes allow homologous chromosome pairs to recombine and ultimately segregate at the two divisions of meiosis I and meiosis II to produce haploid gametes. Although this project has focused on one particular aspect of meiosis, namely cohesin, it is important to describe all the key steps, not only to appreciate the importance of cohesin's roles in meiosis but also to explain the rationale and relevance of the experiments that were undertaken. An outline showing the sequence of key events is shown in Figure 1.

1.2.1 Initiation

In multicellular organisms, meiosis takes place in the reproductive organ known as the gonad or germ line, in which meiosis is initiated from a pool of mitotically proliferating stem cells (Crittenden et al. 2006). These germ cells are set apart from all other somatic cells early in development, and are fated to go on and provide the stem cells from which all eggs and sperm originate. Mechanisms have evolved to maintain this undifferentiated stock by mitotic divisions, while a flow of daughter cells switch into meiosis. In *C. elegans* and *Drosophila* meiosis Notch signaling is important to sustain the mitotic germ cell population (Lopez-Schier and St Johnston 2001; Crittenden et al. 2003). In *C. elegans* other molecules whose expression is restricted to the mitotic region, such as GLP-1 and FBF-2, are necessary to keep nuclei in the mitotic state (Austin and Kimble 1987; Crittenden et al. 1994; Lamont et al. 2004). In mammals, Nodal signaling, which has been connected to Notch, is required for maintaining the proliferative capacity of the germ stem cells in spermatogenesis (Spiller et al. 2012).

A certain proportion of these proliferating cells must switch from mitotic to meiotic cell cycle, which involves undergoing a meiotic S-phase that is slightly different to a standard mitotic S-phase. The balance between proliferation and switch into meiosis is partly dependent on cell positioning and signaling molecule gradients, with a spatially limited mitotic niche created to maintain the stem cell population. In *C. elegans* this niche exists around the distal tip cell (DTC), which is a single cell located at the very beginning of the germline (Kimble and White 1981). As dividing cells move away from the niche around the DTC, the reducing gradient of these proliferation signals coincides with increased levels of proteins that promote the entry to meiosis. Two key factors that trigger meiotic entry are the mutually redundant GLD-1 and GLD-2 (Fox et al. 2011). In mammalian spermatogenesis the mitotic niche is to some extent also defined by spatial positioning with the spermatogonia stem cells residing in the basal layer of the seminiferous tubules (Jan et al. 2012). A complex balance between various signaling molecules controls the switch from mitosis to meiosis in spermatogenesis including GDNF and BMP4. Female mammals and birds do not have a significant pool of proliferating stem cells maintained throughout life, due to meiotic prophase arrest. Instead they undergo a finite period of mitotic proliferation during fetal development and concerted switch to the meiotic cycle (Jimenez 2009). There are reports that a small number of oocytes may arise from oogenesis that initiates after birth from a subset of ovarian stem cells (Woods and Tilly 2013), but the genuine contribution to adult mature follicles is uncertain (Gheorghisan-Galateanu et al. 2014).

The meiosis switch in budding yeast is slightly different being single celled, as no pool of stem cells exists. However it is known that a balance of transcription factors and phosphorylation events coordinate environmental triggers such as low nitrogen levels to initiate the process (Kassir et al. 1988).

1.2.2 S-phase

Although the final round of DNA replication before meiotic prophase begins is often termed premeiotic S-phase, multiple studies have demonstrated that it is required to prepare the genome for successful subsequent events of meiosis and as such can be viewed as a part of meiosis (Watanabe et al. 2001; Baltus et al. 2006). In meiotic S-phase, as in mitotic S-phase, DNA replication begins and then proceeds across the genome from specific sites known as origins of replication (ORC) (Collins and Newlon 1994). The same

core machinery is used in both mitotic and meiotic replication, but the regulation seems to be different in meiosis (Hollingsworth and Sclafani 1993). The most obvious consequence of this difference is that meiotic S-phase takes much longer to complete, in all organisms (Williamson et al. 1983; Jaramillo-Lambert et al. 2007). It is not known exactly why this difference exists as fork lengths and movement rates are similar, but they are likely a result of the different structural and functional requirements of meiotic chromosomes compared to mitotic prophase chromosomes (Cha et al. 2000). The loading of many structural components of the meiotic chromosomes, including cohesin, coincides with the timing of S-phase, but these will be discussed in detail in relation to synapsis and cohesin in later sections.

1.2.3 Homologue pairing

The first brief stage of meiotic prophase is called leptotene, where chromosomes start condensing and acquiring a thread-like appearance that is facilitated by the development of proteinaceous structures known as axial elements (AEs). The next key event is the coordinated searching and stable pairing of homologous chromosomes during zygotene. The mechanism by which homologous pairs achieve pairing has been well studied and varies slightly between species, but all involve active chromosome movements and in most species a spatial restriction of chromosomes within the nucleus (Lui and Colaiacovo 2013). In many organisms, including budding yeast, mammals and monocot plants, this spatial reorganization involves a clustering of chromosomes into a 'bouquet' with both telomere chromosome ends attached to the inner nuclear membrane at the centrosome or spindle pole body in fission yeast, while rest of the chromosome forms loops into the nucleus (Zickler and Kleckner 1998). This not only limits the possible space occupied by the chromosomes but also geometrically sorts them according to length (Schlecht et al. 2004). Although *C. elegans* homologue pairing involves only one chromosome end being fixed to the nuclear periphery, chromosomes still collectively group to one side of the nucleus forming a distinctive crescent shape and thereby achieving the equivalent function of reducing the searchable space. The region of the germ line containing the block of nuclei with this polarised morphology that marks early prophase is called the transition zone.

Active chromosome movements are thought to promote pairing both by bringing the right two chromosomes together before homology can be assessed and stabilized, and by

separating improperly associated chromosomes. Chromosome movement is actually driven by forces generated in the cytoskeleton network outside the nucleus. In *C. elegans*, fission yeast and mouse various experiments using genetics and depolymerizing agents have shown that these forces are generated via microtubules plus dynein motor proteins (Cowan and Cande 2002; Ding et al. 2004; Sato et al. 2009). In budding yeast the polymerization driven movement of actin cables in the cytoplasm provides the movement of chromosomes for pairing (Trelles-Sticken et al. 2005; Koszul et al. 2008). These forces are transferred from cytoskeleton to chromosome via a two-part protein bridge across the nuclear envelope. KASH domain proteins span the outer nuclear membrane connecting to the cytoskeleton network outside and the perinuclear space inside linking with SUN proteins that sit across the inner nuclear membrane (Starr and Fridolfsson 2010), called ZYG-12 and SUN-1 in *C. elegans* (Minn et al. 2009). The SUN proteins provide the point of attachment for chromosome ends at the nuclear periphery. In *C. elegans* phosphorylation of SUN-1 by both polo-like kinase PLK-2 and checkpoint kinase CHK-2 is required for SUN-1 aggregation and clustering of chromosomes that give the transition zone morphology and allow proper pairing (MacQueen and Villeneuve 2001; Penkner et al. 2009).

In order to assess homology during pairing and have stable juxtaposition of homologous chromosomes prior to synapsis two main distinct mechanisms exist. Most organisms have recombination dependent pairing in which the programmed double strand breaks (DSB) by SPO11 that allow COs are also required for homologues to stably pair (Peoples et al. 2002; Page and Hawley 2004). The exact mechanism by which DSB-dependent homologue recognition takes place is not fully understood, but assessment of sequence homology via the recombination machinery might be involved. Alternatively, *C. elegans* and *Drosophila* can achieve stable pairing and synapsis without recombination (Dernburg et al. 1998; McKim et al. 1998). Such homologue recognition is mediated in *C. elegans* though *cis*-acting regions at one end of chromosomes called pairing centres (PCs) that are highly repetitive and recruit zinc-finger binding proteins (Villeneuve 1994; Phillips and Dernburg 2006). HIM-8 specifically binds the X chromosome and ZIM-2 is specific for chromosome II. However, ZIM-1 and ZIM-3 both localize to two different chromosome ends each so a further mechanism of homology assessment must working. These ZIM proteins are presumed to interact via unknown factors to the SUN-1 aggregates.

Interestingly, some degree of homologue juxtaposition is achieved in yeast independently of DSBs (Loidl et al. 1994; Peoples-Holst and Burgess 2005) and recent studies in mouse have also demonstrated significant homologue association independently of DSBs (Boateng et al. 2013; Ishiguro et al. 2014).

1.2.4 Synapsis

Once two homologous chromosomes are successfully paired they can proceed with synapsis, which is the assembly of a stable proteinaceous structure, known as the synaptonemal complex (SC) (Figure 3, A), along the length of the aligned chromosomes. The SC is composed of two lateral elements, which are the rod like chromosome axes or axial elements (AEs) of each homologue, held together by the filamentous zipper-like central element (CE) (Page and Hawley 2004). There is a very regular spacing between the axes of around 100nm in the fully assembled SC of most organisms, including *C. elegans*, which can only be resolved by electron microscopy or super-resolution microscopy (Westergaard and von Wettstein 1972). Synapsis begins in zygotene, the stage that follows leptotene, when chromosomes are still in a bouquet for most organisms, or transition zone in *C. elegans*, and is complete by the pachytene stage, when parallel tracks of chromatin become evenly aligned for the whole length of every pair of homologues.

Before synapsis occurs, the axis of each chromosome must be correctly assembled during leptotene. This involves the creation of a dense protein scaffold on which ~20kb loops of supercoiled chromatin are packed to form the chromosome into a long flexible rod (Novak et al. 2008). Each single axis contains two sister chromatids held together tightly with SCC provided by the cohesin complex. Apart from cohesin, other structural proteins become incorporated into AEs during early prophase (Klein et al. 1999). Cohesin loading in meiosis will be discussed more in later sections.

Apart from cohesin, the best characterised components of axial elements are a family of meiosis-specific proteins characterised by the presence of a HORMA domain (Aravind and Koonin 1998). Budding yeast has a single HORMA-domain protein, Hop1, which is required for proper synapsis and for CO formation (Hollingsworth et al. 1990; Rockmill and Roeder 1990) . Hop1 localizes to AEs during early prophase (Figure 3, A), and was

shown to interact with cohesin subunits through immunoprecipitation (Smith and Roeder 1997; Katis et al. 2010). *C. elegans* has evolved four HORMA-domain proteins that play various essential roles in meiosis and that appear as continuous axial tracks throughout meiosis: HTP-1, HTP-2, HTP-3 and HIM-3 (Aravind and Koonin 1998; Zetka et al. 1999; Couteau et al. 2004; Couteau and Zetka 2005; Martinez-Perez and Villeneuve 2005; Goodyer et al. 2008). Loading of HTP-3 is dependent on cohesin, which itself reinforces proper cohesin loading (Severson et al. 2009). HTP-3 has the most core role being required for the axial localisation of HTP-1, HTP-2 and HIM-3, while loading of HTP-3 does not reciprocally depend on the other three HORMA proteins (Goodyer et al. 2008; Martinez-Perez et al. 2008; Severson et al. 2009). HTP-1, HTP-2 and HIM-3 cannot load in the absence of meiotic cohesin, while cohesin is able to load in worms lacking HIM-3, HTP-1 and HTP-2. Either directly or through the loading of other axial components, HTP-3 is essential for pairing, synapsis and DSB formation (Goodyer et al. 2008). *him-3* mutants fail to pair and cannot load central element components either so fail to form COs (Couteau et al. 2004). *htp-1* mutants are also defective in pairing and CO formation, but display non-homologous pairing and synapsis (Zetka et al. 1999; Couteau et al. 2004; Martinez-Perez and Villeneuve 2005). The HTP-2 protein is 82 % identical to HTP-1, but mutants lacking HTP-2 do not display any obvious defects during meiotic prophase (Martinez-Perez et al. 2008). Two HORMA-domain proteins, HORMAD1 and HORMAD2, have been identified in mouse meiosis, which also play important roles in the formation and monitoring of the SC and in meiotic recombination (Daniel et al. 2011; Kogo et al. ; Shin et al. ; Wojtasz et al. 2012). Unlike *C. elegans* HORMA-domain proteins, HORMAD1 and HORMAD2 are lost from the chromosomes as synapsis is completed (Wojtasz et al. 2009).

Although other components of AEs have been identified, these components do not show the strong conservation in function seen for cohesin and HORMA-domain proteins. For example, budding yeast Red1 is an essential structural component that coordinates synapsis and recombination, but without obvious homologues in other eukaryotes (Loidl et al. 1994; Smith and Roeder 1997). In mouse, SYCP2 and SYCP3 specifically localise to the lateral elements and have been shown to provide a structural scaffold necessary for CE components to attach to (Offenberg et al. 1998; Yuan et al. 2000).

Synapsis requires the assembly of transverse filaments (CE components) that link together the AEs of aligned homologues in a zipper-like fashion (Figure 3, A). In budding

yeast, a single CE component called ZIP1 has been identified, while *C. elegans* has four, SYP-1/2/ 3/4, and mouse so far has five, SYCP1, SYCE1, SYCE2, SYCE3 and TEX12 (Dong and Roeder 2000; MacQueen et al. 2002; Colaiacovo et al. 2003; Smolikov et al. 2009; Fraune et al. 2012). These proteins all have in common a combined polymerizing ability through binding domains that form regular filaments to maintain a consistent SC spacing. In most species initiation of synapsis is dependent on DSBs, and the sites of recombination are the points where synapsis begins (Giroux et al. 1989; McKim et al. 1998; Baudat et al. 2000). However, in *C. elegans* and *Drosophila* synapsis can proceed without DSBs (Dernburg et al. 1998; Liu et al. 2002). In *C. elegans* synapsis starts from the pairing centre end of the chromosome, and the proceeds in a processive manner such that non-homologous synapsis is possible in absence of pairing checkpoints (Dernburg et al. 1998; MacQueen et al. 2005; Martinez-Perez and Villeneuve 2005). The stable context of juxtaposed homologues within the SC is vital for subsequent meiotic recombination steps, as mutants of SC components in yeast, plants, *Drosophila*, *C. elegans* and mammals all have defects in CO formation and delays in repair of DSBs (Lui and Colaiacovo 2013).

1.2.5 DSB formation

Programmed DSBs are a fundamental part of meiosis, since DSBs initiate the process of meiotic recombination that leads to the repair of a subset as inter-homologue COs. These CO events, together with SCC, provide the basis of chiasmata, physical links needed to provide the tension for correct orientation of homologue pairs on the first meiotic spindle (Nicklas 1974). Importantly, CO formation involves the exchange of large sections of DNA between homologous chromosomes generating new combinations of alleles in *cis*, which is essential for evolution.

Meiotic DSBs are created by the conserved endonuclease Spo11, which is related to the DNA topoisomerases (Bergerat et al. 1997; Keeney et al. 1997). Spo11 covalently binds to DNA catalyzing the cutting of a dsDNA molecule from one sister chromatid, leaving the other chromatid intact. Some of these breaks are processed to eventually become COs, while other breaks are processed to end up ligating back to the same chromatid resulting in non-crossovers (NCOs) with unchanged flanking DNA markers and so not forming a link between homologues. In order to assure every homologous pair receives at least one CO, Spo11 must make multiple DSBs per chromosome pair. The positioning of these

breaks and therefore CO sites is not random and preferentially occurs at certain domains or hotspot sites (Gerton et al. 2000).

In budding yeast COs occur mainly in interstitial regions of the chromosome, being suppressed around telomeres and centromeres (Pan et al. 2011). Open chromatin structure was demonstrated to increase DSB initiation and recombination, and on a fine scale most DSBs occur outside ORFs and especially in promoters. Also, regions of cohesin binding were negatively correlated to sites of recombination alluding to accessibility differences due to large-scale chromatin loop structure on the axis. On a broad level *C. elegans* COs are much more common in the end portion of the chromosomes, which are gene poor and less transcriptionally active, with the middle third of the chromosome receiving few COs (Barnes et al. 1995). However, a mark of more open chromatin, H2AK5ac, has been associated with promoting DSB initiation in *C. elegans* (Wagner et al. 2010). Mutations in *C. elegans* condensin, which is related to cohesin, disrupt the pattern of DSB formation confirming a conserved role for chromosome architecture in DSB and CO distribution (Mets and Meyer 2009). Interestingly, in mammals COs are also more common towards chromosome ends and on a local level occur at open chromatin marks, though usually outside genes and, unlike yeast, rarely in promoters (Myers et al. 2005; Chowdhury et al. 2009). Mammals have many specific hotspot sites of very high local CO rate. A zinc finger protein called PRDM9 controls a large number of these hotspots by binding to certain sequence motifs to probably methylate histones and direct Spo11 DSB initiation by affecting chromatin state (Baudat et al. 2009).

1.2.6 Resection and strand invasion

Following DSB formation, subsequent steps of DNA repair require Spo11 removal from the break site (Keeney et al. 1997). As Spo11 is covalently bound to the DNA, the adjoining strand is cleaved a short distance away releasing Spo11 with an attached single stranded oligonucleotide and leaving a single stranded DNA end at the break site (Neale et al. 2005). Com1/Sae2 and the MRX complex composed of Mre11, Rad50 and Xrs2 are required for this cleavage processing (Alani et al. 1990; McKee and Kleckner 1997; Tsubouchi and Ogawa 1998). The exposed single stranded end is then resected 5' to 3' in both directions away from the break leaving a long single stranded overhang. The Exo1 exonuclease is thought to contribute to this full resection in conjunction with the MRX complex (Zakharyevich et al. 2010; Garcia and Nagai 2011).

Following resection, the ssDNA is decorated by strand exchange proteins that form filaments around the DNA and facilitate the invasion of the homologous repair template in one of the chromatids of the homologous chromosome (Hunter and Kleckner 2001). Binding of RPA to the ssDNA is needed to initiate this process, which is then replaced by Rad51 and Dmc1 recombinases (Bishop 1994; Gasior et al. 1998). These single stranded protein covered filaments, together with Rad54 chromatin remodeling protein, allow for homology search and subsequent invasion into a dsDNA molecule of the homologue (Aboussekhra et al. 1992; Shinohara et al. 1992; Mazin et al. 2000). It is thought that the invaded template helix separates to form a displacement loop (D-loop) structure with the invading strand annealing to the complimentary sequence. These protein filaments form discrete foci cytologically that are lost as the next steps of the repair process follow and can therefore be readily used to assess the number and progression of recombination sites during meiosis. *C. elegans* does not have a Dmc1 homologue, so RAD-51 is apparently able to carry out Dmc1 functions. Also unlike most organisms where Rad51 foci peak in leptotene/zygotene, *C. elegans* RAD-51 foci peak in early pachytene and this difference has been attributed to the decoupling of synapsis and DSBs in this system (Alpi et al. 2003).

1.2.7 Repair bias and partner choice

An essential distinction of meiosis from mitosis is that DSBs are predominantly repaired using the homologous chromosome as a template rather than the more spatially proximal sister chromatid, allowing for COs to link homologues. This vital interhomologue (IH) bias is a combination of not only active promotion of strand invasion into the homologue via the strand exchange proteins Rad51/Dmc1 but also by other factors, as well as by the suppression of inter-sister (IS) repair. In budding yeast the core axial components Hop1 and Red1 in combination with Mnd1 appear to be important for this (Zierhut et al. 2004; Niu et al. 2005); displaying a checkpoint mechanism to ensure IH repair regulated by phosphorylation from the yeast ATM/ATR kinase homologues Mec1 and Tel1 (Carballo et al. 2008).

In order to allow IH repair to happen, synapsis with a non-homologous chromosome must be prevented. Hop1 was shown to regulate this in yeast (Latypov et al. 2010) and similarly in *C. elegans* by the axial component HTP-1 (Martinez-Perez and Villeneuve 2005).

Cohesins have also been demonstrated in many organisms to be necessary for IH repair but this may be indirectly by facilitating SC structure and pairing (Klein et al. 1999; Pasierbek et al. 2001; Zierhut et al. 2004). Rec8 has actually been shown, through genetic experiments to actually promote IS repair in budding yeast (Kim et al. 2010), as cohesin is well known to do in the mitotic cell cycle (Strom and Sjogren 2005). It is unclear exactly how cohesins contribute directly to the CO process but it has been hypothesized that the presence of multiple meiotic cohesin complexes in many organisms may help promote IH recombination (Lee and Hirano 2011).

Another alternative form of DNA repair called non-homologous end joining (NHEJ) must be prevented from happening to guarantee IH repair. NHEJ involves the re-ligation of the two ends of a DSB or to any other blunt DNA end by special enzymes such as LIG-4 (Adamo et al. 2010). This results in variable loss of genetic information or potentially translocations and as such is only used as a last resort for most organisms in G1, when homologous recombination is not possible. NHEJ is only active in meiosis under unusual circumstances such as defective synapsis or absence of RAD-51 (Martin et al. 2005; Smolikov et al. 2007).

1.2.8 ZMM CO pathway

Once a D-loop has formed after the invading strand has begun DNA synthesis, second end capture must take place to continue the reciprocal repair process. Second end capture requires that the displaced loop somehow reaches across to anneal with the complimentary sequence on the other exposed single strand of the broken chromatid. DNA synthesis can then proceed using the D-loop strand as a template. The two free synthesized ends are ligated to the 5´ ends where initial DSB resection finished forming a double Holliday junction (dHJ) (Sun et al. 1991; Hunter and Kleckner 2001). Many proteins have been shown to function in this intricate process, several of which collectively grouped into the conserved ZMM network/family, standing for Zip1-4, Mer3, Msh4/5 (Lynn et al. 2007). These are all required to form the appropriate recombination intermediates that ultimately allow for a mature CO to form. In budding yeast and *C. elegans* the Zip3 sumo E3 ligase (ZHP-3 in worms) ultimately localises at foci during meiosis that correlate with CO sites (Agarwal and Roeder 2000) and its loss prevents COs from forming, despite appropriate DSBs being made (Borner et al. 2004; Jantsch et al. 2004). Msh4 and Msh5 also localize to CO sites and seem to promote dHJ formation, while

the Mer3 helicase assists the Rad51 and Dmc1 decorated single strands with stable strand invasion (Hollingsworth et al. 1995; Mazina et al. 2004; Snowden et al. 2004). Various other proteins have been implicated in assuring COs in different species, but the ZMM factors have conserved roles from plants to mice (Chen et al. 2005; Guiraldelli et al. 2013).

1.2.9 CO versus NCO fate

As mentioned earlier, many meiotic DSBs are not repaired as COs, but rather as NCOs, and the fraction of DSBs that are repaired as COs varies depending on the organism. For example, studies in budding yeast studies have shown roughly a 1:1 CO to NCO ratio, while data combining cytological markers of DSBs with genetics estimates a 1:10 ratio in both mice and plants (Mancera et al. 2008; Welz-Voegele and Jinks-Robertson 2008; Drouaud et al. 2013; Odenthal-Hesse et al. 2014).

Some NCOs are known to arise from alternative processing of dHJs by appropriate cleavage and ligation and evidence from budding yeast and *C. elegans* suggests that this is performed by the Top3/BLM/Rmi1 complex (Wang and Kung 2002; Wicky et al. 2004; Zakharyevich et al. 2012). However, most NCOs are thought to result from different processing at an earlier stage. After D-loop formation when DNA synthesis has begun from the invading 3' strand but before second end capture, RTEL1 protein can eject that strand. This strand then anneals back to the other 5' ssDNA end revealed by resection in the opposite direction allowing for DNA synthesis from both strands and an intact dsDNA to be completed by ligation without any sequence loss (Barber et al. 2008a; Youds et al. 2010). Despite this evidence, it still remains a largely open question as to exactly how the CO versus NCO fate is decided. It is possible that local variation in chromatin configuration or SC components around a DSB may favor different recombination intermediates (Kleckner 2006).

1.2.10 CO interference

A phenomenon that is known to affect the likelihood of a DSB becoming a CO is interference, where by the probability of a CO occurring in the vicinity of another CO is much lower than expected by chance (Sturtevant 1915; Muller 1916). Amazingly, despite being described almost a century ago, it is still not fully understood how interference is achieved. An attractive model that has been proposed is a mechanical stress theory, in

which the chromosome is under physical stress or tension that somehow promotes the formation of CO recombination. Once a DSB has committed to becoming a CO this stress is intrinsically relieved, which reduces stress in the surrounding regions (Borner et al. 2004; Kleckner et al. 2004). Transmission of such stress seems more likely via the axis or DNA topology rather than the SC as a whole, given that interference may exist before synapsis (Fung et al. 2004). This model logically links with the concept of CO assurance, ensuring that all homologous pairs receive at least one CO, to CO interference but is yet to be clearly demonstrated (Martini et al. 2006). The extent of interference hugely varies between species: *C. elegans* having the maximum, with only one CO per homologous pair and fission yeast displaying negligible interference (Munz 1994; Hillers and Villeneuve 2003). A recent budding yeast paper demonstrated that Topoisomerase II may play an important role in the mechanism of CO interference (Zhang et al. 2014), which supports the mechanical stress model, via changes to DNA topology.

1.2.11 ZMM independent recombination

In some organisms there exists a fraction of COs that occur independently of the ZMM pathway, as mutants for ZMM complex members or other components in this recombination pathway still create some COs (Hunter and Borts 1997; Borner et al. 2004; Higgins et al. 2004). Such ZMM independent COs are largely reliant on the endonuclease Mus81 and interestingly appear to not be subject to interference mechanisms (Copenhaver et al. 2002; de los Santos et al. 2003; Hollingsworth and Brill 2004). Fission yeast is entirely dependent on Mus81 to resolve recombination intermediates and displays zero interference. However, in *C. elegans* COs seem to be absent in ZMM pathway mutants (de Vries et al. 1999; Zalevsky et al. 1999; Kelly et al. 2000).

1.2.12 Chromosome remodeling

At the end of pachytene and through diplotene once DSBs repair is completed, or nearly completed, a dramatic condensation and remodeling of chromosomes takes place (Figure 3 B). The SC disassembles with central element components largely dissociating from chromosomes while SCC is maintained so that COs become the only physical link between homologues (Storlazzi et al. 2003; Nabeshima et al. 2005). These connections mediated by COs and SCC manifest visibly as chiasmata that persist until they are dismantled during anaphase onset by the regulated removal of cohesin. A homologous pair connected by one

or more chiasma at late prophase is called a bivalent. Chromosome remodeling is especially evident in *C. elegans,* where the presence of a single chiasma per homologue pair results in a particularly clear cytological pattern of events. Simultaneous loss of the SYP-1 central element component from the long arm relative to the CO and loss of the HTP-1 axial component from the shorter arm accompanies condensation and rotation to produce a cruciform bivalent structure (Martinez-Perez et al. 2008). Cohesins and other axial proteins remain localised along the entire length of AEs, apart from some apparent local loss at the chiasma site (Chan et al. 2003; Eijpe et al. 2003; Bhalla et al. 2008).

1.2.13 Meiotic divisions

The ultimate goal of the events of meiotic prophase is to prepare chromosomes for the two rounds of chromosome segregation that ultimately achieves the formation of haploid gametes. The first meiotic division separates the recombined maternal and paternal copies of each homologue pair to opposite poles. This requires that the centromeres of sister chromatids are attached to microtubules from the same pole, a phenomenon called mono-orientation. The attachment to the chromosome is mediated via a complex molecular anchor called the kinetochore, which joins the ends of microtubules to the centromere, itself a specialized heterochromatic region on each chromosome containing particular histone variants (Choo 2001; Santaguida and Musacchio 2009). At metaphase the chromosomes align as the kinetochores attach to microtubules, an alignment made possible through the tension provided by the cohesion surrounding the chiasmata (Watanabe 2012). After chromosomes are correctly oriented, anaphase onset triggers the proteolytic cleavage of the kleisin subunit of cohesin by separase, which results in the loss of cohesion (Kitajima et al. 2003). However, some cohesion must be protected at the first division to allow for sisters to stay attached until they segregate at anaphase II. In most organisms SCC protection during the first division is limited to centromeric regions. While in *C. elegans* and other organisms with holocentric chromosomes, which lack defined centromeres, cohesion is protected in a broader region expanding from the single chiasma to the farthest telomere (Rogers et al. 2002). Similar to a mitotic division, sister centromeres display bi-orientation on the second meiotic spindle and loss of the remaining SCC triggers segregation of sister chromatids to opposite poles. This two-step release of cohesion is one of the most fundamental meiotic events, and hence the regulation and maintenance of cohesion up to this end point is a crucial aspect of meiosis.

1.2.14 Late prophase arrest in mouse and human oocytes

As mentioned earlier, female oogenesis is programmed to pause during late meiotic prophase in mammals and some other vertebrates before the first meiotic division, often called the dictyate arrest (Mira 1998). Amazingly, this phenomenon in mammals is synchronized such that by the time females are born all their eggs for future reproduction have already gone though many key events of meiotic prophase including pairing and recombination. Meiosis only resumes once oocytes are stimulated to mature for each oestrus cycle, which triggers the completion of the first meiotic division. The second division is only completed if the oocyte is fertilised. Dictyate arrest occurs following diplotene, when the central components of the SC have been disassembled (Hodges et al. 2001; Ishiguro et al. 2011). Therefore, the linkages provided by chiasmata, which are sustained by CO events and SCC, must keep homologous chromosomes together from birth until the first meiotic division, two events that can be separated by several decades in women. As mentioned earlier, defects in SCC in arrested oocytes are thought to be a major factor in sudden fertility decline in older women (Angell et al. 1994; Duncan et al. 2012). Though the Duncan et al. study used samples from cancer patients so the relevance to normal oocyte ageing is uncertain. Mammalian spermatogenesis has no prophase arrest, with days rather than decades separating S-phase and the establishment of SCC from the meiotic divisions, which may account for the much less sudden decline in male fertility.

1.3 Cohesin

In eukaryotes, replicated sister chromatids must be physically held together to allow their coordinated segregation during anaphase of mitosis and meiosis. To align the chromosomes correctly to opposite spindle poles prior to segregation, a tensile force must connect sister chromatids and resist the pulling forces from microtubules (Ault and Nicklas 1989). In eukaryotes the solution to this fundamental task is universally provided by the cohesin protein complex that links chromatids together from S-phase until anaphase. This stable cytological association of replicated DNA molecules is known as sister chromatid cohesion (SCC) (Miyazaki and Orr-Weaver 1994).

1.3.1 Core structure and mechanism

Cohesin is part of an ancient group of proteins that regulate chromosome architecture and that are conserved from bacteria to humans (Hirano 2005). In eukaryotes these complexes have diverged with cohesin specializing in some of the most essential roles, most importantly providing SCC. Cohesin-related complexes also include condensin, which affects chromosome compaction and gene expression, and the SMC5/6 complex that has roles in DNA sister repair (De Piccoli et al. 2009; Wood et al. 2010). A Structural Maintenance of Chromosome (SMC) protein dimer forms the core component of all these complexes (Figure 4). SMC structure comprises a curved rod of antiparallel coiled-coils linking tightly to another SMC at both their hinge domains and more dynamically at their globular nuclear binding domains (NBDs) containing both N and C termini (Nasmyth and Haering 2009). ATPase activity has been demonstrated in the NBDs of these SMC proteins and contributes to their function (Lowe et al. 2001). The hinge domains of this SMC dimer are sufficiently flexible to allow for an open U-shape with NBDs apart or with both coiled-coil rods more aligned and NBDs closer together (Haering et al. 2002). The cohesin complex contains a heterodimer of SMC1 and SMC3 that is tightly bound with an alpha-kleisin subunit spanning the NBDs of the SMCs (referred to as simply kleisin hereafter). The kleisin N-terminus binds to SMC3 and the kleisin C-terminus to SMC1 (Nasmyth and Haering 2005). Electron micrographs give strong evidence that this forms a tripartite oval ring of ~50 nm in maximum diameter (Anderson et al. 2002). A fourth cohesin subunit, SCC3 (also called SA1/2 or STAG1/2/3) interacts predominantly via the kleisin subunit and like the other three is essential to provide SCC (Toth et al. 1999; Nasmyth and Haering 2009).

This four-part ring complex composed of SMC1, SMC3, kleisin (SCC1) and SCC3 is widely believed to provide SCC by topological entrapment of chromatin fibres, because the proteolytic cleavage of the kleisin at anaphase by the protease separase, or its experimentally-induced cleavage using the TEV protease, causes sudden loss of cohesion (Uhlmann et al. 1999; Pauli et al. 2008). The physical integrity of this complex must therefore be sufficient to resist forces that try to separate sister chromatids. Although the favored model is for a single cohesin ring to embrace two chromatin fibres as its size permits this and seems the most logical, it remains to be conclusively proven. Other topological models are possible with single rings entrapping single chromatin fibres and interacting with each other to provide cohesion.

1.3.2 Auxiliary factors

Several key auxiliary proteins have been widely documented across most species as having generally conserved roles in regulating cohesin function. I will briefly introduce the canonical mitotic roles of these factors, and then expand further on current knowledge about cohesin and these factors during mitosis and meiosis (Figure 4 shows the key auxiliary factors).

SCC2 and SCC4 are both involved in loading of cohesin onto chromatin and have been collectively termed kollerin (Ciosk et al. 2000; Nasmyth 2011). An important concept with cohesin is that the complex can be loaded or associated with chromatin but is not necessarily cohesive. ECO1 is an acetyltransferase that is known to promote cohesion establishment by mediating post translation modification (PTM), in this case acetylation of two lysine residues in SMC3 (Zhang et al. 2008b). PDS5 is a HEAT-repeat protein that contributes to maintenance of cohesion by largely unresolved mechanisms and predominantly interacts with the complex via binding to the kleisin (Panizza et al. 2000; Shintomi and Hirano 2009). However, PDS5 also mediates destabilization of cohesin from chromosomes in conjunction with WAPL that it binds to in a heterodimer (Kulemzina et al. 2012). WAPL almost universally functions as an antagonizing factor upon SCC and cohesin's association with chromatin (Yu 2013). This allows for dissociation of a major fraction of cohesin from chromosomes without cleavage, prior to anaphase, known as the prophase pathway (Kueng et al. 2006). Separase proteolytically cleaves the kleisin subunit of the remaining complexes at anaphase releasing cohesion, while shugoshin protects removal of cohesin at the centromeres. Below I provide more detailed information about the roles of these factors and the regulation of cohesion.

1.3.3 Subunit diversity

Significant diversity has evolved within the various cohesin complex subunits and factors; the most fundamental is between mitosis and meiosis and these differences are central to this project. Meiosis poses different requirements upon cohesin complexes compared to mitosis; homologue pairing, SC assembly, CO formation, mono-orientation of sister centromeres on the first meiotic spindle, and two-step release of cohesion are unique to meiosis and cohesin is known to play a role in all these events. A prevalent solution to

these meiosis-specific requirements is for organisms to have different kleisin subunits during mitosis and meiosis. During mitosis SCC1 (RAD21/ MDC1) acts as the kleisin subunit (Michaelis et al. 1997). In meiosis SCC1 is predominantly replaced by REC8, a kleisin with meiotic specific functions but that is still cleaved at anaphase by separase and similarly binds to SMC NBDs at its N and C termini (Klein et al. 1999; Gruber et al. 2003; Xu et al. 2005). A direct REC8 orthologue plays essential meiotic roles in nearly all systems studied, and interestingly manages to carry out both mitotic and meiotic functions in the protist *Tetrahymena* (Howard-Till et al. 2013).

Further diversity in meiotic kleisins in addition to REC8 exists in many species. In *C. elegans*, alongside REC-8, two closely homologous and mutually redundant genes *coh-3* and *coh-4* encode kleisin paralogues with roles in SC assembly, CO formation and limited contribution to cohesion, though much about their regulation is still unclear (Severson et al. 2009). An additional kleisin homologue has been identified in *C. elegans* called COH-1 that has slightly cryptic roles in somatic development and possibly in meiosis but having limited meiotic expression (Pasierbek et al. 2001; Mito et al. 2003). Importantly, multiple meiotic kleisins also exist in mammals, with RAD21L expressed throughout most of meiosis (Herran et al. 2011; Ishiguro et al. 2011; Lee and Hirano 2011). In *Drosophila* an additional meiotic kleisin C(2)M that is not an obvious REC8 homologue was also shown to have roles outside cohesion (Lake and Hawley 2012). Even in plants four different kleisin homologues all of which are apparently expressed in meiotic tissue (Yuan et al. 2011). Although some of the particular processes affected by these different homologues have been identified, it remains uncertain why having multiple meiotic kleisins is so prevalent. Furthermore, despite the view of SCC1 being solely a mitotic kleisin, SCC1 has also been detected on meiotic nuclei and possibly has some meiotic function in budding yeast, fission yeast, *C. elegans* and mice (Klein et al. 1999; Watanabe and Nurse 1999; Pasierbek et al. 2001; Mito et al. 2003; Xu et al. 2004; Ishiguro et al. 2011; Llano et al. 2012; Severson and Meyer 2014).

There has also been some diversification of subunits beyond the kleisins. Vertebrates have two versions of SMC1: SMC1α is found in all mitotic cohesin complexes, while SMC1β is only important for meiotic cohesion and synapsis, though there is expression of SMC1α at restricted meiotic stages (Sumara et al. 2000; James et al. 2002; Revenkova et al. 2004). In mice and humans SCC3 has three homologues. STAG1/SA1 and STAG2/SA2 are mainly

mitotic, although STAG2 has been detected at low levels in early meiosis (Prieto et al. 2002). There is a third vertebrate SCC3 paralogue, STAG3/SA3, with meiotic-only expression and that is required for various meiotic processes (Prieto et al. 2001; Hopkins et al. 2014; Winters et al. 2014). There has also been some divergence outside the core subunits; vertebrates have two PDS5 versions and two ECO1 versions, while plants were recently shown to have two WAPL paralogues (Hou and Zou 2005; Losada et al. 2005; De et al. 2014). These will be described in more detail in following sections but no obvious meiotic specificity has so far been observed for these different versions of auxiliary factors.

1.3.4 Cohesin Loading

1.3.4.1 Mitotic loading

The first step of cohesin regulation during the cell cycle is the loading of the complex onto chromatin. Bulk loading happens primarily from telophase through G1/interphase using the major fraction of cohesin complexes that have dissociated from chromatin without cleavage by separase (Kueng et al. 2006; Shintomi and Hirano 2009). There is also significant loading of cohesin after S-phase, although this G2 loaded cohesin does not normally provide SCC (Uhlmann and Nasmyth 1998; Strom and Sjogren 2005; Gerlich et al. 2006). The fact that most of the cohesin loaded seems to be from this recycled pool, plus knowledge that free non-chromatin associated cohesin still forms rings (Gruber et al. 2003), suggests that cohesin is loaded as preformed complexes rather than assembled on DNA from separate subunits.

Loading of intact cohesin complexes very likely involves the transient opening of the ring at the SMC1/SMC3 hinge to entrap chromatin fibres. A study in yeast showed that fusion of either SMC1 or SMC3 NDB to the kleisin C or N terminus respectively, where they usually interact, was viable and allowing cohesin to load, leaving the SMC hinge as the remaining interface (Gruber et al. 2006). They conclusively demonstrated that artificially engineered ligation of the SMC hinge domains stops cohesin from loading and providing SCC. Interestingly, ATP hydrolysis activity of the SMC NBDs at the other end of the complex is also known to be important for proper loading and assembly of cohesin alongside the binding to DNA (Arumugam et al. 2003; Lammens et al. 2004).

Two loading factors conserved from yeasts to humans, SCC2 (NIPBL) and SCC4 (MAU-2), form a separate complex called kollerin that is essential for cohesin loading and therefore allowing cohesion (Michaelis et al. 1997; Ciosk et al. 2000). It is still not known exactly how SCC2/SCC4 promotes loading onto chromatin though a direct interaction has been shown with the cohesin complex (D'Ambrosio et al. 2008). Also, studies that used ChIP to map binding sites of cohesin and SCC2 along the genome found a significant overlap of cohesin and its loader, supporting the idea that SCC2/SCC4 recruits cohesin to DNA (Lengronne et al. 2004; Kogut et al. 2009). However, cohesin binding sites have often been found quite distant from SCC2/SCC4 'docking' sites, giving rise to the theory that cohesin rings can slide along the DNA after loading (Lengronne et al. 2004; Fernius et al. 2013).

In yeast, cohesin was unsurprisingly found to bind most extensively around centromeres where cohesion is most firmly maintained throughout the cell cycle though quite regular enrichment was seen along arm regions in ~1kb blocks interspaced by variable 3-35 kb intervals (Blat and Kleckner 1999; Tanaka et al. 1999). Loading of SCC3 appears to coincide with the other core subunits as a complete ring, because the staining pattern of SCC3 mirrors the other subunits, and its presence is required for cohesin loading (Losada et al. 2000; Hu et al. 2011). It has been suggested that SCC3 binding may contribute to the hinge opening/loading process together with ATP hydrolyis, DNA binding and the SCC2/SCC4 interaction bringing about a transient conformational change (Nasmyth 2011).

1.3.4.2 Meiotic loading

As with cohesin regulation in general, meiotic loading of cohesin is not as well studied as in mitosis. It was first demonstrated in our lab that SCC-2 is required in *C. elegans* for loading of cohesin to meiotic chromosomes (Lightfoot et al. 2011). *scc-2* mutant worms or worms subjected to *scc-2* RNAi had poorly condensed chromatin and defective SC formation plus separated chromatids at late prophase, indicating loss of SCC. It has also been confirmed in budding yeast that SCC2 is needed for meiotic REC8 expression and SCC (Lin et al. 2011). This suggests that the underlying mechanism for cohesin loading in meiosis is similar to mitosis, relying on the SCC2/SCC4 loading complex. Interestingly, a paper in *C. elegans* did show that when a orthologue of the TIMELESS circadian clock protein, *tim-1*, is mutated loading of certain cohesin subunits is abolished (Chan et al. 2003). REC-8 and SCC-3 do not load but SMC1/SMC3 can load and significant SCC is

preserved. As mentioned, kleisin subunits other than REC-8 exist in *C. elegans,* explaining why SCC is not totally lost in *tim-1* mutants, but raises the possibility that cohesin rings may be loaded and cohesive without SCC3 present. Another study in *C. elegans* showed that SCC-3 is loaded during meiosis and that SCC-3 is required for meiotic SCC (Pasierbek et al. 2003), confirming its importance in meiosis as in mitosis.

Although the molecular mechanisms of cohesin loading during meiosis have not been studied in such detail, the loading patterns of the different cohesin subunits and their interactions with other proteins are better documented. As mentioned regarding synapsis, cohesin is central for the formation of the AEs of meiotic chromosomes, the proteinaceous scaffold from which loops of chromatin emanate allowing chromosomes to condense into rod like structures. In mice, loss of SMC1β causes dramatic shortening of the axes and increases in the size of DNA loops (Revenkova et al. 2004). Similarly, mice mutants lacking REC8 have shorter chromosome axes (Bannister et al. 2004). In both worms and mice preventing any cohesin complexes from loading by removing all meiotic kleisins results in uncondensed chromatin, lack of meiotic axes and failure to synapse (Severson et al. 2009; Llano et al. 2012). Budding yeast lacking REC8 and plants lacking SYN1 (REC8 homologue) also have defects in SC formation and synapsis (Bai et al. 1999; Klein et al. 1999). This demonstrates the core role of cohesin loading in forming the chromosome axis and determining SC architecture. Loading of REC8 in most species, including *C. elegans*, starts in premeiotic S-phase (Watanabe and Nurse 1999; Pasierbek et al. 2001; Eijpe et al. 2003) and in yeast REC8 expression before the onset of meiosis is essential to allow mono-orientation and correct segregation (Watanabe et al. 2001). In mammals the other meiotic specific subunits SMC1β, STAG3 and RAD21L only become detectable by IF after S-phase, appearing on chromosome axes at leptotene/zygotene along with other AE proteins (Prieto et al. 2001; Eijpe et al. 2003; Ishiguro et al. 2011). This would seem to preclude them from playing a role in initially establishing cohesion at S-phase, though interestingly these proteins are thought to contribute to SCC (Revenkova et al. 2004; Winters et al. 2014). SCC1 has been observed by IF in yeast, *C. elegans* and mice with the loading and expression only properly starting from late pachytene through late prophase (Prieto et al. 2002; Mito et al. 2003; Ishiguro et al. 2011; Lee and Hirano 2011). The loading pattern of meiosis-specific kleisins other than REC8 is not fully characterised, but recent studies in mice and *C. elegans* suggest that these kleisins are

loaded to chromosomes after the completion of meiotic S-phase (Ishiguro et al. 2014; Severson and Meyer 2014).

1.3.5 Cohesion establishment

1.3.5.1 Mitotic establishment

Cohesin that is loaded to chromosomes is not necessarily cohesive until the complex mediates the stable entrapment of the two chromatin fibres. Establishment is intimately connected to DNA replication, as this is when sister chromatids are produced and SCC is observed immediately after S-phase. Support for this model is given by the fact that although new cohesin subunits associate with chromatin during G2/M, this post-replication reloaded cohesin is unable to provide SCC under normal circumstances (Haering et al. 2004; Strom and Sjogren 2005). It is not really known whether cohesion is established by preloaded complexes that open transiently as replication forks progress, thereby entrapping sister chromatids, or if the soluble pool of cohesin is used. However, the fact that SCC can be established after S-phase if DSBs occur suggests that it may be the latter (Strom and Sjogren 2005; Unal et al. 2007).
It is known that acetylation of SMC3 by the acetyltransferase ECO1 is required for cohesion establishment (Ivanov et al. 2002; Rolef Ben-Shahar et al. 2008; Unal et al. 2008; Zhang et al. 2008b). Specific acetylation of two highly conserved lysine residues in SMC3 by ECO1 is vital for SCC establishment in budding yeast and human cells. Vertebrates have two ECO1 orthologues, ESCO1 and ESCO2, which contribute additively to cohesin establishment (Hou and Zou 2005), while *C. elegans* seems to have a single orthologue that is poorly characterized.

The mechanism by which this acetylation promotes establishment was first hinted at by the observation that deletion of PDS5 in fission yeast suppressed the lethality caused by *eso1* deletion, the ECO1 orthologue (Tanaka et al. 2001). This was further elucidated by repeated findings in budding yeast that a broad spectrum of mutations in the *wpl1* gene (WAPL homologue) could suppress defects in *eco1* mutants (Rowland et al. 2009; Sutani et al. 2009). Also, mutants in specific domains of PDS5 could suppress *eco1* mutant lethality, supporting the earlier finding in fission yeast. It is known that WAPL antagonizes cohesion and that WAPL interacts with cohesin via PDS5 binding (Shintomi and Hirano 2009; Sutani et al. 2009). These findings confirmed that the role of ECO1 in SCC establishment is mainly to counteract the anti-establishment activity of WAPL.

Interestingly, partial separation of sister chromatids persists in *eco1 wpl1* double mutants, indicating that full establishment of SCC may not completely depend on resisting WAPL activity (Sutani et al. 2009). Furthermore, the SMC3 mutations that suppressed the lethality of *eco1* mutants occurred in a domain around the conserved acetylated lysines, confirming their role in establishment (Rowland et al. 2009). Support of this model was given by the fact that budding yeast HOS1 deacetylates SMC3 after it is removed from chromosomes and this is required for these recycled SMC3 molecules to be used for establishing SCC in the next cycle (Borges et al. 2010).
Cohesin loaded after S-phase does not usually establish cohesion and FRAP experiments in both budding yeast and human cells show that a fraction of cohesin is bound very stably to chromatin in prophase (Kurze et al. ; Gerlich et al. 2006). These observations suggest that cohesion is mainly provided by cohesin complexes that become stably associated with chromosomes during DNA replication.

1.3.5.2 Meiotic establishment

Although it is thought that meiotic cohesion must be established by a process similar to that for mitotic cohesion, little is currently known about the regulation and dynamics of cohesion during meiotic prophase. In fission yeast it has been shown that acetylation of SMC3 is important for mono-orientation of chromosomes on the spindle of the first meiotic division (Kagami et al.). This study also suggested SMC3 is deacetylated by a HOS1 paralogue, but these findings remain to be replicated in other organisms. A recent study in *Drosophila* suggests that Eco1 plays a role in maintaining bivalent structure/cohesion during meiotic prophase, suggesting that SMC3 acetylation may also be a regulator of SCC during meiosis (Weng et al. 2014).

1.3.6 Cohesion maintenance

1.3.6.1 Mitotic maintenance

Once cohesion between sisters is established in S-phase it appears that certain processes must help maintain this through until anaphase. The auxiliary factor PDS5 is required to preserve cohesion after S-phase, though the importance seems to vary between species and PDS5 seems to possess a dual role in mediating the opposing effects of WAPL on cohesion. This protein interacts with cohesin more weakly than the core subunits, and the main point of interaction seems to be via the kleisin subunit. In budding yeast PDS5 is completely required for viability, SCC and chromatin condensation (Hartman et al. 2000;

Panizza et al. 2000), whereas in fission yeast it was only found to maintain cohesion or be needed for survival with extended prophase (Wang et al. 2002). In *Sordaria* and *Aspergillus* fungi PDS5 homologues have significant affects on cohesion and condensation but to different degrees (van Heemst et al. 1999; van Heemst et al. 2001). The *C. elegans* homologue of PDS5 called EVL-14 has received limited investigation, with one study mainly suggesting that *evl-14* mutants display mitotic segregation problems and weak meiotic defects that included the presence of occasional univalent in diakinesis chromosomes (Wang et al. 2003). More recent work showed that rapid depletion of PDS5 protein in budding yeast after S-phase had little effect on core cohesin abundance or SCC, suggesting that PDS5 function is temporally linked with replication (Kulemzina et al. 2012). Loss of both PDS5 homologues in human cells was found to paradoxically cause slight local loosening of cohesion at centromeres while also increasing cohesin levels along the rest of the chromosome (Losada et al. 2005). This cohesin destabilization ability of PDS5 has since been supported along side studies of the exclusively anti-cohesion factor WAPL, to which it binds as a dimer (Rowland et al. 2009; Shintomi and Hirano 2009). Vertebrates have PDS5a and PDS5b, which appear relatively redundant in maintaining SCC (Zhang et al. 2009).

The mechanism of cohesin maintenance is not fully understood though work in vertebrate mitotic cells offers some insight. PDS5 acts as a binding site for another factor called sororin that promotes maintenance by preventing WAPL from interacting with PDS5, and thereby inhibiting the removal or antagonistic properties of WAPL (Rankin et al. 2005; Nishiyama et al. 2010). In *Xenopus,* sororin only associates with cohesin from S-phase and this depends on the presence an ECO1 orthologue, ECO2 (Schmitz et al. 2007). This offers a good model to explain the dual effects of not having PDS5, but so far sororin homologues have not been widely identified outside vertebrates and the interacting domains on WAPL and PDS5 that sororin depends on are not conserved. Interestingly, a recent study on fission yeast demonstrated that PDS5 is actually needed for ECO1 acetylation and cohesin establishment (Vaur et al. 2012), blurring the lines between maintenance and establishment.

1.3.6.2 Meiotic maintenance

Cohesion maintenance in meiosis is slightly better studied than establishment, but many questions still remain. The factor PDS5 was initially implicated in helping to maintain

normal cohesion during meiosis in a study on the fungus *Sordaria* (van Heemst et al. 1999). Mutants for *spo76* (the *Sordaria* homologue of *pds5*) showed some mild cohesion defects and abnormal chromosome structure. Also the Spo76 protein localized to chromosome axes. An early study in fission yeast briefly looked at the meiotic requirement for PDS5, where they saw that meiosis in the absence of PDS5 often resulted in reduced and inviable spores implying a role in proper meiosis (Wang et al. 2002). A study in budding yeast did not see PDS5 obviously loaded to chromosomes in meiosis and found that loss of PDS5 did not prevent REC8 from remaining loaded to chromosomes. Though they did see separation of sisters prior to anaphase, implying that PDS5 may help maintain meiotic cohesion (Zhang et al. 2005). However, later work also in yeast did not observe the same effects of PDS5 on maintaining SCC during meiosis, while PDS5 did appear to be loaded to chromosomes (Jin et al. 2009). This is supported by a previous budding yeast study that showed that lack of PDS5 in meiosis triggered cell death suggestive of DNA damage (Ren et al. 2005). It was also shown in fission yeast that loss of PDS5 caused reduced REC8 overall intensity and reduced REC8 binding sites to chromatin at larger intervals using ChIP (Ding et al. 2006). Interestingly, chromosomes appeared more compact and with shortened axes in *pds5* mutants and this depended on REC8, demonstrating a role in cohesion regulation on correct chromosome morphology during meiotic prophase. When the *C. elegans* homologue of PDS5, EVL-14, was mutated it caused relatively mild defects in cohesion at late prophase, with only slightly increased sister separation. Similarly to the yeast studies, REC-8 was able to localize to chromosomes and FISH indicated pairing was achieved (Wang et al. 2003).

An important aspect of cohesion maintenance during meiosis is whether there is fresh loading of cohesin during meiotic prophase, and if this is the case whether reloaded cohesin contributes to cohesion. Two key studies in mice have addressed the functional side of this question. One engineered a mouse strain to have the endogenously expressed version of REC8 to have a TEV inducible cleavage site and also a wildtype sequence transgene of REC8 that can be activated to express during female dictyate arrest. When TEV cleavage is triggered in these mice, any expressed non-cleavable REC8 was unable to provide SCC and resist premature separation of sisters (Tachibana-Konwalski et al. 2010). This demonstrates that reloading of newly expressed REC8 cohesin complexes after diplotene does not significantly contribute to cohesion in arrested oocytes. The other study inactivated the SMC1β gene, that is required for meiotic cohesion in older mouse

mothers, was inactivated by Cre-recombination soon after birth when all oocytes for future reproduction have already entered dictyate arrest (Revenkova et al. 2010). No new functional SMC1β could therefore be expressed in arrested oocytes. This had no impact on reproduction or SCC phenotype in these older mice supporting the same conclusion that cohesin complexes that establish cohesion in early meiosis must very likely be maintained throughout prophase arrest. However, they both do not preclude the possibility that cohesin removed before or during arrest that is not degraded may reload and provide cohesion. Experiments in our lab have found that knockdown of SCC-2 by RNAi from the germline causes loss of chiasmata which would indicate that loading of new cohesin during meiotic prophase is required to maintain or form correct chiasma structure. Furthermore, a recent study in Drosophila this year has observed defects in chiasma maintenance and reduced cohesin association with chromosomes following meiotic knockdown of Deco (*Drosophila* Eco1) (Weng et al. 2014).

1.3.7 Prophase removal

1.3.7.1 Mitotic removal

As indicated already, there is ample evidence showing that significant amounts of cohesin are removed from mitotic chromosomes during prophase, and that this results in cohesion being locally relaxed at chromosome arms. It was first observed in *Xenopus* that a major fraction of cohesin dissociates from chromosome arms by metaphase (Losada et al. 1998). This observation of two different populations of cohesin was confirmed in human cells with most cohesin being removed from the arms, while a small fraction is protected at centromeres until anaphase (Waizenegger et al. 2000). It was then shown that phosphorylation of SCC1 and SA1/2 (SCC3 paralogues) in *Xenopus* by the cell cycle master kinase PLX1 (PLK) may to be important for allowing prophase cohesin removal (Sumara et al. 2002). A more functional study in human cells confirmed that SA2 phosphorylation is required for some prophase removal and that most removal is independent of SCC1 phosphorylation (Hauf et al. 2005). It is estimated that the bulk of cohesin actually dissociates from chromosomes in mitosis without cleavage (~90%) and indeed it has been demonstrated that SCC and segregation are correct if only a small fraction of cohesin is expressed (Losada et al. 1998; Heidinger-Pauli et al. 2010).

This non-cleavage dependent cohesin removal is often referred to as the prophase pathway and is universally mediated by WAPL activity. WAPL is a conserved protein from

yeast to humans but was originally discovered in *Drosophila* where it stands for wings apart-like due to its effects on heterochromatin and gene expression (Verni et al. 2000). Here in flies and initially in yeast certain observations indicated some loss of cohesion in WAPL mutants. However, it was soon clearly demonstrated in human cells that WAPL is responsible for antagonizing cohesion and removing cohesin complexes after they are loaded to chromatin (Gandhi et al. 2006; Kueng et al. 2006). Depletion of WAPL by RNAi prevented the normal removal of most cohesin in prophase and severely limited the resolution of sister chromatid arms at metaphase. Conversely, overexpression of WAPL caused premature loss of SCC. It was shown that SA2/SCC3 is still phosphorylated in absence of WAPL, indicating that WAPL is not required for these modifications but rather they mark cohesin complexes that are susceptible to WAPL. The excess cohesion of cells lacking WAPL caused delays in the mitotic divisions, but separase was eventually able to cleave all cohesin complexes, triggering chromosome segregation. Furthermore, they found that the retention of cohesin on chromatin did not depend on SCC2/SCC4 and they used FRAP to show that loss of WAPL slowed the turnover rate of cohesin on chromatin, though the overall fraction of stably bound cohesin seemed similar. The mechanism of WAPL-dependent cohesin removal was not determined, but both studies found that WAPL interacted with cohesin via the kleisin and SA1/2 (SCC3) subunits and also that it formed a separate dimer complex with PDS5. These studies also reported that loss of WAPL rescued the SCC defect in shugoshin mutants. Shugoshin (SGO1) is a key protector of centromeric cohesion, and without it sister chromatids separate before anaphase disrupting correct orientation and segregation (Salic et al. 2004; McGuinness et al. 2005). This balance between cohesin arm removal by WAPL/ PDS5 and centromeric protection by shugoshin depends on phosphorylation events controlled by PLK1, AuroraB and PP2A (Shintomi and Hirano 2009; Xu et al. 2009). As described above, Sororin is also required for maintaining cohesion in prophase by directly antagonizing WAPL's interaction with cohesin and therefore its ability to oppose cohesion (Nishiyama et al. 2010). Control of phosphorylation of both sororin and shugoshin is essential for protection from WAPL (Liu et al. 2013). All together, the evidence implies that various cohesin subunit PTMs and interaction with WAPL brings about a conformational change in the complex to destabilize the topological entrapment of DNA molecules.

1.3.7.2 Mechanism of cohesin removal by WAPL

Some work has begun to address how WAPL mediates cohesin removal, starting with a study in yeast where they first demonstrated that WAPL can oppose cohesion from complexes that have already established cohesion in S-phase (Chan et al. 2012). Importantly they demonstrated that fusion of SCC1 to SMC3 but not SMC1 bypassed the effects of WAPL on cohesin and the requirement of ECO1 for viability. This strongly suggests that the main exit gate for DNA to escape a cohesin ring during G2 and prophase is the SMC3-kleisin interface. A recent paper in human cells has supported this model for the SMC-3-kleisin exit gate is conserved (Huis in 't Veld et al. 2014). They also demonstrated with FRAP that loss of WAPL increased the half-life of cohesins and the fraction of stable bound cohesin, similar to the original studies in human cells. A recent study in interphase human cells found that WAPL controls the dynamic turnover of cohesin outside mitosis and this can dramatically affect chromosome morphology (Tedeschi et al. 2013). Such control of cohesin dynamics by WAPL has been recently confirmed in budding yeast (Lopez-Serra et al. 2013).

Three papers were published last year that investigated the mode of action of WAPL. One of these studies determined the crystal structure of *A. gossypii* WAPL (Wpl1), determining that WAPL binds to the ATPase domain of SMC3 and suggesting that WAPL may inhibit ATPase activity of SMC3 (Chatterjee et al. 2013). Another study in human cells used rapamycin-mediated heterodimerisation between different cohesin subunits, which allowed accurate temporal control of binding, confirming that the exit gate of cohesin is the SMC3-kleisin interface, while the entry gate is the SMC1-SMC3 hinge (Buheitel and Stemmann 2013). A third study solved the structure of human WAPL and identified that the N-terminus of WAPL binds to PDS5 and to SCC1. The middle region of Wapl likely interacts with the SMC heterodimer while the C-terminus does not appear to be important for association with cohesin but may interact with other effectors (Ouyang et al. 2013). This mechanism of a non-proteolytic exit gate at the interface between SMC3 and the kleisin that is dependent on WAPL was further supported using fluorescent imaging and fusion proteins in *Drosophila* (Eichinger et al. 2013).

In *C. elegans* mitosis, looking at embryo divisions, RNAi of the WAPL homologue was also found to increase cohesin levels on chromatin and lengthen the time to complete segregation, confirming conserved roles in nematodes (Stanvitch and Moore 2008).

1.3.7.3 Meiotic removal of cohesin

Despite the fact that studies in mouse oocytes suggest that there is little replenishment of cohesion during the prophase (Tachibana-Konwalski et al. 2010), whether cohesin is reloaded to meiotic chromosomes between S-phase and the first meiotic division remains an open question. Any active removal of cohesin during prophase is likely to negatively affect cohesion maintenance, but various lines of evidence suggest that cohesin is lost from chromosomes during late prophase. Work in budding yeast meiosis compared cohesin binding sites across the genome in prophase and metaphase synchronized cells using ChIP (Yu and Koshland 2005). They saw that overall binding of SMC1, SCC3 and REC8 was reduced at metaphase implying that some proportion of cohesin complexes are lost by the end of prophase. Cytologically, staining of cohesin components in mice meiosis indicates that, coinciding with SC disassembly, there is a bulk removal of a large amount of cohesin from chromosome axes following late pachytene and into diplotene leaving behind a subset of complexes to maintain SCC (Eijpe et al. 2003; Kouznetsova et al. 2005; Ishiguro et al. 2011). A similar process seems to occur in *C. elegans* during late pachytene/diplotene (Pasierbek et al. 2001; Chan et al. 2003; Pasierbek et al. 2003). At this stage, a rise in the levels of non-chromatin associated cohesin subunits can be seen by IF (Pasierbek et al. 2001; Mito et al. 2003).

It has long been observed that in the diplotene bivalents of mammals and invertebrates that cohesion is visibly relaxed around sites of COs in (Suja et al. 1992; Eijpe et al. 2003; Garcia-Cruz et al. ; Hulten 2011; Calvente et al. 2013). This is indicated by both separation of chromosomes with DNA staining and also the lack of some cohesin subunits at the centres of chiasmata. Indeed, it is expected that some local relaxation of SCC must occur at sites of COs in order to allow chromatids undergoing repair to move away from the sister and towards the homologue for strand exchange. It is thought that DNA recombination at a CO must also lead to an exchange of the structural axis in some way but how cohesion is locally lost around COs or how the different cohesin complex versions control the CO mechanism is unknown. This evidence suggests that a prophase pathway of some sort may exist during meiosis but this has yet to be determined. The recent study of the two Arabidopsis homologues of Wapl (AtWAPL1 and AtWAPL2) showed that a significant portion of SYN1 cohesin subunit is removed at late meiotic prophase of plants, prior to

metaphase I, and this removal is limited in the *Atwapl1 Atwapl2* double mutants (De et al. 2014).

The original study in *Drosophila* that identified WAPL did actually assess some particular aspects of meiosis in *wapl* mutants and found a defect in achiasmate chromosome segregation though meiotic chromosomes were not assessed for cohesin levels or other key events in meiosis (Verni et al. 2000). A recent study in budding yeast briefly assessed meiosis but did not observe obvious defects in spore formation and viability post meiosis in absence of WAPL implying a non-essential role in yeast meiosis (Lopez-Serra et al. 2013). Further study of WAPL during meiosis is clearly needed to understand meiotic prophase removal.

1.3.8 Removal of cohesin at anaphase

Although much cohesin is removed before anaphase some is always protected from WAPL and provides the tension that is essential for correct orientation of bivalents on the spindle. The regulation of cohesin removal during the meiotic divisions has been more extensively studied, and although this is not the focus of the this project, I will give a brief overview of the process without going into as much detail as previous steps of cohesin regulation.

1.3.8.1 Mitotic anaphase

Protection of cohesion at the centromeres is mediated by shugoshin, which in mitotic human cells was shown to maintain sororin on cohesin through recruiting PP2A phosphatase that dephosphorylates sororin. Thereby allowing sororin to bind to PDS5 and prevent WAPL from binding and carrying out its destabilizing activity (Liu et al. 2013). After sister kinetochores are correctly aligned (bioriented) in the metaphase plate, anaphase can proceed with the proteolytic cleavage of SCC1 by separase, which breaks the topological entrapment of sister chromatids (Uhlmann et al. 1999). Thus replicated sister chromatids are separated to different daughter nuclei. Activation of separase is controlled by binding of the inhibitor securin, which in turn is targeted for destruction by the anaphase promoting complex (APC) (Cohen-Fix et al. 1996). Correct attachment and alignment of the chromosomes on the spindle is monitored by the spindle assembly checkpoint (SAC) that once satisfied allows the APC to act.

1.3.8.2 Meiotic anaphase

The first major difference to note in segregation at meiosis compared to mitosis is that sister kinetochores are mono-oriented. REC8 is required for the mono-orientation of kinetochores, displaying one of the key functional divergences between SCC1 and REC8 (Yokobayashi et al. 2003). Supporting this, mutations in the genes for REC8 in *S. pombe* and *Arabidopsis* can switch to biorientation of sister kinetochores in meiosis I (Chelysheva et al. 2005). Another major difference in meiotic anaphase is that two consecutive divisions occur. Also chromosomes reach anaphase with SCC predominantly intact along the arms, rather than solely at the centromeres. For two divisions to be possible only a subset of cohesin complexes must be cleaved at the first division, so that the remaining cohesion can provide the tension required for the correct orientation on the second meiotic spindle. This two-step loss of cohesion is achieved by cohesion being protected at centromeres throughout meiosis I division, while arm cohesion is cleaved.
Phosphorylation of REC8 located on arms targets these cohesin complexes for separase cleavage (Katis et al. 2010). Centromeric cohesin is protected from phosphorylation in meiosis I by the same factor that protects cohesin from removal during mitotic prophase, shugoshin (Kitajima et al. 2006; Ishiguro et al. 2010). PP2A phosphatase is recruited to dephosphorylate the kleisin. Resolution of arm cohesion severs the connections between homologues at chiasmata and the attached sister chromatids travel to the same pole, the remaining cohesin is then cleaved at anaphase II.
C. elegans has holocentric chromosomes without fixed centromeres but the mechanism of meiotic two-step release is analogous to that of organisms with moncentric chromosomes. COs are predominantly positioned towards the ends of chromosomes in *C. elegans,* such that chromosome remodeling around CO sites during late prophase results in the formation of cruciform bivalent with a “long” and “short” arm. The long arm acts as the ‘centromere’ where cohesin is protected through meiosis I, while the short arm acts like the normal arms of monocentric chromosomes, losing cohesion at anaphase I (Schvarzstein et al. 2010). Because *C. elegans* chromosomes only have one CO per pair this method of two step cohesion loss always works, but would seem topologically complicated with extra COs. Two axial proteins HTP-1 and LAB-1 together seem to perform the equivalent function of shugoshin here, being restricted to the long arm where cohesion is protected and are required to prevent premature loss off SCC at anaphase I, possibly by promoting the recruitment of protein phosphatase I (Martinez-Perez et al. 2008) (de Carvalho et al. 2008).

1.3.9 Non-canonical roles of cohesin

Cohesin has important functions outside its role in providing SCC to mediate chromosome segregation (Mehta et al. 2013). Cohesin participates in the control of chromosome morphology by regulating the condensation state of chromatin throughout the cell cycle. As mentioned earlier, cohesin also plays a key role in organising meiotic chromosomes by promoting correct assembly of AEs and SC assembly. Cohesin has also received significant attention in two main cellular processes outside cohesion: DNA repair and gene expression. The former is of more obvious relevance to meiosis, but the latter may also be important.

1.3.9.1 Cohesin and DNA repair

DNA damage is one of the most severe threats to the survival of a cell, potentially causing defective changes to the genome. Accordingly, several sophisticated mechanisms have evolved to repair DNA damage. A DSB can result in chromosome fragmentation or translocation and hence the repair mechanisms for these are especially important. If a DSB happens in G1 then the cell must resort to a NHEJ, which can be deleterious (Wilson et al. 1997). If a DSB occurs in G2 or mitosis there is a sister chromatid of the same sequence close to hand that can be used as a template and ensure information is not lost. Cohesin is important to ensure such homologous recombination (HR) repair can take place correctly (Szostak et al. 1983). In meiosis programmed DSBs are made and these are repaired by a special type of HR to allow inter-homologue COs to form, and cohesin plays an important role as mutants lacking REC8 display a failure in CO formation.

1.3.9.1a Mitotic DNA repair

Lack of cohesin was found to cause hypersensitivity to ionizing radiation and interestingly so did loss of ECO1, which implied cohesion establishment may play a part in HR repair (Sjogren and Nasmyth 2001). It is supposed that cohesin is required because it can keep the sister homologous sequence template in close proximity and possibly may help stabilize strand invasions. If DSBs occur during G2 cohesin becomes particularly enriched in a domain (Heidinger-Pauli et al. 2008)around the break site (Strom et al. 2004). This depends on SCC2/SCC4, showing that de novo loading of cohesin seems occurs, and other

damage response factors like the ATM/ATR kinases are required in this process. This cohesin reloading in response to DSBs coincides with a reinforcement of SCC locally and genome wide, which is known as damage induced (DI) cohesion (Unal et al. 2004; Unal et al. 2007). Along with acetylation of SMC3, phosphorylation of SCC1 at particular residues is required for this DI cohesion (Heidinger-Pauli et al. 2008; Heidinger-Pauli et al. 2009). In addition sumoylation of SCC1 is required for DI cohesion and to oppose WAPL activity (McAleenan et al. 2012; Wu et al. 2012). It was recently reported that DSBs also trigger separase-dependent cohesin removal in regions flanking the DSBS, and that this removal is required for the proper processing and repair of the DSB (McAleenan et al. 2013).

1.3.9.1b Meiotic DNA repair

Cohesin is clearly important for proper repair of DSBs in meiosis as the loss of meiotic cohesin subunits widely results in lack of COs or unrepaired breaks (Klein et al. 1999; Pasierbek et al. 2001; Xu et al. 2005; Severson et al. 2009). However, the specific regulation of cohesin in response to DSBs in meiosis is not well studied and is likely to be have some differences given the very different mode of HR repair that takes place. At present it is unclear exactly what the role of cohesin is in meiotic DSB, though it is clear that there are defects in DSB processing during meiosis in the absence of cohesins. As described in section 1.3.7.3, there is evidence of local loosening of cohesion and loss of cohesin at CO sites, suggesting a fundamental difference with the cohesin reloading and SCC reinforcement that occurs in mitotic cells in response to DSBs (Eijpe et al. 2003; Garcia-Cruz et al. ; Calvente et al. 2013). In budding yeast, REC8 was shown to promote some bias towards sister repair that must be opposed by other SC components (Kim et al. 2010). Also previous work in our lab has shown that overall loading of cohesin by SCC-2 is not only essential for repair of SPO-11-dependent DSBs and CO formation, but also for the DNA damage response pathway (Lightfoot et al. 2011). A requirement for PDS5 in proper repair process in meiosis has been indicated (Storlazzi et al. 2003; Jin et al. 2009). However, further investigation of the regulation of cohesin in DSB repair is needed. Sequence and/or structural differences, as well as specific PTMs, of meiotic-specific cohesin subunits may facilitate the DSB repair mechanisms that meiosis requires. Furthermore, cohesin regulation by auxiliary factors like WAPL may have important effects on appropriate DSB response.

1.3.9.2 Cohesin and gene expression

Cohesin has a long established role in the control of gene expression. The central concept here is that the entrapping ability and topological modulation by cohesin can promote stable interaction of appropriate regions of a gene, such as enhancer and promoter, or maintain separation of regions to switch on or off gene expression. Early indication for this came from identifying mutations in the *Drosophila* SCC2 homologue, Nipped-B, that caused dysregulation of homeobox developmental genes (Rollins et al. 1999). The cohesive function of cohesin and the consequences of not only long-range interactions but also cohesin binding and turnover in mediating have been demonstrated (Rollins et al. 2004; Gause et al. 2010). Furthermore, heterozygous mutations in various cohesin subunits and regulatory factors are responsible for a human disorder called Cornelia de Lange Syndrome (Strachan 2005; Deardorff et al. 2007; Zhang et al. 2009). This is a developmental disorder affecting multiple organs, including the limbs and brain, which indicate gene expression defects. To confirm cohesin effects in gene regulation, a study showed depletion of cohesin from *Drosophila* post-mitotic neurons to cause defective axon pruning that result from deregulated expression of a particular receptor (Pauli et al. 2010).

A role for cohesin in gene regulation has also been well documented in mouse thymocyte development. Loss of cohesin disrupts transcription at a T-cell receptor gene that is important for thymocyte differentiation (Seitan et al. 2012). Cohesin interacts in interphase cells with a key transcription regulator, CTCF, and together they help control gene regulation and even immunoglobulin gene rearrangement by mediating long-range DNA interactions in cis (Hadjur et al. 2009; Degner et al. 2011). The effects of cohesin upon gene regulation in meiosis are yet to be investigated.

1.3.10 Medical impact of meiotic cohesin dynamics

Cohesin is essential for most key meiotic events, such as chromosome morphogenesis and CO formation, and therefore meiotic cohesin is essential for fertility. This is well exemplified by the recent finding that mutations in the meiosis-specific cohesin subunit STAG3 cause premature ovarian failure in women (Caburet et al. 2014). Another particular reason for the relevance of cohesin in human fertility arises from the well known increased risk in aneuploidy with increased maternal age. There are several studies showing evidence that cohesin is gradually being lost from chromosomes in

arrested oocytes and this may cause chiasmata to prematurely fall apart and chromatids to lose cohesion, accounting for increased aneuploidies with maternal age (Mark and Zimmering 1977; Jagiello and Fang 1979; Hodges et al. 2005; Chiang et al. 2010; Garcia-Cruz et al. ; Lister et al. 2010). Cohesion exhaustion from arrested bivalents is now thought to significantly contribute to segregation problems in oocytes of older mothers (Duncan et al. 2012; Handyside et al. 2012; Jessberger 2012; Nagaoka et al. 2012). With this in mind, it is essential to understand how cohesin is regulated or may be removed during meiotic prophase, when oocytes are arrested in mammalian oogenesis.

Studies described earlier regarding SCC maintenance during meiotic prophase found that *de novo* expressed cohesin subunits were unable to mediate the establishment of SCC during dictyate meiotic arrest (Revenkova et al. 2010; Tachibana-Konwalski et al. 2010). However, it still remains completely unknown how cohesin dynamics are controlled during meiotic prophase and whether the factors that may regulate cohesin dynamics, such as WAPL, play important roles during meiotic prophase. Furthermore, even if reloaded cohesins do not contribute to cohesion in arrested oocytes or cohesin is not actively removed during meiosis, cohesin regulation and dynamics during meiosis would be expected to have important affects outside cohesion given the known roles of cohesin on DNA repair, gene expression and chromosome morphology.

1.5 Aims and objectives

The main aim of this project was to investigate whether the cohesin removal factor WAPL has any function during meiotic prophase, especially during the pachytene stage when meiotic recombination is being completed. The hypothesis that cohesin may be actively removed during prophase was based on the observation that local loss of cohesion is known to occur around CO sites (Suja et al. 1992; Eijpe et al. 2003; Hulten 2011; Calvente et al. 2013). Moreover, previous experiments in our group in which the cohesin loader SCC-2 was knocked down after meiotic S-phase suggested that cohesin reloading during meiotic prophase is important for CO formation, and demonstrated a loss of cohesin from pachytene chromosomes (Lightfoot et al. 2011). The fact that impairing cohesin loading in mid prophase (pachytene) resulted in cohesin loss suggested the existence of an active mechanism that removes cohesin during meiotic prophase. WAPL is the most obvious candidate to mediate such cohesin removal activity. More specifically the project set about to determine if WAPL influences the association of cohesin with chromosomes during meiotic prophase, and if in doing so WAPL may affect cohesion and other meiotic events. Alongside this, I hoped to assess the dynamics of meiotic cohesin in vivo by developing FRAP methods using tagged versions of cohesin subunits in the *C. elegans* germ line, and relate to my findings in the investigation of the meiotic roles of WAPL.

Figure 1. Diagram depicting the major events of meiosis

DNA replication at S-phase creates sister chromatids that are held together by sister chromatid cohesion, provided by the cohesin complex. Homologous chromosomes pair and the synaptonemal complex (SC) assembles between them forming a proteinaceous bridge that keeps the aligned homologues in close proximity. DSBs are created in this context some of which become repaired to form COs. After the SC disassembles and chromosomes remodel, COs, together with sister chromatid cohesion, provide the physical attachment between homologues during late prophase. These linkages are known as chiasmata, and the structure formed by two homologous chromosomes connected by chiasmata is called a bivalent. The cohesion holding the chiasmata together is essential for the correct alignment of chromosomes on the spindle. The two-step release of cohesion by the controlled removal of cohesin from different regions of the bivalent at the two meiotic anaphases allows for appropriate chromosome segregation.

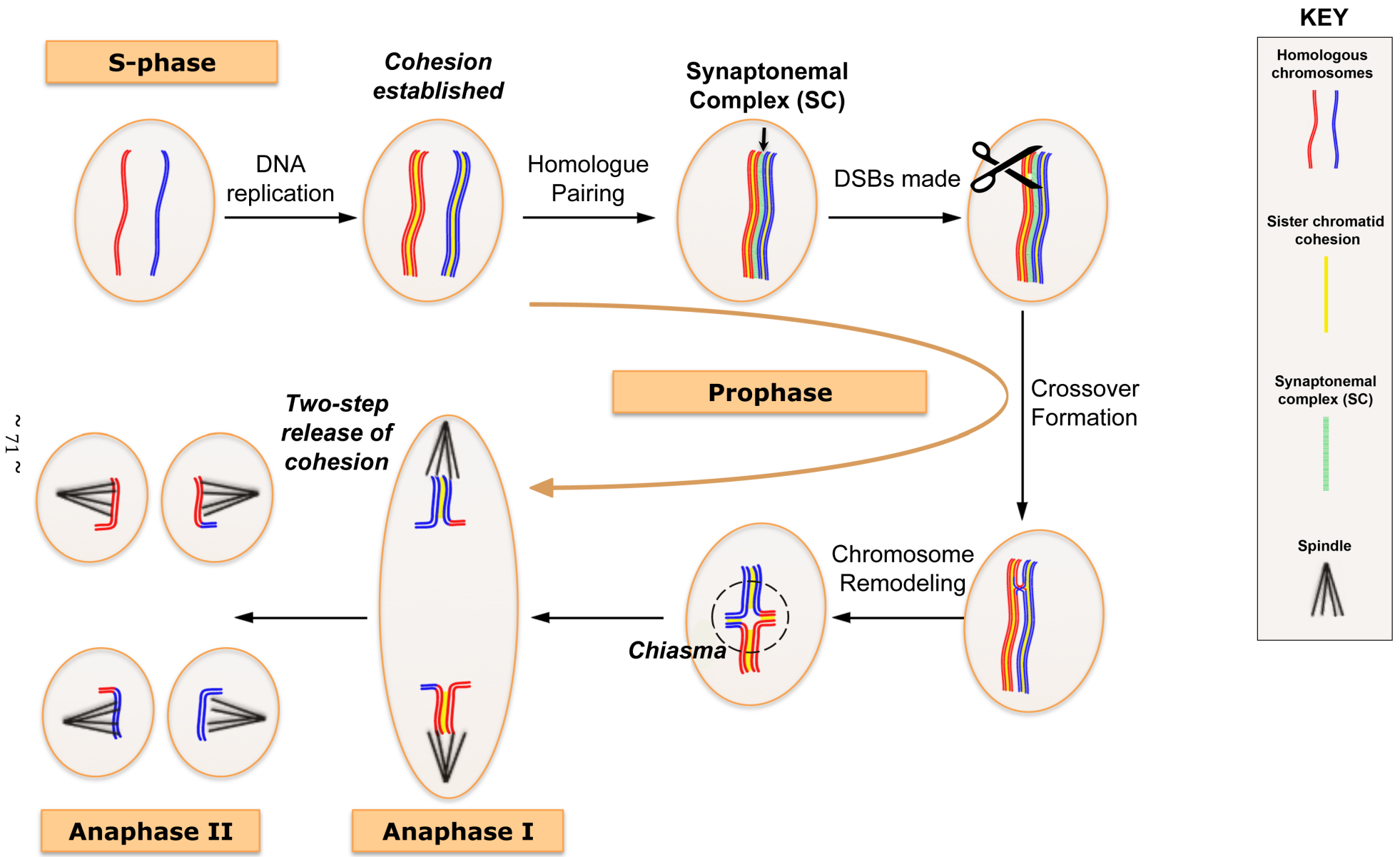
S-phase
Cohesion established
Synaptonemal Complex (SC)
DNA replication
Homologue Pairing
DSBs made
Prophase
Crossover Formation
Two-step release of cohesion
Chromosome Remodeling
Chiasma
Anaphase II
Anaphase I
KEY
Homologous chromosomes
Sister chromatid cohesion
Synaptonemal complex (SC)
Spindle

Figure 2. Diagram of a *C. elegans* germline annotated with key stages and events of meiosis

The germ line displays a whole time-course of meiosis from meiotic S-phase to diakinesis oocytes, which are followed by the meiotic divisions in the embryo that take place in the uterus. The diagram represents a germ line from an adult worm undergoing oogenesis, as are all meiotic nuclei shown in this project. Fertilisation of oocytes occurs at the end of oogenesis with spermatocytes produced in the same germ line at earlier stages in worm development. The position of the nuclei within the germ line, as well as the morphology and condensation of the chromosomes allows the meiotic stage of a nucleus to be readily determined.

*Figure created by colleague Sarah Testori.

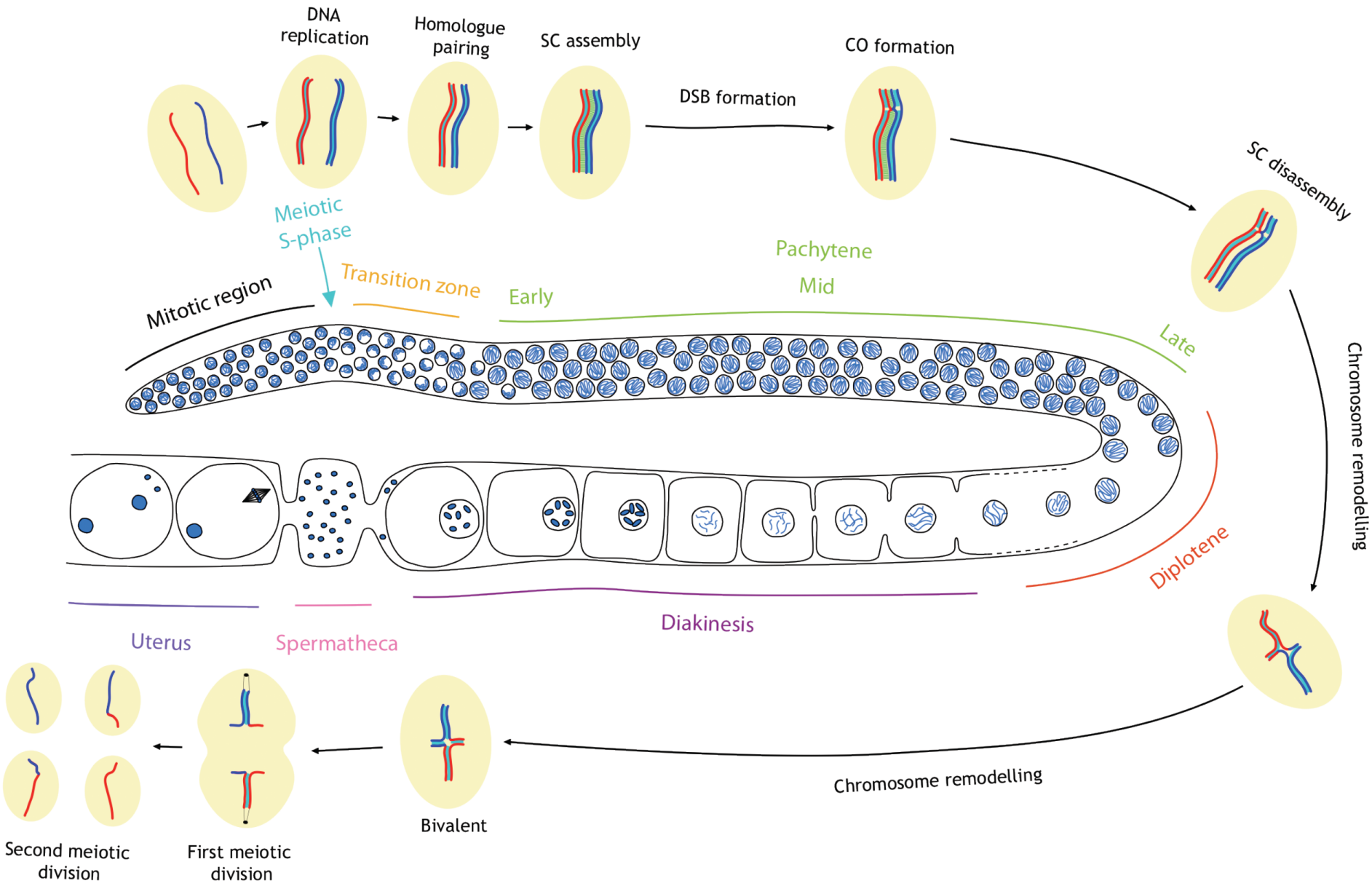
DNA replication
Homologue pairing
SC assembly
DSB formation
CO formation
SC disassembly
Meiotic S-phase
Mitotic region
Transition zone
Early
Pachytene
Mid
Late
Diplotene
Diakinesis
Chromosome remodelling
Uterus
Spermatheca
Bivalent
Chromosome remodelling
First meiotic division
Second meiotic division

Figure 3. Diagrams of SC structure and chromosome remodeling at late meiotic prophase.

A. Depiction of general SC structure. Chromatin loops attach to a core chromosome axis, comprised of meiotic cohesin complexes (REC-8, COH-3/4) and other axial element (AE) components such as HTP-1 (Hop1 in yeast). The central element components such as SYP-1 (Zip1 in yeast) assemble as transverse filaments bridging the two chromosome axes. Typical SC spacing is ~100nm between AEs.

B. Demonstrates chromosome remodeling that occurs from the end of pachytene through diplotene to diakinesis. The SC (purple) disassembles and chromosomes condense while SCC/cohesin (yellow) is maintained along chromosomes apart from some apparent local loss at CO sites. Chromosome arms re-arrange around the sites of COs, which become visible as chiasmata linking each pair of homologous chromosomes. Dashed arrow indicates rotation movement of short arm around the CO to form a cruciform bivalent structure. Note local loss of cohesion around the CO site.

A

The Synamptonemal Complex

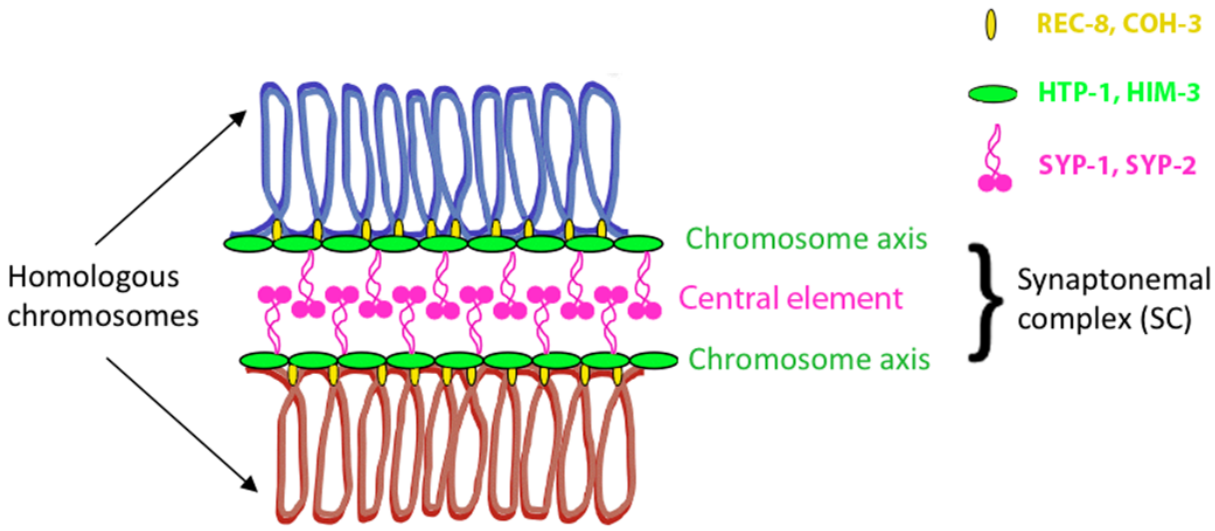

B

Late prophase chromosome remodeling

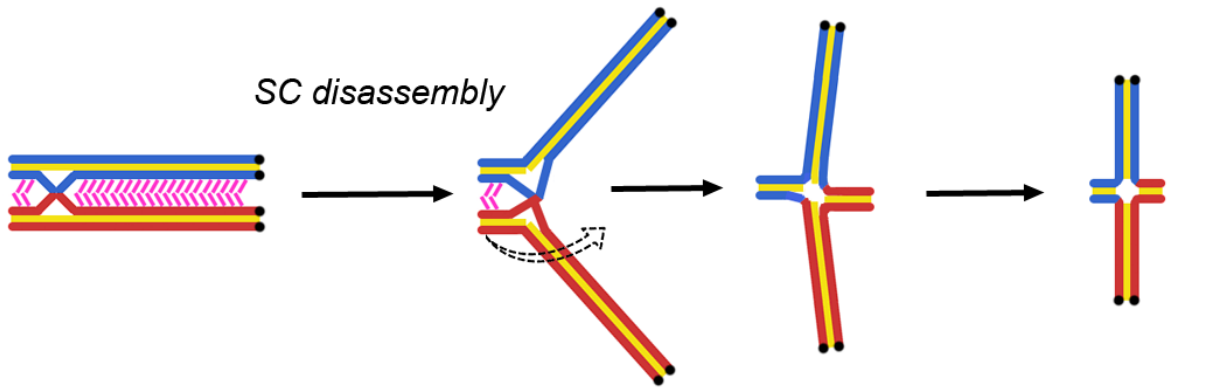

Figure 4. Diagrams of the cohesin complex and regulation of SCC during the mitotic cell cycle.

A. The cohesin complex is shown together with its auxiliary factors. The two SMC subunits form a dimer, bridged by the α-kleisin (SCC1 in mitosis, REC8 typically in meiosis). PDS5 and WAPL are thought to interact via the kleisin to destabilise the ring conformation. ECO1 acetylates SMC3 to oppose WAPL activity.

B. The standard model of cohesin topologically embracing two chromatin fibers to provide cohesion. The different versions of the kleisin subunit found in mitosis and meiosis of *C. elegans* are highlighted in the box.

C. An overview of cohesin regulation during the mitotic cell cycle. Cohesin is loaded to chromosomes before and during S-phase by SCC2/SCC4. Establishment of cohesion is promoted by SMC3 acetylation from ECO1 and maintained by the binding of PDS5. In the event of DSBs in mitosis, extra cohesin is reloaded locally and genome-wide. Most cohesin is removed from chromosome arms by WAPL prior to anaphase without cleavage. Separase cleavage of SCC1 in the remaining loaded complexes releases sister chromatid cohesion at anaphase.

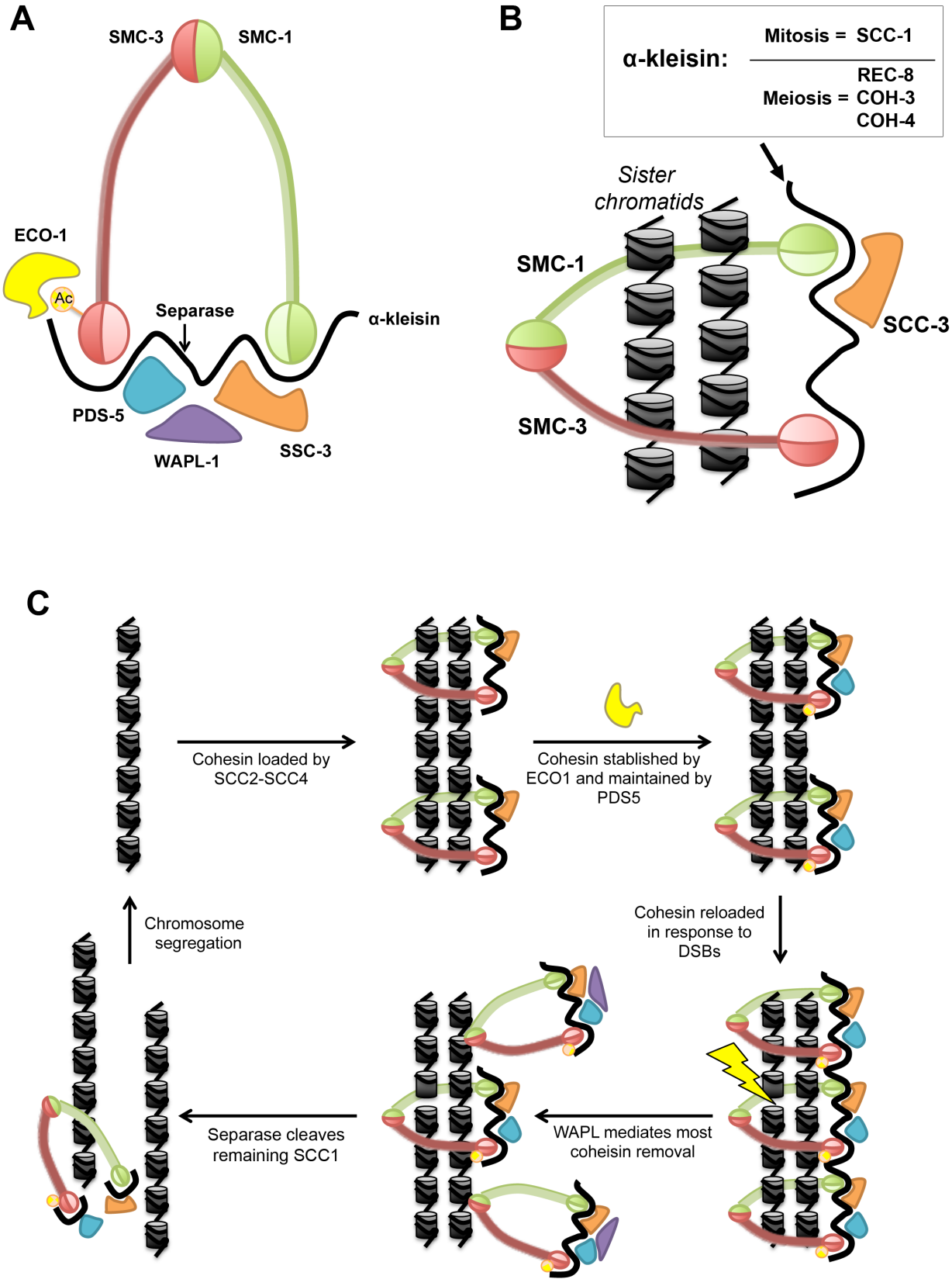
A
SMC-3
SMC-1
ECO-1
Ac
Separase
α-kleisin
PDS-5
WAPL-1
SSC-3
B
α-kleisin:
Mitosis = SCC-1
Meiosis = REC-8
COH-3
COH-4
Sister chromatids
SMC-1
SCC-3
SMC-3
C
Cohesin loaded by SCC2-SCC4
Cohesin stablished by ECO1 and maintained by PDS5
Cohesin reloaded in response to DSBs
WAPL mediates most coheisin removal
Separase cleaves remaining SCC1
Chromosome segregation

CHAPTER 2:

MATERIALS AND METHODS

2.1 C. elegans general methods

2.1.1 General growth conditions

C. elegans strains were maintained on Nematode Growth Media (NGM) plates seeded with either OP50 (Brenner 1974). Media and solutions are described in Table 1. *C. elegans* Bristol strain (N2) was used as wild type controls and all strains were maintained at 20°C, unless otherwise stated. To prevent the population from starving and to provide a constant source of animals from all stages of the life cycle, worms were transferred to a freshly seeded plate every 2-3 days. Starved strains were prevented from becoming desiccated by wrapping parafilm around the plate, and in this way worms were viable for several months.

2.1.2 Handling and observation of C. elegans

Animals were manipulated using a pick made from Platinum wire (Sigma-Aldrich Platinum wire diameter 0.25 mm, Product number: 349402-250MG) welded onto the end of a glass Pasteur pipette. Animals were observed using a Leica MZ75 bench stereoscope or with a Leica MZ16F florescence stereoscope for transgenic worms with visible fluorescent markers.

2.1.3 Genetic crosses and maintaining male stocks

Genetic crosses were typically performed by picking 2-6 males from N2 plates with males onto a plate with a small of OP50 E. coli lawn, together with a single hermaphrodite of the desired genetic background such as a balanced mutation. Male progeny with the genetic variants of interest were appropriately crossed onto other genetic backgrounds until the desired combination of alleles could be brought together. To account for the random assortment and heterozygosity of alleles excess crosses and progeny were picked at all steps to ensure the desired combination was obtained (Brenner 1974). In many crosses I employed a simple technique to limit the number of final progeny by PCR genotyping males after mating had been completed to follow the alleles of interest.

Recombinant chromosomes were made by creating hermaphrodite worms with the appropriate mutations on either chromosome of a homologous pair, through such genetic crosses mentioned above. These hermaphrodites were allowed to self fertilise and large numbers of progeny picked accordingly to the genetic distance between genes of interest. Male stocks were maintained by picking several male worms with 1 or 2 L4 stage hermaphrodites to a single NGM plate. This ensures that hermaphrodites are mated while they were still young adults, resulting in the production of up to 50% of males in the F1 progeny.

2.1.4 Maintaining meiotic mutants

C. elegans meiotic mutants are difficult to maintain, as homozygous strains often have low viabilities. Compounding this, meiotic mutants often have compromised genomic integrity allowing the introduction of novel mutations into the genome when strains are kept as homozygous stocks. Therefore, meiotic mutations were maintained in heterozygosity, by using reciprocal translocations that carried visible markers to balance meiotic mutations, such as *unc*, *rol* and/or GFP expression. From these strains homozygous animals could be obtained, as heterozygous and homozygous animals were easily identifiable on the plates by their visible translocation markers.

2.1.5 Cleaning of C. elegans strains

C. elegans strains occasionally became contaminated with moulds and/or bacteria (different than *E. coli* OP50), which could affect the regular growth of the animals. Uncontaminated cultures were restored by washing with Bleaching Solution. Animals and eggs were washed from their contaminated plate with M9 and pipetted in Falcon tubes containing 10ml of Beaching solution (Table 1). Falcon tubes were left on a nutator for 10 min or until the adult animals had dissolved, leaving no carcasses visible. The worm eggs were pelleted by centrifuging for 1 min at 900 x g in a bench top centrifuge and washed 3 times with 10 ml of H_2O and. Finally the egg pellet was re-suspended in 500 μl of M9 and the eggs were transferred onto fresh OP50 seeded NGM plates. After 12-18 h, the larvae hatched to produce a clean culture.

2.1.6 Freezing of C. elegans strains

A practical, if surprising property of *C. elegans* is that it can be frozen and stored in -80°C freezers, or liquid nitrogen, for many years (Brenner 1974). The early stages of worm development survived the freezing process best, so plates containing large amounts of L1

and L2 were used for the creation of frozen strain stocks. Worms from three plates were washed off using M9 and placed onto a 15 ml falcon tube. This solution was mixed with freezing solution in a 1:1 ratio and 1 ml of this mixture was pipetted into a 3 ml cryotube (Fisher), producing six vials in total. These were immediately transferred to a -80°C freezer. Five vials were stored at -80°C, while 1 test vial was thawed the following day to ensure the strain survived the freezing process.

2.2 DNA methods

2.2.1 Single worm lysis for genotyping

A crude DNA extraction method was used in order to obtain *C. elegans* genomic DNA that could be used as a template for PCR reactions. For single worm extraction, an individual animal was transferred into a 0.2 ml PCR tube containing 10 µl of 1x PCR buffer with proteinase K (see below). The tubes were frozen in liquid N_2 and directly transferred to a PCR thermocycler, using the following program:

70 min at 60°C

15 min at 95°C.

DNA could then be used or stored at -20°C until needed. The same protocol could be used to extract DNA from several worms in a population by simply lysing multiple animals together in the same tube.

1X PCR buffer containing protease K:

Mix 100 µl of 10xPCR mix (100 mM Tris, 500 mM KCl, 15 mM $MgCl_2$ pH 8.3, autoclaved) with 900 µl of H_2O and 50 µl of 20 mg/ ml proteinase K.

2.2.2 Single worm PCR

Using 1-2 µl of DNA extraction as template, a 25µl PCR reaction was set up as follows (or scaled to 50 µl for PCR amplicon sequencing):

10.5 µl H_2O,

12.5µl Taq PCR Master mix (Quiagen)

1 µl of the required primer pair at a 10µM concentration

The annealing temperature used based on the melting temperature (Tm) of each primer pair. The reaction product was checked by running 5 µl of the reaction on an agarose gel

by standard electrophoresis procedures, and cleaned for sequencing using a PCR purification kit (QIAGEN) if necessary.

The following PCR program was run unless specified:

	5 min at 95˚C	x1 cycle
Denaturation	30 sec at 95˚C	x35 cycles
Annealing	30 sec at Tm (default 60˚C)	
Elongation	(60-240)* sec at 72˚C	
	10 min at 72˚C	x1 cycle

* elongation time was adjusted to amplicon size, ~1000 bp per minute

2.2.3 PCR amplicon sequencing

DNA amplicon product from a single or several worm PCR was purified using the Qiagen MinElute PCR purification kit. 50 µl PCR reaction volume was used for sequencing to obtain sufficient product. At last step of the kit DNA was eluted from the column using 10 µl H_2O. DNA was quantified using Qubit or running aliquot on gel electrophoresis with marker. Sequencing pre-mix was made with PCR product at roughly 10 ng per 100bp of sequence and 3.2 pmole of primer per sample mix. Individual sample mix was made for forward or reverse primers separately. Total mix volume was made up to 10 µl and given to the CSC genomics laboratory to carry out following steps of sequencing procedure using fluorescent labeled nucleotides and ABI3730xl instrument.

2.2.4 Taqman CO qPCR mapping

The technique of rapid reliable genotyping of SNPs using TaqMan™ RT-PCR technology has been established for some time (Livak et al. 1995; Chen et al. 1997). The application of Taqman genotyping to map CO distribution has been developed in our lab by Leticia Labrador. Briefly, 5 Hawaiian strain SNP variants were chosen for each chromosome spaced evenly by physical distance. The genotyping of the SNPs can map 4 broad intervals spanning most of a chromosome. Animals must be created in which have one chromosome within a homologous pair contains all N2 wildtype SNPs and the other homologue has all Hawaiian version SNPs (Figure 30). COs will occur between the two homologues making recombinant chromosomes with a mix of both N2 and Hawaiian SNPs at different positions. These recombining hermaphrodites must be outcrossed to either

N2 or Hawaiian background and individual progeny picked to genetically isolate any recombinant chromosomes. Self-progeny of such isolated chromosomes in a single worm should represent on a population level the founding genotype. The genotyping of the 5 SNPs mapped CO events to broad genetic intervals.

2.2.4.1 Whole plate DNA extraction

Worms collected from starved final plates from mapping crosses (Figure 30) by washing with M9 + 0.1% Triton X-100 into 15ml tube balanced up to 10ml. This suspension was centrifuged at 2000 rpm for 2 min. Supernatant was removed and worm pellet was washed 3 times likewise with deionised water. Final pellet after washing was re-suspended in 150ml of worm lysis buffer and transferred to individual 200ml PCR tube (50 mM KCl, 10 mM Tris pH 8.2, 2.5 mM MgCl2, 0.45% NP-40, 0.45% Tween 20, 0.01% gelatin: just before use add 6 ml 10 mg/ml proteinase K). Worms were then lysed with PCR machine lysis program: 1hour 10 min 60 C^o, 15 min at 95 C^o. DNA was precipitated by first transferring of lysis solution into 1.5 ml tube, leaving behind undissolved. 450 ml of ethanol and 15 of ml sodium acetate were added to the lysis solution. This was left at -20 C^o overnight and then centrifuged at 13000 rpm for 30 min to pellet DNA precipitate. Ethanol/acetate was then poured off and DNA pellet dried at room temperature. DNA was then resuspended in 100 ml water and diluted out 1 in 4 into four replicate 96 well plates, sealed with film and stored at -20C^o.
Plates at -20 C^o. Control mapping DNA was also obtained from replicates of plain N2, Hawaiian and N2/Hawaiian heterozygous worms with the same method: extracting DNA from starved plates as above. For heterozygous controls F1 L4s from a cross between N2 and Hawaiian were picked and left to starve.

2.2.4.1 Taqman probe genotyping

QIAgility Robot (Qiagen) was used to automate PCR setup for qPRC Taqman probe genotyping. The robot was programmed with QIAgility software (version 4.11.0) to load the Rotor-Disc 100. Each reaction well contained 12 ml final volume: 7.68 ml of General master mix and 4.32 ml of genomic sample DNA dilution. General master mix was made up in the following ratio: 6 ml Type-it Fast SNP Probe PCR Master Mix (2X concentration) from Qiagen kit 206042, 0.3 ml Taqman custom probe (40X concentration), 1.38 ml water. Appropriate probe for relevant SNP of interest was used for each general master mix. SNP1: -15.9 (149586), pkP2132,T/A. SNP2: -6.23 (3629598), CE2-125, G/C. SNP3: +0.50 (7158542), pkP2149, T/C. SNP4: +3.41, (11305690), CE2-190, A/C. SNP5: +27.3,

(14808011), CE1-226, G/T. For full 96 well plate the Rotor-Disc 100 allowed for a single control reaction for N2, Hawaiian, heterozygote and water blank. After robotic pipetting, Rotor-Discs were sealed using Rotor Disc heat sealing film (981601) and Corbett Gene-disc Heat Sealer HS-01. SNPs were detected by cycling on the Corbett Rotor-Gene (RG6000). Cycle settings comprised a 94 C^o initial activation step for 10 min then 40 cycles of 92 C^o for 15 seconds, 60 C^o for 105 seconds. This can be adjusted empirically to sample quantity and probe efficiency. Fluorescence was measured every cycle at both channels: Green 470nm gain 5 and Yellow 530nm gain 5. A genotyping graph is plot with cycle amplification curves as part of the running software and final output data is grouped into genotypes using control samples. Genotyping data is exported as excel file for analysis. In cases of poor genotype grouping Q-solution was added, as described in the Type-it Fast Probe PCR manual. Genotype results for all 5 SNPs on chromosomes II were combined to give full chromosome genotype for each sample. Data filtering entailed grouping of samples into mother plates from which the F3 final progeny of the crosses were picked (see Figure 30). Absence of any N2 SNPs in any progeny from a mother plate indicated ancestral worm was not a true cross progeny at F1 cross and therefore F2 hermaphrodite mother carried no N2 DNA as required. Successful cross at F2 was ensured for *wapl-1* mutant mapping by rescue of *wapl-1* fertility defects in F3.

2.2.5 CGH array mapping

2.2.5.1 Genetic crosses and DNA extraction

To obtain appropriate mapping DNA a combination of genetic crosses was employed. N2 males were crossed to balanced hermaphrodites to produce *fq9* heterozygous males with N2 background. These were crossed to full Hawaiian (CB4856) hermaphrodites to produce F2 hermaphrodites heterozygous for all N2 and Hawaiian SNPs and heterozygous for *fq9* mutation. 400 self progeny L4 worms (F3) were picked to individual plates. ~100 *fq9* homozygote recombinants were identified by their reduced fertility and at 48 hours post L4 were manually picked into a 1.5 ml tube with of 1ml (M9 + 0.1% Triton X-100) for washing. Worms were centrifuged at 2000 rpm for 2 min and supernatant removed. Worms were washed with water 3 times. Maximum water was removed and final pellet frozen at -80 C. Puregene Genomic DNA Tissue Kit (Qiagen) used to extract DNA from worm pellet as follows. Worms were thawed, and appropriate volume of Cell Lysis Solution and proteinase K was added and mixed by inversion. Worms incubated at 55°C for 3 hours with inversion every hour. 3ml of RNase A then added followed by incubation

at 37°C for 1 hour with inversion every 15 min. Lysate was then incubated on ice for 1 min. 200ml Protein Precipitation Solution added to lysate and vortexed briefly. Mix was then incubated on ice for 5 min and centrifuged at 13000 rpm for 3 min at 4°C to pellet precipitated proteins. Supernatant containing DNA was transferred into 600ml of isopropanol and mixed by gentle inversion (~50 times). This is mix was centrifuged at 4°C at 13000 rpm for 15 min to pellet/smear DNA onto tube. Supernatant was removed and pellet washed 3 times by re-suspending in 600 ml of 70% ethanol. Final pellet was air dried for 30 min to remove all ethanol. The DNA then was dissolved in 100ml DNA Hydration Solution (Qiagen).

2.2.5.2 DNA quality check and CGH array

DNA concentration was measured using the Qubit fluorospectrometer (Invitrogen). Working Solution is made in the ratio of 1µL Quant-iT Reagent to 199 µL Quant-iT Buffer (Invitrogen). Calibration Standards made using 10 µL of stock solution dsDNA Standard #1 (0 ng/µL) and #2 (10 ng/µL) from kit with 190 µL Working Solution, mixed in 0.5mL thin-walled PCR tubes. For the mapping sample 4 µL of purified DNA solution was mixed with 196 µL of the Working Solution (final volume of 200µL). Repeat measurements of the sample DNA were made after calibration. DNA quality was checked with NanoDrop® ND-1000 Spectrophotometer (Buhler et al. 2009). Remaining sample was then sent to our collaborators in the Moerman laboratory British Colombia, Canada who labeled the DNA and performed the CGH tiling array (Flibotte et al. 2009) and processed the data as SNP signal plots shown in chapter 8.

2.2.6 Whole genome sequencing

Whole genome sequencing (WGS) was performed to identify all possible candidate mutations within the *fq9* mutant, particularly in the 400 Kb region mapped by the CGH array. This WGS approach has been successfully applied to the mapping of C. elegans mutations (Hillier et al. 2008; Sarin et al. 2008). WGS was done using Illumina TruSeq technology. As instructed the purified ethanol precipitated DNA from fq9 homozygous mutant worms was sheared using an E210 sonicator (Covaris) for 45 and then analysed on 8% PAGE gels. DNA fragments of 200-300 were excised and eluted from the gel slices overnight using the MiniElute Gel Extraction kit (Qiagen). Genome libraries were prepared using the paired-end tag (PET) protocol as described in the TruSeq DNA Sample Preparation Guide. Briefly, this involved DNA end repair and formation of 3′ adenosine overhangs which are ligated to chosen Illumina PE adapters (with 5′ overhangs). Adapter-

ligated products were purified and amplified by 10 PCR cycles with the PE primer. PCR products of the desired size range were purified from adapter ligation artifacts using 8% PAGE gels. DNA quality was assessed and quantified using Nanodrop spectrophotometer and a Bioanalyser (Agilent). Average library fragment size was 371 bp, which corresponds to ~250 bp genomic fragment with 60 bp adaptor sequence on either end. Sequencing of the library was done Illumina HiSeq2500 sequencers. The total reads sequenced above the basic filter was ~237 million. These were assembled into a whole genome sequence by alignment to the reference N2 genome using ELAND (efficient large-scale alignment of nucleotide databases). This gave an average depth of coverage of 126X and a 99.8% of bases sequenced at greater than 15X coverage. Results were marked for non-synonymous versus synonymous and filtered for exonic changes to the reference genome.

2.2.7 Transgenic MosCI insertion

Recent development of the Mos1 Single Copy Insertion (MosSCI) developed by Roberts & Bessereau (2007) and improved by the Jorgensen lab, has been used for the creation of all transgenic lines for this study. Most transgenes shown in the results were made by my colleagues Sarah Testori and Consuelo Barroso. Briefly, a tagged gene is cloned into a vector containing a functional copy of the unc-119 gene and ~1.5kb of sequence which has homology to a chromosomal locus with a Mos1 site. Mos1 excision is induced by expression of Mos1 transposase and gene insertions are generated by repair of the double stranded break. This occurs by homologous recombination between the break ends and the regions of homology within the vector. It is therefore necessary to use the appropriate C. elegans strain and vector combination. REC-8::GFP, SCC-3::GFP and GFP::WAPL-1 were all inserted at the Chromosome II locus (ttTi5605, EG4322 strain) using the pCFJ151 plasmid vector. COH-3::mCherry was inserted at the Chromosome I locus (ttTi4348, EG6701 strain) using the pCFJ352b plasmid vector. All constructs used were produced by gene synthesis and cloned into the MosSCI vectors by GeneScript.

2.2.7.1 Generation of transgenic strains

The strains injected in order to generate transgenic lines all contain a mutation in the *unc-119* gene, which acts as a positive marker as worms in which the *unc* phenotype has been recovered to wild type by injection, are easily identifiable. Young adult worms are injected into that were picked as L4 the previous day.

Worms are injected with the transgene construct directly into their germline. To select true inserts from non-inserted extrachromosomal array, a number of positive and

negative selection markers are used. Positively injected worms are be identified by the presence of *non-unc* progeny, as the *unc-119* phenotype is rescued by the presence of the functional gene in the transgene vector. In addition to this three negative selection mCherry fluorescent markers are co-injected with transgene vector. The mCherry expression is driven by pharyngeal, neural and muscle promoters that can be seen under a fluorescent microscope without moving the worms from the plates. These marker vectors they are not targeted for insertion so as these animals pass through successive generations the extrachromosomal plasmid arrays are lost. Non-*unc*, non-mCherry worms can then be assessed for full insertions by PCR sequencing. Correct transgene insertions can be crossed into the appropriate mutant background to assess function.

2.2.7.2 Preparation of injection mix

All plasmid constructs were transformed into chemically competent DH115α *E. coli* cells, grown up and plasmid harvested with QIAprep Spin Miniprep Kit (QIAGEN). The DNA concentration was measured and the following 10X stock injection mix shown in the table below was made and stored at -20°C. On the day of injection, a 1X mix was made diluting with water and the addition of the transgene vector to a final concentration of 50ng/µl.

Table 1: Co-injection MosCI selection vectors

Plasmid	Description	Final concentration
pCFJ601	Peft-3::transposase	500ng/µl
pGH8	Prab-3::mCherry (Pan-neuronal)	100ng/µl
pCFJ90	Pmyo-2::mCherry (pharynx muscle)	25ng/µl
pCFJ104	Pmyo-3::mCherry (body muscle)	50ng/µl

2.3 Cytological Methods

2.3.1 Ethanol fixation and quick DAPI staining

Ethanol fixation followed by DAPI staining is a quick and simple way to observe *C. elegans* chromosomes cytologically. Approximately 20 worms were picked to 8 µl M9 buffer on a superfrost charged slide (VWR scientific). As much liquid as possible was wicked away using filter paper until the worms were left in only a small volume of M9. 10 µl 95% ethanol was added to the slide and air-dried. This was repeated to fully dehydrate the worms. 8 µl of 2µg/ml DAPI was added and a 22 x 22 glass cover slip was placed on the

top of the worms. Animals were viewed on a Leica DMRB microscope using 20X, 40X, or 63X lenses and imaged with a Leica DFC300 FX camera.

2.3.2 Immunostaining of C. elegans meiosis

A slightly modified protocol for immunostaining staining was carried out as described in Howe et al. (2001). Worms were synchronised by transferring L4s to a fresh NGM plate and allowing them to mature for 18hr, unless otherwise specified, yielding a population of young adults. 20 to 30 age matched adult worms were picked into 15 µl egg buffer (118 mM NaCl, 48 mM KCl_2, 2 mM $CaCl_2$, 2 mM $MgCl_2$, 5 mM HEPES, at pH 7.4) with 0.1% tween on a 22 x 22 glass cover slip. The animals were carefully dissected just behind the pharynx using a fine needle in order to achieve optimum gonad extraction. Germlines were fixed by the addition of 15 µl 2% paraformaldehyde (PFA) in egg buffer and 0.1% tween. Pipetting gently ensured an even mix of PFA throughout and aided in extruding the gonads. 15µl of the solution was then removed and the remaining solution covered with a superfrost charged slide (VWR scientific). The dissections were fixed for a total 5 min from the addition of the PFA and then immediately immersed in liquid N_2. The cover slip was removed using a razor blade and the slide placed in -20°C methanol.

Slides could be stored in -20°C methanol ~24 hours but ideally were processed in the same day. Minimum immersion in methanol was aiding adherence of the germlines to the slides. The slides were washed 3 x 5 min in PBST (1x PBS, 0.1 % Tween) in coplin jars before being blocked for 1 hr in 0.7 % BSA in PBST. 50µl of primary antibody diluted in PBST was added to each slide and covered with a parafilm cover slip. Slides were incubated in a dark humid chamber at room temperature (RT) ON. The primary antibody was then washed off by 3 x 10 min washes in PBST in coplin jars. 50 µl of the appropriate Alexa secondary antibody (Invitrogen) in PBST was then added at a dilution of 1:300. Another parafilm cover slip was placed over the slides and they were again incubated for 2 hr RT in the dark in a humid chamber. Finally, the secondary antibodies were washed off by 3 x 10 min washes in PBST in coplin jars. 75µl of 2µg/ml DAPI in water was added to the slides and left in the dark for 5 min. This was removed by a 5 min wash in PBST and the slides mounted by the addition of 15 µl of vectashield (Vector labs). A 22 x 40 glass cover slip was used to seal the immunostaining.

For observation of fixed embryos worms were cut in the middle of the body to release maximum embryos and larger numbers of worms were used as the embryos do not adhere well.

2.3.2.1 TRITON-X100 protocol

A version of immunofluorescence was performed for some experiments using TRITON X-100 detergent to wash out nucleoplasmic protein. In this case TRITON X100 replaced Tween in the PBST buffer for all subsequent stages after snap freezing. Extra slides for each genotype are required because the stronger detergent causes more germlines to dislodge from the slide.

Table 2: Antibodies used for immunofluorescence

Antibody	Host	Main Staining	Dilution	Source
SMC-1	Rat	Cohesin complex	1:300	Dr Barbara J. Meyer (UC Berkely)
SMC-3	Rabbit	Cohesin complex	1:200	Millipore (AB3914)
REC-8	Rabbit	Cohesin complex	1:200	SDIX
COH-3	Rabbit	Cohesin complex	1:1000	Novus Biologicals (49290002)
COH-3/4	Rabbit	Cohesin complex	1:1000	SDIX (serum)
HTP-1	Rabbit	Axial element	1:200	SDIX (serum)
SYP-1	Chicken	Central element	1:300	SDIX
RAD-51	Rabbit	Recombination intermediates	1:10000	SDIX
GFP-488	Rabbit	Transgenic GFP proteins	1:200	InvitroGen

2.3.3 Deltavision microscopy

Immunostained germlines were imaged using a DeltaVision Deconvolution Microscope developed by Applied Precision (DeltaVision system core, Olympus 1X70 microscope, CoolSNAP$_{HQ}^2$ Monochrome camera). Germlines were imaged in a series of Z-stacks that required deconvolution to reverse the optical distortion. Images in different z-axis planes were analysed and processed in softWoRx (version 3.7.1) and were subsequently flattened into a two-dimensional projection. The relatively large size of a *C. elegans*

germline prohibited imaging of the whole structure in a single field and so several fields were required. Reconstruction of the whole image germline could be achieved manually using Photoshop (Adobe) or automatically with ImageJ.

2.3.5 Whole nucleus mean fluorescence intensity quantification

Mean whole nuclear fluorescence was quantified with an ImageJ macro written by D. Dormann and K. Hng. Quantification was performed on raw deltavision files acquired under identical microscope settings. Briefly, an oval is manually drawn to define a nucleus ROI within which mean fluorescence intensity is quantified for each Z-stack and automatically averaged across the chosen range of stacks. This measurement is performed on the desired number of nuclei within an image producing an excel table with the mean intensity values plus a reference image with a numerical ID to distinguish nuclei. Only nuclei with stacks covering the whole nuclear volume were used. These mean nuclear intensities were then grouped from multiple images to calculate overall average intensity for a certain staining, meiotic stage and genotype.

2.3.5 Lineprofile fluorescence intensity range quantification

Fluorescence intensity lineprofiles were made using the SoftWoRx Line Profile tool. 1024x1024 pixel raw deltavision image stacks were opened in SoftWoRx (version 2.0) and maximum intensity projections made of the minimum stacks containing nuclei of interest. Well-stained nuclei that were not overlapping with neighbours and showing 3 or more parallel axial cohesin tracks were chosen and cropped to 91x91 pixel square, typically leaving a small margin. The lineprofile was then placed across the nucleus perpendicular to the axes, either horizontally or vertically. The position of the line was chosen to give at least 3 axial defined peaks of roughly similar size to control for measurement of overlapping tracks. Data from the lineprofile was captured to an excel file which could be plotted to a graph of intensity over pixel number (0-91). Peak to trough fluorescence intensity ranges (ΔF) were calculated for all peaks within a nucleus (Figures 21, 22 & 23).

2.3.6 Quantification of ZHP-3 foci

Quantification of the recombination intermediate ZHP-3 was carried out on α-GFP immunostained germlines of worms containing the ZHP-3:GFP transgene (Bhalla et al. 2008) in the N2 wildtype background or crossed into the homozygous *wapl-1* (*tm1814*)

background, picked as F1 from nT1 balanced worms. Images were acquired using a Delta Vision deconvolution Microscope (Deltavision system core, Olympus 1X70 microscope, CoolSNAP$_{HQ}^2$ Monochrome camera) as in 2.5.2. softWoRx (version 3.7.1) was used to scan through the Z-stacks. Foci were counted within the 3D context of the nuclear space.

2.3.7 Quantification of DAPI-stained bodies in diakinesis oocytes

Diakinesis staged *C. elegans* nuclei were quantified from germlines processed as in 2.3.2, either with full immunostaining for secondary observations or directly stained with DAPI after initial washes. Images of the -1 and -2 diakinesis were acquired on a Delta Vision Deconvolution Microscope developed by Applied Precision (Deltavision system core, Olympus 1X70 microscope, CoolSNAP$_{HQ}^2$ Monochrome camera). The following settings were used for acquisition: DAPI excitation and emission, 2% intensity, 0.05 s exposure and 100x oil immersion objective. Deconvolved images were converted into maximum intensity projections and cropped to the size of an individual nucleus using ImageJ. These cropped images were analysed in CellProfiler to identify each DAPI stained body, calculating the number of bodies per nucleus as well as the area of each individual body. Analysis on wildtype and mutants with known diakinesis chromosome phenotypes was performed to determine the area in pixel of different DAPI mass types (Figure 33). This allows unbiased automatic identification of DAPI mass types according to their area, with a bivalent 500-1000 pixels, a univalent 250-500 pixels, an individual sister 120-250 pixels, and a fragment less than 120 pixels. Multiple repeats of these diakinesis quantifications were pooled to determine frequency histograms of body areas.

2.4 Live imaging

2.4.1 FRAP imaging

FRAP live imaging has not been previously applied to the *C. elegans* germline according to the literature and therefore the following procedure was developed through a combination of adapting previous live imaging techniques used for *C. elegans* in our lab and elsewhere together with FRAP live imaging protocols used in other systems plus empirical testing with our system (Baudrimont et al. ; Gause et al. 2010; Labrador et al. 2013). The Leica TCS SP5 confocal scanning microscope was used as this has a built in FRAP wizard and previous FRAP experiments have commonly been performed with confocal microscopy including some cohesin FRAP experiments. All FRAP imaging was in

2D and at room temperature. Using Prior to starting all individual FRAP experiments, nuclei at desired stage within a germline were chosen for having 3 or 4 clear parallel axial tracks to facilitate ROI boundary definition and visual recovery to chromosome axis. Z-position was always set initially so axial tracks within the bottom third of the nucleus were visible for the two nuclei of interest. 7x zoom was used for all FRAP imaging runs, for consistency, giving reasonable resolution of individual chromosomes but allowing for some X-Y movement. Bleach ROI was set before starting FRAP run and always covered around half of the nucleus for both chosen nuclei plus a margin of ~1/4 of a nucleus width. Similar overall bleach area size was maintained.

2.4.1.1 Live worm slide preparation

L4 worms of transgenic strain were picked in morning before imaging the following day. This meant adults imaged were always ~30 hours post L4 giving large germlines for ease of imaging and staging of nuclei. Worms were picked from progeny of single mother worms and normal germline expression was checked in at least 20 adults by inspection of live worms using a Leica DMRB fluorescence microscope. 5 adult worms were picked to a 5 µl drop of M9 buffer containing 2mM levamisole. The drop was placed onto a small fresh 5% agarose pad. Agarose pads were made by dropping molten agar (5% agar dissolved in M9) onto the centre of a glass and placing a second slide on top, spaced by strips of plastic sheet ~0.1 mm. Solidified agarose pads were cut to 1cm squares with a razor blade immediately prior to each experiment. After M9 liquid drop and worms were added to the pad a small coverslip was gently placed on top (18x18 mm Menzel-Glaser). The coverslip was then sealed on all edges using a 50/50 mix of Vaseline (Sigma-Aldrich) and Paraffin oil (Sigma-Aldrich) painted on with a small brush. Slides were initially viewed under bright field illumination with 10x objective and the eyepiece of the Leica SP5 microscope. Worms to image were chosen for well positioned visible germlines with desired staged nuclei close to coverslip and not obscured by other organs. Then the 60x oil immersion lens was switched to and the Z-position adjusted to start fluorescence imaging.

2.4.1.2 High resolution FRAP microscope settings

For the high resolution FRAP a greater degree of control was required for monitoring the position of nuclei between full high resolution images and so the FRAP wizard was used for the: single pre-bleach image, the single bleaching and the first post bleach image (t=0). Then subsequent time-points were manually acquired, not within the FRAP wizard. The

acquisition images for the high resolution were all taken with the following settings: 100 Hz scanning speed, 3 times line averaging, 1 AU pinhole. SCC-3::GFP and REC-8::GFP were imaged with 488 laser at 30% overall power and 10% sub-power for acquiring, HyD detector set to 502 nm – 552 nm range, at 300 gain. COH-3::mCherry was imaged with the 561 laser (non-variable overall power) and 10% imaging power, HyD detector set to 590 nm – 680 nm range, at 350 gain. A single bleach image was used for both laser lines with zoom-in setting, 60% sub-power for the 488 laser. After a single t = 0 s time-point with the FRAP wizard, all subsequent time-points were acquired manually and following a clock timer. The following time-points were always used t = +0, +5 min (300 s), +10 min (600 s) and + 15 min (900 s). Despite immobilization methods, internal movement of organs plus nuclei drift typically required constant monitoring and manual Z position and sometimes X-Y position adjustment to maintain focus on chromosome axes of interest. Between long time-points general Z-position of bleached nuclei was monitored by very low intensity imaging (1400 Hz) to minimize acquisition bleaching. Images were exported as tiffs and contrast adjusted equally for an image series to visualise axial fluorescence.

2.4.1.3 Low resolution FRAP microscope settings

Low resolution FRAP settings were used with regular time-points for producing recovery curves to estimate the dynamics of the whole mobile fraction. The following conditions were used for all transgenes: 400 Hz scanning speed, 1 times line averaging, 3 AU pinhole. SCC-3::GFP and REC-8::GFP were imaged with 488 laser at 30% overall power and 10% sub-power for acquiring, HyD detector set to 502 nm – 552 nm range, at 150 gain. COH-3::mCherry was imaged with the 561 laser (overall power not adjustable) and 8% imaging power, HyD detector set to 590 nm – 680 nm range, at 150 gain. 100% sub-power was used for bleaching in both laser lines. 3x pre-bleach images were used at 1.3 s intervals (minimum with given settings). A single bleach image was set at 100% laser sub-level power for 488, zoom-in setting. Post-bleach imaging was in two phases: 10x 3 s followed by 20x 15 s (total post bleach of 300 s) or 26x 15 s (total post bleach of 390 s). As mentioned, constant adjustment was requited to maintain correct position of the nuclei. For the low resolution imaging, the acquisition experiment time-points were themselves used for monitoring position.

2.4.1.4 GFP::WAPL-1 FRAP

GFP::WAPL-1 FRAP imaging required very different settings to the fluorescent cohesin subunits due to much faster recovery dynamics. The following conditions were used:

1400 Hz scanning speed, 1 times line averaging, 3 AU pinhole, 488 laser with 30% overall power and 10% imaging power, HyD detector set to 502 nm - 552nm range and 150 gain. Two bleach images were required to significantly bleach with such fast scan speed, at 100% laser sub-level power, zoom-in setting. Post-bleach imaging was made much shorter due to full rapid recovery but still carried out in two phases: 20x 0.19 s followed by 14x 4 s (total 60s). Z position adjustments were rarely required for the shorter imaging period.

2.4.1.5 FRAP analysis and curve fitting

To create a FRAP recovery curve, imaging time series files (.lif) were opened in ImageJ and mean fluorescence intensity was measured for different defined ROIs using a macro written by Keng Hng to allow adjustment of ROI position through time series. The bleached half and unbleached half of a nucleus were defined by four sided, semi-hexagons and the background was sampled by a small circle within the germline area but some distance from bleach area (Figure 40). Output means for the 3 ROIs for each time point were pasted into excel for processing. All bleached and unbleached values were first subtracted the mean background fluorescence. Then post bleach values were corrected for acquisition bleaching during post-bleach imaging by normalizing with the change in fluorescence of the unbleached half, adapted from (Phair et al. 2004). As is typical, bleached half values were simultaneously normalised as relative intensities of the pre-bleach intensity (mean of the final two pre-bleach images). These 'double normalised' bleach ROI values were then subject to a final normalisation by setting the initial post-bleach difference to 1.0, by dividing all values by the initial difference (Stenoien et al. 2001). This allows averaging of image series for any repeats and easier comparison of different transgenes/stages with varying bleach depth.

The fully normalised values were fitted with a curve in GraphPad software. If possible a two-phase exponential association curve was used as described in previous studies (Molk et al. 2004; Gerlich et al. 2006; Gause et al. 2010). Sometimes a single exponential component (one-phase association) gave a better fit to the data in which case this was used.

2.4.2 Embryo meiotic division imaging

Strains used for live imaging of embryo divisions had the H2B::mCherry transgene either in the N2 wildtype background or in the *wapl-1* homozygous background. The transgene is a bombardment insertion created by the McNally lab UC Davis (McNally et al. 2006) and

obtained from Alex Dammermann at the MFPL, Vienna. A technique was used similar to that described in the McNally et al paper and further elaborated in (Maddox and Maddox 2012). Briefly, ~24 hours post L4 hermaphrodites were dissected by cutting in the middle of the body to release embryos in a drop of isotonic embryo imaging medium on a glass slide, composed of the following. 60% v/v Leibowitz-15 media, 20 % fetal bovine serum (heat activated: 30 min at 56°C; Invitrogen), 25 mM HEPES pH 7.4, 5 mg/ml inulin (Sigma-Aldrich) (Shelton and Bowerman 1996). Coverslips with a 2% agarose pad were gently placed on top of the drop after a ring of Vaseline had been applied round the drop at a distance of ~5 mm. This prevented pressure of the coverslip damaging the fragile embryos and also sealed the medium drop from evaporation during imaging. Transmission light was used to search for correctly staged and oriented embryo while minimizing bleaching of the transgene.

Data collection was performed using a wide-field Delta Vision Deconvolution system (Applied Precision) equipped with an Olympus 1X70 microscope, softWoRx (version 3.7.1) software. Following imaging settings were used: fast acquisition, wavelength then Z, open shutter for each exposure, fast/aggressive for camera readout mode, CoolSNAP-HQ2 camera, live imaging settings on the illumination controls, mCherry option (575 nm excitation, 632 nm emission), The following general imaging settings were used: 32% light intensity, 0.1 s exposure, 60x objective, 512x512 pixel image size, 1x1 binning. Images of meiotic divisions were acquired in a series of 1mm-spaced Z-stacks (9-12 stacks) to encompass movements in 3D and follow both polar bodies and daughter chromosome movement simultaneously, with a regular time lapse of 5s intervals for total of 3–15 minutes depending on starting stage and focus. Image stacks were projected and brightness was adjusted to visualise chromosomes. Movies were then made from these time-series using SoftWoRx.

2.5 Protein methods

2.5.1 Analysis of whole-worm protein extracts by Western blot

Seventy 24 hours post-L4 worms were collected in 1X TE (10 mM Tris-HCl pH 8, 1 mM EDTA) supplied with complete protease inhibitor (Roche), washed twice with 1X TE 0.1% Triton-X and freeze-thawed three times in liquid nitrogen. Worms were then resuspended in 40 µl of 1X Laemli buffer and boiled for 10 minutes. Extracts were run on a 10% acrilamide gel and transferred on nitrocellulose for 1 hour at 4 °C, blocked for 1 hour in

5% milk TBST (1x TBS
0.1% Tween) and then incubated primary antibody, anti WAPL- 1 (1:3000, Rabbit, SDIX). The secondary antibody for the blot shown was anti-rabbit HRP-conjugated (Jackson Laboratories, 1:5000, goat). Incubation of secondary antibodies was carried out for 1 hour at room temperature in 5% milk TBST. Detection of bands was with standard ECL (Amersham) and film.

2.5.2 Germline nuclei isolation and protein fractionation from *C. elegans* cultures

Large cultures of *C. elegans* were prepared by seeding twenty 100mm NGM plates with 1 ml of OP50 bacteria (obtained from resuspending 2 liters of an overnight *E. coli* culture in a final volume of 40 ml). Between 5000 to 6000 *C. elegans* embryos were added to each 100 mm plate, and the plates were incubated at 20 °C for three days. Young adult worms were collected and transferred to 50 ml tubes by washing the plates with M9, and tubes were left on a rack for 15 minutes to allow the worms to pellet by gravity, at which time most of the M9 was removed and fresh M9 solution was added. This washing step was repeated 3 times. The final wash was performed using NP buffer (10 mM HEPES-KOH pH 7.6, 1mM EGTA, 10 mM KCl, 1.5 mM MgCl2, 0.25 mM Sucrose, add 1 mM PMSF and 1 mM DTT) containing protease inhibitors and worms were pelleted by centrifugation at 600 g for 2 minutes. 0.5 to 1 ml of this worm pellet was used to isolate nuclei. Nuclei were isolated from whole worms as described in (Haenni et al.). Briefly, worms were broken using a cooled metal Wheaton Dura-Grind dounce tissue grinder and the resulting suspension was filtered first using a 100 µm mesh, followed by a second filtration with a 40 µm mesh. The filtered solution was then centrifuged at 300 g for two minutes at 4 °C, and the supernatant from this step, which contains nuclei, was further centrifuged at 2,500 g for 10 minutes at 4 °C. The resulting supernatant was used as cytosolic fraction, while germ line nuclei were contained in the pellet. In order to separate the nuclear soluble and the DNA-bound insoluble protein fractions from these nuclei, we used a Qproteome Nuclear Protein Kit from (Qiagen) according to manufacturers instructions.

2.5.3 Immunoprecipitation of GFP::WAPL-1 and REC-8::GFP

Soluble and insoluble protein extracts from the above described method were combined for these IP experiments and total volume of IP mix was made up to 750 µl with buffer D (20mM HEPES Ph 7.9, 150 mM KCL, 20% v/v glycerol, 0.2 mM EDTA, 0.2% TRITON X-100

and supplemented with protease inhibitor cocktail (Roche, c0mplete ULTRA). 50 µl of buffer D washed GFP-TRAP beads (gta-20, Chromotek) were added to the IP mix and incubated for two and half hours at 4 °C with constant mixing. Complexes bound to the GFP-TRAP beads were harvested by centrifugation at 7,300 rpm for two minutes at 4 °C. The beads were then washed a total of 5 times, before resuspending them in 30 µl of SDS-PAGE sample buffer. Immunoprecipitated proteins were eluted by boiling the beads in the SDS-PAGE sample buffer at 95 °C for 10 minutes.

2.5.4 Mass spectrometry for IP

2.5.4.1 REC-8::GFP IP

Immunoprecipitated protein elution was run on a 10% acrylamide gel for 20 minutes (fixed 80V), and then stained overnight using colloidal Coomassie (ProtoSafe). Each gel lane was excised into 5 equal horizontal bands along the entire length of the gel lane. Gel pieces were subjected to overnight trypsin digestion at 37°C. Peptides were extracted from the gel using acetonitrile and mixtures were subsequently dried to completeness using a vacuum centrifuge. Dried peptides were resuspended in 0.1% trifluoroacetic acid (TFA) and subjected to LC-MS analysis using an Ultimate3000 nano HPLC coupled to a LTQ-Orbitrap-Velos mass spectrometer. A top 10 CID method was implemented with full MS scans acquired in the Orbitrap mass analyser. All data analysis was performed using the MaxQuant-Andromeda bioinformatics suite (Cox and Mann 2008). The data was searched against the *C. elegans* FASTA database downloaded from Wormbase. Intensity based absolute quantification was used to estimate abundance. A target-decoy approach using the reverse model was used to calculate posterior error probabilities (PEP) for protein identification. To estimate relative enrichment comparison was made to a previous mass spectrometry dataset of whole nuclear extract obtained by sonicating intact meiotic nuclei. Whole nuclei were isolated at pellet stage (2500g) with no fractionation. Mass spectrometry method was the same for the whole nuclear extract. Summed intensity values for each protein were normalised as a proportion of the total summed intensities for that sample. Fold over max between immunoprecipitation and whole nucleus samples was calculated with these normalised values for each protein. Then fold over max IP values were divided by fold over max whole nucleus values for a measure of relative fold enrichment, this output was used to sort the list. Log2 of this fold enrichment was shown in the final results table. Proteins with zero detection in the whole nucleus control and present in the immunoprecipitation were given infinite values and

assigned to the top of the list, and then ordered by raw intensity. A threshold of at least 2 peptides was set as a quality control filter.

2.5.4.2 GFP::WAPL-1 IP

For this experiment three samples were run: GFP::WAPL-1 immunoprecipitated protein, input of the immunoprecipitation (control 1) and mock immunoprecipitation with N2 worms and anti-GFP chromotek beads (control 2). As with the REC-8:GFP IP, sample was run on a 10% acrylamide gel for 20 minutes (fixed 80V), and then stained overnight using colloidal Coomassie (ProtoSafe). The gel was processed in the same way as in 2.5.4.1 and digested with trypsin and subjected to LC-MS analysis using an Ultimate3000 nano HPLC coupled to a LTQ-Orbitrap-Velos mass spectrometer. The data was searched against the *C. elegans* FASTA database downloaded from Wormbase. Best protein score was used instead of PEP as a confidence filter.

2.5.5 Phosphoproteomics

From either post-irradiation N2 or control N2 non-irradiated worms, germline enriched nuclei were obtained after douncing and initial filtration with nylon membranes followed by two centrifugation steps (as described in section 2.5.2). The supernatant from the 2500 g centrifugation was removed and nuclei pellet was used directly without fractionation extraction. Nuclei pellet was washed with ice-cold PBS buffer supplemented with phosphatase inhibitors (1 mM Na3VO4 and 1 mM NaF). The cells were then lysed and proteins denatured in 8 M urea, 20 mM HEPES (pH 8.0) supplemented with phosphatase inhibitors (1 mM Na3VO4, 1 mM NaF, 2.5 mM Na4P2O7, 1 mM ß-glycerol-phosphate). Cell lysates were further homogenized by sonication and insoluble material was removed by centrifugation at 20,000×g for 10 min. Protein concentration in the supernatants was calculated by Bradford analysis and samples containing 500 µg. Proteins were further processed for phosphoproteomic LC–MS/MS analysis following trypsin digestion, digestion clean-up using Reversed-Phase SPE (OASIS) and phosphopeptide enrichment using TiO2 affinity chromatography was performed as described by (Larsen et al. 2005).

2.6 γ-irradiation of *C. elegans*

Radiation experiments were carried out using an IBL 637 cell irradiator containing a caesium-*137* source. Irradiation for the experiments shown in this thesis was carried out directly on large NGM E. coli seeded plates with adult worms (18 hr post L4). Worms were exposed irradiation for the appropriate number of seconds to result in ~15Gys dose.

Table 3: Main solutions and buffers used

Name	Composition	Use
NGM	3 g NaCl 2.5 g Bactopeptone 20 g Agar H_20 up to 1 l 1 ml 1M $MgS0_4$ 1 ml 1M $CaCl_2$ 1 ml 1M Cholesterol (5 mg/ml in EtOH) Autoclave and add 25 ml Potassium Phosphate (1 M, pH 6.0) Dispense into 60 mm petri dishes	Growth media for *C. elegans* strains
M9	5.8 g Na_2HPO_4 3.0 g KH_2PO_4 0.5 g NaCl 1.0 g NH_4Cl dH_2O up to 1liter	Short-term preservation of *C. elegans* in liquid.
Bleaching Solution	5.5 ml H_20 2.5 ml 2M NaOH 2 ml of bleach	Cleaning of the strains of *C. elegans*
Freezing Solution	5.85 g NaCl 6.8 g KH_2PO_4 300 g Glycerol 5.6 ml 1M NaOH dH2O up to 1 l Autoclave and add 300 µl of 1 M $MgSO_4$	Cryopreservation of *C. elegans* strains
10 X PCR Lysis Buffer	100 mM Tris 500 mM KCl 15mM $MgCl_2$ pH 8.3 Add Proteinase K to 1XPCR Lysis Buffer before use to a final concentration of 1mg/ml	DNA extraction
10 X EGG Buffer	118 mM NaCl 48 mM KCl_2 2 mM $CaCl_2$ 2 mM $MgCl_2$ 5 mM HEPES pH 7.4	Immunostaining
10 X PBS	0.2 M Sodium phosphate 1.5 M NaCl pH 7.4	Immunostaining

CHAPTER 3: RESULTS

CHARACTERISATION OF MEIOSIS IN *wapl-1* MUTANTS

3.1 Objectives

The overall objective of this project was to investigate if cohesin is dynamically associated with meiotic chromosomes between S-phase and the first meiotic division. In particular, a central aim was to determine whether the factor known as WAPL (WAPL-1 in *C. elegans*) regulates cohesin binding to meiotic chromosomes, as it has been shown to do in studies of mitotic cells (Gandhi et al. 2006; Kueng et al. 2006). A central approach to address this question was to assess how loss of WAPL-1 from meiotic cells may affect the association of cohesin with chromosomes in meiotic prophase. In mitotic cells WAPL limits the amount of cohesin from chromosomes and thereby anagonizes SCC and controls chromatin morphology (Shintomi and Hirano 2009; Tedeschi et al. 2013). If WAPL does limit the association of cohesin with meiotic chromosomes, it would be expected to affect the various functions of meiotic cohesin. Outside its role in SCC, cohesin is known to be important in chromosome morphology, SC assembly, DSB repair and chromosome segregation during meiosis (Klein et al. 1999; Kitajima et al. 2003; Ding et al. 2006; Severson et al. 2009; Kim et al. 2010; McNicoll et al. 2013). Thus, my initial goal was also to determine whether loss of WAPL-1 caused any problems in the normal progression of these meiotic events.

3.2 Meiotic defects of *wapl-1(tm1814)* mutants

A direct approach to understand the role of any factor in a biological process is to functionally remove this factor, in this case a protein, from the organism or cell type/tissue. In order to investigate the role of WAPL-1, I took advantage of a deletion allele, *wapl-1(tm1814)*, generated by the National Bioresource Project (Japan), which generated a 548 bp deletion that starts 167 bp before the ATG start site of the *wapl-1* gene and is predicted to delete exons 1, 2 and part of 3 (Figure 5 A). The deletion was intially confirmed and followed by PCR. The *wapl-1(tm1814)* allele was outcrossed several times into worms of wildtype background (N2) to remove other possible mutations present in original mutant strain. Following outcrossing, the *wapl-1(tm1814)* allele was maintained

in heterozygosity by genetic balancer *nT1*, which includes a reciprocal translocation between chromosomes IV and V. In this way homozygous *wapl-1(tm1814)* mutant worms could be continually isolated from heterozygous mothers. From simple inspection, *wapl-1* (*tm1814*) homozygote worms have some noticable developmental and reproductive problems that included sick looking worms, vulva defects, locomotion problems and the production of few offspring. These defects suggested that WAPL-1 plays roles in both somatic cells and during meiosis. Despite these defects, many adult worms do develop, with slightly small but complete germlines allowing the study of meiosis in *wapl-1(tm1814)* mutants.

3.2.1 *tm1814* is a null allele of *wapl-1*

The *tm1814* allele is predicted not to express a protein product as it lacks the start site and promoter region (Figure 5 A), but it was important to demonstrate that it is a real null allele. Western blot analysis of whole worm extracts probed with α-WAPL-1 antibodies revealed a strong band at the expected molecular weight (84 KDa) in extracts prepared from wildtype worms, but not extracts made from *wapl-1* (*tm1814*) homozygous mutants (Figure 5 B). The blot also shows extracts from transgenic worms expressing GFP::WAPL-1 in the *wapl-1* (*tm1814*) homozygous background, a clear band is seen at the predicted larger molecular weight from the fused tag. This further demonstrates the specificity of the α-WAPL-1 anibodies. Ponceau staining shows that similar overall amount of protein was extracted from the 100 worms of each genotype. The adult worms used for the Western blot were 24 hours post L4 larval stage, which is the same age used for other experiments described in following sections. The *tm1814* allele therefore provides a tool to test how loss of WAPL-1 affects meiosis, hereafter referred to as the *wapl-1* mutant.

3.2.2 *wapl-1* mutants display fertility defects

The ultimate outcome of successful meiosis is the production of gametes with the correct number of chromosomes, which give rise to embryos that develop into healthy adult organisms. *C. elegans* hermaphrodites normally produce a large number of internally fertilised embryos in a very processive manner. If defects in meiosis occur, gametes often continue to be produced and fertilized, but the resultant embryos can suffer from aneuploidy, causing aberrant development and unhatched embryos (Lui and Colaiacovo 2013). Thus, the presence of developmentally arrested embryos gives a quantifiable

indication of meiotic defects. Brood size is clearly reduced in *wapl-1* mutants, ~73 laid embryos compared to ~227 in wildtype worms (Figure 6 A & B). Normally the percentage of laid embryos that are unhatched (embryonic lethality) is very low, as shown by the 0.3% in wildtype controls, whereas *wapl-1* mutant worms have a greatly increased embryo lethality of 20.8% (Figure 6 A & C). Embryonic lethality is due to aneuploidy of the autosomes, while missegregation of the X chromosomes results in a high incidence of males (HIM phenotype) among the progeny. However, the quantification shown in Figure 6 did not find an increase in male progeny among adults in *wapl-1* mutants, 0.1% males in both mutants and controls. Some preliminary counts had observed a slightly higher number of males in the *wapl-1* mutants but these may not have been detected in the final count due to them being very small and therefore regarded as larval arrested instead of adult. The fraction of laid eggs that show larval arrest can be calculated from the difference between the total laid eggs and the total dead eggs plus the adult worms. The larval lethality for this mutant is ~28%, which like embryo lethality is also known to arise from aneuploidy (Adames et al. 1998). These results suggested that WAPL-1 may play an important role in ensuring the formation of viable gametes, but some of the embryonic defects could also be due to the expected mitotic roles of WAPL-1, as specifically implied by a study of the embryonic divisions following knockdown of *wapl-1* (Stanvitch and Moore 2008).

3.2.3 *wapl-1* mutant DAPI phenotype

Visualizing chromosomes by DAPI staining of dissected germ lines shows that *wapl-1* mutants have short germ lines with reduced numbers of nuclei, especially from pachytene onwards (Figure 6 D & E). This may be due to increased apoptosis, which could reflect meiotic errors, or by problems in the mitotic divisions that precede meiosis. A consistent phenotype seen by DAPI staining is that pachytene chromosomes appear shorter, wider and spaced further apart, indicating greater condensation and possibly altered SC structure. This effect on morphology is most obvious when looking at stained nuclei by scrolling through the Z-axis on a microscope or in image series, though it can be appreciated to some extent in the projection images that show more space between the chromosomes (Figure 6 Di & Ei). This altered morphology was further demonstrated by a quantification performed by Sarah Testori from our laboratory. The total length of the SC in pachytene nuclei was measured by tracing the length of HTP-3, an axial element protein (Goodyer et al. 2008). The total axial length per nucleus was 28% shorter in the *wapl-1*

mutant: 32 µm in WT and 23 µm in *wapl-1* mutant (*t*-test – P = <0.000001). This is likely an underestimation of the difference due to some overlap caused by the projection of Z-stacks.

Diakinesis oocytes of *wapl-1* mutants always contained 6 equal sized DAPI-stained bodies: in several hundred oocytes that I observed as part of various experiments none had more than 6 bodies. This indicates that, similar to WT controls, homologous chromosomes are linked by COs in *wapl-1* mutants. Although this phenotype was not quantified, no greater than 6 bodies were observed in hundreds of diakinesis nuclei across many experiments. This suggests that both the ability to make COs and SCC are not overtly defective without WAPL-1.

3.2.4 Meiotic divisions are disrupted in *wapl-1* mutants

Despite the normal appearance of diakinesis oocytes with 6 bivalents, the fertility defects of *wapl-1* mutants (3.2.2) suggest that defects in chromosome segregation may occur during the meiotic divisions. Also, an excess of cohesin and cohesion predicted by loss of WAPL-1 would be expected to manifest as a problem during chromosome segregation (Kueng et al. 2006; Stanvitch and Moore 2008; Lopez-Serra et al. 2013). One of the best ways to assess the meiotic divisions is to observe them by live imaging using a fluorescent marker of chromosomes (Maruyama et al. 2007). An mCherry-tagged histone (H2B) transgene allows visualization of the meiotic divisions in the early embryo. In the wildtype embryos the two polar bodies generated during the meiotic divisions of the oocyte remain quite compact once extruded, and stay close to the cortex of the embryo, especially the first polar body (Figure 7 A & B) (McNally and McNally 2005). In contrast, in *wapl-1* mutant oocytes the first polar body often splits into two or more masses and appears to attempt a division of its own simultaneously with the anaphase II division (Figure 7 C & D). This phenotype was consistently observed, to a varying degree, in all embryos imaged, suggesting that inappropriate meiotic segregation patterns occur when WAPL-1 is absent. Also, the second polar body in the wildtype though it does occasionally show some movement it ultimately remains on the outside of the embryo and ends up close to the first polar body. However, in the *wapl-1* mutant background the second polar body is often highly mobile and occasionally moves back to the middle of the embryo and becomes involved in the mitotic divisions, a defect never seen in wildtype controls. Furthermore, 'wandering' chromosomes are more often seen in the mutant embryos,

whereby apparently single chromosomes temporarily jump out from one set of chromosomes towards another set. This defect is highlighted in panel of Figure 7 Ci compared to control panels Figure 7 Ai and Bi. These defects, which are rarely or never seen in the meiotic divisions of wildtype embryos, can be best appreciated in movies made from live images taken from early embryos (Movie 1 and Movie 2, on CD). These defects may in part account for the impaired fertility described in previous sections because the production of aneuploid nuclei due to the aberrant behaviour of chromosomes, including the polar bodies, could result in developmental failure. Also it is possible that dysregulation of the meiotic spindle arising from the loss of WAPL could interfere with the mitotic segregation.

3.2.5 WAPL-1 is expressed in meiotic prophase nuclei

The results shown so far indicate a role for WAPL-1 during meiosis, but it was important to determine the localization of WAPL-1 throughout meiosis, especially during meiotic prophase. It was not possible to obtain a α-WAPL-1 antibody that showed a consistent staining pattern that was completely absent in the mutant germlines. However, a GFP::WAPL-1 transgene was created that included the endogenous promoter and 3' UTR regulatory region and inserted as a single copy (MosSCI). α-GFP immunofluorescence revealed that GFP::WAPL-1 is expressed in nuclei throughout meiotic prophase, consistently peaking at late pachytene/diplotene (Figure 8 A). This logically suggests that WAPL-1 may control particular events at this stage such as chromosome remodeling (Storlazzi et al. 2003; Nabeshima et al. 2005; Bhalla et al. 2008; Martinez-Perez et al. 2008). The transgene is also highly expressed in the mitotic tip and apparently drops upon entry to meiosis; implying WAPL-1 may exert some temporal regulation during meiosis. Zoomed-in images, reveal that WAPL-1 is found as a diffuse staining that surrounds chromosomes inside the nucleus (Figure 8 B). To check whether underlying patterns of WAPL-1 on chromatin were being masked by a larger fraction of unbound diffuse protein, immunofluorescence was performed using TRITON-X detergent to further permeabilise the nuclei and wash out protein not stably bound to chromatin. Most GFP::WAPL-1 appeared to be lost from meiotic nuclei and no underlying axial patterns were seen (Figure 8 C). This suggests that any interactions that may exist with cohesin or any other chromatin proteins must be mainly transient with no significant chromatin-bound fraction. Analogous results and similar conclusions have been obtained studying WAPL in mitotic cells (Kueng et al. 2006; Chan et al. 2012).

The images shown in Figure 8 are from a strain homozygous for the GFP::WAPL-1 transgene and the *wapl-1(tm1814)* mutation. This strain displays a large rescue of the fertility defects observed in *wapl-1* mutants (Figure 6 A), and worms appear wildtype in gross morphology. Embryo lethality drops significantly from 20.8% to 4.2% though this definitely does not reach the negligible levels of the wildtype worms. The number of adult worm is higher in the transgenic strain but again does not reach the wildtype adult brood size. The incomplete rescue of the fertility defects of *wapl-1* mutants by the GFP::WAPL-1 transgene may be caused by the apparent reduced expression of GFP::WAPL-1 compared to endogenous WAPL-1 (Figure 5 B). In addition, the remaining low levels of embryonic lethality may be due to mitotic defects in the embryo. In fact, experiments described in later sections demonstrate that GFP::WAPL-1 provided WAPL-1 functionality during meiosis (see later).

An alternative explanation for the incomplete rescue of the fertility defects of *wapl-1* mutants by the GFP:WAPL-1 transgene is that the GFP tag affects the functionality of WAPL-1. Thus, we also built a strain expressing a non-tagged version of WAPL and crossed this transgene into the *wapl-1(tm1814)* mutant background. This transgene rescued the fertility defects of *wapl-1* mutants to a larger extent than the GFP::WAPL-1 transgene, but it also displayed residual levels of embryo lethality, suggesting that expression levels of the transgene are at least partially responsible for the absence of complete rescue. Some of the incomplete rescue may well also be caused by slight disruption of protein function from the GFP tag. Similar to the GFP::WAPL-1 the WAPL-1 (no tag) transgene also provides WAPL-1 function during meiosis (see later).

3.3 Effect of WAPL-1 on the level of axis-associated cohesin

The evidence presented in previous sections of this chapter strongly suggests a meiotic role for WAPL-1. The key question is whether WAPL-1 is regulating cohesin binding to chromosomes during meiosis, as it has been shown to do in mitotic cells (Kueng et al. 2006; Shintomi and Hirano 2009). The amount of cohesin associated with a chromosome is thought to affect cohesion as well as overall chromosome morphology. Cohesin removal by WAPL during late mitotic prophase facilitates loss of cohesion on chromosome arm regions at late prophase, while the opposite situation exists when WAPL is absent.

Therefore, it was vital to understand how WAPL-1 affects cohesin association with chromosomes during meiosis, and this was primarily assessed in this project by using immunofluorescence to visualize meiotic cohesin in *wapl-1* mutant and wildtype germlines. Comparison of staining patterns mainly focused on stages up till late pachytene, as from diplotene chromosome morphology becomes less uniform and more dispersed and therefore hard to quantifiably compare.

3.3.1 Effect of WAPL-1 on SMC-3 at late pachytene

As explained in the chapter 1, there are multiple cohesin complexes, differing in their kleisin subunit, present during *C. elegans* meiosis (Pasierbek et al. 2001; Severson et al. 2009; Severson and Meyer 2014). REC-8, COH-3 and COH-4 appear as meiosis-specific kleisins, while COH-1 and SCC-1, which are also expressed in somatic tissues, do not appear to play major roles during meiosis. The presence of different meiotic cohesin complexes offers multiple putative targets for WAPL-1 to enact upon. The non-kleisin subunits of cohesion are thought to be the same in mitotic and meiotic cohesin complexes, and these are SMC-1, SMC-3 and SCC-3. The SMC subunits form the core of the complex with the kleisin while evidence suggests that SCC-3, though essential for cohesion, possibly has a more supplementary function and associates with the complex slightly less robustly in both mitosis and meiosis (Nasmyth and Haering 2009; Kulemzina et al. 2012; Calvente et al. 2013). Therefore patterns of SMC subunits give the most reliable readout of broad effects, as they will be common to all cohesin complexes at all stages. α-SMC-3 staining revealed that in the *wapl-1* mutant there is an increase in the amount of cohesin associated with chromosomes compared to wildtype (Figure 9 A). This is evident from both the brightness and the definition of the axial pattern, which was most obviously affected at late pachytene. All the images are acquired and processed identically such that intensity of immunofluorescence is directly comparable and gives a measure of the amount of protein at specific locations.

Although images shown are representative there was some variation between nuclei of any stage and between germ lines within each genotype, and so a quantitative assessment was necessary. This was true for all cohesin immunofluorescence experiments. A good approximation of the amount of protein stably associated with chromosome axes is the overall average intensity of the immunofluorescence of a nucleus. This is because although intensity is averaged across the whole nuclear space, including the non-

chromosome regions, chromosome-bound protein disproportionately contributes to fluorescence intensity, while individual soluble molecules contribute little to overall signal. The mean nuclear fluorescence intensity of SMC-3 was measured in many nuclei over several germlines (Figure 9 B) and found to be significantly higher in the *wapl-1* mutant: 810 compared to 646 in the wildtype. A two-tailed *t*-test (unequal variance) showed this to be a significant with a P value of less than 0.0001. This result indicates that WAPL-1 is required in meiotic prophase to limit the amount of cohesin binding to chromosomes.

3.3.2 Effect of WAPL-1 on SMC-3 at early meiotic stages

Whole nucleus mean-fluorescence quantification was also done on nuclei from transition zone (corresponding to leptotene and zygotene stages) and early pachytene, where different meiotic events are taking place (Figure 10A). The results are represented by the bar graph in Figure 10 B, showing mean fluorescence to be still significantly greater at early pachytene of the mutant but with only a 9.2% increase compared to 25.5% at late pachytene. While at transition zone the increase in mean intensity was only 3.2% and statistically insignificant. These results indicate that WAPL-1 is affecting cohesin dynamics to varying extent at different stages of meiosis. Interestingly, this corresponds with the GFP::WAPL-1 expression pattern which peaked at late pachytene.

3.3.3 Effect of WAPL-1 on REC-8 at late pachytene

Given that my SMC-3 experiments show an overall increase of axis-associated cohesin in *wapl-1* mutants, it was important to find out whether this limiting effect of WAPL-1 on meiotic cohesin affected all cohesin complexes in the same manner. Meiotic complexes only differ by their kleisin subunit in *C. elegans* and these fit into two functional types. REC-8 is the canonical meiotic cohesin found in all organisms and provides the key cohesive roles. COH-3 and COH-4, which are closely related to each other in sequence and function, are more nematode specific with much looser sequence homologues in distant species, though multiple meiotic kleisins are also present in mouse and plants (Bai et al. 1999; Bhatt et al. 1999; Severson et al. 2009; Herran et al. 2011; Lee and Hirano 2011; Yuan et al. 2012; Ishiguro et al. 2014). Focusing on the more canonical cohesin complex first, immunofluorescence with α-REC-8 in *wapl-1* mutants shows that the there is surprisingly little overall change in chromosome association compared to wildtype

controls (Figure 11 A). Whole nuclear fluorescence intensity shown in Figure 11 B demonstrates this minimal effect of WAPL-1 upon overall REC-8 levels at late pachytene: 561 mean intensity in wildtype nuclei and 583 in *wapl-1* mutants. A *t*-test confirmed that this 3.9% increase is not quite significant, P value = 0.054.

3.3.4 Effect of WAPL-1 on REC-8 at early meiotic stages

Nuclear distribution of REC-8 is also not grossly affected by loss of WAPL-1 at earlier stages of meiosis, as is shown by the α-REC-8 staining in Figure 12 A. Whole nuclear intensity quantification of α-REC-8 confirms that the levels of REC-8 on meiotic chromosomes are not overtly affected during meiosis. This result implies that other cohesin complexes that don't contain REC-8 may be particularly affected by WAPL-1.

3.3.5 REC-8::GFP patterns agree with α-REC-8

This result is quite surprising given the changes that are seen with SMC-3. Also the quality of staining with the α-REC-8 antibody shown was not particularly clean and quality issues existed with a separate antibody showing high background. So to confirm the surprising result, REC-8 patterns were assessed using a fully functional REC-8::GFP transgene that had been generated in the lab and can allow much cleaner α-GFP immunofluorescence. The transgene, as well as a *rec-8* (*ok978*) null mutation, were crossed to the *wapl-1* background. Anti-GFP staining revealed that REC-8 binding to chromosomes does not significantly change in the presence or absence of WAPL-1. Figure 13 A and B demonstrate this finding with the REC-8::GFP transgene, which corroborates the results seen with α-REC-8 staining.

3.3.6 WAPL-1 affects COH-3 association with meiotic chromosomes at late pachytene

Going on the assumption that all cohesin complexes contain SMC subunits and a kleisin, the results seen with SMC-3 and REC-8 logically imply that cohesin containing other kleisins must be more affected by WAPL-1. COH-3 and COH-4 are the other well-described meiosis specific kleisins. Immunofluorescence with α-COH-3 antibodies revealed a dramatic increase in the amount of COH-3 on chromosomes of *wapl-1* mutant germ lines. This was immediately clear when looking through a microscope eyepiece from the overall brightness and greatly increased contrast of staining from chromosome axis to

nucleoplasmic space. The panels in Figure 14 A demonstrate this, as in the case of SMC-3 this effect appeared to be more dramatic at late pachytene. Mean nuclear fluorescence intensity of α-COH-3 was quantified in many nuclei as with SMC-3 and REC-8 and confirmed by quantification that COH-3 levels are much higher in the *wapl-1* mutant: 772 compared to 498 in the wildtype. A two-tailed *t*-test (unequal variance) showed this difference to be significant, with a P value of less than 0.0001. This is a ~55% increase in COH-3 mean nuclear intensity and clearly suggests that cohesin complexes containing COH-3 as their kleisin, and by similarity perhaps also COH-4 (see below), are highly sensitive to the destabilizing effect of WAPL-1 on meiotic chromosomes. In contrast, complexes with REC-8 as their kleisin are largely insensitive to WAPL-1. Interestingly, visually and quantitatively the increase seen with the SMC-3 staining is an intermediate between COH-3 and REC-8 responses. This fits with the model that SMC subunits are common to all cohesin complexes with different kleisin subunits defining distinct meiotic functions.

3.3.7 α-COH-3/4 antibody resolves α-COH-3 specific issues

Though the α-COH-3 antibody used for the experiment just described demonstrates a clear increase of COH-3 staining in *wapl-1* mutants, the use of this antibody has some technical difficulties. Firstly, the antibody generally has a weak staining that results in high background levels and some discontinuous staining on axial elements. Also, the staining usually disappears at diplotene in both wildtype and mutant. However, visualization of COH-3 expressed from a functional COH-3::mCherry transgene reveals continuous axis staining and persistence of COH-3 until diakinesis. On the other hand, this COH-3 transgene displays big variations in expression between different worms, especially in the *wapl-1* mutant background, which made it impractical for quantitative measurements. To address these issues, another anti-COH-3 antibody was tested that showed significantly improved staining quality, and whose signal persisted in diakinesis oocytes. In addition, this COH-3 antibody also appears to recognize some epitopes on the COH-4 protein, since some axial staining is observed in the *coh-3* mutant that is lost in the *coh-3; coh-4* double mutant (see Figure 15). Referred to hereafter as α-COH-3/4, this provides both an improved quality of staining and a quantitative tool to assess the levels of COH-3 and COH-4 simultaneously.

3.3.8 α-COH-3/4 displays increased chromsome levels in *wapl-1* mutant

Immunofluorescence with the α-COH-3/4 shows a large increase in the levels of axis associated COH-3/4 in *wapl-1* mutants compared to wildtype controls (see Figure 16 A). The tracks are brighter and much better defined in the absence of WAPL-1, especially at late pachytene. Quantification of whole nuclear fluorescence intensity again confirms this significant increase: an average of 841 in the mutant and 584 in the wildtype nuclei. A two-tailed *t*-test (unequal variance) showed this to be a significant with a P value of less than 0.0001. This ~45% increase supports the conclusion that different cohesin complexes have very different sensitivity to WAPL-1 depending on their kleisin subunit.

Observation of whole mounted *wapl-1* mutant germ lines stained with the α-COH-3/4 antibodies suggested that the increase in COH-3/4 staining is more pronounced in late pachytene, as it was the case for SMC-3. However, whole nucleus intensity quantification finds there to be a similar increase in both transition zone and early pachytene nuclei in the *wapl-1* mutant: 42% and 43% increases respectively both of which are highly significant with *t*-test P values of >0.0001 (Figure 17). This discrepancy with the qualitative impression may be due the slightly crude nature of the quantification, in that it averages all nuclear staining including non-chromosome regions.

3.3.9 α-COH-3/4 and α-REC-8 double staining in *wapl-1* mutants

The changes in chromosome association of the different kleisins appear quite convincing given that the quantification was performed on many nuclei of several germlines and from multiple slides within each genotype to account for variations that often occur in the immunofluorescence process. However, a good way to also demonstrate the different effects of WAPL-1 on the different cohesin complexes is to simultaneously stain germlines with both α-COH-3/4 and
α-REC-8. This double immunofluorescence shown in Figure 18 confirmed that when COH-3/4 levels are strongly increased on chromosomes, in the same nuclei REC-8 levels are not overtly affected.

3.3.10 Mean nuclear intensity of different cohesin subunits

Figure 19 combines the results of the immunofluorescence whole-nucleus quantification for REC-8, COH-3/4 and SMC-3 for just late pachytene data. Also, shown above the corresponding columns is a zoom-in of representative nuclei. This highlights the different sensitivity to WAPL-1 displayed by the different kleisins. Late pachytene is of particular focus due to the fact that this is the place of highest WAPL-1 expression, and also because this stage is easily identifiable within the *C. elegans* germ line. In addition, it is most interesting to know the effect of WAPL-1 on cohesin, and potentially SCC, near the later stages of meiotic prophase because this when dictyate arrest occurs in human oocytes.

The graph in Figure 20 combines the mean fluorescence data from all three stages analysed for REC-8, COH-3/4 and SMC-3. The consistently higher levels of COH-3/4 in *wapl-1* mutants contrast with the consistently unchanged levels of REC-8. It is interesting to note that for wildtype nuclei there is a small drop seen in the mean intensity from the transition zone to pachytene for both REC-8 and SMC-3 but not for COH-3/4. Smaller nuclear volume at transition zone may explain the higher mean fluorescence for REC-8 and SMC-3. While the later expression and loading pattern normally observed for COH-3/4 likely accounts for the lower intensity for this subunit at earlier stages.

3.3.11 WAPL-1 transgenes restore normal COH-3/4 chromosome levels in *wapl-1* mutant background

The clear increase in chromosome bound COH-3/4 in *wapl-1* mutant provides a tool to test the meiotic specific function of the WAPL-1 transgenes. Therefore, α-COH-3/4 immunofluorescence was carried out on the strains with GFP::WAPL-1 and WAPL-1[no-tag] transgenes in the *wapl-1* mutant background. Wildtype and *wapl-1* mutant germ lines were also stained in the same experiment for control comparisons (same dataset as Figure 16 & 17). The panels in Figure 21 demonstrate that amount of COH-3/4 on late pachytene chromosomes of both transgenic strains are restored to levels much closer to wildtype than the *wapl-1* mutant. Insufficient germ lines were obtained for reliable whole nucleus mean quantification, but pilot analysis shows mean intensity to be closer to wildtype than the mutant. This result not only shows the meiotic functionality of the transgenes, but also supports the conclusion that the phenotypes observed in *wapl-1* mutants are indeed due to lost functions from absence of the WAPL-1 protein.

It is noticeable that germ lines from the GFP::WAPL-1; *wapl-1* strain have marginally brighter and more defined axial COH-3/4 staining than both the wildtype and WAPL-1[no-tag] phenotypes. This may be accounted for by reduced expression of the GFP::WAPL-1 (Figure 5 B) and/or partial interference of the tag on the protein function.

3.4 Measurement of axis-bound versus nucleoplasmic cohesin

The quantification of whole-nucleus cohesin levels seems to give a fairly good indication of the amount of cohesin associated with axial elements, since this bound fraction disproportionally contributes to the overall fluorescence intensity compared to the nucleoplasmic fraction. However, the values from the quantification do not represent the impressive extent to which WAPL-1 appears to affect cohesin distribution. In order to represent this in a quantitative way a line profile/line plot feature was employed. For this measurement, initially a line is drawn at will through an immunofluorescence image, in this case transecting several axial elements in a single nucleus projection, and a profile is given with the precise individual pixel intenisty values along that line (see Figure 22 A & B). As with the whole nucleus quantification, this was done on non-deconvolved images because deconvolution algorithms distorts the inensity values making them not proportional to raw intensity, and so incomparable quantitatively. The values are plotted to give a graph lineplot showing peak staining at chromosome axes and troughs at non-chromatin regions. The difference between peak and trough intensies (ΔF) is a measure of the balance between chromosome associated and nucleoplasmic protein (see Figure 22, 23 and 24 parts A & B), which WAPL-1 is known to regulate in mitosis (Kueng et al. 2006; Gause et al. 2010; Tedeschi et al. 2013). The line profile analysis was performed on the same image datasets used for the whole nucleus quantification.

3.4.1 SMC-3 line profile analysis

Line profile fluorescence intensity ranges of α-SMC-3 staining in late pachytene nuclei of wildtype and *wapl-1* mutants are displayed in the scatterplot in Figure 22 C. This demonstrates that there is a strong increase in the SMC-3 values in the mutant with an average difference of 290 compared to 183 in wildtype nuclei. A *t*-test shows this to be highly significant, P = < 0.0001. This is a ~59% increase; roughly double the increase seen with the whole-nucleus mean intensity quantification. The line profile offers a better

quantitative representation of the increase in axis-associated cohesin in *wapl-1* mutants. As can be seen from the example nucleus in Figure 22 A, the α-SMC-3 peak (green profile) corresponds well with the position of a DAPI peak (blue profile) supporting the conclusion that the cohesin staining peak is actually at the chromosome axis. This result strongly suggests that WAPL-1 is controlling the stable association of a significant fraction of cohesin complexes in meiosis.

3.4.2 REC-8 line profile analysis

Line profile fluorescence intensity ranges of α-REC-8 staining in late pachytene nuclei of wildtype and *wapl-1* mutants are displayed in the scatterplot in Figure 23 C. This shows a much smaller increase fluorescence difference in the mutant compared to the α-SMC-3 staining with an average ΔF of 185 and 147 in the wildtype nuclei. A *t*-test does show this to be significant, unlike the case with the whole nucleus quantification, with a P value of 0.0008. This ~27% increase in the mutant from the wildtype is considerably more than the 3.9% increase seen with the whole nucleus REC-8 quantification. One may conclude that there may actually be some effect upon REC-8 association with chromosomes when WAPL-1 is absent that is not apparent from qualitative inspection. Or alternatively, increased chromosome compaction in the *wapl-1* mutant simply concentrate the fluorescence that is loaded resulting in higher peak values even if overall amount loaded is unchanged. Either way the increase in axial intensity is far less for the REC-8 than for COH-3/4 confirming the more limited sensitivity of REC-8 to WAPL-1 (see Figure 25).

3.4.3 COH-3/4 line profile analysis

Line profile fluorescence intensity ranges of α-COH-3/4 staining in late pachytene nuclei of wildtype and *wapl-1* mutants are displayed in the scatterplot in Figure 24 C. This shows a dramatic increase in fluorescence difference in *wapl-1* mutants, with an average ΔF of 395 compared to 184 in wildtype nuclei. A t-test shows this to be very significant with a P value of much less than 0.0001. This is a ~114% increase in the mutant and more than double the increase seen with the whole nucleus COH-3/4 quantification (44%). Interestingly the COH-3/4 ΔF increase in the mutant is close to double the SMC-3 increase (114/59 = 1.9) and the SMC-3 increase is close to double that with REC-8 (59/27 = 2.2). This intermediate response with the SMC-3 to loss of WAPL-1 again implies that SMC-3 molecules may fall into two major populations: some forming complexes with COH-3/4

and others in a complex with REC-8. This pattern is demonstrated in Figure 25 by combining line profile results for all three subunits, with a similar but more exaggerated overall pattern to the whole nucleus quantification (Figure 19).

3.5 WAPL-1 affects chromosome remodeling during diplotene

During diplotene, as the SC is disassembled, meiotic chromosomes are structurally remodeled. At this stage chiasmata, the physical linkages provided by inter-homologue CO events and SCC, become visible, and chromosome condensation is also evident. Moreover, the position of the CO event is key in the remodeling process, as SC central region components are retained in the interval between the CO and the closest telomere, while axial elements components HTP-1/2 are specifically removed from that interval (Nabeshima et al. 2005; Martinez-Perez et al. 2008; Qiao et al. 2012). Cytological evidence also suggests that cohesion association with chromosomes changes during this stage, as the amount of nucleoplasmic cohesin seems to be increased while chromosome-associated cohesion levels appear to be reduced (Eijpe et al. 2003; Bhalla et al. 2008; Herran et al. 2011). This is seen as a greater immunofluorescence 'haze' throughout the nucleus, while chromosome axial staining becomes weaker and less defined, which is particularly evident with the SMC subunits (Figure 26). It would be predicted that such changes in dynamics might be regulated by WAPL-1, given its known role in regulating the association of cohesin with chromosomes in condensing mitotic chromosomes.

3.5.1 Staining patterns of cohesin during diplotene in *wapl-1* mutant

It was readily observed in the germ lines used for cohesin immunofluorescence quantification experiments (see section 3.3 & 3.4) that *wapl-1* mutants have an altered phenotype in diplotene nuclei. The nucleoplasmic 'haze' of cohesin staining seen in wildtype diplotene nuclei is considerably reduced in *wapl-1* germ lines, while cohesin staining at axial elements remains more defined (see Figure 26). This effect is most clear with SMC-3, despite the fact that COH-3/4 seems to be more strongly affected at late pachytene, as demonstrated in sections 3.3 and 3.4. α-SMC-1 immunofluorescence shows a similar effect in diplotene nuclei of *wapl-1* mutants, with reduced nucleoplasmic haze and more defined chromosome staining (see Figure 27 A). Limited availability of the α-SMC-1 antibody prevented the use for the pachytene quantification experiments but general staining patterns at pachytene also replicate those seen with α-SMC-3.

Although the α-COH-3/4 staining does not exhibit the strong reduction in the nucleoplasmic haze seen for the SMC subunits in diplotene nuclei of *wapl-1* mutants, the definition of axial staining is increased compared to wildtype. The axial rod-like pattern of pachytene persists for longer into diplotene in the *wapl-1* mutant compared to the wildtype, where it usually appears more dispersed. To highlight this difference deconvovled images with adjusted contrast are shown to focus on the chromosome staining only (see Figure 27 B). This apparent delay in the remodeling process in the absence of WAPL-1 is also observed from the overall morphology of the chromatin as shown by DAPI staining. Chromosomes appear less compacted and more elongated in the *wapl-1* mutant. Both nuclei shown in Figure 27 B are from early diplotene stage at the point just before nuclei first spread out into single file progressing down the germ line (see arrows marked (C) and (D) in Figure 28). REC-8 staining does not show clear changes in diplotene nuclei of *wapl-1* mutants, however a slight persistence of axial formation is observed. These observations suggest that WAPL-1 is required for correct chromosomes remodeling during diplotene.

3.5.2 SYP-1 and HTP-1 remodeling during diplotene

As mentioned above, SC and axial element components undergo striking changes in localisation during diplotene. In *C. elegans,* the central element protein SYP-1 (MacQueen et al. 2002) is removed from the chromosomal interval between the CO and the furthest telomere, while the axial element components HTP-1/2 acquire a reciprocal staining pattern to SYP-1, being lost from the interval between the CO and the closest telomere (Martinez-Perez et al. 2008). Therefore these proteins provide markers to assess the progression of chromosome remodeling. Immunofluorescence with α-HTP-1/2 and α-SYP-1 antibodies found that these proteins display a reciprocal staining pattern in diplotene nuclei of *wapl-1* mutants, with minimal overlap of the two channels (see Figure 28 & 29). However, while the chromosomal region containing SYP-1 staining rapidly becomes condensed to a short stretch in wildtype diplotene nuclei (Figure 29 Ai & Aii), SYP-1 persists in long chromosomal tracks in diplotene nuclei of *wapl-1* mutants (Figure 29 Bi & Bii). By late diplotene/early diakinesis the region containing SYP-1 eventually becomes well condensed in *wapl-1* mutants, as in the WT (Figure 29 Aiii & Biii). Condensation of α-HTP-1 staining is also somewhat delayed in the *wapl-1* mutant, but the

effect is less obvious because a significant degree of elongation in the staining is retained, unlike the SYP-1. Such delays in the remodeling events in the *wapl-1* mutants correlate well with the altered cohesin dynamics that I observed at this stage. It is likely that WAPL-1 affects the remodeling of SYP-1 and HTP-1/2 indirectly, through altered cohesin dynamics, although a direct effect of WAPL-1 on SC components cannot be ruled out.

3.5.3 Structure of diakinesis bivalents

Although the overall appearance of diakinesis bivalents in *wapl-1* mutants is similar to that seen in wildtype controls (see Figure 6 Dii & 5 Eii), this does not rule out defects in the internal structure and distribution of cohesin in these bivalents. Unfortunately the immunofluorescence of cohesion subunits does not work very effectively or reliably in diakinesis oocytes, which makes it difficult to perform quantitative measurements of cohesin staining. However, as described in the whole nucleus quantification, a functional and stably expressed REC-8::GFP transgene was crossed into the *wapl-1* mutant background. Immunofluorescence with α-GFP in this strain was much cleaner at diakinesis than for the α-REC-8 for endogenous REC-8. No obvious increase in overall REC-8 intensity was observed in *wapl-1* diakinesis bivalents, but some irregularities seem to be more common with fewer typical cruciform shaped bivalents.
Transgenes for other cohesin subunits were either not made yet, not successfully crossed to the *wapl-1* background or had expression problems during immunofluorescence experiments. Future experiments with alternative methods of transgenic tagging will hopefully reveal how WAPL-1 affects the distribution the different cohesin subunits and bivalent structure in diakinesis bivalents.

3.6 Meiotic DSB repair in *wapl-1* mutants

One of the key roles of cohesin outside SCC is in the effective response and repair of DSBs. In mitosis cohesin's association with chromatin and its function are affected in response to DSBs. After DSB formation during G2/M extra cohesin is reloaded to chromatin, reinforcing cohesion (Strom et al. 2004; Unal et al. 2004; Strom and Sjogren 2005). The loading factors SCC2/SCC4 are required for this process (Unal et al. 2007) and cohesion reinforcement requires various PTMs that appear to oppose the releasing activity of WAPL (Heidinger-Pauli et al. 2008; Heidinger-Pauli et al. 2009; McAleenan et al. 2012). Presence of cohesin in meiosis seems to be essential for recombination and CO formation

(Klein et al. 1999; Pasierbek et al. 2001; Xu et al. 2005; Llano et al.). However, how meiotic cohesin is regulated to facilitate repair and respond to meiotic DSBs remains largely unknown. It was shown in our lab that the overall loading of cohesin by SCC-2 is required to repair DSBs and make COs. PDS5 has also been implicated in proper repair of breaks in meiosis, though how PDS5 might be affecting cohesin exactly is not clear (Storlazzi et al. 2003; Jin et al. 2009). Given the role of WAPL-1 demonstrated so far in limiting the association of cohesin with meiotic chromosomes, it seemed possible that WAPL-1 may function in the local loss of cohesion and removal of cohesin around CO sites (section 1.3.7.3).

3.6.1 RAD-51 foci in *wapl-1* mutants

An important step in meiotic DSBs processing is the binding of RAD-51 to single stranded DNA revealed by resection (Bishop 1994). RAD-51 and other factors allow these single strands to invade the homologous chromosome and initiate homologous repair. At certain stages of meiosis this binding of RAD-51 can be seen as distinct staining foci. When DSB repair progresses into the formation of COs or NCOs single stranded DNA is no longer exposed and RAD-51 foci disappear. Thus, foci of RAD-51 that mark early repair intermediates are a good measure of the progression of DSB repair during meiosis. So to determine how WAPL-1 might affect meiotic DSB repair, wildtype and *wapl-1* mutant germlines were stained with α-RAD-51 antibodies. In wildtype nuclei, numbers of RAD-51 foci peak at early pachytene and gradually decrease so by the end of pachytene few foci remain indicating most breaks are repaired (Alpi et al. 2003). Similar patterns were seen in the wildtype control germ lines (Figure 30). In *wapl-1* mutant germlines, the number of foci per nucleus not only appears somewhat higher than the wildtype at early pachytene (Figure 30 C), but this peak number of foci is more prolonged into mid pachytene (Figure 30 D). By late pachytene the number of RAD-51 foci do appear to drop back levels more similar to wildtype controls (Figure 30 E). A full quantification of this phenotype has been carried out by Sarah Testori from our lab, which confirms that there are significantly greater numbers and more prolonged RAD-51 recombination intermediates in the *wapl-1* mutant. This suggests that in absence of WAPL-1 increased stability or rather reduced dynamics of cohesin on meiotic chromosomes interferes with the appropriate and timely repair of DSBs.

3.6.2 ZHP-3 foci in *wapl-1* mutants

To further investigate how DSB repair is affected by loss of WAPL-1, ZHP-3 foci, which mark CO-fated recombination events, were assessed. ZHP-3 is one of the ZMM group of proteins that collectively contribute to the formation of mature COs from the earlier recombination intermediates. ZHP-3 decorates axial elements during early pachytene, but becomes restricted to single focus per homologue pair by the very end of pachytene and into diplotene, usually with 6 foci per nucleus marking the single CO per homologous pair that occurs in *C. elegans*. The best way to clearly visualize the ZHP-3 protein is using a ZHP-3::GFP transgene, which was crossed onto the *wapl-1* mutant background. α-GFP immunofluorescence shows that although the axial tracks of ZHP-3 may persist slightly longer in *wapl-1* mutants, 6 clear foci invariably appear (Figure 31 A). Quantification of over one hundred nuclei from several germ lines demonstrates that there is no difference in the number of ZHP-3 foci at diplotene in the absence of WAPL-1. This indicates that CO number, at least in the ZMM pathway, is not regulated by WAPL-1 and increased association of COH-3/4 on chromosomes does not seem to affect CO interference or assurance.

3.6.3 CO position mapping

Although total number of COs does not appear to be altered by loss of WAPL-1 the position of COs may be affected. CO positioning follows a distinctive statistical pattern along chromosomes that is not random or proportional to physical distance (section 1.2.5). In *C. elegans* CO frequencies are higher in the end portions of chromosomes, while central regions display lower frequencies, giving a U-shape to a mapping frequency distribution (Barnes et al. 1995; Rockman and Kruglyak 2009). The exact reason for this distribution is not certain however it is possible that chromosome architecture and SC structure may determine this distribution landscape. Therefore, the altered chromosome structure in *wapl-1* mutants, shown in previous sections, could influence CO distribution. Furthermore not all COs are marked by ZHP-3 foci and so a comprehensive mapping would reveal any such additional hidden COs. To test this a combination of genetic crosses and SNP detection using Taqman qPCR technology was used.

3.6.3.1 Genetic set-up of CO mapping

To map COs a Hawaiian strain of *C. elegans* is used because it has a large number of SNPs spread throughout all chromosomes that are not found in the N2 background (Hillers and Villeneuve 2003; Lim et al. 2008). For this mapping experiment, worms carrying one chromosome within a particular homologous pair with all Hawaiian SNP variants and the other chromosome within the pair with all N2 SNPs were created (Figure 32 A; F3 hermaphrodites). Simultaneously, to test the effect of a particular mutation, such as *wapl-1*, the worm must also be homozygous for the desired mutation. In order to set this up, the *wapl-1* mutation had to be out-crossed to the Hawaiian background until a chosen chromosome had become homozygous for Hawaiian SNPs; in this case chromosome II.

Heterozygous *wapl-1* males with WT background had to be crossed to the homozygous Hawaiian chromosome II plus homozygous *wapl-1* strain (Figure 32 A; F1) because *wapl-1* mutant males have very low mating success. As a result only 50% of the progeny from the F1 cross were homozygous for *wapl-1,* but all had a Hawaiian and WT version or chromosome II. The progeny from the correct ~50% of crosses were crossed to Hawaiian males so that any recombined informative chromosomes from the F2 hermaphrodites would become isolated from the further recombination events, which could mask the CO position. Individual F3 hermaphrodites were picked to individual plates and reproduced to starvation. The DNA extracted from such whole plates is representative of the SNP identity of the individual parent worm due to genetic randomness on a population level. The equivalent experiment was carried out in the wildtype background as a control (Figure 32).

3.6.3.2 Mapping distribution

The position of COs was mapped to particular intervals using Taqman qPCR probes for five particular SNPs spaced by roughly even physical distance across chromosome II (green bars, Figure 32 C) but uneven genetic distance (red bars, Figure 32 C). The genetic position of these SNPs is given in Figure 32 B legend. The position of a CO is identified by the change in genotype between two SNPs from homozygous Hawaiian (all red, 32 A) to heterozygous N2/Hawaiian (blue/red, 32 A). The results of the CO mapping in the *wapl-1* mutant and wildtype background are shown in the frequency distribution graph in Figure 32 B. There appears to be a change in overall distribution in the *wapl-1* mutant with a reduction in the COs from the two intervals at the end of the chromosome and an increase

in COs at the middle two intervals. This coordinated change in the pattern would imply a genuine affect from the absence of WAPL-1 on CO distribution. However, Chi-squared tests demonstrate that the differences in CO frequency are only significant to P value of <0.05 at interval C. It is therefore hard to conclude whether WAPL-1 really does affect overall CO distribution. The lack of statistical significance at other intervals is partly due to the relatively few number of plates/chromosomes that could be included in the final dataset, which was due to imperfect mating efficiency, meaning that some F2 hermaphrodites were not true cross progeny from the F1 cross. To determine this, all F3 plates were recorded for their mother plate from the F2 cross and if none of the offspring for a particular mother plate showed even a single N2 SNP then that group were not usable as they were unlikely to derive from true cross progeny in the F1 cross. This quality control filtered out a significant number of mapped samples from being used in the frequency distribution: 77 out of 156 analysed.

Furthermore there appears to be a possible issue with the N2 control data because some frequencies differ from the expected frequency distributions calculated from the genetic intervals in the reference map on Wormbase (Figure 32 C, red bars). This is most notable with interval A where the expected frequency is 0.097 while the control data gave 0.188, almost double. Due to the possibility of the control data being faulty, Chi-squared tests were also performed comparing *wapl-1* mutant frequencies and expected CO frequencies for that sample size calculated from genetic intervals (Figure 32 C, red bars). Despite the small increase in the value at interval C, this remains the only interval showing a significant difference to the *wapl-1* dataset.

The relative physical distance between marker SNPs in base pairs is also included, represented by the green bars. It is interesting to note that the two intervals with large discrepancies between the expected frequency and physical distance ratio (red versus green) are the same intervals in which the *wapl-1* mutant shows greater deviation from the expected (blue versus red). Further experiments with larger numbers and also assessing CO distribution on other chromosomes would be needed to confirm if this trend is real.

A final result to note from the CO mapping is that not a single double CO was observed in *wapl-1* mutant samples, suggesting that interference is not obviously disrupted by loss of WAPL-1 and in agreement with the ZHP-3 foci quantification.

3.7 Summary of results

The most important finding to be demonstrated in this chapter is that WAPL-1 controls the association of certain cohesin complexes with chromosomes during meiotic prophase. In the absence of WAPL-1 a much greater amount of COH-3/4 is localized to chromosomes, whereas cohesin complexes containing REC-8 are much less sensitive to WAPL-1. SMC-3 consistently shows an intermediate response to loss of WAPL-1, implying that both COH-3/4 and REC-8 loaded on chromosomes are within the context of the cohesin complex. In somatic cells, WAPL limits the stable association of cohesin with chromatin (Shintomi and Hirano 2009) and this work for the first time demonstrates an analogous role for WAPL in meiosis. The different sensitivity of different cohesin complexes depending on their kleisin subunit was less expected and may highlight an important functional divergence in these meiotic kleisins.

Also, results presented in this chapter confirm that WAPL-1 is expressed during meiosis, as previous studies indicated (Kuroda et al. 2005; Zhang et al. 2008a), and that loss of WAPL-1 causes various defects during meiosis. WAPL-1 is required for normal fertility levels, and absence of WAPL-1 results in errors in the meiotic divisions of oocytes. Another key meiotic event disrupted by loss of WAPL-1 is DSB repair, as demonstrated by the accumulation of RAD-51 repair intermediates.. Furthermore, chromosome remodeling at diplotene is delayed and chromosome/SC morphology appears more condensed in *wapl-1* mutants. Together these results support the conclusion that WAPL-1 is an important factor in regulating meiotic chromosome structure and function, likely by controlling the association of COH-3/4 cohesin complexes with chromosomes. See Table 4 for a summary of the key findings on the effect of WAPL-1 on the various meiotic factors described in chapter 3.

Table 4: Summary of proteins/factors investigated in the *wapl-1* mutant

Protein	Function/ Location	Phenotype when absent	Effect of *wapl-1* mutation on protein
SMC-3	Cohesin subunit in all complexes, mitosis also. Found in chromosome axis throughout meiosis	Loss of SCC, homologue pairing, COs and delayed DSB repair	Increased association with chromosome axis (↑SCC). Reduced nucleoplasmic protein, especially at diplotene
REC-8	Conserved meiotic kleisin subunit of cohesin. Loaded before entry to meiosis. Important for SCC	Loss of COs, minimal SCC, delayed DSB repair	Chromosome association not overtly altered, (effect on SCC uncertain but never compromised when REC-8 present)
COH-3	Nematode only meiotic kleisin subunit of cohesin. Loaded after entry to meiosis. Important for synapsis and DNA repair not for SCC	When COH-4 also absent = loss of COs, failure of synapsis and delayed DSB repair. SCC not affected.	Dramatic increase in association of COH-3/4 with chromosome axis (↑SCC). Reduced nucleoplasmic protein throughout meiosis
SYP-1	Conserved central element component of the SC. Loads in early meiosis upon synapsis, lost from long arm in diplotene	Lack of synapsis, stable pairing and COs. Excess DSBs & delayed repair.	Loads to SC as in WT but delayed remodeling at diplotene
HTP-1	Axial element component of HORMA domain family. Loads in early meiosis, lost from short arm in diplotene	Non-homologous synapsis, excess DSBs and delayed repair. Lack of COs.	Loads to SC as in WT, possibly increased levels associated with chromosomes
RAD-51	DNA repair factor that decorates exposed single stranded DNA at DSB sites. Foci on chromosomes, peaking at early pachytene	Homologous repair defective, fragments and masses at diakinesis	Increased numbers of foci per nucleus that persist later
ZHP-3	Recombination factor needed for COs, member or the ZMM network. Forms foci at CO sites	Lack of COs	No obvious effect. 6 foci per nucleus, as in WT
H2B (Histone)	Core histone, marks all DNA. Polar bodies are condensed and remain on cortex at meiotic divisions	*(not relevant)*	Polar bodies dispersed and appear to attempt own divisions. PB2 sometimes moves into

Figure 5. *tm1814* is a null allele of *wapl-1*

A. Diagram showing the predicted structure of the *C. elegans wapl-1* gene. Exons are shown as green blocks and introns as black lines. Horizontal distance is proportional to sequence length in base pairs. The deletion allele *tm1814* is depicted by the lower blue block.

B. Western blot of whole worm extracts made from 100 worms per genotype. Lane 1 marker, lane 2 wildtype, lane 3 *wapl-1* (*tm1814*) mutant and lane 4 GFP::WAPL-1 homozygous transgene in *wapl-1* mutant background. α-WAPL-1 antibody raised to the N-terminus peptide sequence gives a strong band at expected size (~84 kDa) in WT extract but not *wapl-1* mutant extract. α-WAPL-1 recognises GFP::WAPL-1 transgene, seen by the higher band at the combined predicted size (~120 kDa). Ponceau staining of the same blot shows similar total protein loading (lower window Ponceau staining has been digitally compressed on the vertical scale).

A

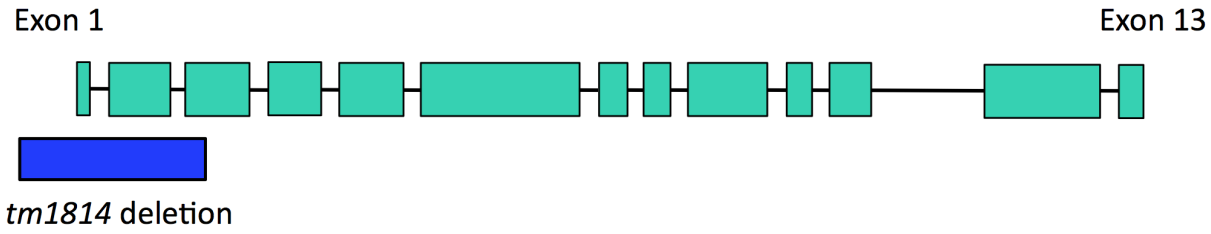
Exon 1
Exon 13
tm1814 deletion

B

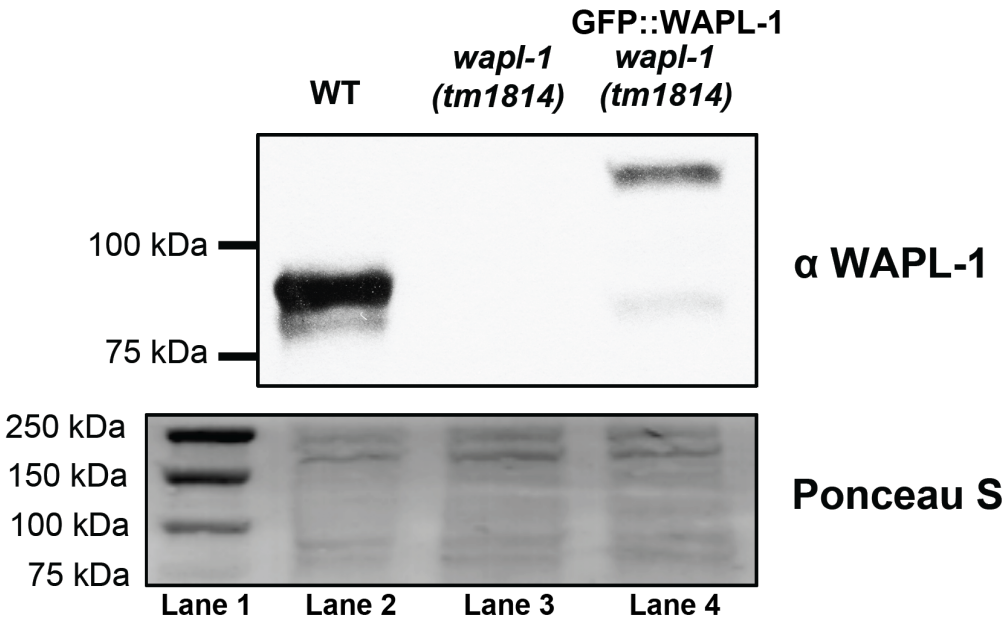
WT
wapl-1 (tm1814)
GFP::WAPL-1 wapl-1 (tm1814)
100 kDa
75 kDa
α WAPL-1
250 kDa
150 kDa
100 kDa
75 kDa
Ponceau S
Lane 1
Lane 2
Lane 3
Lane 4

Figure 6 . *wapl-1* mutant egg count and DAPI phenotype

A. Table of egg counts for wildtype (WT) *wapl-1* mutant and GFP::WAPL-1 transgene in the *wapl-1* mutant background. Total fertility quantified in multiple individual worms (number of repeats = n). First row = sum total. Other rows = mean values.

B. Bar graph representing average number of adult offspring per worm in WT and *wapl-1* mutant (See table, A). Error bars = standard deviation.

C. Bar graph representing average percentage of unhatched embryos laid per worm in WT and *wapl-1* mutant (See table, A).

D. Deconvolved projections showing a whole WT germ line stained with DAPI. (Di) Late pachytene panel. (Dii) Diakinesis oocyte example.

E. Deconvolved projections showing a whole *wapl-1* germ line stained with DAPI . Note the spacing out of nuclei at diplotene occurs earlier in the mutant and the number of diakinesis nuclei is ~5 in the mutant compared to ~10 in the more curved wildtype example. (Ei) Late pachytene panel. (Eii) Diakinesis oocyte example.

N.B. Egg count experiment (A, B, C) performed by Nuria Ferrandiz-Diaz

A

	WT	*wapl-1*	GFP::WAPL-1
Total embryos laid	1137 (n = 5)	1427 (n = 10)	1558 (n = 10)
Mean adult brood size	227.4	73.4	147.3
Embryo lethality	0.3%	20.8%	4.2%
Male incidence	0.1%	0.1%	0.1%

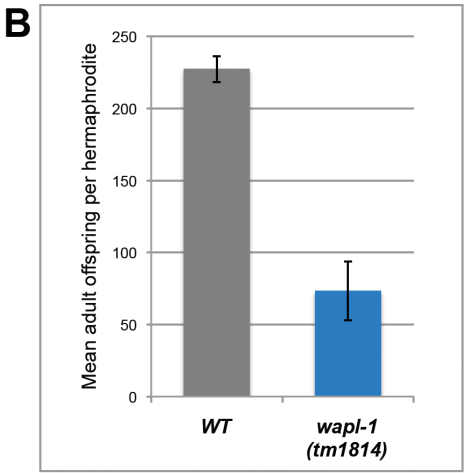

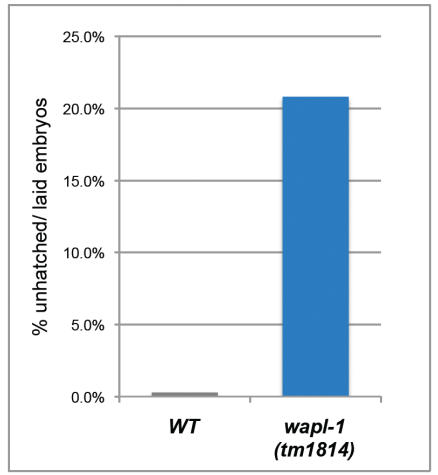

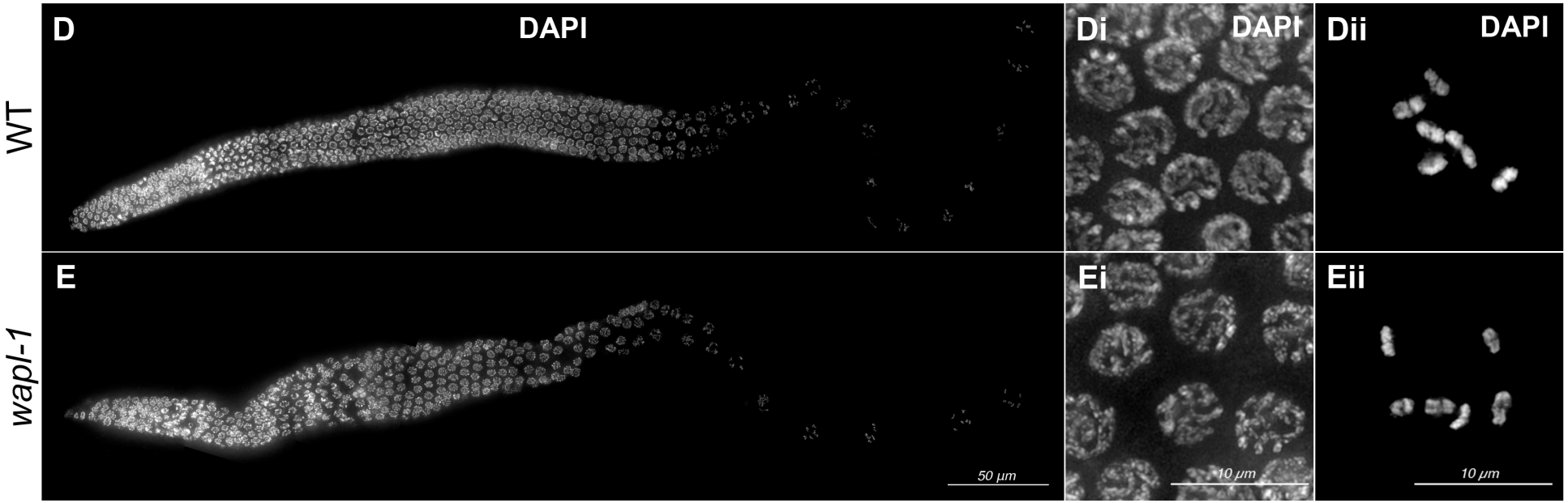

Figure 7. Live imaging of meiotic divisions reveals defects in *wapl-1* mutants

Still images form live imaging of embro divisions, using fluorescently tagged histone (H2B::mCherry) in wildtype and *wapl-1* mutant. Movies from image sequences are included (Movie 1, Movie 2)

A. Wildtype example 1. (Ai) Chromosomes closely grouped at metaphase II. (Aii) Compact polar body 1 (PB, white arrow) at anaphase II (pink arrows = segregation movement). (Biii) both polar bodies remaining on the edge of the embryo (PB1 and PB2) as pro-nuclei migrate.

B. Wildtype example 2. (Bi) Chromosomes closely grouped at metaphase II. (Bii) Compact polar body 1 (white arrow) at anaphase II (pink arrows = segregation movement). (Biii) both polar bodies remaining on the edge of the embryo and compact (PB1 and PB2) as pro-nuclei fuse. (Biv) Polar bodies remain on edge of embryo and compact at first mitotic anaphase (pink arrows = segregating chromosome movement)

C. *wapl-1* example 1. (Ci) Wandering chromosome (red arrow) at metaphase II. Note the abnormal morphology of polar body 1 (left of arrow).(Cii) Polar body 1 in two clumps (white arrow) at anaphase II (pink arrows = segregation movement). (Ciii) Polar body 1 still as two parts and polar body 2 (PB2) moving towards the mid embryo.

D. *wapl-1* example 1. (Di) Poolar body 1 in two clumps (white arrow) at anaphase II (pink arrows = segregation movement). (Dii) Polar body 1 (PB1) still as two parts and polar body 2 (PB2) moved to centre of embryo as pro-nuclei fuse (faint aggregate above). Note likely wandering chromosome between PB2 and pro-nuclei. (Diii) PB2 moves between segregating chromosomes at anaphase II and is pulled by tension from poles. (Div) PB2 appears decondensed and attached and to one mitotic nucleus on left at telophase.

Ai
METAPHASE II
20 µm
Aii
ANAPHASE II
Aiii
Histone(2B)::mCherry
PB2
PB1
Biv
MITOTIC ANAPHASE
PB2
PB1
WT movie (1)
Bi
METAPHASE II
30 µm
Bii
ANAPHASE II
Biii
PB2
PB1
WT movie (2)
Ci
METAPHASE II
20 µm
Cii
ANAPHASE II
Ciii
PB1
PB2
wapl-1 movie (1)
Di
ANAPHASE II
20 µm
Dii
PB1
PB2
Diii
MITOTIC ANAPHASE
PB1
PB2
Div
wapl-1 movie (2)

Figure 8. GFP::WAPL-1 transgene expression during meiotic prophase.

A. GFP::WAPL-1 transgene expression in a dissected germ line from transgenic worms carrying a single-copy insertion of the *GFP::wapl-1* and the *wapl-1(tm1814)* mutation . Upper panel is α-GFP only, lower panel is DAPI (blue) and α-GFP (green) merged. Deconvolved assembled projections. Expression peaks within meiosis at late pachytene diplotene.

B. Panel of late pachytene from the germ line shown in (A). Normal immunofluorescence protocol stained for DAPI and α-GFP, (as in Figure 7, A). Note the diffuse nuclear pattern of GFP::WAPL-1.

C. Late pachytene nuclei from transgenic worms carrying a single-copy insertion of the *GFP::wapl-1* and the *wapl-1(tm1814)* mutation. TRITON-X strong detergent washes used in immunofluorescence protocol stained for DAPI and α-GFP. Note GFP::WAPL-1 is largely absent from nuclei, indicating nucleoplasmic localization of WAPL-1.

N.B. These images are deconvovled and display adjusted to highlight expression pattern rather than compare levels.

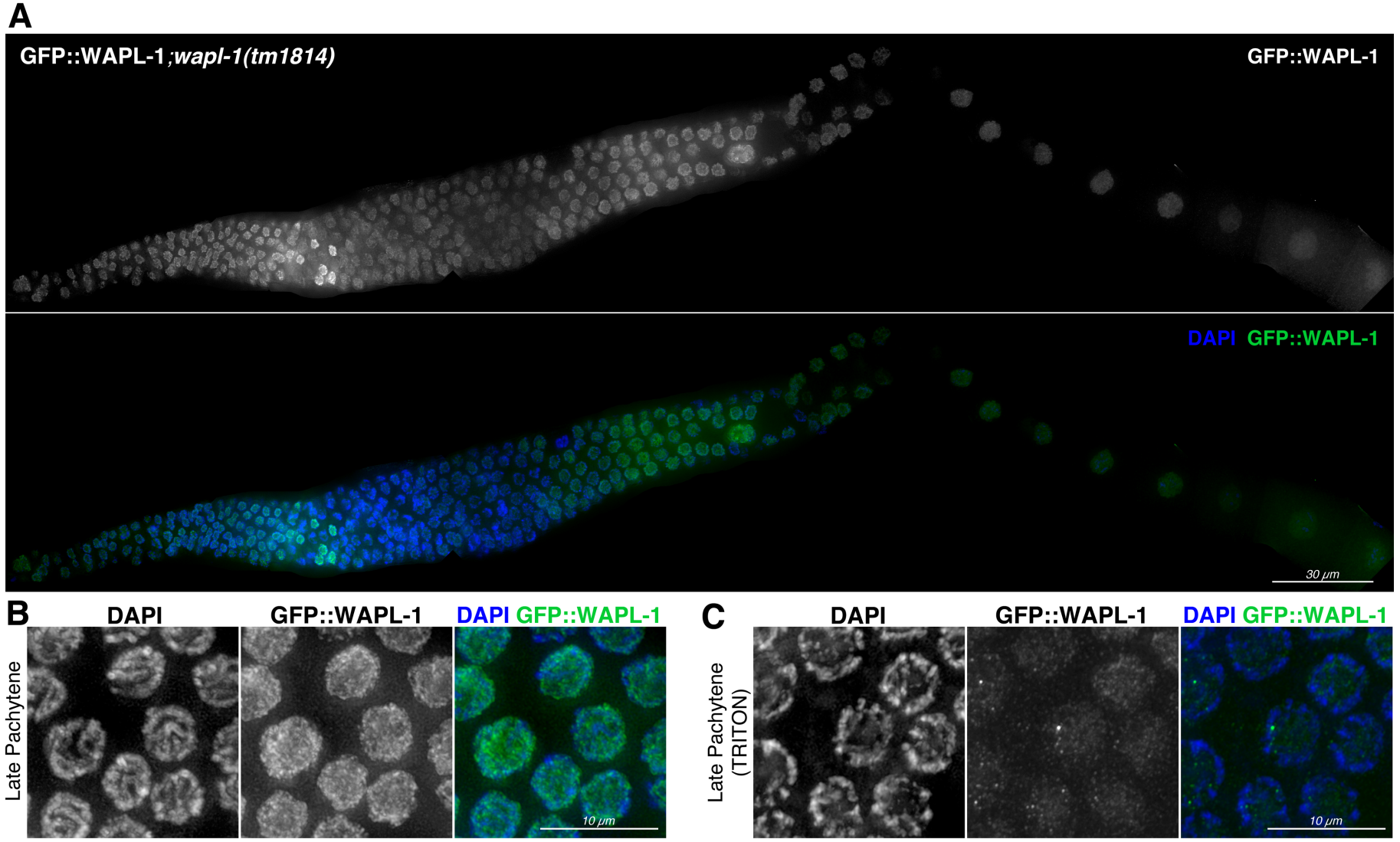
A
GFP::WAPL-1;wapl-1(tm1814)
GFP::WAPL-1
DAPI GFP::WAPL-1
30 μm
B
DAPI
GFP::WAPL-1
DAPI GFP::WAPL-1
Late Pachytene
10 μm
C
DAPI
GFP::WAPL-1
DAPI GFP::WAPL-1
Late Pachytene
(TRITON)
10 μm

Figure 9. SMC-3 levels are increased on late pachytene chromosomes in *wapl-1* mutants

A. Late pachytene panels from typical examples of wildtype and *wapl-1* mutants stained with α-SMC-3 antibody and DAPI. Images are raw non-deconvolved images obtained with the same microscope settings and SMC-3 display scale set with identical min/max values. DAPI adjusted to similar levels visually to allow relative SMC-3 levels to be observed in merged panels.

B. Whole nuclear mean fluorescence intensity of late pachytene α-SMC-3 averaged across 0.2 μm Z-stacks, measured with FIJI macro. Value represented by bar chart is overall mean intensity averaged from many nuclei across multiple germlines. 20 nuclei measured per germline from late pachytene stage. 14 germlines of WT (mean = 646 +/-8.6, 280 nuclei). 16 germlines of wapl-1 mutant (mean = 810+/-9.6, 320 nuclei). Y-axis is mean intensity per pixel (arbitrary units). Error bars = SEM.

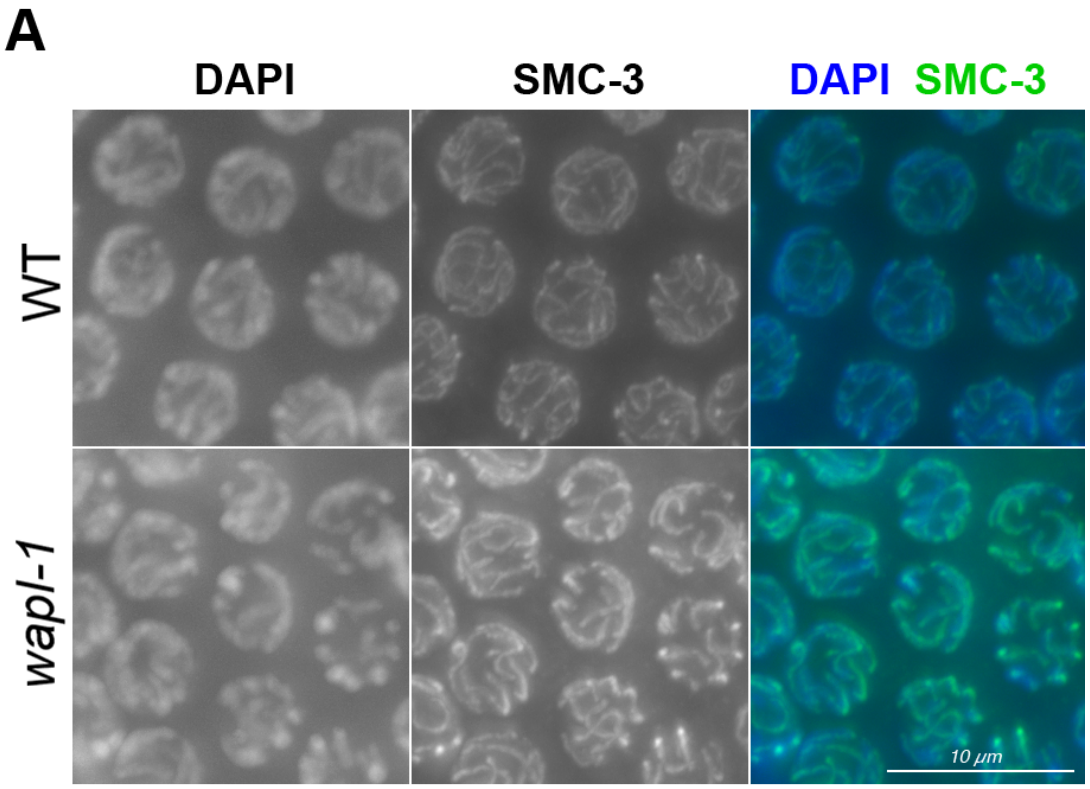
A
DAPI
SMC-3
DAPI SMC-3
WT
wapl-1
10 μm

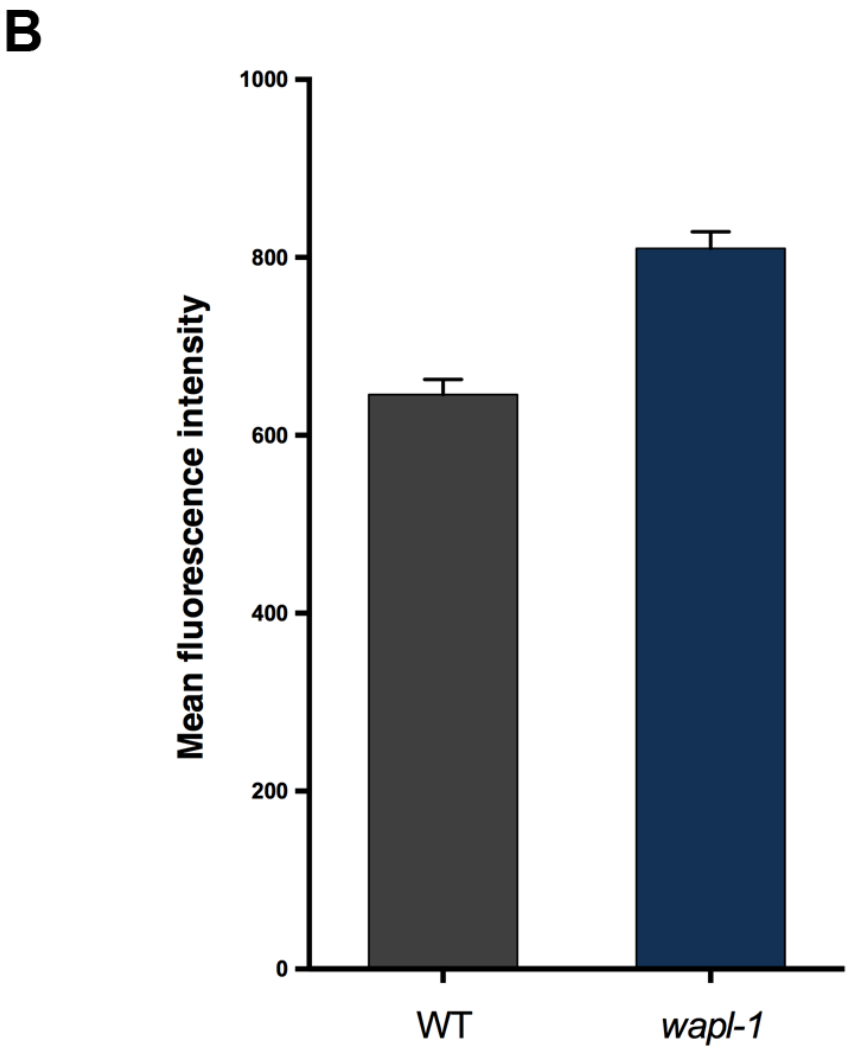
B
Mean fluorescence intensity
1000
800
600
400
200
0
WT
wapl-1

Figure 10. SMC-3 immunostaining appears less affected at earlier meiotic stages in *wapl-1* mutants

A. Transition zone (TZ) nuclei from wildtype and *wapl-1* mutant stained with α-SMC-3 antibody and DAPI. Final images produced by identical methods (see Figure 9, A)

B. Whole nuclear mean fluorescence intensity of α-SMC-3 staining from TZ (see Figure 10, A), early pachytene (panels not shown) and late pachytene (see Figure 9, A). Same experiment and germlines used from Figure 9. Bars represent overall mean intensity (method as described in 9, B). Nuclei measured per germline – TZ = 15, EP and LP = 20. TZ: 12 germlines of WT (mean = 730 +/-12.8, 180 nuclei), 10 germlines of *wapl-1* mutant (mean = 753+/-18.6, 150 nuclei); not significant. Early pachytene: 14 germlines of WT (mean = 653+/-8.7, 280 nuclei). 12 germlines of *wapl-1* mutant (mean = 713+/-10.8, 240 nuclei); **** p = < 0.0001. Late pachytene: same dataset as Figure 9, B; **** p = < 0.0001. Error bars = SEM.

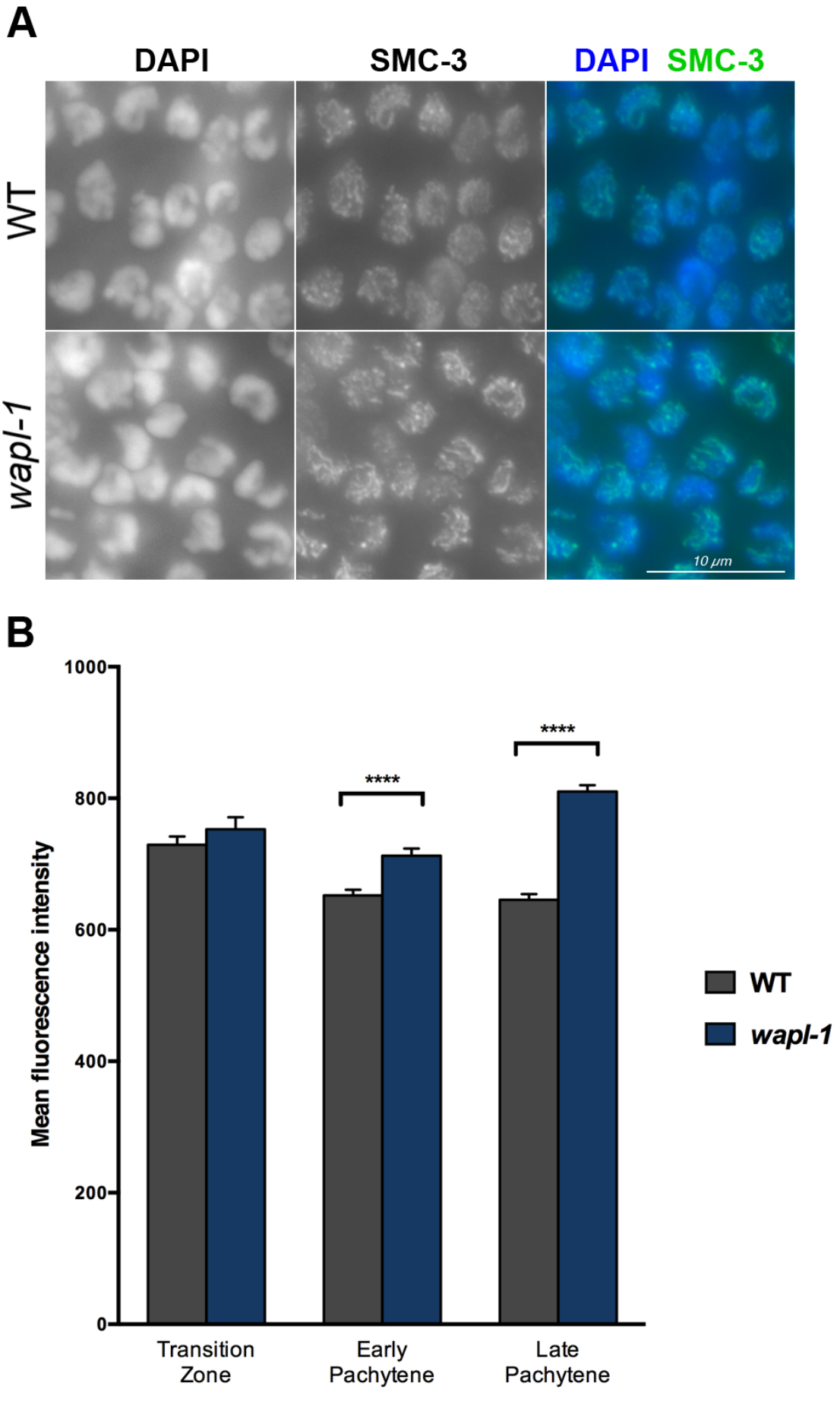
A
DAPI
SMC-3
DAPI SMC-3
WT
wapl-1
10 µm
B
Mean fluorescence intensity
1000
800
600
400
200
0
****
****
Transition Zone
Early Pachytene
Late Pachytene
WT
wapl-1

Figure 11. REC-8 cohesin levels are not strongly increased on *wapl-1* mutant late pachytene chromosomes

A. Late pachytene panels from typical examples of wildtype and *wapl-1* mutant stained with α-REC-8 antibodies and DAPI. Final images produced by identical methods (see Figure 9, A).

B. Whole nuclear mean fluorescence intensity of late pachytene α-REC-8. Bars represent overall mean intensity (method as described in 9, B). 6 germlines of WT (mean = 561 +/-9.5, 120 nuclei). 6 germlines of wapl-1 mutant (mean = 583+/-6.2, 120 nuclei). Error bars = SEM.

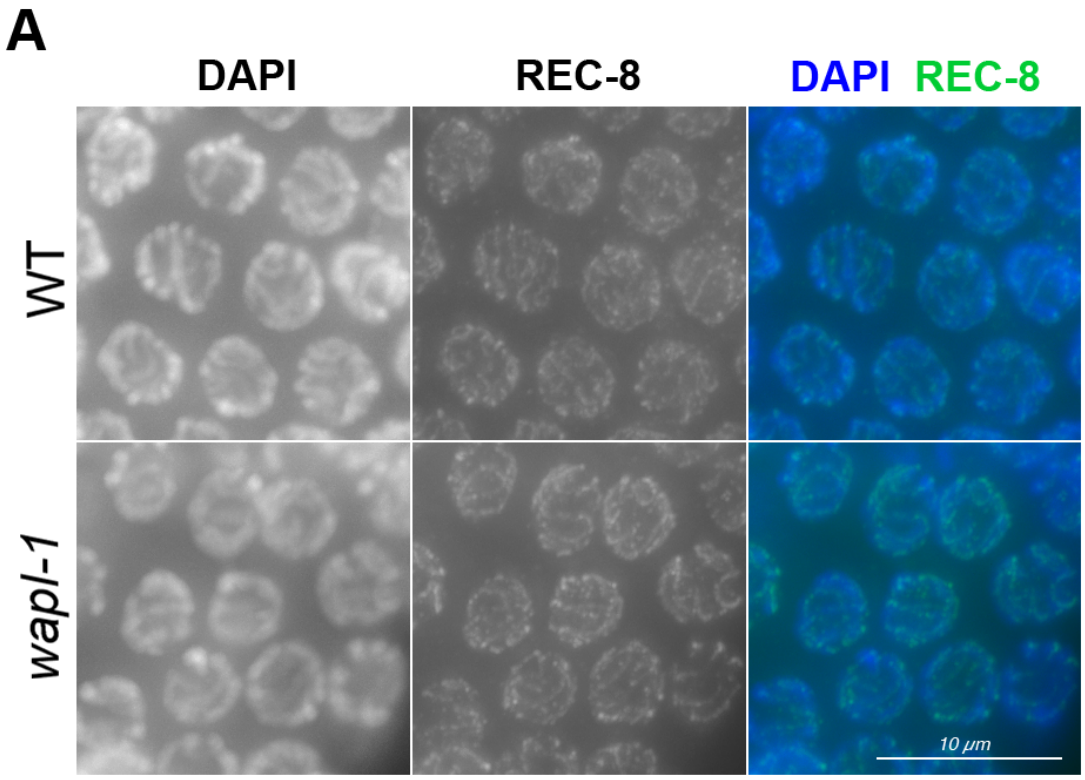
A
DAPI
REC-8
DAPI REC-8
WT
wapl-1
10 μm

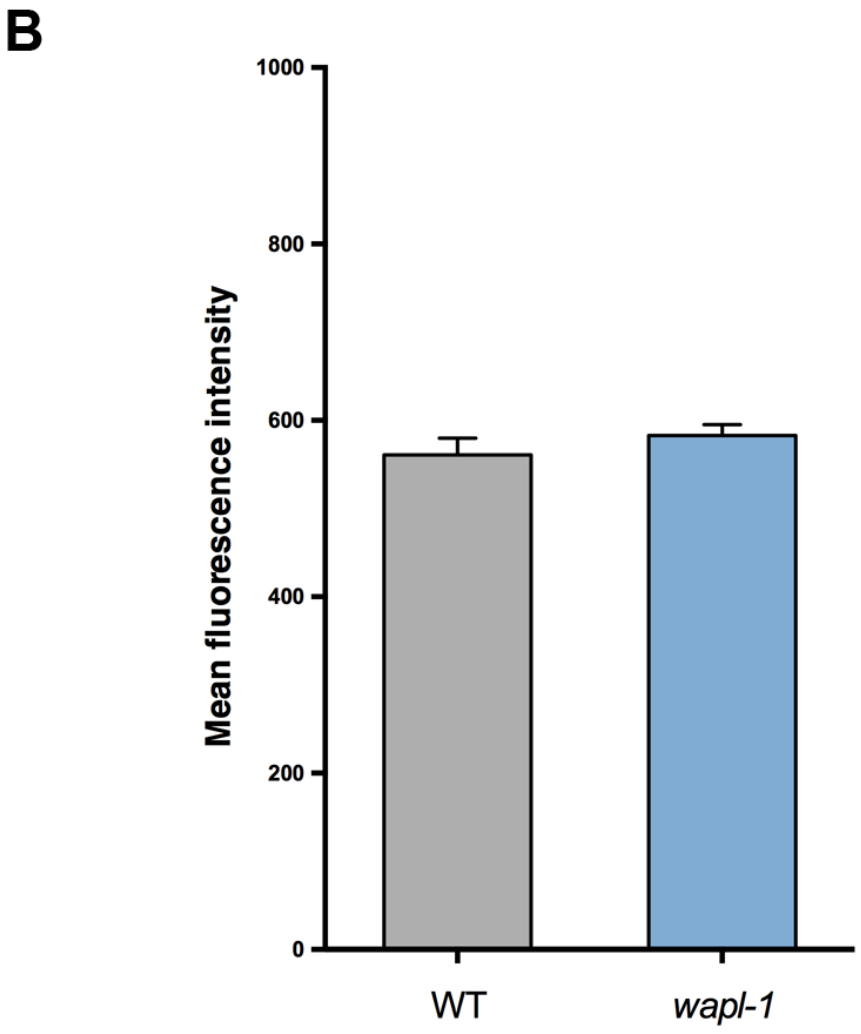
B
Mean fluorescence intensity
1000
800
600
400
200
0
WT
wapl-1

Figure 12. α-REC-8 immunostaining is similar during early prophase in *wapl-1* mutants and wildytpe controls.

A. Transition zone (TZ) nuclei from wildtype and *wapl-1* mutants stained with α-REC-8 antibody and DAPI. Final images produced by identical methods (see Figure 9, A)

B. Whole nuclear mean fluorescence intensity of α-SMC-3 staining from TZ (see Figure 12, A), early pachytene (panels not shown) and late pachytene (see Figure 11, A). Same experiment and germlines used from Figure 11. Bars represent overall mean intensity (method as described in 9, B). Nuclei measured per germline – TZ = 15, EP and LP = 20. TZ: 5 germlines of WT (mean = 644 +/-15.6, 75 nuclei), 6 germlines of *wapl-1* mutant (mean = 667+/-11.4, 90 nuclei); not significant. Early pachytene: 5 germlines of WT (mean = 588+/-14.4, 100 nuclei), 6 germlines of *wapl-1* mutant (mean = 573+/-5.1, 120 nuclei); not significant. Late pachytene: same dataset as Figure 11, B; not significant. Error bars = SEM.

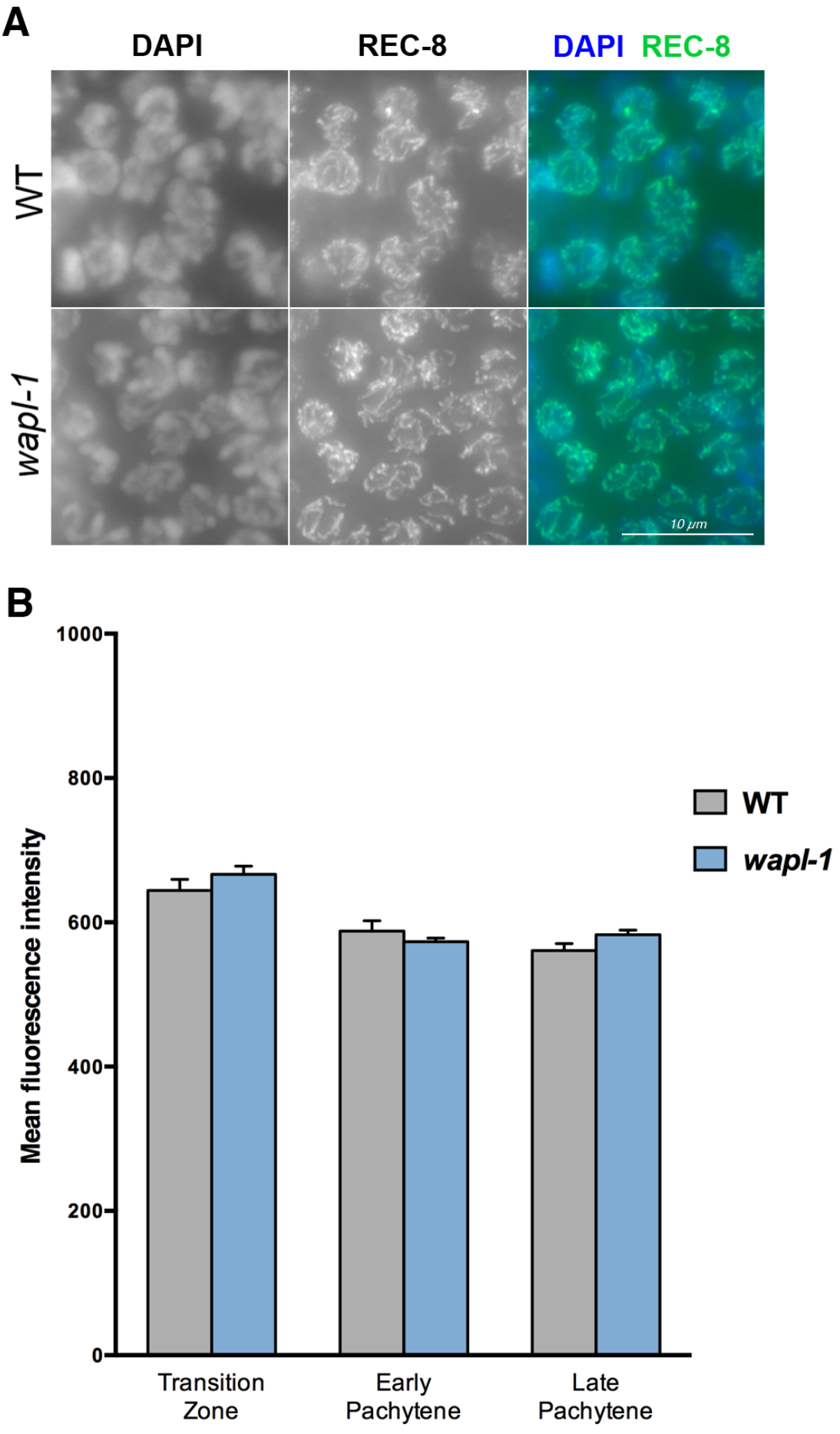
A
DAPI
REC-8
DAPI REC-8
WT
wapl-1
10 μm
B
Mean fluorescence intensity
1000
800
600
400
200
0
WT
wapl-1
Transition Zone
Early Pachytene
Late Pachytene

Figure 13. REC-8::GFP levels are not affected by WAPL-1.

A. Late pachytene panels of REC-8::GFP; *rec-8* (wildtype background) and REC-8::GFP; *wapl-1; rec-8* (*wapl-1* mutant) stained with á-GFP antibody (conjugated) and DAPI. Final images produced by identical methods (see Figure 9, A).

B. Whole nuclear mean fluorescence intensity of late pachytene REC-8::GFP. Bars represent overall mean intensity (method as described in 9, B). 5 germlines of WT background, 10-15 nuclei measured per germline (mean = 899 +/-17.1, 65 nuclei). 9 germlines of *wapl-1* mutant, 10-20 nuclei per germline (mean = 945+/-16.9, 135 nuclei); not significant. Error bars = SEM.

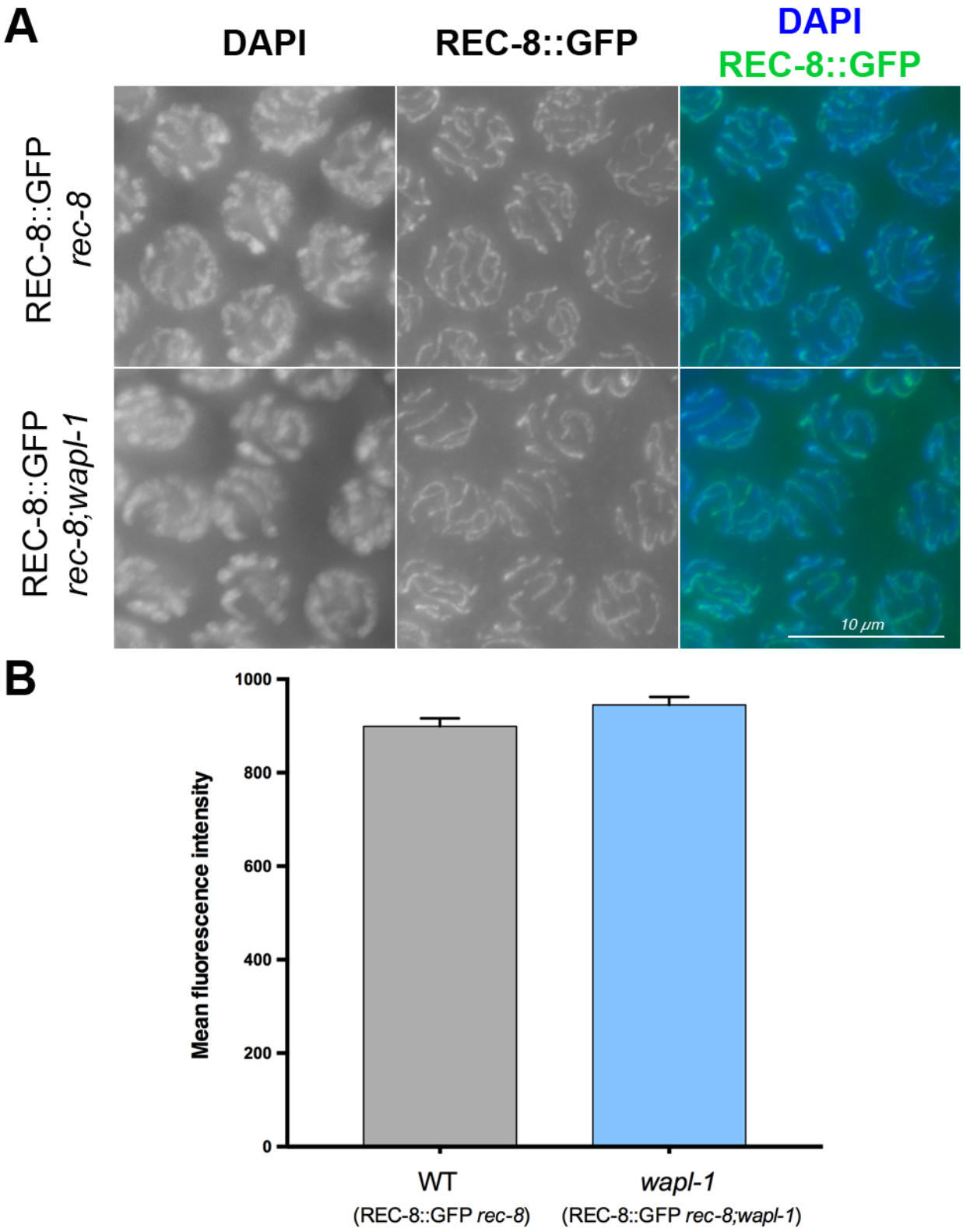
A
DAPI
REC-8::GFP
DAPI
REC-8::GFP
REC-8::GFP
rec-8
REC-8::GFP
rec-8;wapl-1
10 μm
B
Mean fluorescence intensity
1000
800
600
400
200
0
WT
(REC-8::GFP rec-8)
wapl-1
(REC-8::GFP rec-8;wapl-1)

Figure 14. COH-3 cohesin levels are dramatically increased on *wapl-1* mutant late pachytene chromosomes

A. Late pachytene nuclei from wildtype and *wapl-1* mutants stained with α-COH-3 antibody and DAPI. Final images produced by identical methods (see Figure 9, A).

B. Whole nuclear mean fluorescence intensity of late pachytene α-COH-3. Bars represent overall mean intensity (method as described in 9, B). 15-20 nuclei per germline. 6 germlines of WT (mean = 498 +/-5.5, 114 nuclei). 6 germlines of wapl-1 mutant (mean = 772+/-11.7, 147 nuclei). Error bars = SEM. **** P = < 0.0001; *t*-test.

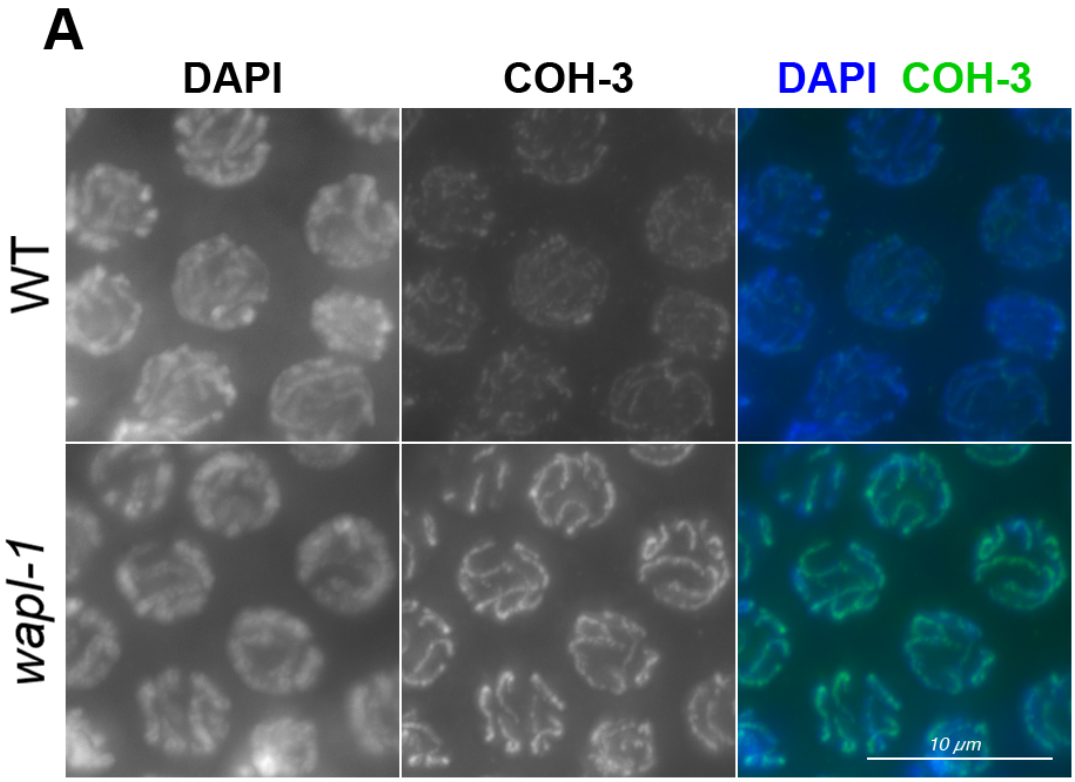
A
DAPI
COH-3
DAPI COH-3
WT
wapl-1
10 μm

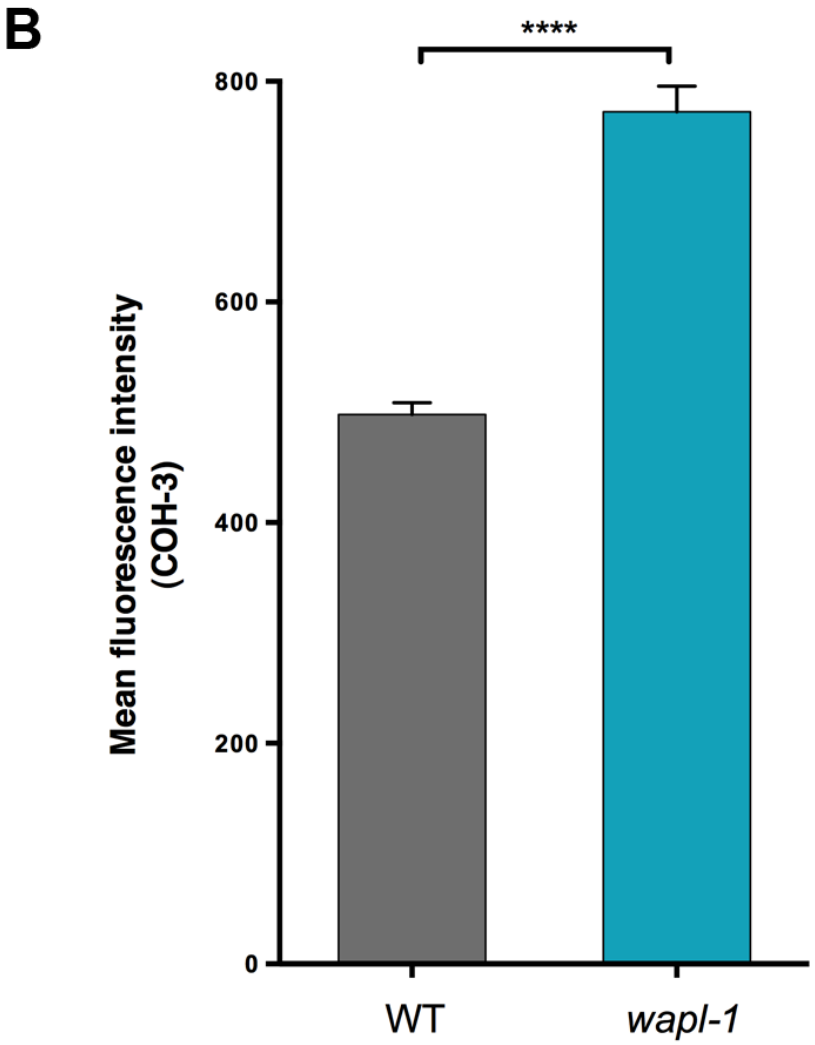
B
****
800
600
400
200
0
Mean fluorescence intensity (COH-3)
WT
wapl-1

Figure 15. Non-affinity purified antibody serum recognises both COH-3 and COH-4

α-COH-3/4 antibodies recognises both COH-3 and COH-4. Only shows blank staining in *coh-3; coh-4* double mutants. Final images produced by identical method (as described in Firgure 9, A)

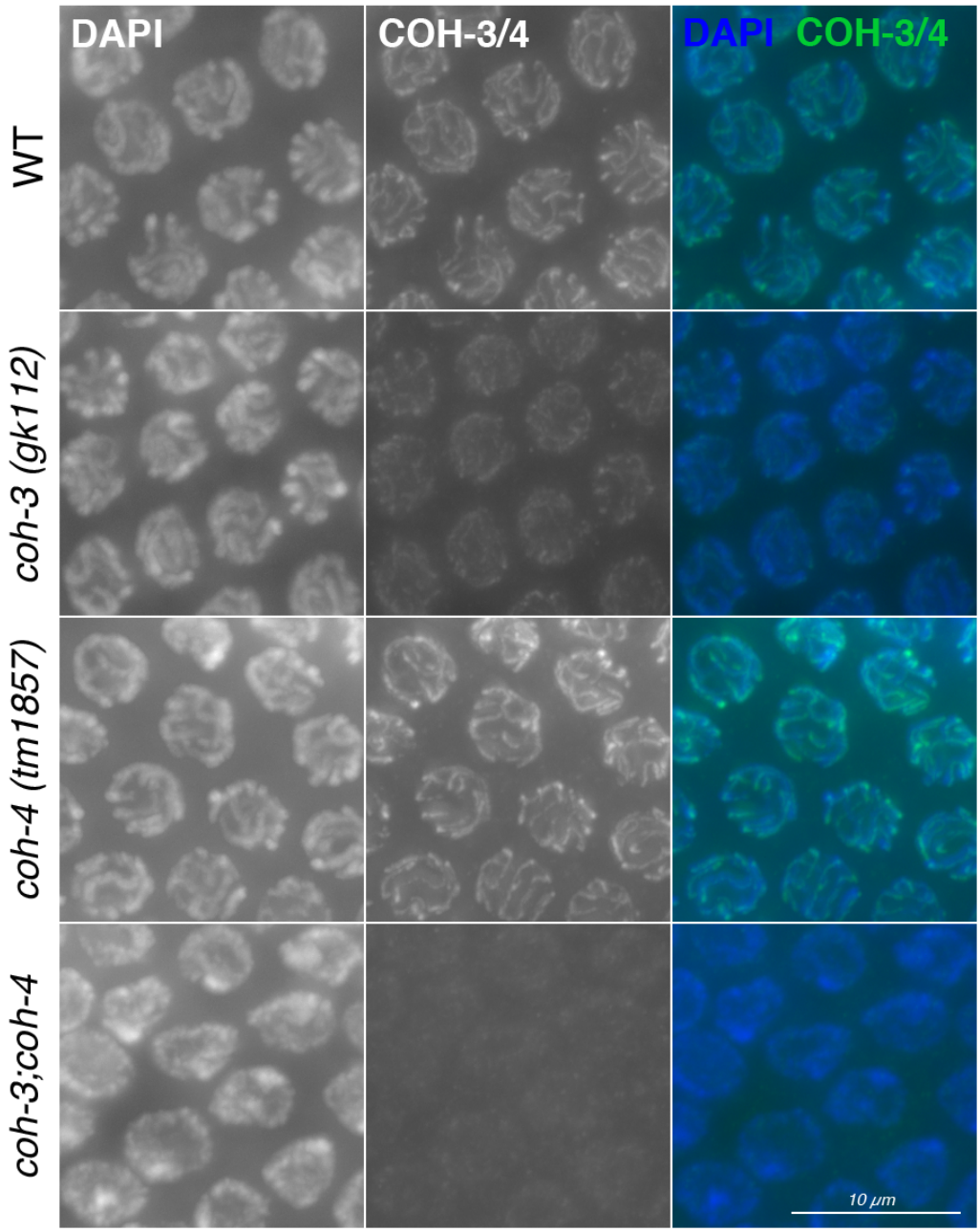
DAPI
COH-3/4
DAPI COH-3/4
WT
coh-3 (gk112)
coh-4 (tm1857)
coh-3;coh-4
10 μm

Figure 16. α-COH-3/4 immunostaining also shows increase on late pachytene chromosomes of *wapl-1* mutant

A. Late pachytene nuclei from wildtype and the *wapl-1* mutant stained with α-COH-3/4 antibody and DAPI. Final images produced by identical methods (see Figure 9, A).

B. Whole nuclear mean fluorescence intensity of late pachytene α-COH-3/4 (serum). Bars represent overall mean intensity (method as described in 9, B). 10 germlines of WT, 200 nuclei (mean = 584 +/-8.7). 9 germlines of wapl-1 mutant, 180 nuclei (mean = 841+/-16.3). Error bars = SEM.

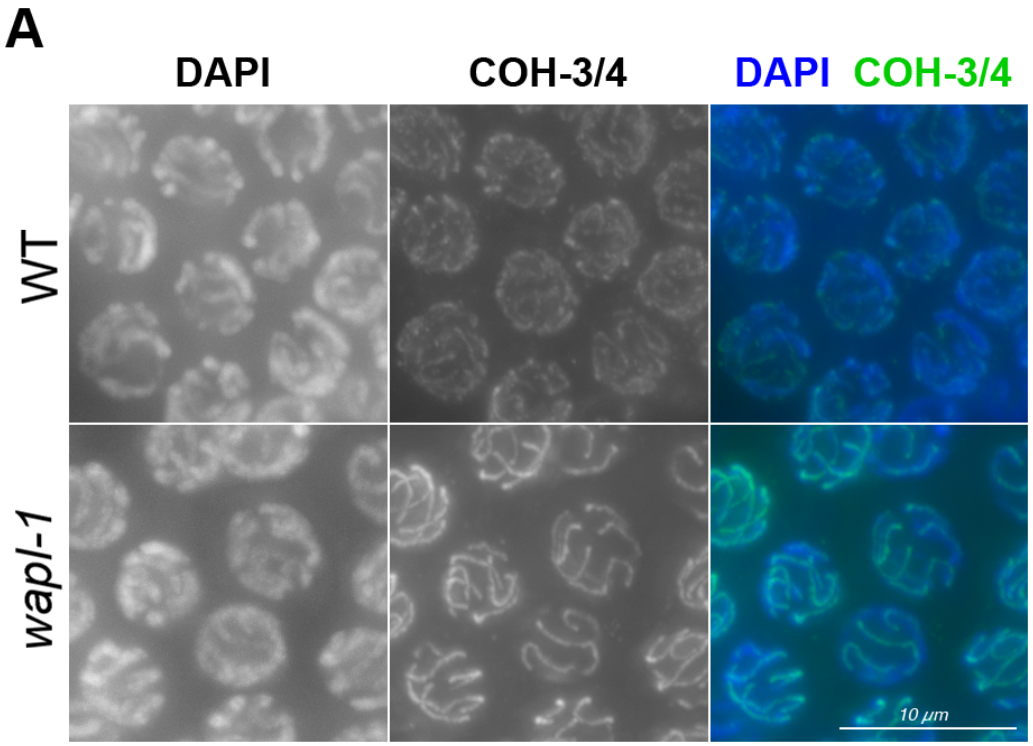
A
DAPI
COH-3/4
DAPI COH-3/4
WT
wapl-1
10 μm

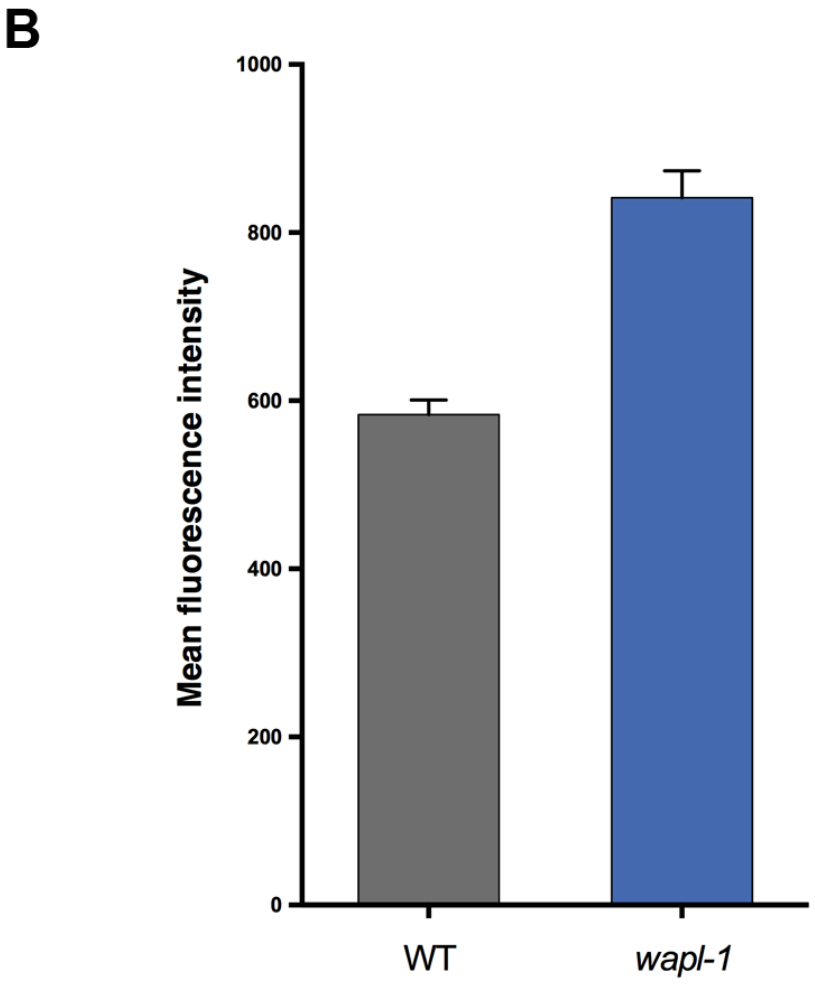
B
Mean fluorescence intensity
1000
800
600
400
200
0
WT
wapl-1

Figure 17. α-COH-3/4 immunostaining is increased on chromosomes at early meiotic stages in *wapl-1* mutants

A. Transition zone (TZ) stage nuclei of wildtype and the *wapl-1* mutant stained with α-COH-3/4 (serum) and DAPI. Final images produced by identical methods (see Figure 9, A)

B. Whole nuclear mean fluorescence intensity of α-COH-3/4 staining from TZ (see Figure 17, A), early pachytene (panels not shown) and late pachytene (see Figure 16, A). Same experiment and germlines used from Figure 16. Bars represent overall mean intensity (method as described in 9, B). Nuclei measured per germline – TZ = 15, EP and LP = 20. TZ: 8 germlines of WT (mean = 468 +/-5.8, 160 nuclei), 8 germlines of *wapl-1* mutant (mean = 665+/-15.7, 160 nuclei); **** P = < 0.0001. Early pachytene: 8 germlines of WT (mean = 535+/-6.2, 160 nuclei), 8 germlines of *wapl-1* mutant (mean = 767+/-19.5, 180 nuclei); **** P = < 0.0001. Late pachytene: same dataset as Figure 16, B; **** P = < 0.0001. Error bars = SEM.

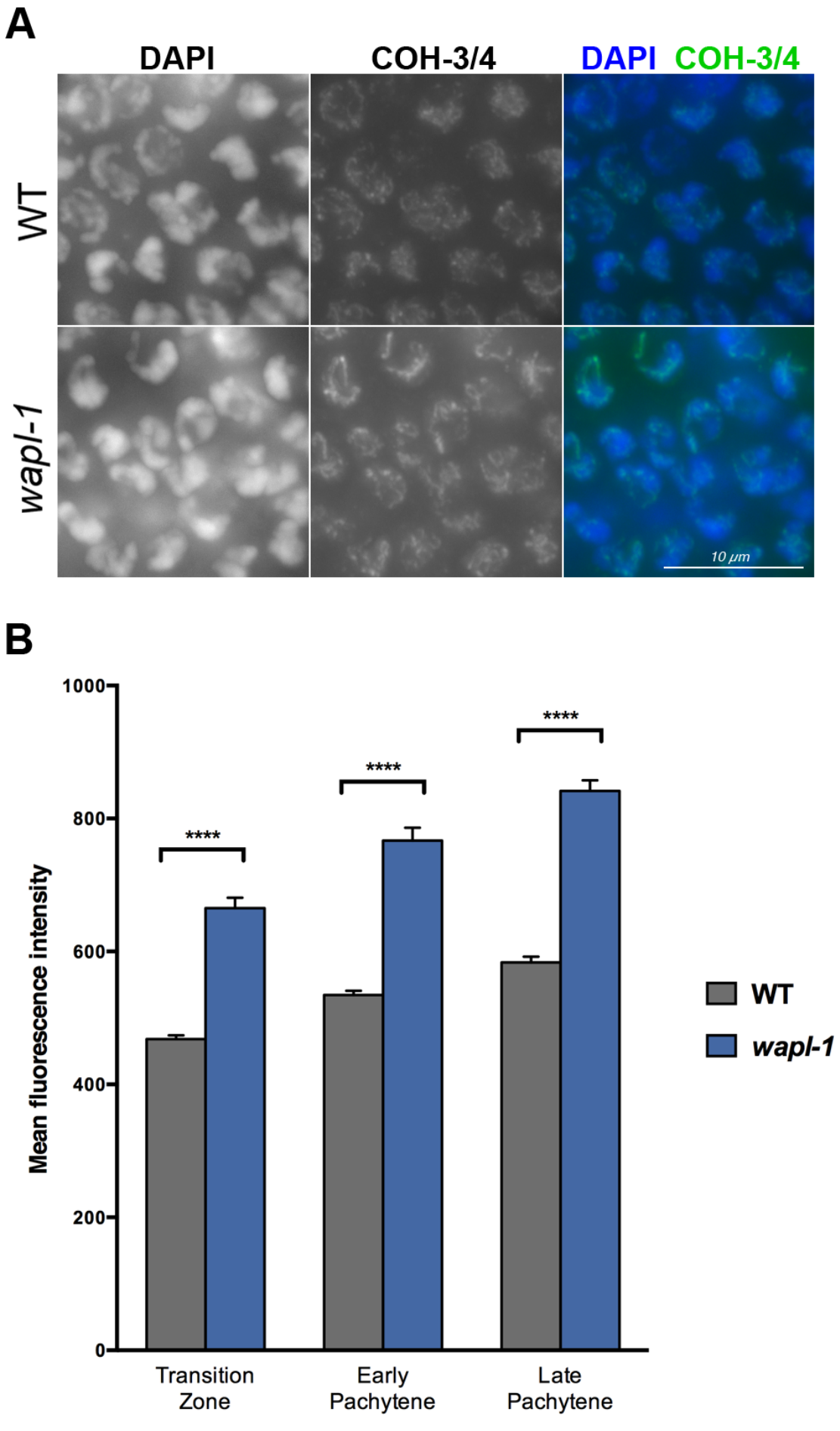
A
DAPI
COH-3/4
DAPI COH-3/4
WT
wapl-1
10 μm
B
Mean fluorescence intensity
1000
800
600
400
200
0
****
****
****
Transition Zone
Early Pachytene
Late Pachytene
WT
wapl-1

Figure 18. α-COH-3/4 and α-REC-8 co-staining in wildtype and *wapl-1* mutants

Late pachytene nulei of wildtype and *wapl-1* mutant costained for both α-COH-3/4 and α-REC-8. Note that COH-3/4 is increased on chromosomes but not REC-8 in the wapl-1 mutant. Images produced by identical methods (as in Figure 9, A).

COH-3/4 REC-8
REC-8
COH-3/4
DAPI
10 µm
WT
wapl-1

Figure 19. WAPL-1 has variable affect on different cohesins at late pachytene

A. Single late pachtyene nucleus of α-REC-8, α-COH-3/4 and α-SMC-3 immunostaining from wildtype and the *wapl-1* mutant, taken from same panels shown in Figures 9, 11 & 16.

B. Bar chart combining analysis of late pachytene nuclei for α-REC-8, α-COH-3/4 and α-SMC-3. Corresponding stainings in part A are shown above appropriate columns. Note intermediate response of SMC-3 between REC-8 and COH-3/4. **** P = < 0.0001, ns = not significant; *t*-test. Error bars = SEM.

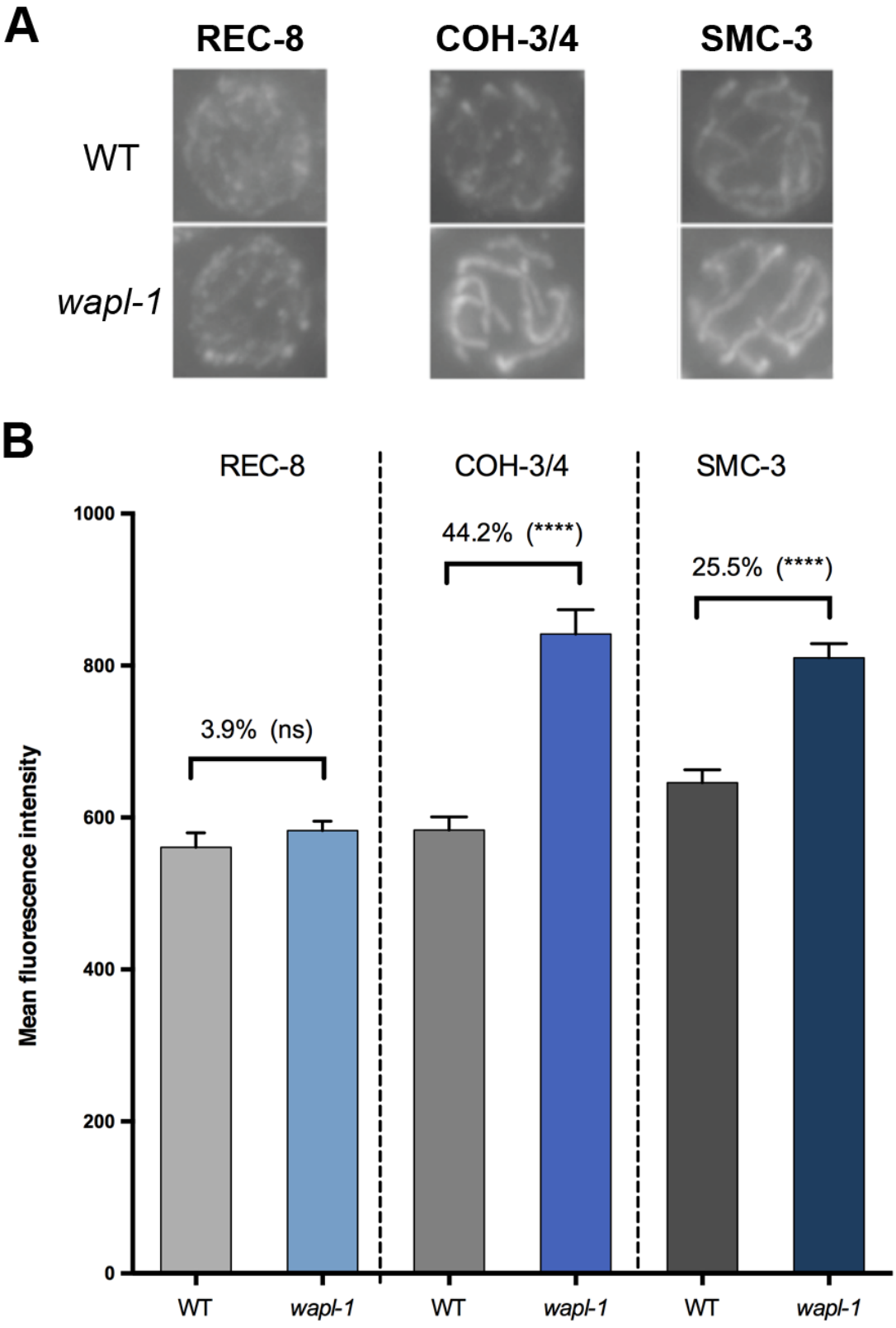
A
REC-8
COH-3/4
SMC-3
WT
wapl-1
B
REC-8
COH-3/4
SMC-3
Mean fluorescence intensity
1000
800
600
400
200
0
3.9% (ns)
44.2% (****)
25.5% (****)
WT
wapl-1
WT
wapl-1
WT
wapl-1

Figure 20. Effect of WAPL-1 on different cohesin subunit stainings at different meiotic stages

Whole nucleus mean intensity of α-REC-8, α-COH-3/4 and α-SMC-3 immunofluorescence at different stages of meiosis in WT and *wapl-1* mutant; tranzition zone (TZ), early pachytene (EP) and late pachytene (LP). Graph combines data shown in Figure 10, Figure 12 and Figure 17. Grey shades = WT. Blue shades = *wapl-1* mutant. Asterisks indicate significant differences in mean nuclear intensity between wildtype and *wapl-1* mutants.

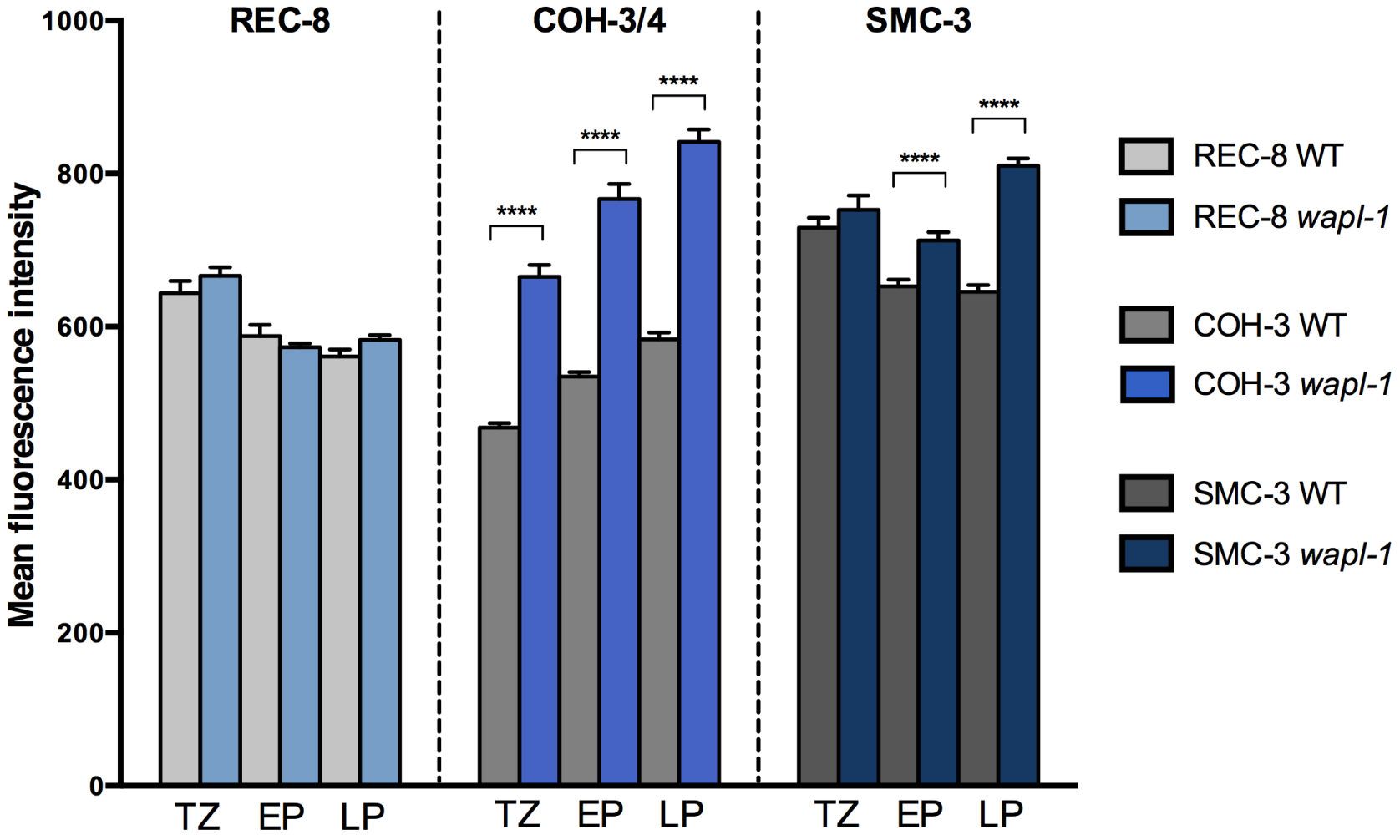
REC-8
COH-3/4
SMC-3
Mean fluorescence intensity
1000
800
600
400
200
0
TZ
EP
LP
****
REC-8 WT
REC-8 wapl-1
COH-3 WT
COH-3 wapl-1
SMC-3 WT
SMC-3 wapl-1

Figure 21. WAPL transgenes rescue *wapl-1* mutant meiotic phenotypes

α-COH-3/4 staining in strains carrying transgenes of the WAPL-1 endogenous sequence tagged with GFP on the N-terminus or with no tag crossed to the *wapl-1* (*tm1814*) homozygous background. Note second row, for both transgenic strains the COH-3/4 pattern and intensity is more similar to wildtype nuclei. Fourth row shows a single nucleus zoom-in taken from the corresponding panel in second row. Images produced by identical methods described in Figure 9. A.

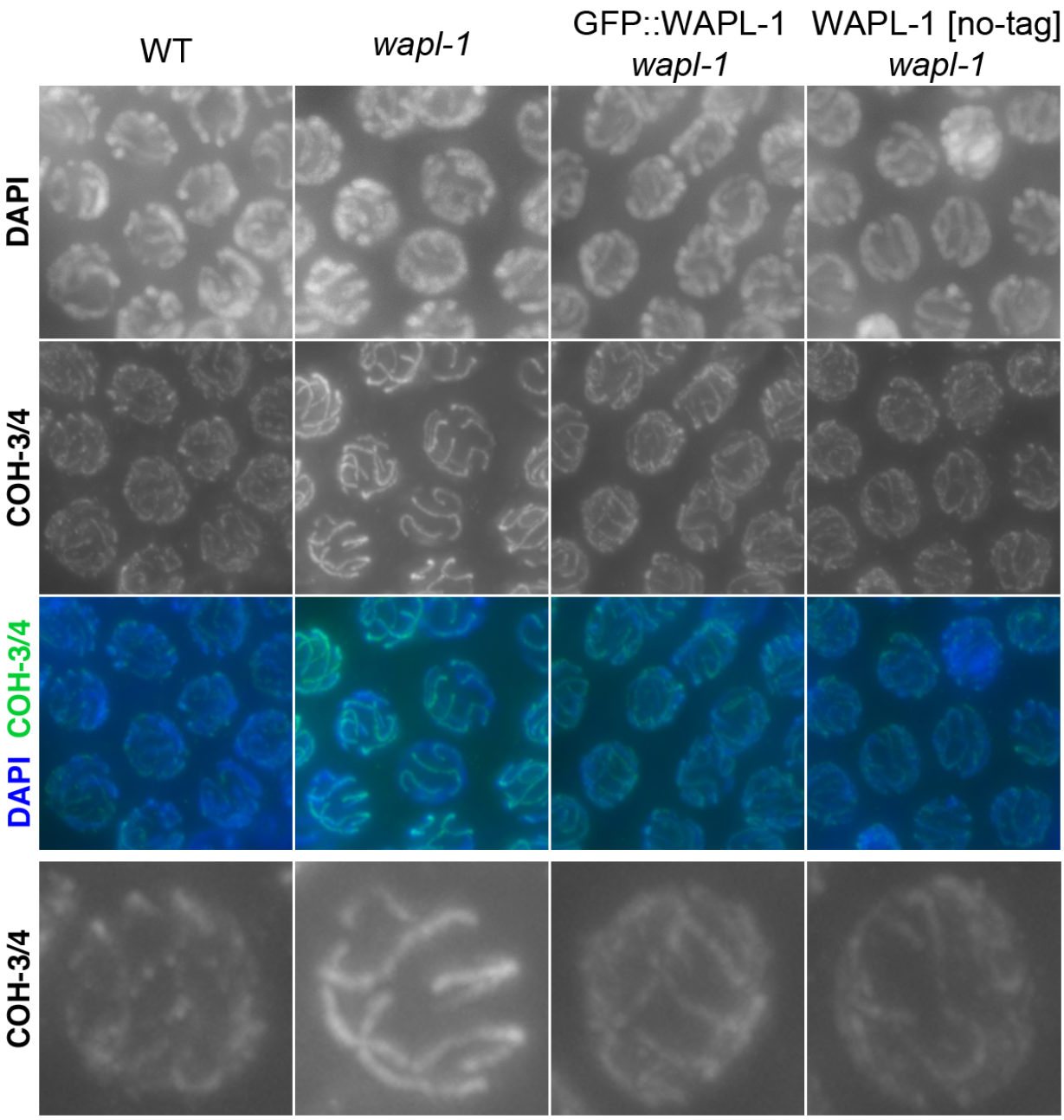
WT
wapl-1
GFP::WAPL-1
wapl-1
WAPL-1 [no-tag]
wapl-1
DAPI
COH-3/4
DAPI COH-3/4
COH-3/4

Figure 22. Lineprofiles of α-SMC-3 staining

A. Single late pachytene nucleus stained with α-SMC-3 and DAPI. Lineprofile position (horizontal yellow line) chosen perpendicular to chromosome axis direction. Green peaks correspond to SMC-3 chromosome axial staining, Blue peaks mark DAPI staining of chromatin. Non-deconvolved image.

B. Graph plotting α-SMC-3 immunofluorescence intensity lineprofile (same example as part A). Dotted lines mark peak and trough pixel intensity values. Arrow indicates fluorescence range between peak and trough: ΔF (Axis to nucleoplasm difference).

C. Scatterplot of multiple SMC-3 lineprofile ranges (ΔF), for wildtype and *wapl*-1 nuclei at late pachytene. Each point = single ΔF value as shown in part B. 3-5 ΔF values were measured per nucleus and two nuclei per germline. 14 wildtype gemlines (mean = 183 +/-6.3) and 16 *wapl-1* mutant germlines (mean = 290 +/-8.4). Significant difference with *t*-test; p = <0.0001.

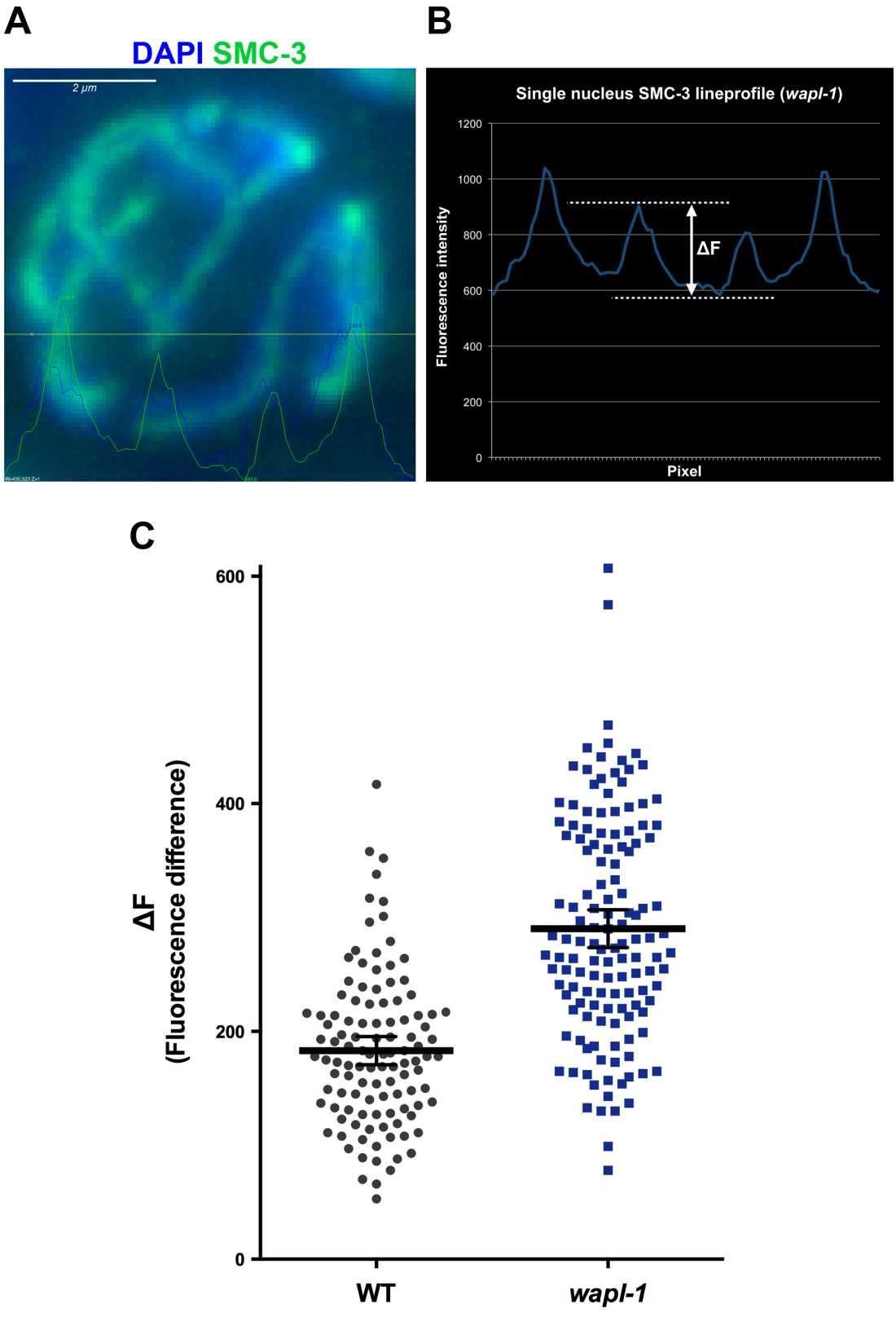
A
DAPI SMC-3
2 µm
B
Single nucleus SMC-3 lineprofile (wapl-1)
Fluorescence intensity
1200
1000
800
600
400
200
0
ΔF
Pixel
C
ΔF
(Fluorescence difference)
600
400
200
0
WT
wapl-1

Figure 23. Lineprofiles of α-REC-8 staining

A. Single late pachytene nucleus stained withα-REC-8 and DAPI. Lineprofile position at vertical yellow line. Green peaks = REC-8 chromosome axial staining, Blue peaks mark DAPI staining of chromatin. Non-deconvolved image.

B. Graph plotting α-REC-8 immunofluorescence intensity lineprofile (same example as part A). ΔF = peak to trough fluorescence intensity range (as described in 22, B).

C. Scatterplot of multiple REC-8 lineprofile ranges (ΔF), as described in 21, C. 6 wildtype gemlines (mean = 147 +/-7.8) and 6 mutant germlines (mean = 185 +/-7.9). Significant difference shown with *t*-test; p = 0.0008.

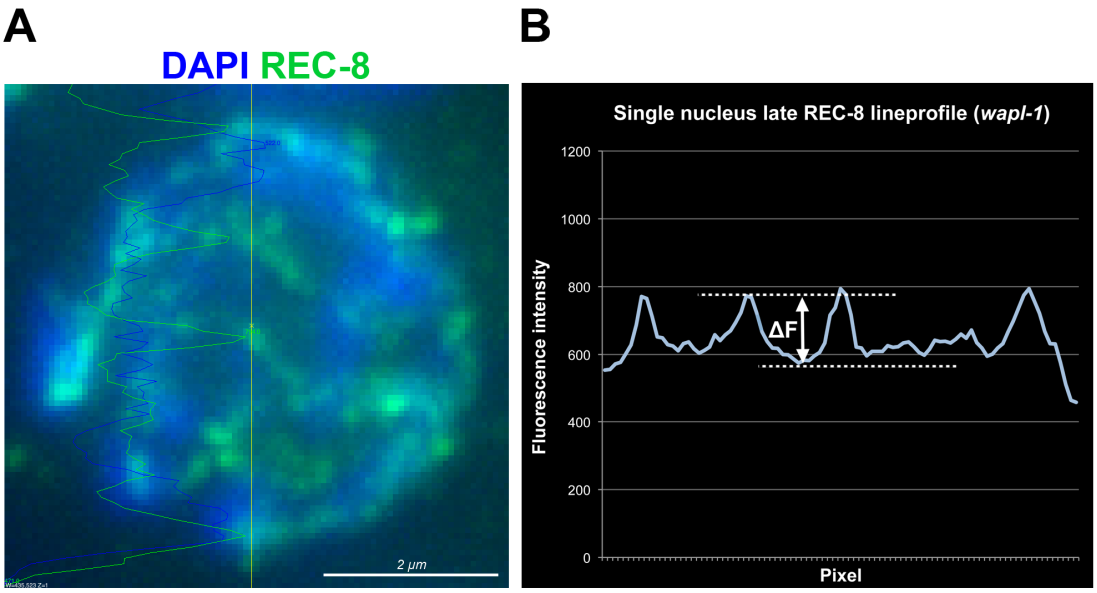
A
DAPI REC-8
2 µm
B
Single nucleus late REC-8 lineprofile (wapl-1)
Fluorescence intensity
1200
1000
800
600
400
200
0
ΔF
Pixel

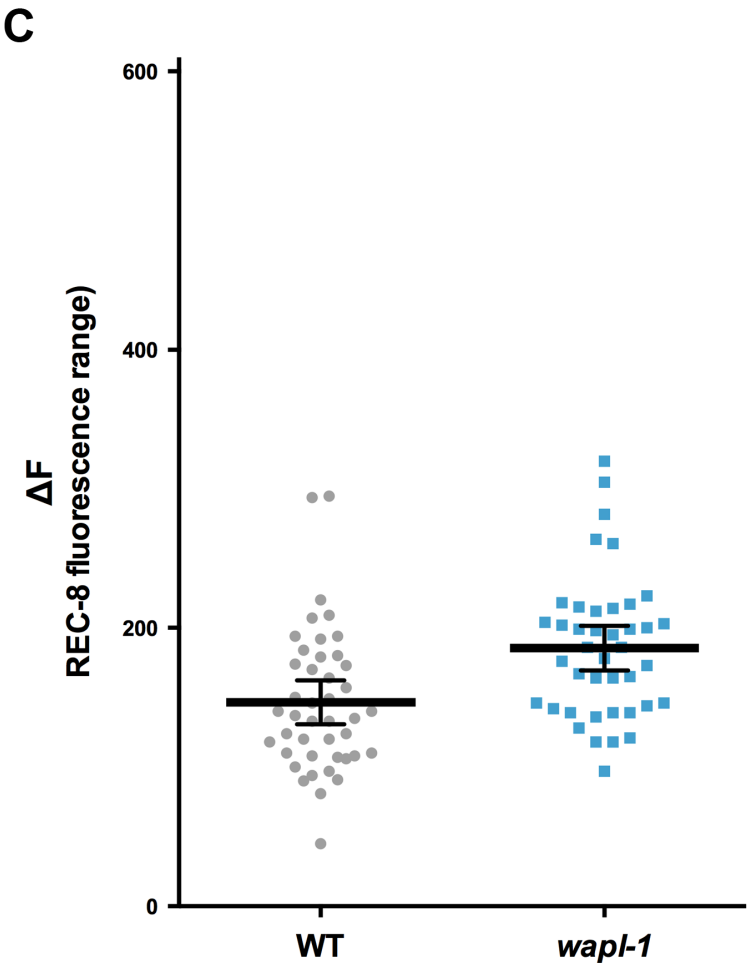
C
ΔF
REC-8 fluorescence range)
600
400
200
0
WT
wapl-1

Figure 24. Lineprofiles of α-COH-3/4 staining

A. Single late pachytene nucleus stained withα-COH-3/4 and DAPI. Lineprofile position at horizontal yellow line. Green peaks = COH-3/4 chromosome axial staining, Blue peaks mark DAPI staining of chromatin. Non-deconvolved image.

B. Graph plotting α-COH-3/4 immunofluorescence intensity lineprofile (same example as part A). ΔF = fluorescence intensity range (as described in 22 B).

C. Scatterplot of multiple COH-3/4 lineprofile ranges (ΔF), as described in 21, C. 10 wildtype gemlines (mean = 184 +/-7.8) and 9 mutant germlines (mean = 395 +/-13.3). Significant difference shown with *t*-test; p = < 0.0001.

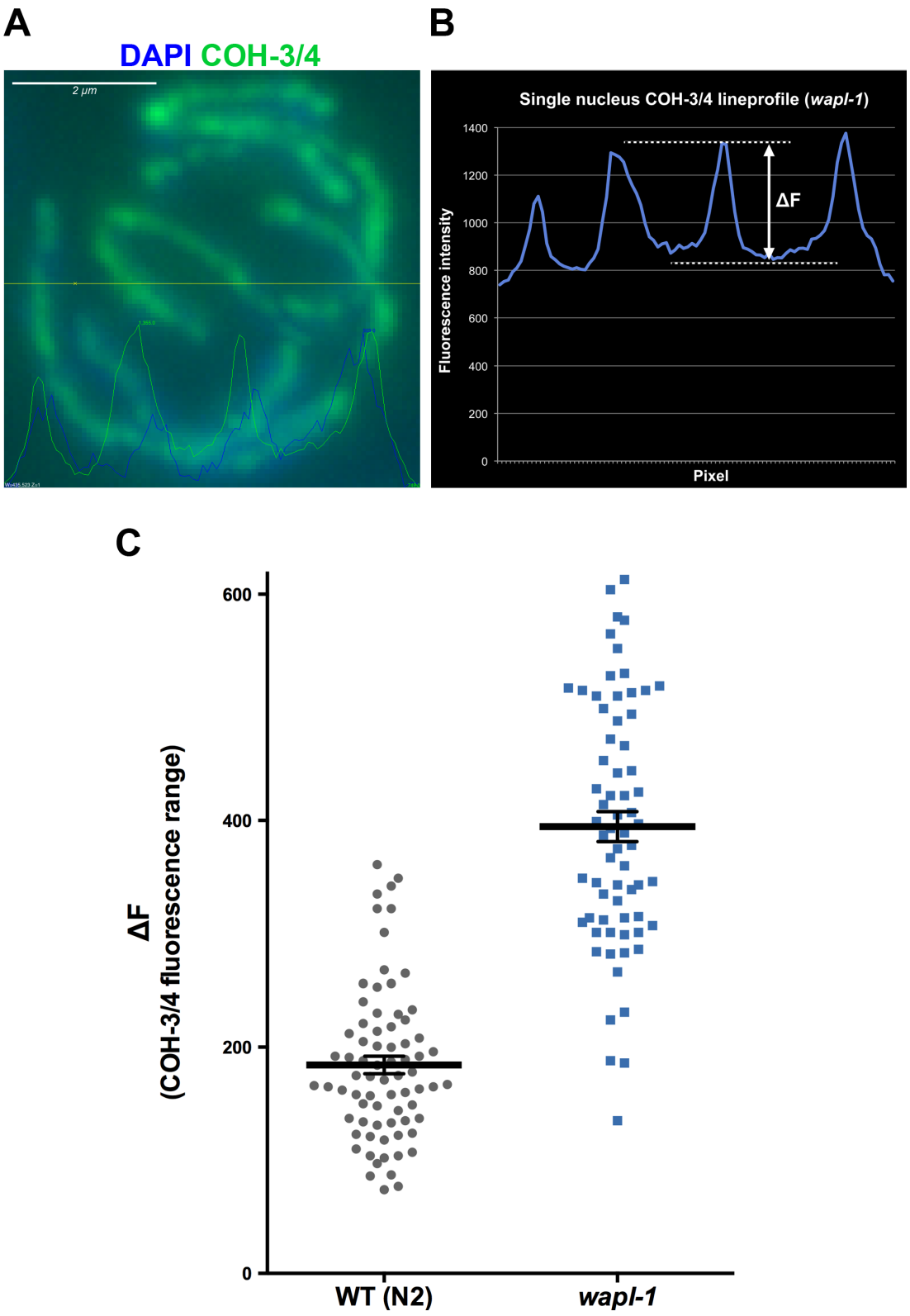
A
DAPI COH-3/4
2 µm
B
Single nucleus COH-3/4 lineprofile (wapl-1)
Fluorescence intensity
1400
1200
1000
800
600
400
200
0
ΔF
Pixel
C
ΔF
(COH-3/4 fluorescence range)
600
400
200
0
WT (N2)
wapl-1

Figure 25. Fluorescence lineprofiles for α-REC-8, α-COH-3/4 and α-SMC-3 in wildtype and *wapl-1* mutant

Fluorescence linprofile intensity ranges (ΔF) for α-REC-8, α-COH-3/4 and α-SMC-3 staining in late pachytene nuclei of wildtype and *wapl-1* mutants. Combined datasets from Figure 22, Figure 23 and Figure 24. Note larger relative increases in *wapl-1* mutant compared to increases in mean nuclear fluorescence (Figure 19). Also note the intermediate response of SMC-3 to loss of WAPL-1.

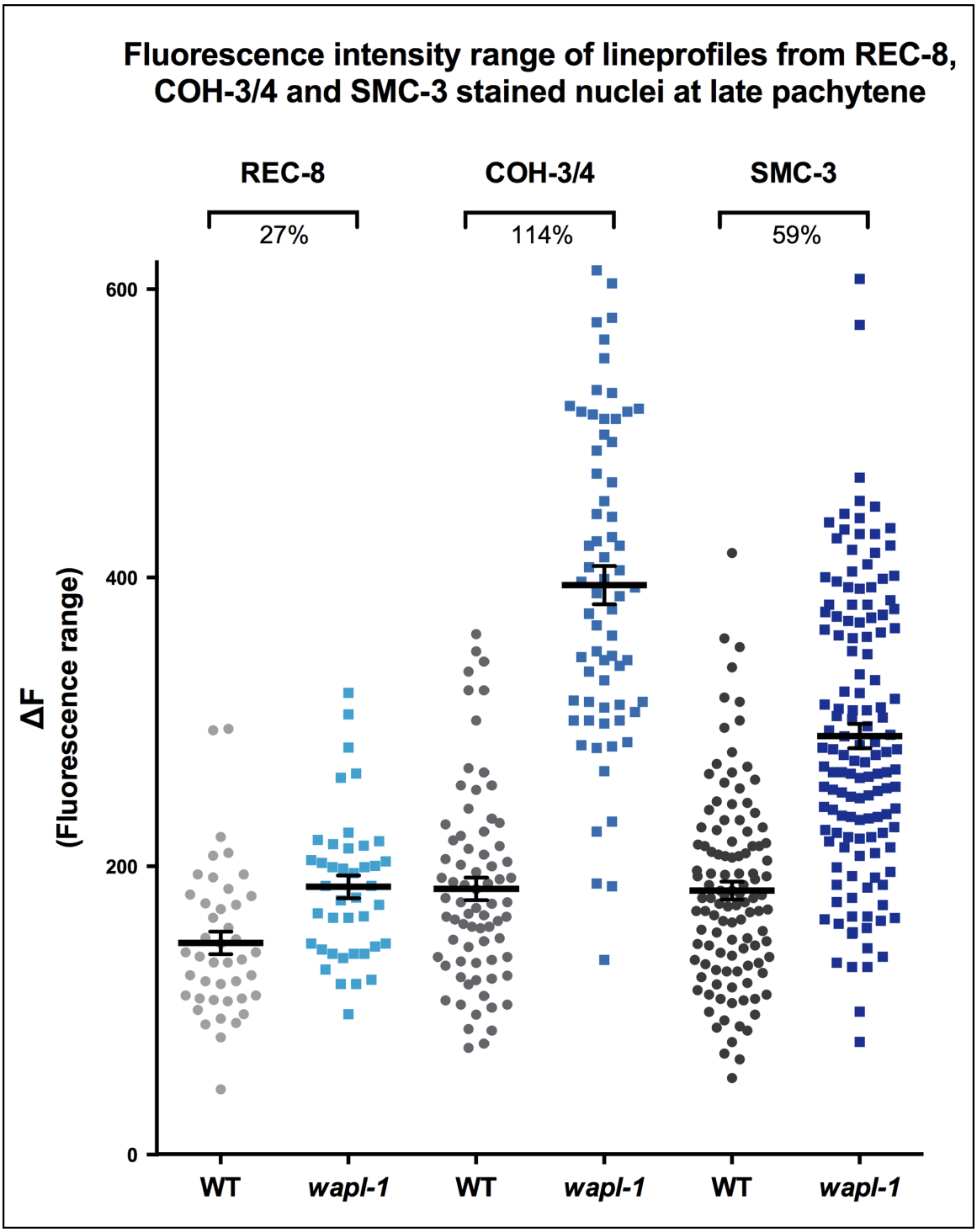
Fluorescence intensity range of lineprofiles from REC-8, COH-3/4 and SMC-3 stained nuclei at late pachytene
REC-8
COH-3/4
SMC-3
27%
114%
59%
ΔF
(Fluorescence range)
600
400
200
0
WT
wapl-1
WT
wapl-1
WT
wapl-1

Figure 26. Diplotene α-SMC-3 staining in wildtype and *wapl-1* mutants

Late pachytene and diplotene nuclei in wildtype and the *wapl-1* mutant stained with α-SMC-3 and DAPI. Images obtained through identical method as described in Figure 9, A. Note wildtype nuclei have a high level of nucleoplasmic staining and axial staining is not clear while the *wapl-1* mutant nuclei show reduced nucleoplasmic staining and increased axial staining.

DAPI SMC-3
SMC-3
20 µm
20 µm
WT
wapl-1

Figure 27. α-SMC-1 and α-COH-3/4 patterns are affected in the *wapl-1* mutant

A. α-SMC-1 and DAPI staining in diplotene nuclei from wiltype and wapl-1 mutant germlines. Final images produced by identical methods as described in Figure 9, A. Note reduced nucleoplasmic staining in *wapl-1* mutant and increased axial definition.

B. α-COH-3/4 and DAPI staining in early diplotene nuclei from wildtype and *wapl-1* mutant germlines. Images shown are deconvolved and contrast adjusted to highlight axial staining. Note both DAPI and COH-3/4 staining patterns remain more elongated in the *wapl-1* mutant, showing delayed remodeling.

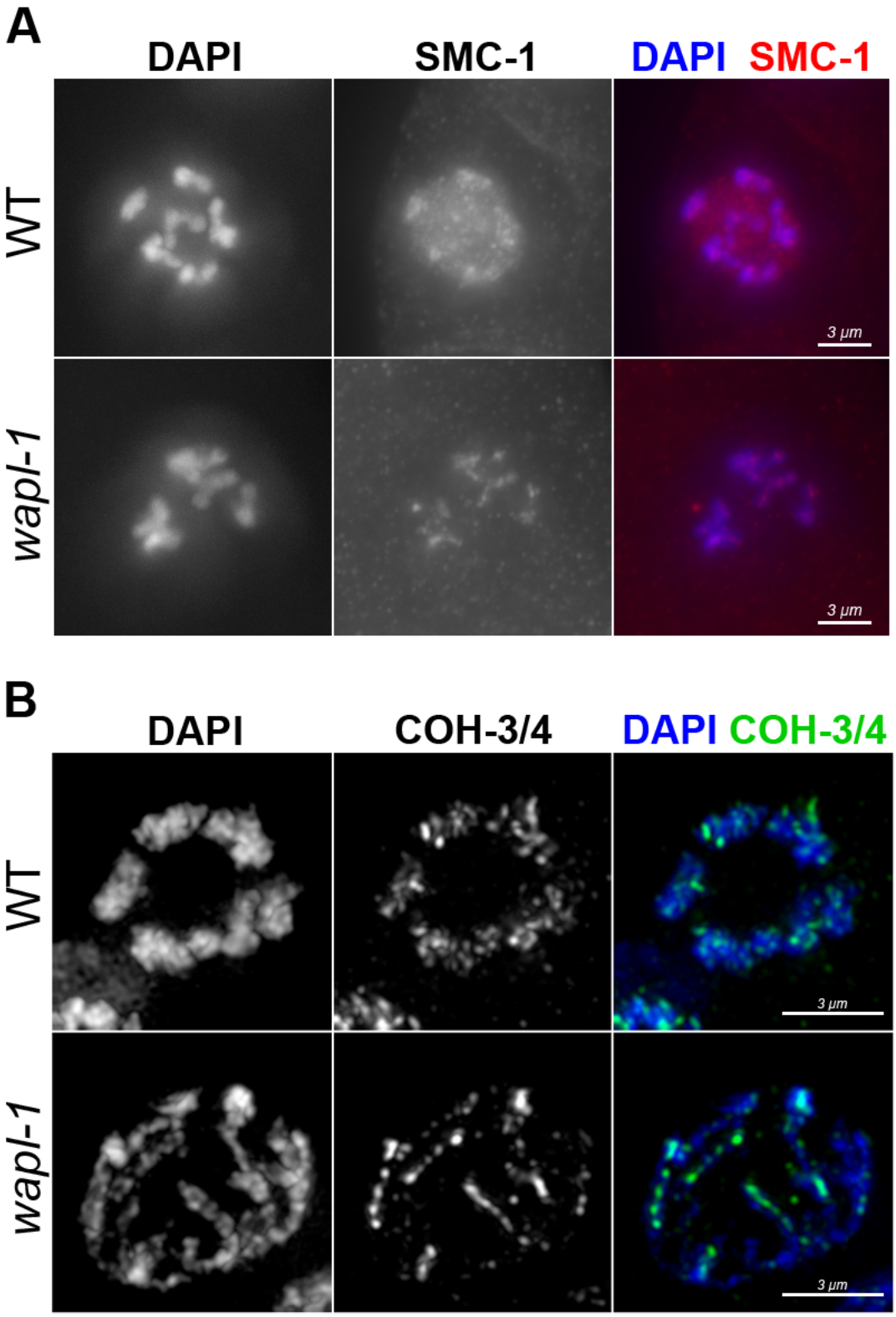
A
DAPI
SMC-1
DAPI SMC-1
WT
wapl-1
3 µm
3 µm
B
DAPI
COH-3/4
DAPI COH-3/4
WT
wapl-1
3 µm
3 µm

Figure 28. SYP-1 and HTP-1 staining confirm delayed remodeling in *wapl-1* mutant

A. Diplotene stage of a wildtype germline stained for α-SYP-1, α-HTP-1 and DAPI. Arrows and letters Ai, Aii & Aiii mark nuclei shown in zoom-in panels in following Figure 29.

B. Diplotene stage of a *wapl-1* mutant germline stained for α-SYP-1, α-HTP-1 and DAPI. Arrows and letters mark nuclei shown in zoom-in panels in following Figure 29.

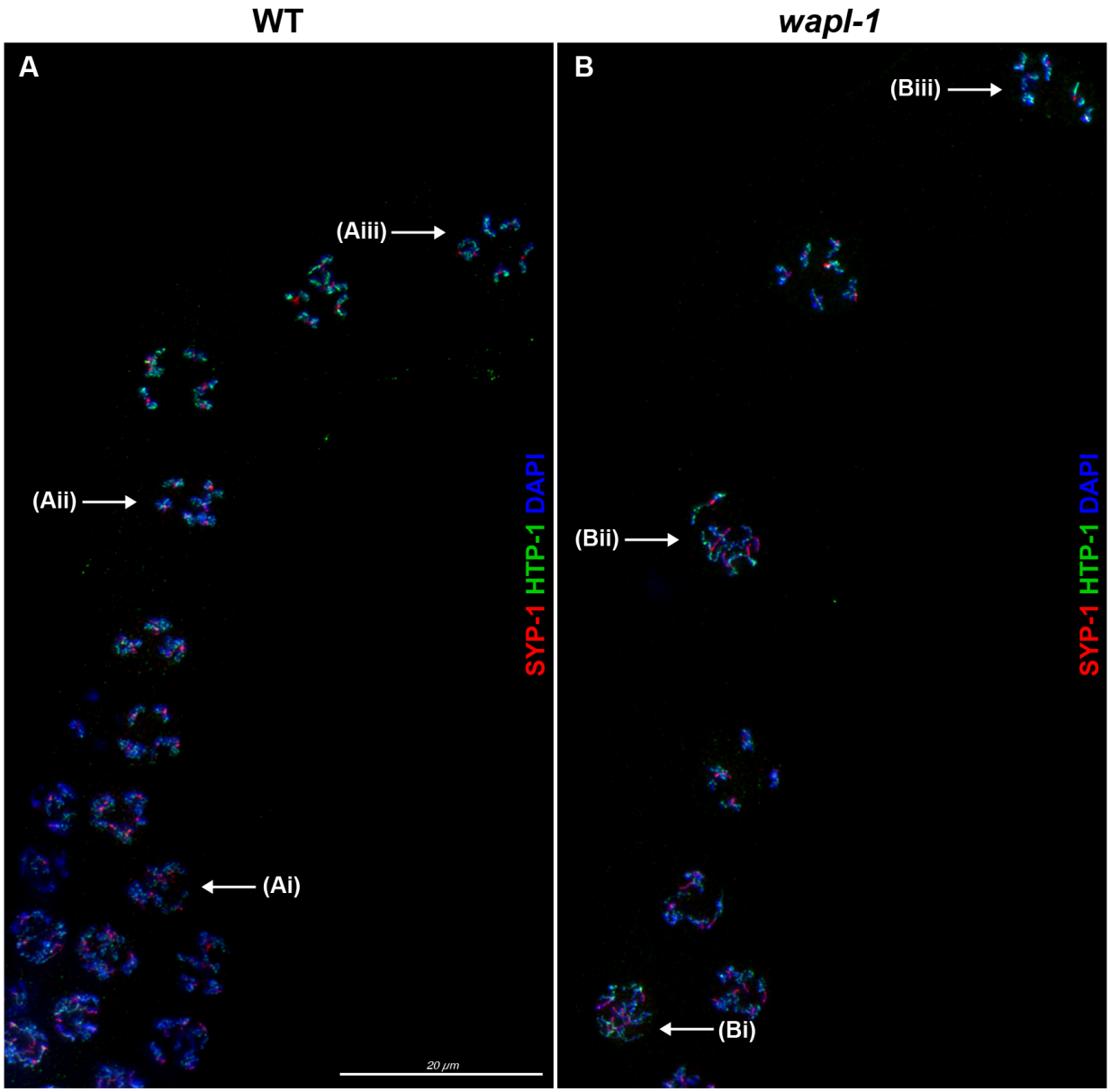
WT
wapl-1
A
B
(Aiii)
(Aii)
(Ai)
(Biii)
(Bii)
(Bi)
SYP-1 HTP-1 DAPI
SYP-1 HTP-1 DAPI
20 µm

Figure 29. SYP-1 and HTP-1 staining confirm delayed remodeling in *wapl-1* mutant (part 2)

Ai. Wildtype early diplotene nucleus stained with α-SYP-1 and α-HTP-1 shows some elongated staining.

Bi. *wapl-1* mutant early diplotene nucleus stained with. SYP-1 shows more extensive elongated/axial pattern than wildtype at early diplotene.

Aii. Mid diplotene wildtype nucleus stained with α-SYP-1 and α-HTP-1. SYP-1 staining appears quite compact, minimal elongation.

Bii. Mid diplotene *wapl-1* mutant nucleus stained with α-SYP-1 α-HTP-1. SYP-1 still shows significantly elongated staining.

Aiii. Late diplotene wildtype nucleus stained with α-SYP-1 and α-HTP-1. SYP-1 appears as very compact foci.

Biii Late diplotene *wapl-1* mutant nucleus stained with α-SYP-1 and α-HTP-1. SYP-1 appears as compact foci, no longer showing elongated staining as seen at mid diplotene.

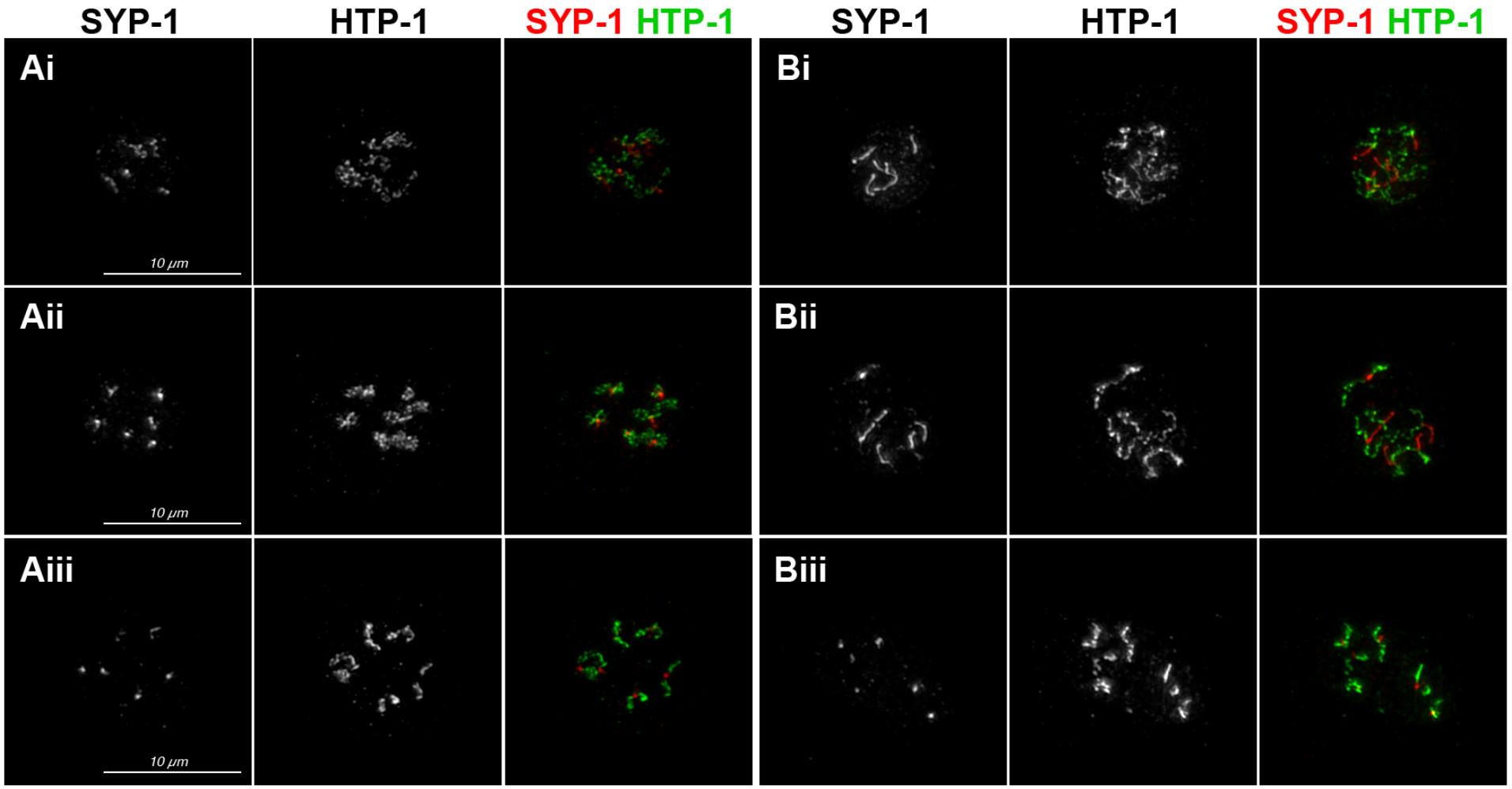
SYP-1
HTP-1
SYP-1 HTP-1
SYP-1
HTP-1
SYP-1 HTP-1
Ai
Aii
Aiii
Bi
Bii
Biii
10 μm
10 μm
10 μm

Figure 30. α-RAD-51 staining in the wildtype and *wapl-1* mutant

A. Wildtype germline from mitotic tip to late pachytene stained for DAPI and α-RAD-51. Lower part shows α-RAD-51 only. Pachytene sub-stages shown in parts C, D and E are marked by arrows.

B. *wapl-1* mutant germline from mitotic tip to late pachytene stained for DAPI and α-RAD-51. Lower part shows α-RAD-51 only. Pachytene sub-stages shown in panels C, D and E are marked by arrows.

C. Early pachytene of wildtype and *wapl-1* mutant stained for DAPI and α-RAD-51. Note the higher number of RAD-51 foci in *wapl-1* mutant.

D. Mid pachytene of wildtype and *wapl-1* mutant stained for DAPI and α-RAD-51. Note the higher number of RAD-51 foci in wapl-1 mutant.

E. Late pachytene panels of wildtype and *wapl-1* mutant stained for DAPI and α-RAD-51. Note similar low numbers of RAD-51 foci are seen in wildtype and the *wapl-1* mutant..

N.B. Deconvovled images.

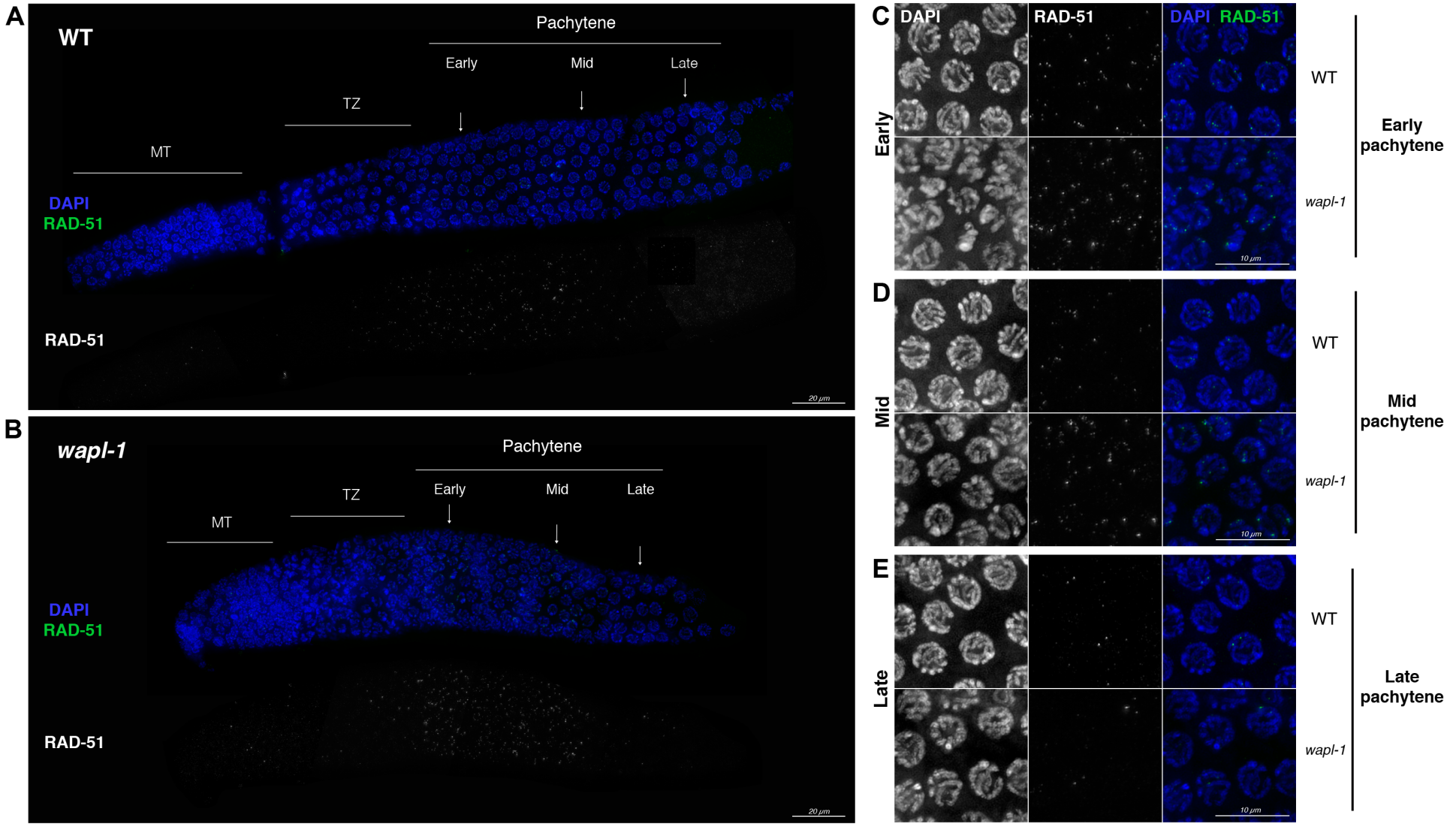
A
WT
Pachytene
Early
Mid
Late
TZ
MT
DAPI
RAD-51
RAD-51
20 μm
B
wapl-1
Pachytene
TZ
Early
Mid
Late
MT
DAPI
RAD-51
RAD-51
20 μm
C
DAPI
RAD-51
DAPI RAD-51
Early
WT
wapl-1
Early pachytene
10 μm
D
Mid
WT
wapl-1
Mid pachytene
10 μm
E
Late
WT
wapl-1
Late pachytene
10 μm

Figure 31. ZHP-3::GFP foci indicate CO number is not affected in *wapl-1* mutant

A. ZHP-3::GFP transgene in the wildtype and *wapl-1* mutant background at late pachytene is visualised by α-GFP staining. DAPI staining is also show (red). A white circle highlights a single nucleus example with six foci. Images are deconvolved.

B. Quantification of ZHP-3::GFP foci in late pachytene/early diplotene stage of wildtype and *wapl-1* mutants. Bar chart displays the percentage of nuclei with number of foci per nucleus. There is a majority of 6 foci per nucleus in both wildtype (97% of 119 nuclei) and *wapl-1* mutant (98% of 124 nuclei).

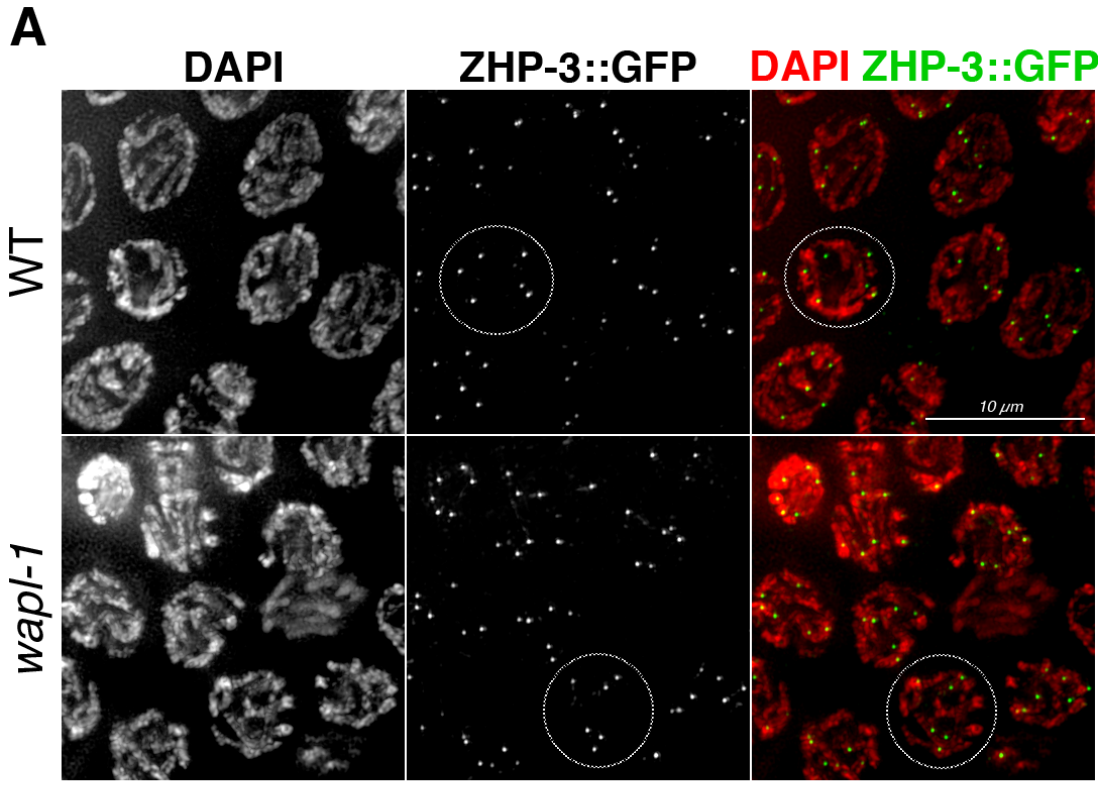
A
DAPI
ZHP-3::GFP
DAPI ZHP-3::GFP
WT
wapl-1
10 µm

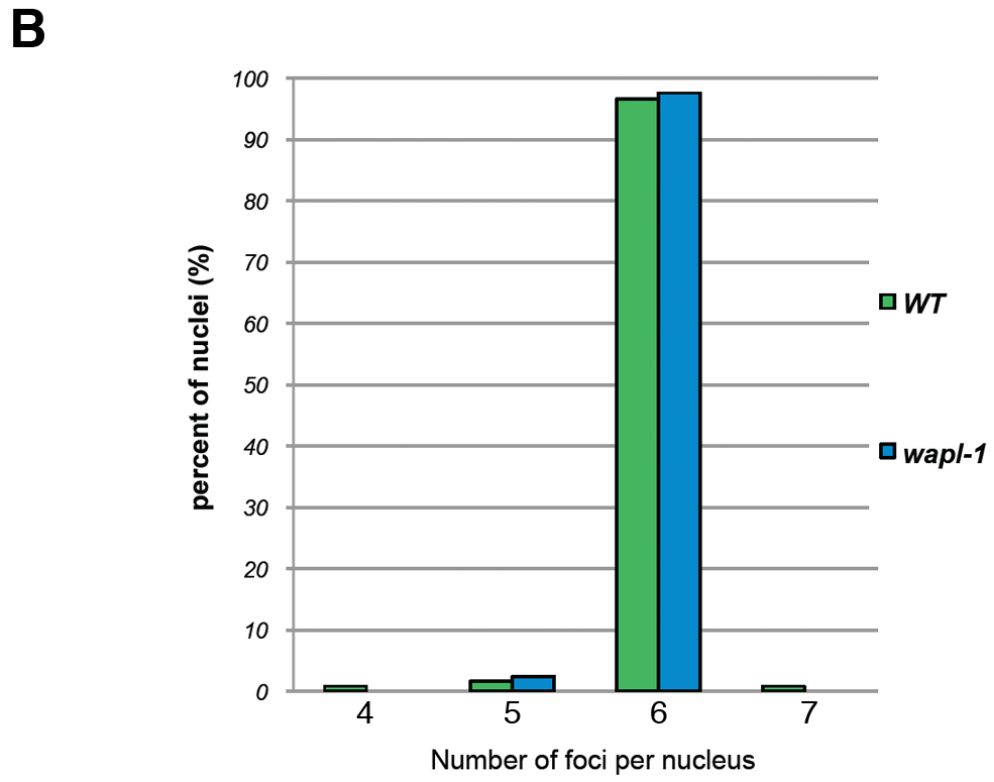
B
100
90
80
70
60
50
40
30
20
10
0
percent of nuclei (%)
4
5
6
7
Number of foci per nucleus
WT
wapl-1

Figure 32. Effect of WAPL-1 on CO distribution

A. Diagram showing genetic crosses carried out to set up the mapping of CO distribution on chromsome II in *wapl-1* mutant background. Males heterozygous for *wapl-1* mutation and homozygous for wildtype (N2) SNPs were obtained by crossing N2 to *wapl-1* balanced worms (F0). These *wapl-1* heterozygous males were crossed to hermaphrodites homozygous for *wapl-1* (*tm1814*) mutation and homozygous for Hawaiian SNPs on chromosome II (F1). Hermaphrodite offspring from F1crosses were mated to normal Hawaiian males (F2). ~50% of F2 hermaphrodites were homozygous *wapl-1* and heterozygous for chromosome II N2/Hawaiian SNPs, as required. Hermaphrodite offspring from appropriate F3 crosses were picked onto individual plates and DNA extracted from starved plate for mapping (F4).

B. Bar chart representing the frequency of crossovers occuring in wildtype (grey) and *wapl-1* mutant (blue) at the genetic interval between two SNPs as a fraction of total chromosomes measured. Interval A = between SNP 1 and SNP 2(-15.9<>-6.23). Interval B = betweeen SNP 2 and SNP 3(-6.23<>+0.5). Interval C = between SNP 3 and SNP 4 (+0.5<>+3.41). Interval D = between SNP 4 and SNP 5 (+4.31<>+27.3).

C. Bar chart representing crossover distributions of wildype and *wapl-1* mutants (same data Figure 32, B) plus expected crossover frequencies from genetic distance (red) and physical distance as a relative ratio of bp distance (green).

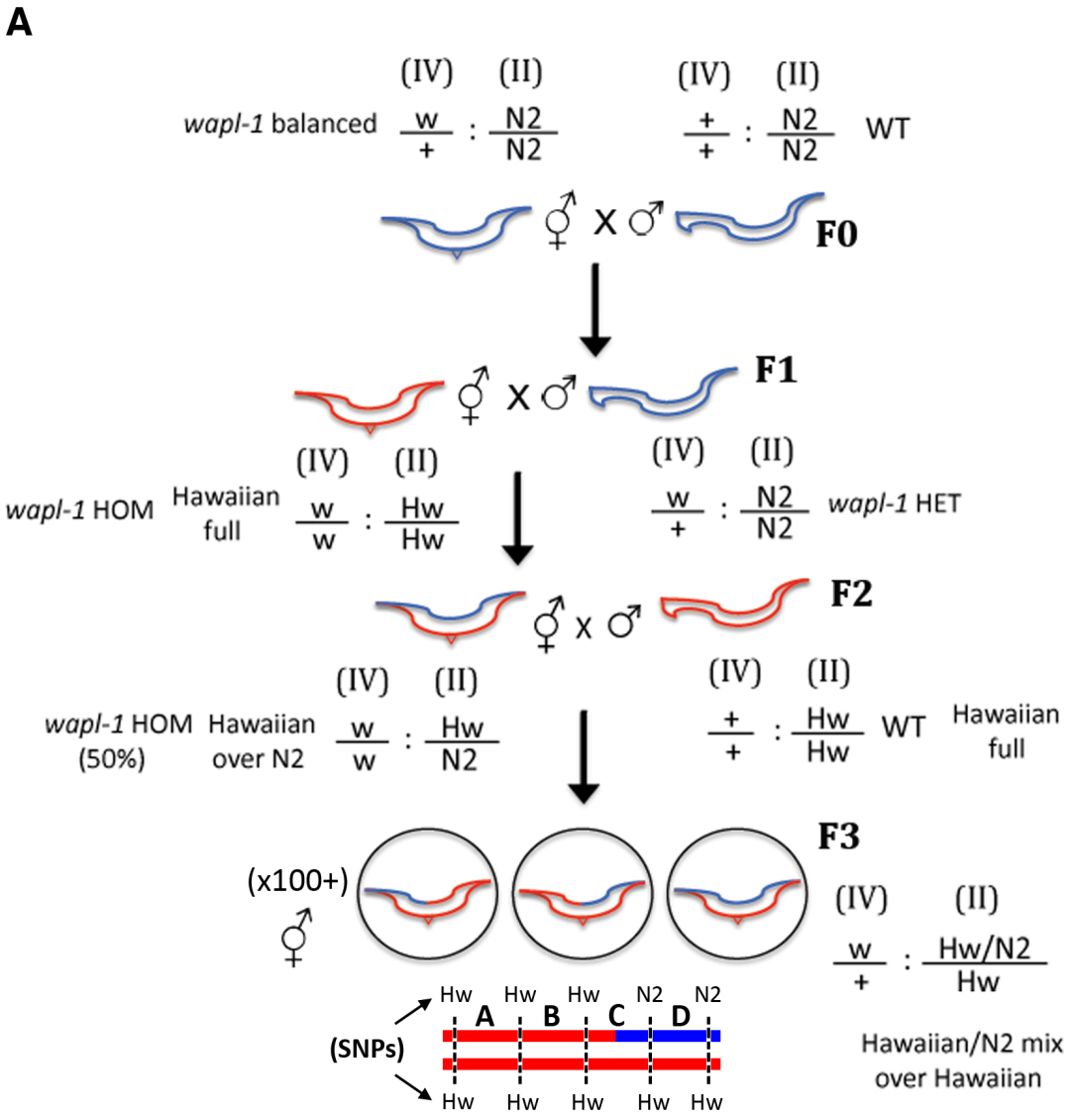
A
(IV) (II)
wapl-1 balanced w/+ : N2/N2
(IV) (II)
+/+ : N2/N2 WT
F0
F1
wapl-1 HOM Hawaiian full
(IV) (II)
w/w : Hw/Hw
(IV) (II)
w/+ : N2/N2 wapl-1 HET
F2
wapl-1 HOM (50%) Hawaiian over N2
(IV) (II)
w/w : Hw/N2
(IV) (II)
+/+ : Hw/Hw WT Hawaiian full
F3
(x100+)
(IV) (II)
w/+ : Hw/Hw
(SNPs)
Hw Hw Hw N2 N2
A B C D
Hw Hw Hw Hw Hw
Hawaiian/N2 mix over Hawaiian

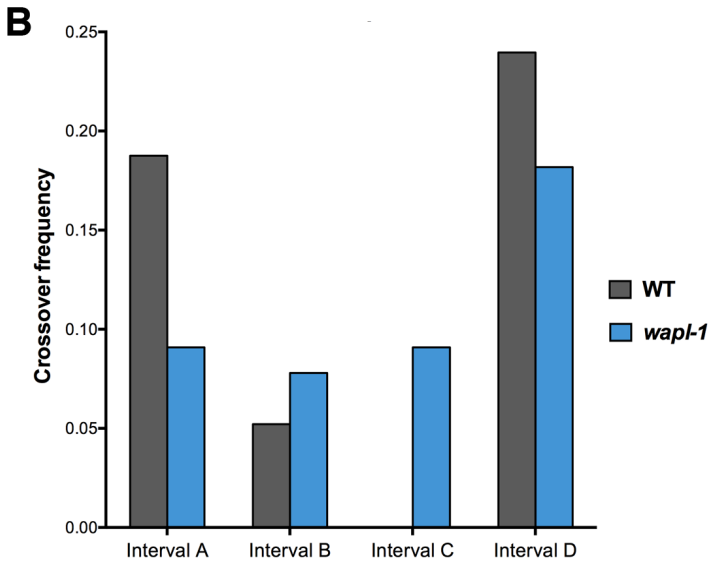
B
Crossover frequency
0.25
0.20
0.15
0.10
0.05
0.00
Interval A
Interval B
Interval C
Interval D
WT
wapl-1

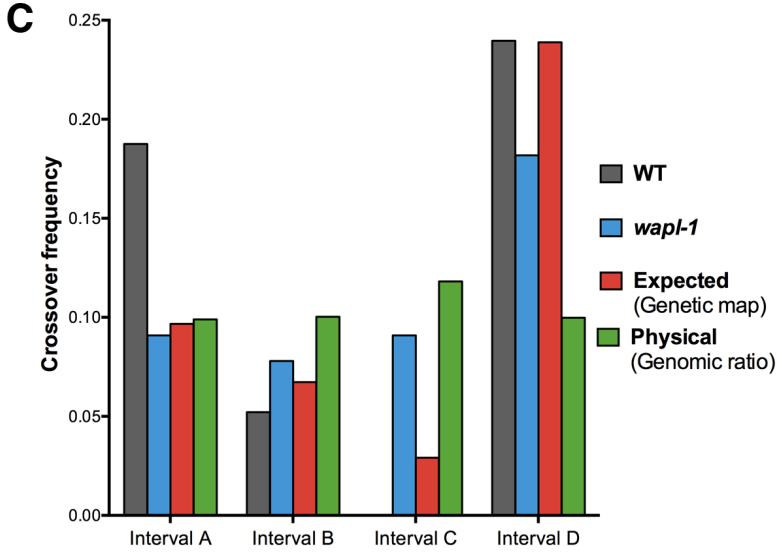
C
Crossover frequency
0.25
0.20
0.15
0.10
0.05
0.00
Interval A
Interval B
Interval C
Interval D
WT
wapl-1
Expected (Genetic map)
Physical (Genomic ratio)

CHAPTER 4: RESULTS

EFFECT OF WAPL-1 ON COHESION DURING MEIOTIC PROPHASE

4.1 Objectives

The cohesin complex plays roles in a range of processes during meiosis, including DSB response and repair, synapsis, and chromosome condensation and remodeling (Lightfoot et al. 2011; McNicoll et al. 2013), some of which have been investigated in chapter 3 and by other members of our laboratory. However, the cannonical function of cohesin during meiosis is to provide cohesion (Petronczki et al. 2003), as it is in mitosis. The results presented in chapter 3 demonstrate that WAPL-1 appears to negatively regulate the amount of cohesin bound to chromosomes, and that in the absence of WAPL-1 defects in DNA repair, chromosome remodeling and chromosome segregation are evident during meiosis. However, the previous chapter did not explore how WAPL-1 affects SCC during meiotic prophase, and a main aim of this work was to test whether whether WAPL-1 regulates the "cohesiveness" of the different meiotic cohesin complexes during prophase. In order to achieve this, I investigated the effect of WAPL-1 in genetic backgrounds in which cohesion is compromised to different extents. I also aimed to investigate whether the worm homologue of ECO1, the factor that acetylates SMC-3 and is required to establish SCC in mitosis, has any function in meiotic cohesion.

4.2 Genetically compromised meiotic cohesion can test for WAPL-1 cohesion role

C. elegans is particularly amenable for the investigation of meiotic SCC, since nuclei at all meiotic stages are present as a temportal/spatial gradient in each germ line. Moreover, although worms have a pachytene checkpoint that triggers apoptosis of nuclei with defects in DSB repair or synapsis, this checkpoint is leaky and therefore some defective nuclei keep progressing through meiotic prophase, meaning that SCC defects can be assessed at all meiotic stages. This is important because defects in SCC are more easily

detected in diakinesis oocytes, when the strong chromosome condensation, and the separation of chromosomes inside the nucleus allow an easy evaluation of cohesion. Most experiments in this chapter are focused on the final two oocytes of the germ line (-1 and -2 diakinesis).

In order to assess whether WAPL-1 is limiting cohesion at all during meiosis in *C. elegans* it was necessary to identify a situation where cohesion is actually clearly compromised, since cohesion is very robust in wild type oocytes. A key requirement of a genetic background for this experiment to test whether cohesion is being limited by WAPL-1 is that cohesion is theoretically possible, such that all components of an intact cohesin ring are present, genetically at least. This is made easier by the fact that multiple meiotic kleisin exist in *C. elegans*, as they do in humans, so different versions of the cohesin ring can exist differing on their kleisin subunit (Pasierbek et al. 2001; Bannister et al. 2004; Severson et al. 2009; Gutierrez-Caballero et al. 2011; Herran et al. 2011; Ishiguro et al. 2011). However, unless all three meiotic kleisins are absent from otherwise normal worms there is no clear-cut cohesion loss. The *rec-8* single mutant displays a complete failure in inter-homologue crossover formation, but only partial cohesion defects, with sister chromatids remaining loosely attached at diakinesis (Pasierbek et al. 2001). DAPI staining of diakinesis oocytes in *rec-8* mutants reveals 12 distinct bilobed chromatin bodies, with occasional small fragments (Figure 33 A). Single mutants of the other two meiotic kleisins (COH-3 and COH-4) do not display obvious meiotic defects, however *coh-3; coh-4* double mutants display a lack of chiasmata, but no defects in SCC (Severson et al. 2009). DAPI staining of diakinesis oocytes in *coh-3; coh-4* double mutants reveals 12 compact chromatin bodies (univalent) that are morphologically indistinguishable from other crossover deficient mutants (Figure 35). Previous studies have shown that combining mutations in *rec-8* with mutations in other non-cohesin genes, such as *spo-11* or SC components, leads to a severe impairment in SCC in diakinesis oocytes (Colaiacovo et al. 2003; Severson et al. 2009). Since COH-3/4 cohesin complexes remain intact in these genetic backgrounds, they provide a genetic tool to test if WAPL-1 affects meiotic cohesion.

4.2.1 WAPL-1 antagoinizes cohesion in *rec-8 spo-11* double mutants

Double mutants for *rec-8* and the endonuclease *spo-11* (*ok79*) which catalyzes the formation of meiotic DSBs, were shown to have full separation of sister chromatids in

diakinesis oocytes (Severson et al. 2009). A very recent study suggests that the defect in cohesion of *rec-8 spo-11* double mutants is due to the fact that cohesion provided by COH-3/4 cohesin complexes requires DSB-dependent phosphorylation of COH-3/4 (Severson et al. 2009; Severson and Meyer 2014). Nevertheless, *rec-8 spo-11* double mutants provide an ideal tool to test if WAPL-1 affects meiotic cohesion. The *wapl-1* (*tm1814*) mutation was crossed to the *rec-8* and *spo-11* mutations to create a single recombined chromosome IV with all three mutations. DAPI staining to visualize chromatin in diakinesis oocytes clearly shows that *wapl-1; spo-11; rec-8* triple mutants have a rescue of the cohesion defect seen in *rec-8 spo-11* double mutants (Figure 33 A). The number and shape of chromatin bodies in *wapl-1; spo-11; rec-8* triple mutants much more closely resembles the *rec-8* single mutant that than the *spo-11; rec-8* double. This cohesion rescue was strikingly penetrant, with no oocytes appearing to contain more than 12 chromatin bodies. Diagrams below each panel highlight the cohesion phenotype in the example oocytes. Quantification of this rescue by manually counting the bodies in 3D in many oocytes is represented in the bar chart in Figure 33 B. Average number of DAPI-stained bodies per oocyte is ~19 in *spo-11; rec-8* and ~11 in *wapl-1; spo-11; rec-8* which approaches the theoretical 24 individual chromatids and 12 sets of cohesive sister chromatids respectively. A *t*-test gave an extremely significant difference between the two genotypes. Experiments in our laboratory using FISH (performed by Sarah Testori) confirmed that the reduction in DAPI-stained bodies in diakinesis oocytes of *wapl-1; spo-11; rec-8* triple mutants is indeed due to rescued cohesion between sister chromatids. These results show that WAPL-1 limits cohesion during meiotic prophase, likely by antagonizing the cohesive function of cohesin complexes containing COH-3/4. This conclusion is because COH-3/4 are the available meiotic kleisin subunits, with REC-8 absent, and furthermore experiments shown in chapter 3 demonstrate that chromosome association of COH-3/4 is limited by WAPL-1.

4.2.2 WAPL-1 antagoinizes cohesion in *rec-8 syp-1* double mutants

The cohesion rescue seen by removing WAPL-1 from *spo-11 rec-8* double mutants is quite convincing, but since DSBs are an essential part of the meiotic program, it was important to test whether WAPL-1 could limit cohesion in the presence of DSBs. Another genetic background that has been observed where cohesion is very compromised but DSBs are present is a combination of mutations in *rec-8* and a synaptonemal complex central element (Colaiacovo et al. 2003; Severson and Meyer 2014). *syp-1* (*me17*)*; rec-8* double

mutants display severe chromosome fragmentation in diakinesis oocytes, indicating major problems in chromosome stability, despite the fact that COH-3 and COH-4 are present in this background and so intact rings are potentially available (Figure 34 A). This background makes an ideal genetic tool to test WAPL-1 functionality in the presence of DSBs. Crossing the *wapl-1* mutation onto this background dramatically and consistently rescued the chromosome fragmentation defect, and results in diakinesis oocytes that much more closely resemble *rec-8* single mutants (Figure 34 A).

The complex fragmentation phenotype of the *syp-1; rec-8* mutant is difficult to manually quantify due to the high numbers and small size of the DAPI-stained bodies, as well as the presence of some larger masses with unclear boundaries. So to quantify the differences I developed an automated quantification pipeline with a combination of Image J and Cell Profiler software to identify and measure distinct bodies from the DAPI-stained diakinesis oocytes (see 4.3 for set up). Examples are shown with outlines of bodies identified with the pipeline in Figure 34 B. The analysis had to be run on 2D projections of Z-stacks and so due to overlap the absolute number of bodies does not give such a representative readout, however the exact area size of all identified bodies is known and the distribution of sizes gives a very good representation of the phenotype. The area sizes were sorted into area categories with ranges that correspond to different types of chromosome bodies: chromosome fragments, individual sister chromatids, univalents (attached sisters but no crossovers), bivalents (homologous pairs attached by a crossover) and clusters (overlapping, indistinguishable, entangled or ligated combinations of the other types). Figure 34 C shows a frequency histogram of many bodies grouped from multiple oocytes of either genotype and demonstrates the difference in distribution of sizes from *syp-1; rec-8* to the *wapl-1; syp-1; rec-8* rescue. The most common category (modal) shifts from fragments to univalents in the rescue genotype, replicating the qualitative observations of individual oocytes. The fragments category drops from 49% of bodies to 11% in the rescue background, ~78% decrease. While the univalents category increases from 16% to 48% of bodies in the rescue background, ~200% increase. This clearly demonstrates that WAPL-1 is also limiting cohesion in the presence of DSBs.

4.2.3 Loss of WAPL-1 improves weakened cohesion of *rec-8* mutants

It is clear from the experiments shown above that WAPL-1 is actively limiting some cohesive function during meiotic prophase, but it was important to determine if the effect

of WAPL-1 on cohesion can be assessed in a less compounded and less severe background than *rec-8; spo-11* or *rec-8; syp-1*. As noted in chapter 1, diakinesis oocytes of *rec-8* single mutant contain bilobed univalents with sister chromatids weakly attached to each other and occasional small fragments. The chromatin connection between sisters very often appears minimal, so the univalent are seen as two balls of chromatin sitting next to each other. Thus, *rec-8* single mutants offer a genetic background to test whether WAPL-1 can improve a more subtle weakening of cohesion. Indeed the *wapl-1; rec-8* double mutant does seem to have univalents that are less bi-lobed and chromatids that are more closely associated (Figure 36 A). However, the phenotype seemed to be slightly variable so to try to quantitatively assess this improvement, many images were taken of both genotypes and processed with the automated analysis pipeline. The quite conservatively defined parameters result in the bi-lobed univalents of *rec-8* mutant being predominantly resolved as separate bodies, while the univalents of the *wapl-1; rec-8* double are more often identified as single continuous body (Figure 36 B). The frequency histogram in Figure 36 C produced from >60 oocytes of each genotype demonstrates this improvement in cohesion. Although inspection of the images also gives the impression of slightly reduced number of small fragments this was not represented in the frequency histogram.

4.3 Set up of automated analysis parameters and area categories

The size ranges and the parameters for the analysis software described in the previous sections were defined by informed measurements and empirical adjustment using control genotypes of known typical chromosome phenotype and cohesion status (see Figure 35). A relatively good set of parameters and size ranges were found, which scored the expected category (chromosome fragments, sister chromatids, univalent or bivalents) of each genotype as the most common (47% or over) chromatin body area size. There are several reasons why the different genotypes are not perfectly grouped by the analysis. There are some inherent geometric problems from 2D analysis of 3D stacks that will be discussed later. Also the actual phenotype of the *syp-1; rec-8* genotype clearly has a mixture of chromatin bodies ranging from fragments to large aggregated masses, as well as the universal fact that any bodies that are not biologically attached can stochastically be in very close spatial proximity at the moment of fixation, as chromosomes are mobile.

The analysis appears to be sufficient to graphically represent some clear differences between different cohesion phenotypes from a dataset series of images.

4.4 Improved cohesion by removal of WAPL-1 depends on COH-3 and COH-4

The rescue of cohesion defects in *wapl-1; rec-8, spo-11* and *wapl-1; rec-8; syp-1* mutants, suggest that WAPL-1 antagonizes cohesion provided by cohesin complexes containing the remaining known meiotic kleisins COH-3 or COH-4. However, it was essential to definitively demonstrate this by testing if removal of COH-3 and COH-4 from the triple mutants would cause cohesion defects. Mutations in *coh-3* and *coh-4* genes were crossed into the *wapl-1; spo-11; rec-8* background to make a quintuple mutant and as expected separation of sister chromatids was restored to diakinesis oocytes (Figure 37 A). Although many separated sisters were always seen in oocytes of the quintuple mutant, the overall number of DAPI bodies seemed a bit lower than in *spo-11; rec-8* double mutant and some occasional clumping of several sister-sized bodies was detected. Many images of the three genotypes shown in Figure 37 A were put through the automated analysis for an unbiased quantification. The frequency histogram of these analyses clearly shows that the modal area size category shifts back from 45% univalents in the triple to 56% sisters in the *coh-3; coh-4; wapl-1; spo-11; rec-8* mutant confirming that the cohesion rescue is largely dependent on COH-3 and COH-4 (Figure 37 B). The fact that the percentage of sisters does not reach the 69% seen for the *spo-11; rec-8* seems largely due to the occasional occurrence of clumps of more than two chromatids that are identified as bivalents or clusters and disproportionately reduce the sister category.

Two other experiments that are not shown in figures support the idea that both COH-3 and COH-4 are targets of WAPL-1. Firstly, a quadruple mutant was isolated of *coh-3; wapl-1; spo-11; rec-8* with COH-4 not mutated that mostly looks like the *wapl-1; spo-11; rec-8* triple mutant, only occasionally displaying separated sister chromatids. Secondly, a transgene containing COH-3::mCherry was crossed onto the *coh-3; coh-4; wapl-1; spo-11; rec-8* quintuple background and this reverts back to a phenotype of mostly intact cohesion at diakinesis with occasionally more than 12 univalents, similar to the *coh-3; wapl-1; spo-11; rec-8* quadruple mutant. The fact that in both these cases there is some occasional loss of cohesion occurs also reveals a limit to the redundancy of COH-3 and COH-4.

4.5 Cohesin staining at late pachytene correlates with WAPL-1 cohesion rescue

It is clear from the experiments shown in chapter 3 that the loss of WAPL-1 from otherwise wildtype background causes an increase in the amount of cohesin associated with chromosomes, most strikingly at late pachytene. It was of natural interest to find out whether the improvements in cohesion described in previous sections of this chapter correlate with similar increases in the levels of cohesin on chromosomes in these multiple mutant backgrounds as might be logically expected. Since all the genetic backgrounds that we used for the cohesion rescue experiments lacked REC-8, we decided to focus on the staining pattern of COH-3/4. In fact, the findings from both the immunofluorescence and cohesion experiments point to COH-3/4 as the main target of WAPL-1 activity. It would of course be interesting to compare cohesin staining in the same diakinesis nuclei where cohesion phenotypes were scored. However, poor efficiency and reliability of staining at the later stages with the available antibodies meant that comparison of levels at diakinesis were not practical. Furthermore, comparison with the findings in other experiments shown in chapter 3 was desirable, so I decided to focus the analysis on late pachytene nuclei. It was also clear from the expression pattern of GFP::WAPL-1 along the germline and the cohesin immunofluorescence quantification that late pachytene nuclei contain the largest concentration of WAPL-1, suggesting important activity of the protein at this stage.

4.5.1 Association of COH-3 with chromosomes in *wapl-1; spo-11; rec-8*

The most convincing demonstration that WAPL-1 affects COH-3/4 function is the dependency on COH-3/4 of the cohesion rescue seen in *wapl-1; spo-11; rec-8*. α-COH-3 immunofluorescence on *wapl-1; spo-11; rec-8* germ lines found that the COH-3 signal associated with axial elements at late pachytene is stronger compared with the *spo-11; rec-8* (Figure 38). This suggests that the levels of cohesin associated with chromatin in late pachytene give an indication of its cohesive function, as it has been shown in mitotic cells (Gandhi et al. 2006; Kueng et al. 2006; Shintomi and Hirano 2009). Thus, WAPL-1 may be limiting the cohesive ability of COH-3/4 cohesin complexes in the *spo-11; rec-8* mutant by reducing their stable association with chromatin. As expected, the *wapl-1; spo-11; rec-8; coh-3; coh-4* mutant has blank staining for α-COH-3, supporting the prediction

that the *coh-3* (*gk112*) mutation is effectively a null allele, which was also confirmed by Western blot (data not shown).

4.5.2 *wapl-1; syp-1; rec-8* mutants display increased COH-3/4 staining on late pachytene chromosomes

It was important to determine whether the correlation between cohesion phenotype, as assessed in diakinesis oocytes, and the cohesin staining in late pachytene nuclei also applied in other situations where compromised cohesion is rescued by loss of WAPL-1. As with the cohesion rescue itself, it is especially important to see if this correlation occurs when DSBs are taking place and hence a situation more analagous to wildtype meiosis. α-COH-3/4 immunofluorescence shown in Figure 39 A demonstrates that COH-3/4 staining in axial elements is far stronger in late pachytene nuclei of *wapl-1; syp-1; rec-8* compared to *syp-1; rec-8*. The corresponding representative cohesion status at diakinesis can be seen in the same row, as is fully demonstrated in Figure 34. This result is similar to the situation in the *wapl-1; spo-11; rec-8*, however, the extent of WAPL-1's effect on distribution seems to to be far greater in this case because overall nuclear levels of COH-3/4 are significantly higher. Comparing merged channel panels, the *syp-1; rec-8* nuclei have a quite blue appearance with minimal contribution from the red channel, while nuclei of the *wapl-1; syp-1; rec-8* appear much more pink in colour with a greater contribution from the red channel. Mean nuclear fluorescence was not quantified but images shown are representative. Similar results were obtained using the α-COH-3 antibody.

4.5.3 *wapl-1; rec-8* mutants display increased COH-3 staining on late pachytene chromosomes

Another genetic background in which I wished to investigate if loss of WAPL-1 results in increased COH-3 staining was the *rec-8* mutant. COH-3 is clearly more enriched on chromosomes in late pachytene nuclei of *wapl-1; rec-8* compared to *rec-8* mutants, demonstrating again a correlation between the amount of COH-3 cohesin seen at late pachytene and improved cohesion in diakinesis oocytes (Figure 39 B). Furthermore, a strong overall increase in COH-3 nuclear levels is observed in the *wapl-1; rec-8* mutant, similar to the *wapl-1; syp-1; rec-8* rescue. In the same way, this effect is especially evident in the merged panel where the intensity of the red channel (COH-3) is much brighter,

giving a pinker overall color to the *wapl-1; rec-8* mutant. The mean nuclear fluorescence intensity was not quantified but the images shown are representative of the average phenotype from multiple germ lines.

Interestingly, removal of WAPL-1 from *rec-8* and *rec-8 syp-1* resulted in much higher levels of COH-3 staining than when WAPL-1 is removed from *spo-11 rec-8*, suggesting that DSBs may influence the amount of COH-3 bound to axial elements. Thus, DSBs may be somehow regulating the extent to which WAPL-1 affects the levels of axis-associated cohesin.

4.5.4 Effect of WAPL-1 on cohesion and COH-3 staining *in coh-4; rec-8* double mutants

COH-3 and COH-4 appear to be functionally redundant, as evidenced by the fact that *coh-3 coh-4* double mutants display a crossover failure, while *coh-3* and *coh-4* single mutants appear wildtype (Severson et al. 2009). However, I found that removal of REC-8 (using the *rec-8* mutation) from the *coh-4* single mutant induced major cohesion defects in diakinesis oocytes (Figure 38). The same phenotype was seen in the *rec-8; coh-3* double mutant (data not shown). Strikingly, the genetic loss of WAPL-1 from these compromised backgrounds results in strong improvements in cohesion at diakinesis, with few fragments and ~12 continuous equal-sized DAPI stained bodies. α-COH-3 immunofluorescence in late pachytene nuclei of *wapl-1; coh-4; rec-8* triple mutant found a significant increase in the amount of axis-associated COH-3 staining compared to *coh-4; rec-8* (Figure 40). These results provide further support for the idea that WAPL-1 regulates COH-3/4 binding to chromosomes, and that DSBs also contribute to this regulation.

4.6 WAPL-1 expressed from transgenes show meiotic anti-cohesive function

To further support the finding that WAPL-1 limits SCC during meiosis, the two transgenes expressing WAPL-1 protein, mentioned in chapter 3, were crossed to the *wapl-1; spo-11; rec-8* triple mutant background. In this triple mutant, absence of endogenous WAPL-1 results in a complete rescue of SCC at diakinesis, with ~12 univalent bodies compared to ~24 separated sister chromatids in the *spo-11; rec-8*. If the WAPL-1 transgenes are

meiotically functional then the SCC rescue at diakinesis should be abolished. As expected, a clear 'de-rescue' was seen when both GFP::WAPL-1 and WAPL-1 (no tag) transgenes were crossed into the *wapl-1; spo-11; rec-8* triple mutant background (Figure 41 A). In both these instances the diakinesis oocytes consistently show separation of sister chromatids with much greater than 12 DAPI stained bodies, appearing to be much more similar to the *spo-11; rec-8* double mutant. To confirm this result, images of all four of the following genotypes were analysed with the automated pipeline: a) *spo-11; rec-8*, b) *wapl-1; spo-11; rec-8*, c) GFP::WAPL-1; *wapl-1; spo-11; rec-8* and d) WAPL-1 (no tag); *wapl-1; spo-11; rec-8.* The frequency histograms of these four genotypes are displayed in Figure 41 B. Both genotypes with the transgenes have a clear modal area size category of 'sisters' and overall patterns of distribution are similar to the *spo-11; rec-8* double mutant. t-tests confirm that that the distributions are changed by the presence of the WAPL-1 transgenes ($p = <0.0001$). This again demonstrates that WAPL-1 protein limits the SCC provided by COH-3/4 during meiosis. Furthermore, this confirms the meiotic function of WAPL-1 transgenes and supports the validity of other experiments performed with these transgenes.

4.7 SMC-3 acetylation on meiotic cohesin

In mitosis a fundamental step in establishing cohesion is the acetylation of conserved lysine residues in the SMC-3 subunit by Eco1 acetyltransferase (Unal et al. 2008; Zhang et al. 2008b). It has been well demonstrated that this post-translational modification of cohesin is largely required for the purpose of conferring resistance to WAPL-1 (Chan et al. 2012; Lopez-Serra et al. 2013). The role of Eco1 in meiosis is largely unknown although there was a study this year that demonstrated that loss of Eco1 from Drosophila meiotic cells after they have entered meiosis causes defects in SC structure, lack of CO maintenance and segregation problems (Weng et al. 2014). There is one clear orthologue of Eco1 in *C. elegans* called *F08F8.4* but there is no evidence of it having been studied. We obtained an 318 bp deletion allele of *F08F8.4* generated by the National Bioresource Project called *tm5441*. The homozygous mutants of *tm5441* are highly sterile and sick, indicative of developmental problems. However, surprisingly in over 100 worms observed there appeared to not be any loss of cohesion or lack of COs indicated by any greater than 6 bodies at diakinesis. This very preliminary observation suggested that *F08F8.4* may not be required for meiotic SCC or CO formation/maintenance in *C. elegans*.

Unfortunately we did not have an anti-ECO-1/ F08F8.4 antibody to check by Western blot or IF whether the *tm5441* allele is a null. Interestingly, preliminary experiments observed some rescue of the sterility seen in the *tm5441* (*F08F8.4*) mutants by the addition of the *wapl-1 tm1814* mutation to the background, though this could arise from the mitotic roles of WAPL-1.

Unfortunately attempts were unsuccessful to raise an antibody to recognize acetylation of *C. elegans* SMC-3 at the conserved lysines. Furthermore, attempts to make transgenic lines with an acetyl mutant or mimic at the conserved lysines were also unsuccessful due to the very large size of the SMC-3 gene in *C. elegans*. Further work is clearly needed to determine whether acetylation of SMC-3 and Eco1 are important in *C. elegans* meiotic cohesin regulation.

4.8 Summary of results

In this chapter it has been clearly demonstrated that WAPL-1 limits SCC during meiotic prophase. Various mutant genetic backgrounds with compromised SCC, both with and without DSBs, show significant improvement at diakinesis when combined with the *wapl-1* mutation. This suggests that WAPL-1 may be antagonising meiotic SCC irrespective of DSB events and therefore may be limiting SCC not just in these compromised backgrounds but also in wildtype meiosis. It was demonstrated that WAPL-1 dependent SCC rescue is specifically provided by COH-3 and COH-4. Furthermore, all the SCC compromised backgrounds identified involve the loss of REC-8 and while COH-3/4 are present. This strongly indicates that the anti-cohesion activity of WAPL-1 targets cohesin complexes containing COH-3/4 but not those with REC-8. This finding is in agreement with the results in chapter 3 showing WAPL limits the association to chromosomes of cohesin complexes containing COH-3/4 but not REC-8. Results in this chapter also show increases in the association of COH-3/4 with the chromosome axis in the SCC rescued backgrounds lacking WAPL-1. Together these findings indicate that WAPL-1 specifically limits the stable association of cohesin complexes containing COH-3/4 and thereby severely limits their ability to provide SCC. While cohesin complexes containing REC-8 are insensitive to WAPL-1 activity. This fundamental difference in the sensitivity of different meiotic cohesin complexes to WAPL-1 may be important for their known functional divergence (Pasierbek et al. 2001; Severson et al. 2009). Preliminary investigation into whether SMC-

3 acetylation and Eco1 affect meiotic SCC was not conclusive but further study will reveal the exact mechanism by which WAPL-1 antagonises COH-3/4 during meiosis.

Table 5. Summary of phenotypes described in chapter 4

Strain/mutant	Pachytene chromatin	Diakinesis phenotype	COH-3/4 pachytene loading
Wild type (N2)	Thick organised tracks, homologues synapsed	Six DAPI bodies comprised of homologues linked by COs together with SCC	Loaded in axial tracks with some nucleoplasmic protein
rec-8	Relatively organized tracks	12 bi-lobed univalents with sister chromatids weakly attached and some small fragments	Loaded in thin axial tracks
spo-11; rec-8	Relatively organized tracks	~24 separated sister chromatids. Loss of SCC	Loaded in thin axial tracks
wapl-1; spo-11; rec-8	Compact thick tracks	12 univalents of continuous DAPI bodies. Rescue of SCC	Loaded in thick, defined axial tracks. Reduced nucleoplasmic staining
syp-1; rec-8	Very thin disorganized tracks	Mixture of many small fragments and chromatin aggregates and long threads. Separated sisters	Loaded in thin discontinuous tracks
wapl-1; syp-1; rec-8	Compact thick tracks	12 univalents of continuous DAPI bodies. Rescue of SCC and fragmentation	Loaded in thick, defined axial tracks. Reduced nucleoplasmic staining. Brighter overall staining
wapl-1; rec-8	Compact thick tracks	12 univalents of quite continuous DAPI bodies. Improvement in SCC.	Loaded in defined tracks, reduced nucleoplasmic and brighter overall staining
coh-3; coh-4; wapl-1; spo-11; rec-8	Very thin disorganized tracks	~24 separated sister chromatids. Loss of SCC	No COH-3/4 staining as mutant for both genes
GFP::WAPL-1 (& no tag); *wapl-1; spo-11; rec-8*	Relatively organised tracks	~24 separated sister chromatids. Loss of SCC	_Loaded in axial tracks, like wildtype, but <u>not</u> thick and defined

Figure 33. Loss of WAPL-1 rescues SCC defect in *spo-11; rec-8* mutant backround

A. Diakinesis oocytes of the *rec-8* single, *spo-11; rec-8* double and *wapl-1; spo-11; rec-8* triple mutants stained with DAPI. Images are projections of deconvolved files. Below each oocyte is a diagram depicting a model of the chromatin bodies for each genotype, presence of SCC is represented by a yellow band. Homologues are of the same colour and can be seen as separated individual sister chromatids or as univalents with sisters attached.

B. Bar chart showing mean number of distinct DAPI bodies per diakinesis oocyte in *spo-11; rec-8* (mean=19.1, n=94) and *wapl-1; spo-11; rec-8* (mean=11.2, n=85). Bodies were manually counted in 3D. (P value **** = 1.2×10^{-21}, t-test). Error bars = SEM.

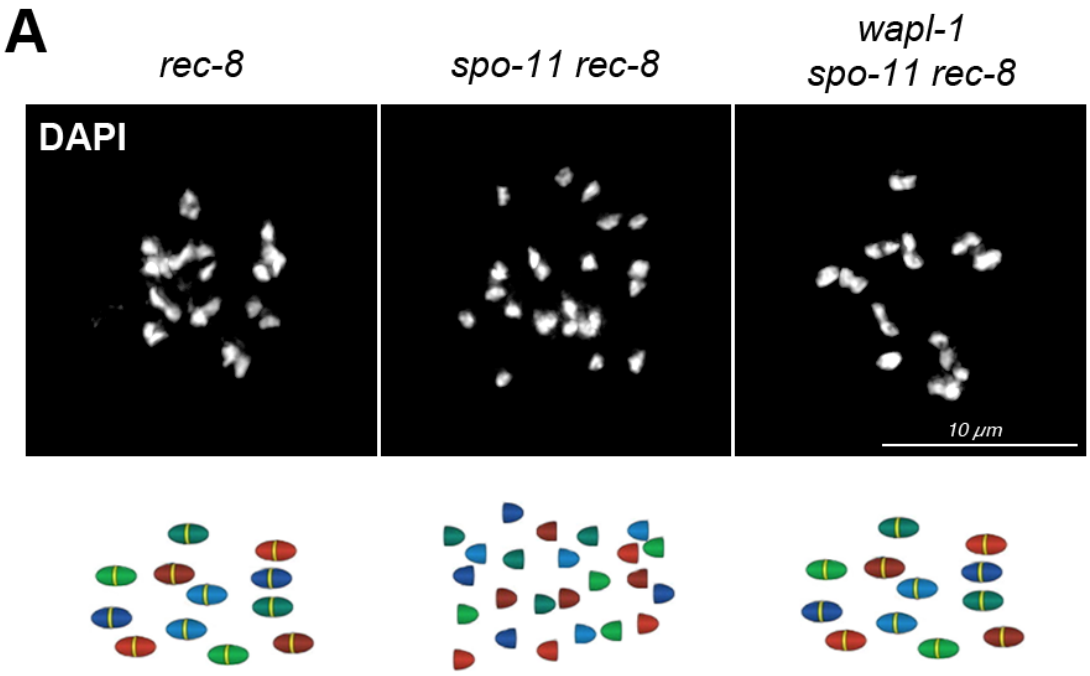
A
rec-8
spo-11 rec-8
wapl-1
spo-11 rec-8
DAPI
10 µm

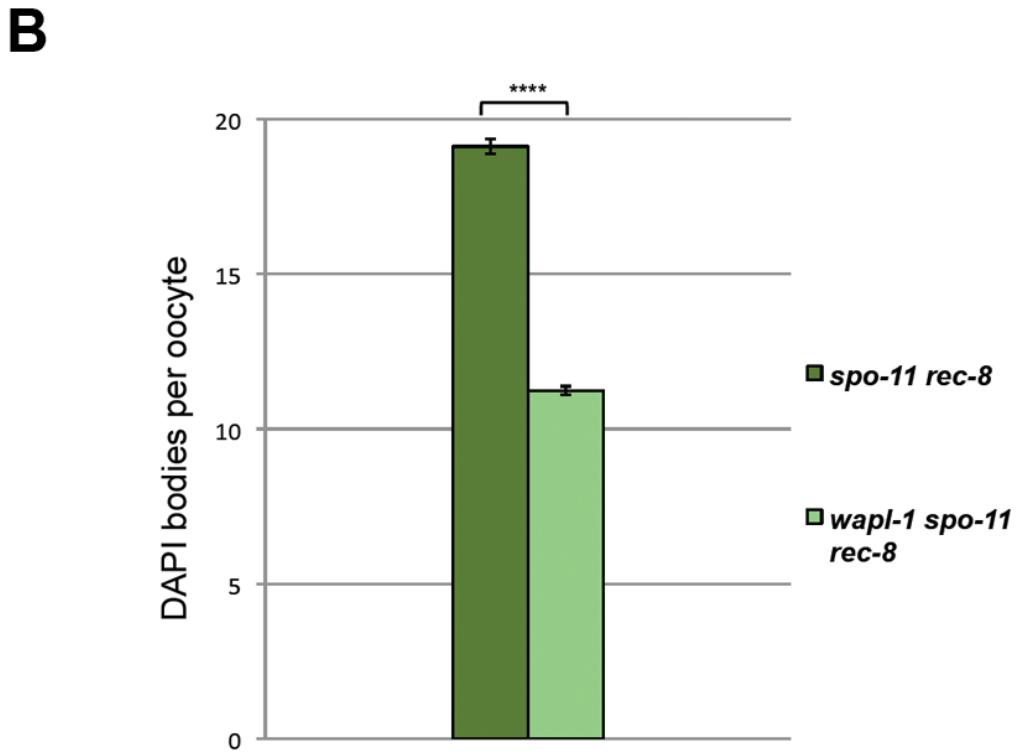
B
****
20
15
10
5
0
DAPI bodies per oocyte
spo-11 rec-8
wapl-1 spo-11
rec-8

Figure 34. Loss of WAPL-1 rescues SCC defects in *syp-1; rec-8* mutant background

A. Diakinesis oocytes of *rec-8* single, *syp-1; rec-8* double and *wapl-1; syp-1; rec-8* triple mutants stained with DAPI. Images are projections of deconvolved files.

B. Diakinesis oocytes of *syp-1; rec-8* and *wapl-1; syp-1; rec-8* mutants stained with DAPI, red lines mark the boundaries of individual DAPI bodies defined by automated analysis with CellProfiler software. Analysis and images shown are projections of deconvolved files.

C. Frequency histogram of DAPI body area sizes in pixels, obtained from CellProfiler analysis on *syp-1; rec-8* (n=52) and *wapl-1; syp-1; rec-8* (n=36). Area size outputs (per oocyte) were grouped for each genotype to calculate the total histogram. Area size category bins were defined by control genotypes (see Figure 35) The most common area size category represents the typical SCC and CO status for each genotype. The modal category for the *syp-1; rec-8* oocytes is fragmented chromosomes (49%) while in *wapl-1; syp-1; rec-8* triple mutants show a modal category of univalents (48%).

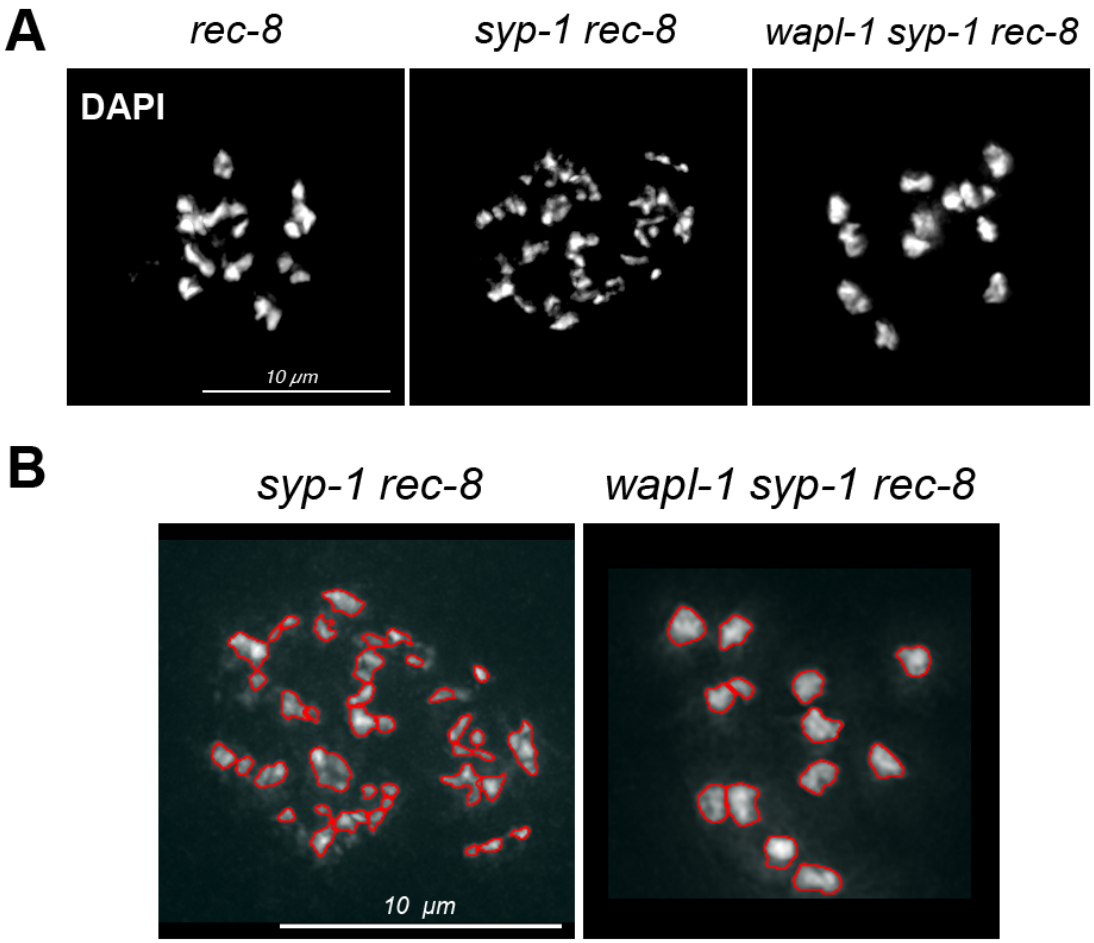
A
rec-8
syp-1 rec-8
wapl-1 syp-1 rec-8
DAPI
10 µm
B
syp-1 rec-8
wapl-1 syp-1 rec-8
10 µm
C
Fraction of DAPI bodies in area category
0.6
0.5
0.4
0.3
0.2
0.1
0
0-120 fragments
120-250 sisters
250-500 univalents
500-1000 bivalents
1000-8000 clusters
Pixels
syp-1 rec-8
wapl-1 syp-1 rec-8

Figure 35. Calibration of CellProfiler automated analysis for diakinesis DAPI bodies

Frequency histograms of diakinesis DAPI body area distribution from CellProfiler analysis for calibration of analysis parameters and area size categories. Area size unit = pixels, Y-axis = relative frequency of bodies for genotype. Repeats of each genotype were used to obtain average distribution. Wildtype (n=40) with a modal category of bivalents, 46% (cohesion intact and COs made). *coh-3; coh-4* double mutants (n=61) with a modal category of univalents, 66% (cohesion intact but no COs). *spo-11; rec-8* double mutants (n=116) with a modal category of sisters, 69% (separate sister chromatids with no cohesion). *syp-1; rec-8* (n=52) with a modal category of fragments, 49% (fragmented chromosomes and loss of cohesion). The clusters/overlap catergory (1000-8000 pixels) corresponds to masses or unresolved groups of bodies larger than a bivalent. Typical example DAPI stained oocytes are shown next to the appropriate genotype label.

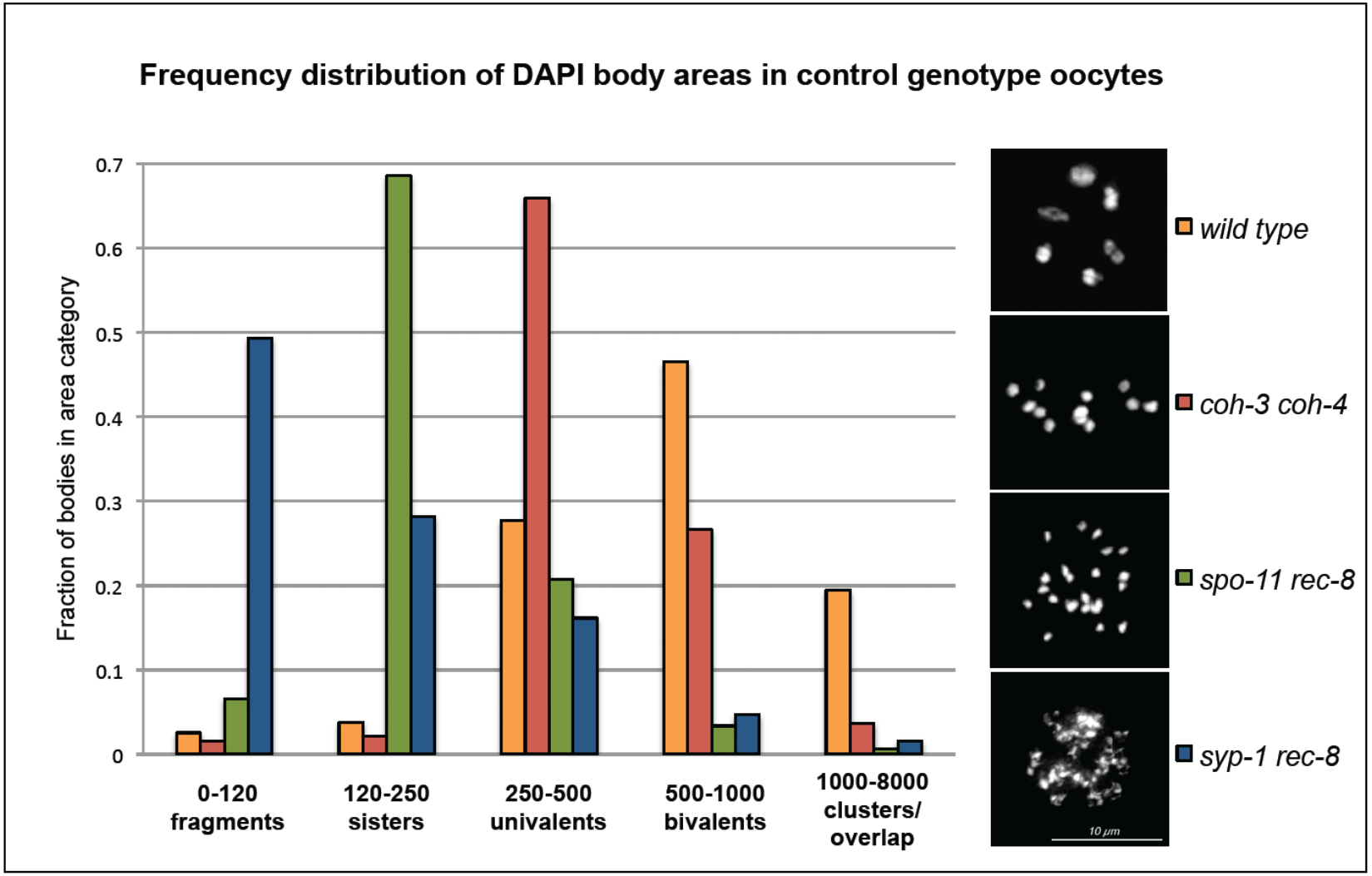
Frequency distribution of DAPI body areas in control genotype oocytes
Fraction of bodies in area category
0.7
0.6
0.5
0.4
0.3
0.2
0.1
0
0-120 fragments
120-250 sisters
250-500 univalents
500-1000 bivalents
1000-8000 clusters/ overlap
wild type
coh-3 coh-4
spo-11 rec-8
syp-1 rec-8
10 µm

Figure 36. Loss of WAPL-1 improves weakened SCC in *rec-8* mutant background

A. Diakinesis DAPI stained oocytes of *rec-8* and *wapl-1; rec-8* mutants. *rec-8* mutants show bilobed loosely connected univalents. *wapl-1; rec-8* double mutants have less bilobed and more continuous bodies.

B. Diakinesis oocytes of *rec-8* and *wapl-1; rec-8* mutants stained with DAPI, red lines mark the boundaries of individual DAPI bodies defined by automated analysis with CellProfiler software. Analysis and images shown are projections of deconvolved files.

C. Frequency histogram of DAPI body area sizes (pixels), from CellProfiler analysis on *rec-8* (n=67) and *wapl-1; rec-8* (n=63). Area size outputs were grouped for each genotype before calculating frequencies. Area size categories are as defined in Figure 35. The modal category of bodies for the *rec-8* mutant are 'sisters' (47%). Note the loose connection between sisters is often not represented by the automated analysis. The modal category of bodies identified in *wapl-1; rec-8* double mutant are 'univalents' (38%).

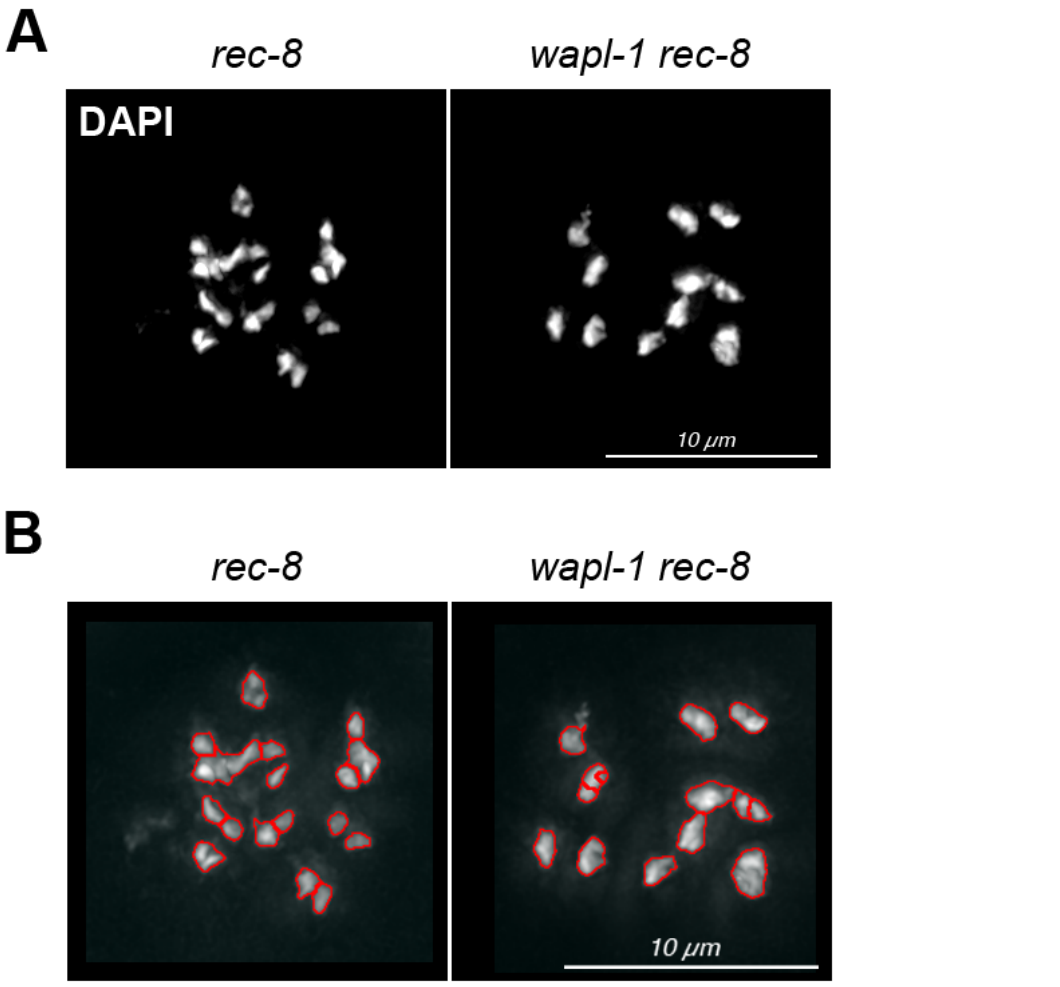
A
rec-8
wapl-1 rec-8
DAPI
10 μm
B
rec-8
wapl-1 rec-8
10 μm
C
Fraction of DAPI bodies in area category
0.6
0.5
0.4
0.3
0.2
0.1
0
0-120 fragments
120-250 sisters
250-500 univalents
500-1000 bivalents
1000-8000 clusters
rec-8
wapl-1 rec-8

Figure 37. SCC rescue in *wapl-1; spo-11; rec-8* mutant depends on COH-3 and COH-4

A. DAPI stained diakinesis oocytes of *wapl-1; spo-11; rec-8* double mutant, *wapl-1; spo-11; rec-8* triple mutant rescue and *coh-3; coh-4; wapl-1; spo-11; rec-8* quintuple mutant de-rescue. A. Below each oocyte is a diagram depicting chromosome status (as described in Figure 33 A.)

B. Frequency histogram of DAPI body area sizes (pixels) from CellProfiler analysis on diakinesis oocytes of *spo-11; rec-8* (n=116), *wapl-1; spo-11; rec-8* (n=90) and *coh-3; coh-3; wapl-1; spo-11; rec-8* (n=76). Area size outputs were grouped for each genotype before calculating overall frequencies. Area size categories were defined as shown in Figure 35. Modal area size categories are identified for each genotype: 'sisters' for *spo-11; rec-8* (69%), 'univalents' for *wapl-1; spo-11; rec-8* (45%) and 'sisters' in *coh-3; coh-4; wapl-1; spo-11; rec-8* (56%).

A

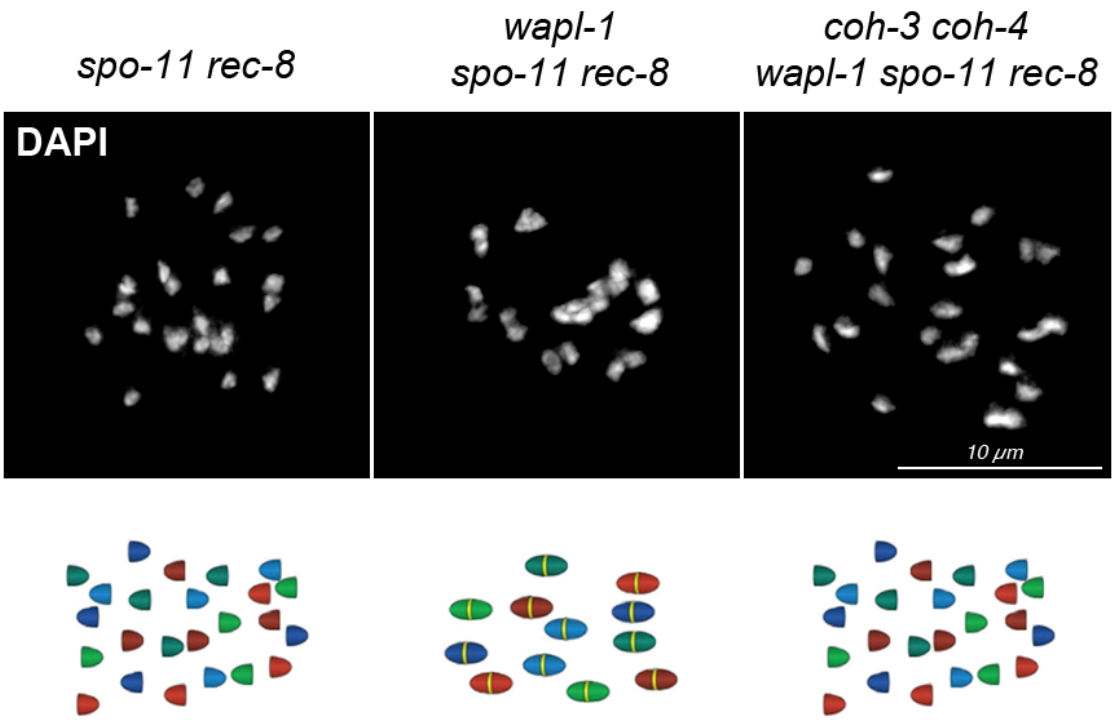
spo-11 rec-8
wapl-1 spo-11 rec-8
coh-3 coh-4 wapl-1 spo-11 rec-8
DAPI
10 µm

B

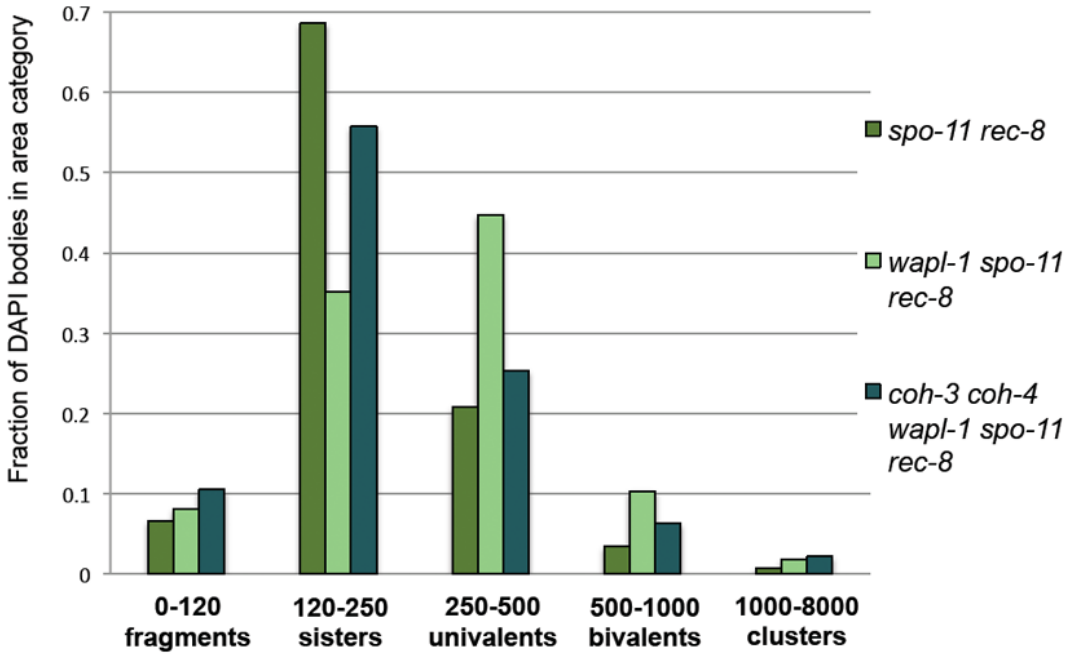
Fraction of DAPI bodies in area category
0.7
0.6
0.5
0.4
0.3
0.2
0.1
0
0-120 fragments
120-250 sisters
250-500 univalents
500-1000 bivalents
1000-8000 clusters
spo-11 rec-8
wapl-1 spo-11 rec-8
coh-3 coh-4 wapl-1 spo-11 rec-8

Figure 38. α-COH-3 staining is increased on late pachytene chromosomes of *wapl-1; spo-11; rec-8* mutant

The first image of each row shows a DAPI stained deconvolved projection of a diakinesis oocyte for that genotype demonstrating the cohesion phenotype. The remaining images of each row show DAPI and α-COH-3 staining, non-deconvolved for intensity comparison.

A. *spo-11; rec-8* mutant. Note the loss of SCC at diakinesis and high level of diffuse nucleoplasmic α-COH-3 staining and lack of clear axial pattern and late pachytene.

B. *wapl-1; spo-11; rec-8* mutant. Note the SCC rescue at diakinesis and greater axial α-COH-3 staining at late pachytene and reduced nucleoplasmic staining. Overall brightness does not appear much greater than the *spo-11; rec-8* mutant.

C. *coh-3; coh-4; wapl-1; spo-11; rec-8* quintuple mutant. There is a lack of SCC at diakinesis, as shown in Figure 37. Note the blank COH-3 staining as expected in a *coh-3* mutant background.

DAPI
COH-3
DAPI
COH-3
DAPI
A
B
C
10 µm
10 µm
Diakinesis
Late pachytene
spo-11 rec-8
wapl-1
spo-11 rec-8
coh-3 coh-4
wapl-1 spo-11 rec-8

Figure 39. Increased α-COH-3/4 staining correlates with improved SCC in *wapl-1; syp-1; rec-8* and *wapl-1; rec-8* mutants

N.B. α-COH-3/4 used for part A recognises both COH-3 and COH-4 protein. α-COH-3 used for part (B) recognises only COH-3.

A. Rescue of fragmentation in *wapl-1; syp-1; rec-8*, (as quantified in Figure 34) is accompanied by increased association of COH-3/4 to chromosomes and greater overall brightness, indicating strong increase.

B. Improvement of SCC in *wapl-1; rec-8* (as quantified in Figure 36) is accompanied by increased association of COH-3 to chromosomes and greater overall brightness, indicating strong increase.

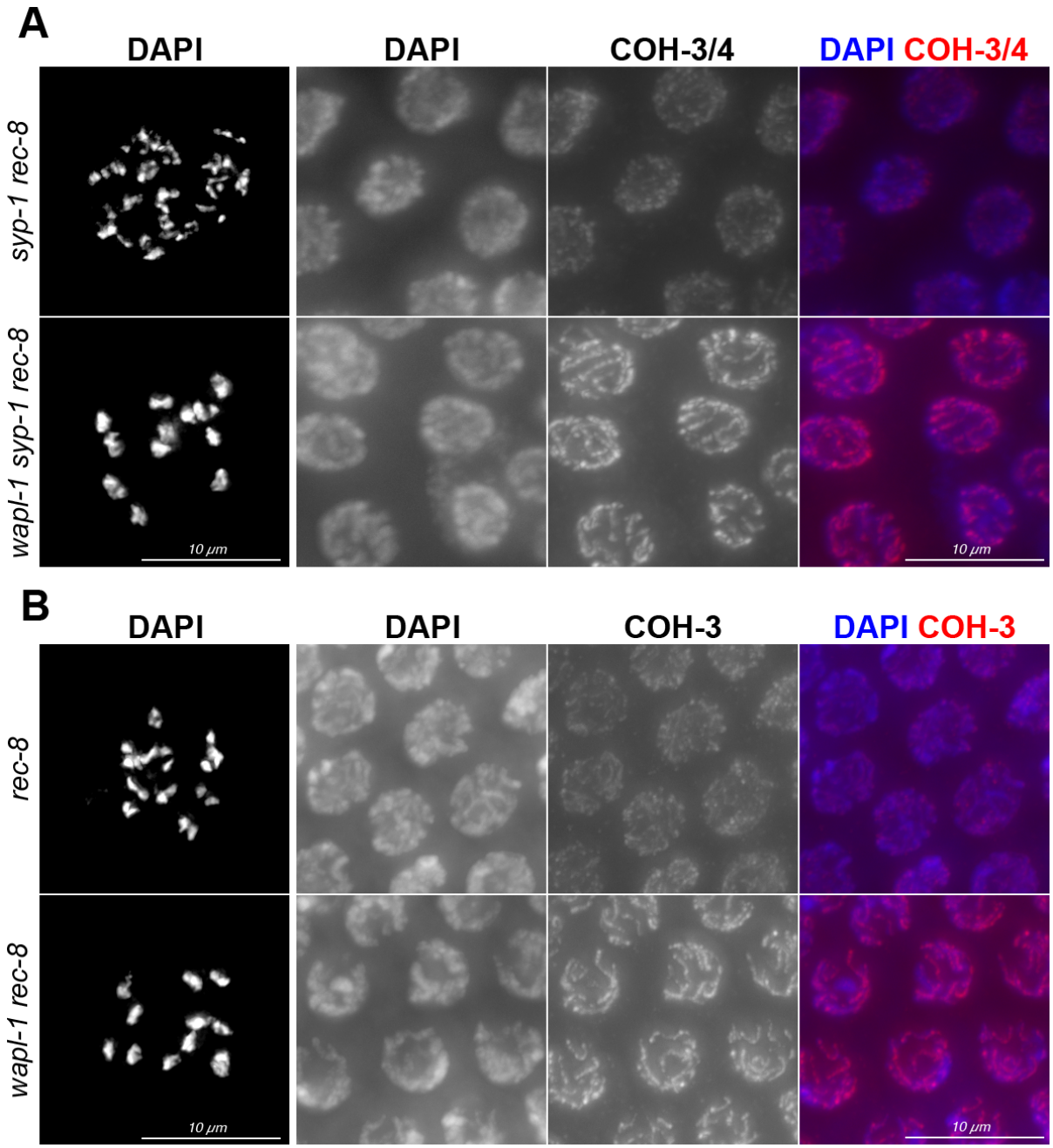
A
DAPI
DAPI
COH-3/4
DAPI COH-3/4
syp-1 rec-8
wapl-1 syp-1 rec-8
10 μm
10 μm
B
DAPI
DAPI
COH-3
DAPI COH-3
rec-8
wapl-1 rec-8
10 μm
10 μm

Figure 40. SCC rescue in *wapl-1; coh-4; rec-8* background and late pachytene α-COH-3 staining

Cohesion is also compromised in *coh-4; rec-8* double mutants. Chromosome fragments (see red arrows) and entangled chromatin masses are regularly observed at diakinesis. *wapl-1; coh-4; rec-8* triple mutants rarely have fragments or masses at diakinesis. Late pachytene panels show α-COH-3 and DAPI staining, non-deconvovled. Note the much higher level of COH-3 on chromosomes of *wapl-1; coh-4; rec-8* compared to the *coh-4; rec-8* mutant.

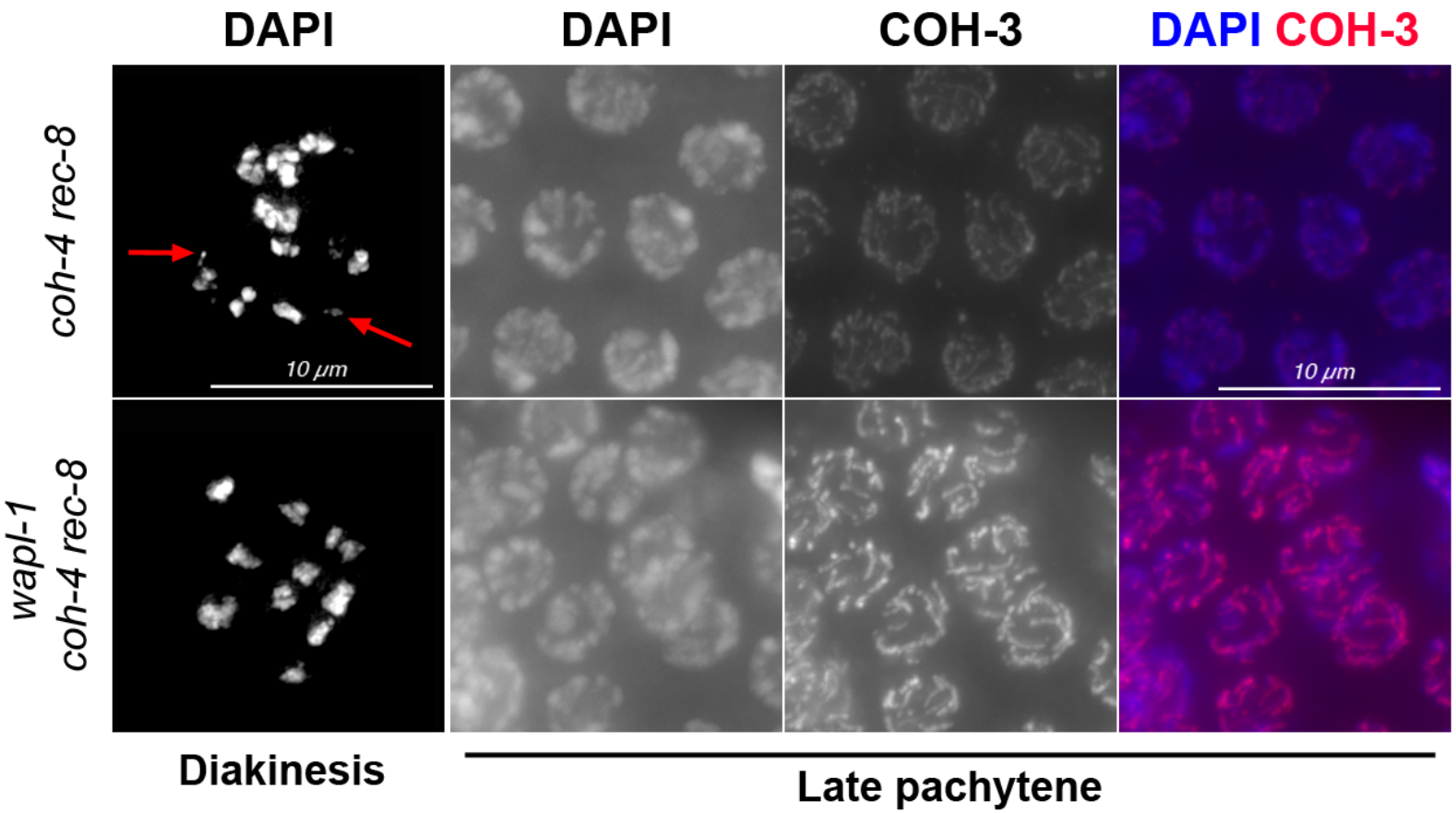
DAPI
DAPI
COH-3
DAPI COH-3
coh-4 rec-8
wapl-1
coh-4 rec-8
10 μm
10 μm
Diakinesis
Late pachytene

Figure 41. WAPL-1 transgenes show meiotic anti-cohesive function

A. Diakinesis oocytes stained with DAPI show SCC rescue in *wapl-1; spo-11; rec-8*. 'De-rescue' of SCC when GFP::WAPL-1 or WAPL-1 (no tag) transgenes were crossed *wapl-1; spo-11; rec-8* mutant rescue background, demonstrating meiotic anti-cohesion function. Cohesion status is highlighted by diagram below panel.

B. Frequency histogram of DAPI body area sizes (pixels) from CellProfiler analysis on *spo-11; rec-8* (n=37), *wapl-1; spo-11; rec-8* (n=50), GFP::WAPL-1; *wapl-1; spo-11; rec-8* (n=50) and WAPL-1 (no tag) transgene; *wapl-1; spo-11; rec-8* (n=48). Area size categories were defined as in Figure 35. The modal area categories of identified bodies are 'sisters' for *spo-11; rec-8* (55%), 'univalents' for *wapl-1; spo-11; rec-8* (46%) and 'sisters' for both transgenes in the *wapl-1; spo-11; rec-8* background - GFP::WAPL-1 (60%) and WAPL-1 (no tag) (62%).

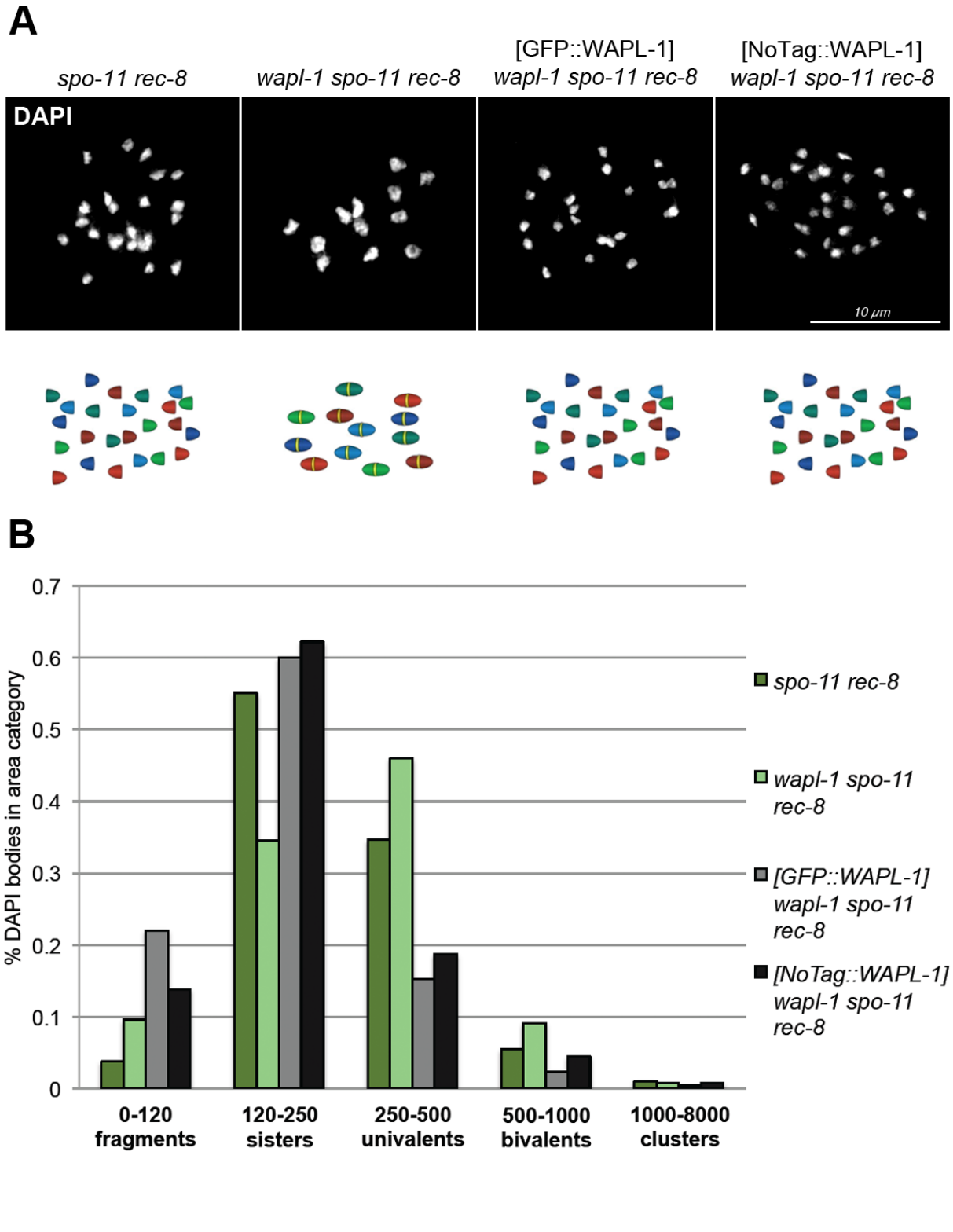
A
spo-11 rec-8
wapl-1 spo-11 rec-8
[GFP::WAPL-1]
wapl-1 spo-11 rec-8
[NoTag::WAPL-1]
wapl-1 spo-11 rec-8
DAPI
10 µm
B
% DAPI bodies in area category
0.7
0.6
0.5
0.4
0.3
0.2
0.1
0
0-120 fragments
120-250 sisters
250-500 univalents
500-1000 bivalents
1000-8000 clusters
spo-11 rec-8
wapl-1 spo-11 rec-8
[GFP::WAPL-1] wapl-1 spo-11 rec-8
[NoTag::WAPL-1] wapl-1 spo-11 rec-8

CHAPTER 5: RESULTS

INVESTIGATING COHESIN DYNAMICS *IN VIVO* DURING MEIOTIC PROPHASE

5.1 Objectives

Experiments shown in previous chapters have demonstrated that WAPL-1 controls the association of cohesin with meiotic chromosomes, thereby limiting their overall cohesive function. Several previous studies on mitotic cohesin have shown that the WAPL functions to antagonise cohesin by increasing the dynamic turnover of cohesin in live nuclei (Gerlich et al. 2006; Kueng et al. 2006; Bauerschmidt et al. ; Gause et al. 2010; Chan et al. 2012; Cunningham et al. 2012; Eichinger et al. 2013; Tedeschi et al. 2013). The evidence suggests that WAPL works by destabilising the stable association of cohesin complexes on chromatin. It was unknown whether there is any dynamic turnover of cohesin during meiosis, but our finding that WAPL-1 is active in *C. elegans* meiosis implies that cohesin turnover may occur during pachytene. It was also of interest to determine if the different sensitivity to WAPL-1 of cohesin complexes containing REC-8 or COH-3/4 may also correspond with different dynamics within the nucleus in vivo. Elucidating if cohesin is dynamically associated with chromosomes during meiotic prophase could have important implications for our understanding of meiotic events in which cohesin is known to play a role, such as SC assembly and recombination. In addition, the existence of cohesin turnover during meiotic prophase could affect our understanding of why SCC degrades in arrested oocytes of older women, an important question in meiosis (Jessberger 2012; Nagaoka et al. 2012). Therefore, a major objective of my PhD was to develop FRAP live imaging for the *C. elegans* germline using fluorescently tagged transgenes expressing functional cohesin subunits. This chapter describes the results of such cohesin FRAP experiments, as well as FRAP experiments using a WAPL-1 transgene.

5.2 FRAP imaging of meiotic cohesin

To our knowledge, FRAP live imaging had not been applied to the *C. elegans* germline, and indeed to cohesin in any meiotic system. One reason for pursuing this technique in my

project is that *C. elegans* is especially amenable to live imaging because the whole organism is transparent. The clear organised time-course of the worm germ line also allows for easy staging of meiotic nuclei. For fluorescence imaging of cohesin, transgenes encoding different subunits fused to fluorescent tags were inserted into the genome and crossed onto the corresponding mutant background for an assessment of functionality. This was achieved for three subunits: REC-8, COH-3 and SCC-3 with assistance from Consuelo Barroso and Sarah Testori. SCC-3 is the fourth core subunit and like SMC1/3 is thought to be common and necessary for all cohesin rings (Toth et al. 1999; Losada et al. 2000; Wang et al. 2003; Nasmyth and Haering 2009). Having the most robust bright expression, the SCC-3::GFP; *scc-3* strain was used to set up the conditions for the FRAP imaging and analysis (Figure 42).

Through empirical testing and by collaborating with the microscopy facility, challenges to both the imaging and analysis process were overcome. In order to obtain FRAP recovery curves with regular time points, relatively low-resolution settings were defined (Figure 42 A). The analysis method used was based on the traditional double normalisation for background and acquisition bleaching (Phair et al. 2004), plus a third normalisation for bleach depth to aid comparison within and between datasets (Royen et al. 2008; Eichinger et al. 2013). This process is demonstrated with an example of a late pachytene nucleus expressing SCC-3::GFP and a final triple normalised curve (Figure 42, C). The data points from such curves were then averaged from repeat experiments for each cohesin subunit and meiotic stage to obtain a mean FRAP curve. All subsequent figures in this chapter display this type of averaged curve.

5.2.1 SCC-3::GFP FRAP

5.2.1.1 Late pachytene recovery curve

Initially, late pachytene was the focus for the FRAP experiments given the results shown in chapter 1 that the later stages of meiotic prophase seem to be especially affected by WAPL-1. The late pachytene FRAP curve for SCC-3::GFP reveals a significant total mobile nuclear pool of SCC-3 of around 29% (Figure 43 B). The mobile pool is estimated from the plateau value of the exponential two-phase association curve fitted with GraphPad. A double exponential curve gave a better fit than a single phase exponential, similar to some previous studies of cohesin FRAP in mitotic cells (Gerlich et al. 2006; Gause et al. 2010).

Overall this implies that the remaining ~70% of SCC-3 is stably associated with meiotic chromosomes at this stage, over this 5 minute time scale (Eichinger et al. 2013).

The overall half-life from of the late pachytene SCC-3 curve is ~30 s, which is in the same order seen with cohesin FRAP experiments in mitosis. Though it is thought that FRAP half-lives values cannot accurately be compared between different systems or experimental conditions. The two-phase curve has two exponential components with different decay rate constants giving very different individual half-lives. The fast component making up about a third of the mobile pool has a half-life of 2 s while the slow component making up the other two thirds has a half-life of 79 s. The two components from exponential FRAP curves have been used in some studies to determine models of distinct sub-fractions: 'free unbound' versus 'weak dynamic bound' (Gause et al. 2010). Such studies used alternative type of analysis to make their curves, which was not suitable for my data. Therefore in the following FRAP experiments described here, the two components are not attributed exclusively to different biological fractions. Instead, the larger slower component is taken as a general indicator of dynamics, as is the overall half-life. A longer half-life (more gradual plateau) typically implies more extensive binding events within that mobile pool and shorter half-life (more abrupt plateau) typically implies a situation more akin to freely diffusing molecules, hence less turnover on chromosomes (Phair and Misteli 2001; Lippincott-Schwartz et al. 2003).

5.2.1.2 Chromosome reloading

From the monitoring required in these low-resolution FRAP experiments it was clear that a considerable proportion of mobile SCC-3 was reloading back to chromosomes. However, the 'low resolution' images obtained from these curve-data settings do not show this very convincingly (Figure 42 A). Therefore, I developed higher resolution FRAP settings with only 4 timepoints that better display reloading. The panels in Figure 43 A quite clearly demonstrate the recovery of SCC-3::GFP back to chromosome axes. As can be seen from the intensity of the axes in the unbleached halves this chromosome recovery is far from reaching pre-bleach levels. This is in line with the FRAP curves showing a larger stable bound fraction. Together, these results suggest that although much of cohesin is stably associated with chromosomes at late pachytene, a reasonable mobile fraction is dynamically turning over on chromosomes at late pachytene.

5.2.1.3 Early pachytene recovery curve

It was of interest to find out if the dynamics of SCC-3::GFP turnover were changed at different meiotic stages, where different meiotic events occur. Early pachytene presented the most suitable stage to assess for altered dynamics that was still technically feasible, unlike transitions zone or diplotene/diakinesis. The mean normalised recovery curve for SCC-3::GFP at early pachytene is shown in Figure 43 C, along with a control late pachytene curve from concurrently acquired dataset different to that shown in Figure 43 B. The early pachytene curve plateaus significantly lower than the late pachytene controls: 23% mobile fraction versus 31% mobile fraction respectively. This is a around a quarter less in the early pachytene suggesting a different balance of nuclear SCC-3 fractions exists at this stage. It is possible that there is less SCC-3 turning over on chromosomes or that there is less free mobile molecules. High-resolution images show chromosome reloading still occurs at early pachytene (data not shown), though it is hard to judge if there is less reloading compared to late pachytene.

The slow component of the early pachytene curve has a slightly shorter half-life (75 s) than the late pachytene controls (97 s). This change implies that there may be an increase in the dynamic population of SCC-3 at late pachytene compared to earlier stages. Such a conclusion would agree with the result from the SMC-3 immunofluorescence whole nucleus quantification showing a stronger effect of losing WAPL at late pachytene and therefore increased WAPL dependent dynamics (Figure 10). It should be noted that the half-life of the late pachytene controls is slightly longer than for the original late pachytene experiment (Figure 43 B), but this is most likely due to necessary adjustments to the imaging settings to account for unplanned microscope repairs. Importantly, the half-lives of early and late pachytene in Figure 41 C are directly comparable because they were acquired over the same imaging sessions with identical settings. The same is true for the equivalent figures for the other cohesin subunits (Figure 44 C and 45 C).

5.2.2 REC-8::GFP FRAP

5.2.2.1 Late pachytene recovery curve

A REC-8::GFP transgene provided the possibility to assess the dynamics of REC-8 compared to the other cohesin subunits. As with SCC-3::GFP, late pachytene was initially

assessed and the mean REC-8::GFP FRAP curve revealed a plateau recovery of ~16% of the total pre-bleach level (Figure 44 B). This is considerably lower than the 29% seen with the SCC-3::GFP, indicating that there is a smaller mobile pool of REC-8 than SCC-3, and conversely that a greater proportion of REC-8 is stably associated with chromosomes. As well as this, the overall shape of the REC-8::GFP curve is quite different, plateauing much more quickly than the SCC-3::GFP and is almost completely flat after only ~150 s. This change in shape is reflected by the half-life values. Overall the curve has a half-life of ~15 s, only half as long as the SCC-3::GFP overall half-life of ~30 s. From the two-component breakdown the slow component half-life is calculated at 29 s, less than half as long as for SCC-3::GFP (79 s). A shorter half-life of REC-8 implies less dynamic turnover on the chromosomes at late pachytene and the small mobile pool of REC-8 is behaving more similarly to freely diffusing molecules. This would agree with the immunofluorescence result showing that REC-8 is not very sensitive to WAPL-1.

5.2.2.2 Chromosome reloading

From the low-resolution FRAP experiments there appeared to be almost zero recovery of REC-8::GFP back onto chromosome axes, and therefore the 16% mobile pool seen in the curve arises predominantly from free mobile recovery into the bleached half. The same high resolution FRAP settings used for SCC-3::GFP confirmed this observation to be true with hardly any chromosome reloading of REC-8::GFP (Figure 44 A), at least over the 10 minute (600 s) timescale of these experiments. The 600 s post bleach image has negligible chromosome axial patterns in the bleached halves of the nuclei. Only a couple of very faint patches of continuous fluorescence can be seen on the regions where chromosomes should be. This is in stark contrast to the clear reloading to axial elements seen with SCC-3::GFP. This finding is in line with the FRAP curve in that the larger majority of REC-8::GFP appears to be stably immobilised, around 85%.

5.2.2.3 Early pachytene recovery curve

The mean recovery curve for REC-8::GFP at early pachytene is shown in Figure 44 C, along with a control late pachytene curve, again from a concurrently acquired dataset that is different to that shown in Figure 44 B. The early pachytene curve plateaus at an even lower value than the late pachytene controls: 12% mobile fraction versus 16% mobile fraction at late pachytene. It is important to note that the 16% plateau value of the late pachytene controls is very similar to the first late pachytene dataset. Similar to the SCC-

3::GFP, the mobile fraction is around a quarter less in early pachytene suggesting a different balance of nuclear fractions exists at this stage. This could mean either that there is less REC-8 turning over on chromosomes during early pachytene, or rather that there are less free mobile molecules. The slow component of the early pachytene curve has a shorter half-life than the late pachytene controls, 33 s versus 51 s. This change implies there may be a slightly increased dynamic population of REC-8 turning over at late pachytene. However, high-resolution images show minimal chromosome reloading of REC-8::GFP at both stages (early pachytene not shown), suggesting that the increased late pachytene mobile pool for REC-8 is largely from free unbound REC-8 without increased turnover.

5.2.3 COH-3::mCherry FRAP

5.2.3.1 Late pachytene recovery curve

A COH-3::mCherry transgene was used to determine COH-3/4 dynamics in pachytene and to compare them to those of the other subunits analysed so far. The high sensitivity of COH-3 to WAPL demonstrated in previous chapters suggested that COH-3 complexes display strong turnover on axial elements. When crossed into the single mutant *coh-3* background, COH-3::mCherry displays an axial nuclear pattern, but the expression levels of the transgene seem to fluctuate considerably between different animals compared to the SCC-3::GFP; *scc-3* and REC-8::GFP; *rec8* strains. Given the redundancy of COH-3 and COH-4, the COH-3::mCherry transgene was crossed to the double mutant *coh-3*; *coh-4* background, which showed that the transgene expressed a fully functional COH-3 that rescued the meiotic defects of *coh-3*; *coh-4* double mutants. The transgene expression was more stable in the double mutant background, however dynamics are not expected to be completely normal in the absence of COH-4. A solution was provided by the much more stable expression shown in a strain containing REC-8::GFP and the *rec-8* mutation as well as the COH-3::mCherry and *coh-3* mutation. This combined transgene strain is the one used for the FRAP experiments shown in Figure 45 and 46, marked as COH-3::mCherry; *coh-3*.

The late pachytene FRAP curve for COH-3::mCherry reveals the presence of a significant mobile pool of COH-3 at late pachytene of ~26% (Figure 45 B). This is much larger than the REC-8 mobile pool (16%), in agreement with the greater sensitivity of COH-3/4 to WAPL-1. As well as a significantly larger mobile fraction than the REC-8::GFP, the overall

shape of the COH-3::mCherry curve is very different with some noticeable incline still present after 400 s, while the REC-8::GFP curve is completely flat by ~150 s. This slow recovery rate is represented by a much longer overall half-life of the best-fit curve at ~60 s compared to the ~15 s for the REC-8::GFP. This COH-3::mCherry curve has two components like the other two subunits. In accordance with the overall half-life, the slow component has a far longer half life of 148 s compared to the corresponding 29 s of the REC-8::GFP. These observations suggest that mobile COH-3 is involved in more extensive binding events, meaning a larger dynamic fraction and resulting in slower movement into the bleached half (Lippincott-Schwartz et al. 2003). This conclusion would fit with the results of in chapter 3 and 4 that demonstrate COH-3/4 to be highly sensitive to WAPL-1. Evidence in mitosis has shown that sensitivity of cohesin complexes to WAPL does translate to higher turnover on chromatin and reduced stable association (Kueng et al. 2006; Shintomi and Hirano 2009; Tedeschi et al. 2013).

5.2.3.2 Chromosome reloading

As with the SCC-3::GFP it was immediately apparent during the monitoring of the curve data imaging that the COH-3::mCherry was recovering significantly to chromosomes. High resolution FRAP imaging of COH-3::mCherry at late pachytene revealed a clear recovery along chromosome axes in the bleached half of the nucleus (Figure 45 A). This definite dynamic turnover fits with the slower half-life from the FRAP curves and contrasts with the REC-8::GFP experiments. Though the chromosome recovery is clear it only reaches a fraction of the initial level. This agrees with the estimated mobile pool size showing that overall, around three quarters of COH-3 is stably bound to chromosomes. It was not possible to quantify the chromosome-specific recovery accurately in the high-resolution images, but visual judgment would estimate under a quarter of the unbleached levels.

5.2.3.3 Early pachytene recovery curve

As for the REC-8::GFP and SCC-3::mCherry, I also determined the recovery curve of COH-3::mCherry in early pachytene nuclei. A mean recovery curve for early pachytene COH-3::mCherry is shown in Figure 45 C, together with late pachytene COH-3::mCherry (controls) curve, again acquired concurrently and a different dataset from the original late pachytene dataset (Figure 45 B). The most immediate observation is that the overall mobile fractions appear similar at both meiotic stages, as evidenced from the general overlap of data points and curves throughout the imaging period. This is unlike both SCC-

3::GFP and REC-8::GFP early pachytene curves, which show clear divergence in curve shape from quite early on (Figure 43 C and Figure 44 C). Quantitatively, however, the curves fitted to the two datasets give a misleading impression with quite different final plateau values of 24% and 33% despite similar values for their final few data points. Also, the plateau value of 33% predicted from the late pachytene COH-3::mCherry (controls) curve is very different from 26% seen in the first experiment on late pachytene nuclei (Figure 45 B). A likely explanation for these discrepancies is that the early pachytene COH-3::mCherry curve has a good fit and should be a reliable dataset being is calculated from 20 repeats, however, the late pachytene COH-3::mCherry (controls) curve is averaged from only 4 repeats due to technical issues. As a result some data points inevitably deviate significantly from the best-fit curve by chance fluctuation, skewing its shape. Therefore, the actual mobile fraction for the late pachytene COH-3::mCherry (controls) is concluded to be close to the final data points (~25%) or fractionally higher, as is the case for all other curves shown. With this in mind, the first dataset for late pachytene COH-3::mCherry (Figure 45 B) will also be used to support comparison of half-lives to the early pachytene data.

The slow component half-life of the early pachytene curve is calculated to be 88 s, much shorter than the 214 s slow component half-life of the late pachytene (controls). The late pachytene (controls) half-life is considerably longer than the equivalent value from the 148 s of the initial late pachytene COH-3::mCherry dataset (Figure 45 B). However, even comparing the early pachytene data to this more reliable previous late pachytene dataset, the slow component half-life is considerably shorter at early pachytene: 88 s versus 148 s. Therefore, despite the appearance of similar mobile fraction and shape there may be underlying changes in COH-3/4 dynamics from early to late pachytene. This result suggests there may be greater dynamic turnover at late pachytene. The same experiment with more repeats of the late pachytene controls is required to confirm this conclusion. High-resolution FRAP displays chromosome recovery of COH-3::mCherry at early pachytene (data not shown), this seems similar to late pachytene (Figure 45 A). Though it is possible that the high-resolution FRAP may not be able to distinguish some subtle changes to dynamics. Interestingly, the fact that overall mobile pools are similar between stages would agree with the finding that α-COH-3/4 whole nuclear quantification at early and late pachytene shows similar increases in the *wapl-1* mutant (Figure 17).

5.2.4 Comparison of FRAP curves of different cohesin subunits

5.2.4.1 Late pachytene

If the late pachytene FRAP curves are compared for all three subunits (Figure 46 A), it is immediately noticeable that the SCC-3::GFP mobile pool and curve shape is generally more similar to the COH-3::mCherry mobile pool than to REC-8::GFP. As described, this implies both SCC-3 and COH-3 are likely to have significant dynamic turnover, while REC-8 is expected to have much less. However, it is also immediately clear that the SCC-3::GFP curve, though generally similar, does plateau significantly higher than COH-3::mCherry, implying that that there is a larger mobile pool of SCC-3::GFP than of CH-3 mCherry. If a single molecule of SCC-3 is actually present in every cohesin complex, then one would expect that the mobile pool of SCC-3 would be an intermediate between COH-3 and REC-8, in an analogous way to the intermediate response with the α-SMC-3 staining quantification (Figure 19 & Figure 25). There are several possible reasons why an SCC-3 mobile pool is not intermediate. One explanation could be the presence of other kleisin subunits known to be expressed during meiosis, SCC-1 and COH-1, which could result in other cohesin complexes not accounted for by REC-8 or COH-3/4 (Pasierbek et al. 2001; Mito et al. 2003). Another explanation could be that SCC-3 has binding dynamics of its own, outside of the intact cohesin complex, which is implied from a study with human cells (Kulemzina et al. 2012). In terms of chromosome turnover, the curve shape and half-life of cohesin FRAP experiments may in fact provide a more reliable characteristic for comparison (Gause et al. 2010). Interestingly, the half-life values for COH-3::mCherry are roughly twice as long as for SCC-3::GFP and roughly four times as long as the REC-8::GFP. So in terms of half-life the SCC-3::GFP does have a more intermediate phenotype (Figure 19 & Figure 25).

5.2.4.2 Early pachytene

Comparing the early pachytene curves for all three subunits (Figure 46 B), the most striking observation is that COH-3::mCherry and SCC-3::GFP appear to be extremely similar. REC-8::GFP early pachytene curve is clearly very different from the other two subunits, with a small mobile pool and more rapid plateau. Calculated from the curves, the COH-3::mCherry mobile pool is ~24% and slow component half-life is 88 s, while the SCC-3 has a ~23% mobile pool and slow component half-life of 75 s. These similar dynamics at early pachytene could be interpreted as meaning that the dynamics of SCC-3 are largely

defined by the dynamics of COH-3/4 complexes at this stage. While the limited REC-8 dynamics, ~12% mobile pool and ~33 s half-life, contribute relatively little to overall SCC-3 dynamics.

5.2.5 COH-3::mCherry in the *coh-3; coh-4* double mutant background

As mentioned earlier, the COH-3::mCherry transgene was crossed into the double mutant *coh-3; coh-4* mutant background to demonstrate transgene functionality because the two genes are mutually redundant (Severson et al. 2009). This strain provided a way to indirectly infer whether COH-4 may be displaying some dynamic turnover. This was not directly possible because a fluorescently tagged transgene for COH-4 has not been made yet. In a normal meiotic nucleus, if COH-3 and COH-4 are presumed to have relatively similar function and dynamics then there is likely to be a competition for binding/association sites along the chromosomes. If either one is removed, while expression of the other remains relatively similar, then lack of binding competition would result in changes to dynamics of the remaining protein. One would predict that the stable fraction of the remaining protein might increase, while the overall mobile pool would decrease.

This is indeed what seems to happen in the COH-3::mCherry; *coh-3; coh-4* strain (Figure 47). The FRAP curve obtained for the COH-3::mCherry; *coh-3; coh-4* strain shows the overall mobile fraction to be reduced compared to the COH-3::mCherry; *coh-3* (single) strain: 16% versus 26% respectively (Figure 47 B). Also, in the double mutant background the COH-3::mCherry recovery is faster with the curve appearing to plateau quicker. The half-lives reflect this difference in shape with the COH-3::mCherry; *coh-3; coh-4* (double) having an overall half-life of 25 s and a slow component half-life of 55 s. While the COH-3::mCherry; *coh-3* recovery is much slower having an overall half-life of ~60 s and a slow component half-life of 148 s (same dataset as Figure 45 B). This implies that loss of COH-4 does change the balance of dynamics for COH-3 and therefore that COH-4 is likely to have a significant mobile pool. High-resolution FRAP at late pachytene (Figure 47 A) does show some recovery to the chromosome axis for the COH-3::mCherry; *coh-3; coh-4* (double) but not quite to the level seen in the single mutant background (Figure 45 A).

It is important to note that the COH-3::mCherry; *coh-3; coh-4* curve shown in Figure 47 B was only imaged till 300 s post-bleach because this strain was actually imaged prior to the COH-3::mCherry; *coh-3*. The longer 400 s imaging period was used in response to the slower rate of plateau seen with the single mutant background.

5.2.6 FRAP experiments in the *wapl-1* mutant background

5.2.6.1 COH-3::mCherry

The FRAP experiments shown so far support the findings from the previous results chapters: the higher sensitivity of COH-3/4 to WAPL-1 compared to REC-8 does translate into a greater recovery to chromosomes following photo bleaching, as well as larger mobile pool and slower recovery. Such affects would be predicted from the current understanding of the model for WAPL-1, which is thought to destabilise the association of cohesin complexes with chromatin (Chan et al. 2012; Ouyang et al. 2013; Tedeschi et al. 2013). However, to truly integrate these different approaches to understand cohesin regulation I wanted to assess how cohesin dynamics in vivo are affected by loss of WAPL-1. For COH-3::mCherry there was a slight issue because the transgene in the single *coh-3* mutant background alone has unstable expression. Therefore, instead a strain containing the COH-3::mCherry in the double mutant *coh-3; coh-4* background plus the *wapl-1* mutation with more stable expression was used. This was compared to the double mutant background without the *wapl-1* mutation (as shown in Figure 47). The FRAP curves in Figure 46 B show that in the *wapl-1* mutant background the COH-3::mCherry does indeed have a reduced mobile fraction: 14% in the *wapl-1* mutant compared to 18% in the controls. However, this is not a significant difference at several timepoints, as evidenced by the overlap of error bars. Regarding the half-lives, it is important to mention that for these particular datasets there was a better fit and more normal curve shape with a single-phase curve than a double-phase curve. Importantly, a single-phase model also fits the previous COH-3::mCherry; *coh-3; coh-4* dataset well (Figure 47 B), implying it may be an appropriate model to use. Therefore single-phase curves are shown in this experiment (Figure 48 B). Single-phase curves only give one overall half-life value with no separate components. The *wapl-1* background (COH-3::mCherry *wapl-1; coh-3; coh-4*) has a 60 s half-life compared to 40 s in the controls (COH-3::mCherry *coh-3; coh-4*). This longer half-life, together with the reduced mobile pool, suggests that WAPL-1 may be controlling the live dynamics and turnover of COH-3 during meiosis. High-resolution FRAP supports this conclusion from the curve data because the COH-3::mCherry *wapl-1; coh-3; coh-4* strain

appears to show less recovery onto the chromosomes (Figure 48 A). More experiments with larger sample sizes and ideally in the single mutant background are required to determine the full extent of the effect of WAPL-1 on COH-3 and COH-4 dynamics.

5.2.6.2 REC-8::GFP

If REC-8 is largely insensitive to WAPL-1 activity, then the loss of WAPL-1 should not increase the stability of REC-8. Therefore combining the *wapl-1* mutation with the REC-8::GFP transgene should not result in a smaller mobile pool and or delayed recovery half-life. The graph in Figure 48 C displays mean FRAP curves for REC-8::GFP in the *rec-8; wapl-1* mutant background and the *rec-8* alone background (controls). In the absence of WAPL-1, REC-8::GFP shows a considerably higher mobile pool of ~ 26% than in the controls with ~17%. This opposite trend from the COH-3::mCherry in the *wapl-1* mutant background supports the conclusion that in normal meiosis WAPL-1 is not antagonising REC-8. However, it is surprising that the mobile fraction of REC-8::GFP increases in the absence of WAPL-1, as one would have expected that REC-8::GFP dynamics may not be affected by WAPL-1. This apparent contradiction could be explained considering that the increased levels of chromosome-bound COH-3/4 cohesin complexes may leave less binding sites on the axis for REC-8. Another consideration with this result is that the REC-8::GFP; *rec-8* strain was grown completely homozygously so that there is selection for appropriate expression of the REC-8 transgene. While the REC-8::GFP *wapl-1; rec-8* strain had to be grown with the transgene homozygous but both the *wapl-1* and *rec-8* mutations balanced and then picked as homozygotes for the experiment, due to genetic postitions of the genes. Therefore in this strain there is not selection for expression over generations of maintaining it. However, importantly the general shape and half-life remains similar in the *wapl-1* background. They both have overall half-lives of ~25 s while the REC-8::GFP; *wapl-1; rec-8* strain has a slow component half-life of 32 s and the REC-8::GFP; *rec-8* control has a slow component half-life of 36 s. Therefore, the increase in mobile pool does not seem to be accompanied by a significant change in the turnover dynamics implying that the larger mobile pool arises mainly from a larger free unbound fraction. Overall the results from the REC-8::GFP FRAP support the previous findings in that REC-8 is not sensitive to the antagonistic effects of WAPL-1. The stable association of REC-8 with chromosomes is not limited by WAPL-1 activity.

5.3 GFP::WAPL-1 FRAP

The GFP::WAPL-1 transgene provided an opportunity to assess the dynamics of WAPL-1 during meiosis. From inspection of the live and fixed imaging of germlines expressing GFP::WAPL-1, there does not appear to be a significant stable chromosome-bound fraction of WAPL-1, because instead of axial tracks as with the cohesin subunits, an even diffuse nuclear pattern is seen (Figure 8). These observations suggest a relatively weak or transient interaction of WAPL-1 with chromatin, as similarly indicated for mitotic prophase from previous experiments (Kueng et al. 2006; Kulemzina et al. 2012). FRAP of a fluorescently tagged WAPL was investigated in yeast mitotic prophase cells where it was found to have a very fast half-life (Chan et al. 2012). Initial trial FRAP experiments with the GFP::WAPL-1 in *C. elegans* meiosis confirmed the patterns that were seen in the fixed germ lines. WAPL-1 shows a diffuse nuclear staining lacking any axial pattern and the expression peaks towards the end of pachytene into diplotene. It is also noticeable that the GFP::WAPL-1 is loosely enriched around the outer part of the nucleus where the chromosomes are located, making a hollow even sphere. The signal recovery of GFP::WAPL-1 after photo bleaching is extremely fast, therefore the fastest possible imaging settings were used. Still images from an example GFP::WAPL-1 FRAP experiment are shown in Figure 49 A. By 4 s post bleach the bleached halves of the affected nuclei appear equalised with the unbleached halves. The mean FRAP curve from many repeat experiments shown in Figure 49 B clearly demonstrates that there is almost complete recovery back to 1.0, meaning that the mobile pool of GFP::WAPL-1 comprises more of less 100% of the protein in the nucleus. The curve fitted to the data gives a predicted plateau of 0.99 (99% mobile fraction), which strongly implies that effectively all WAPL-1 is mobile and none is involved in stable association with chromosomes. The overall half-life of GFP::WAPL-1 is ~1 s. The half-life of the fast component of the two-phase curve, which is the majority component in this case unlike the cohesin subunits, is 0.8 s. Such rapid recovery is far quicker than any of the cohesin subunits and together with the full mobility suggests that there is very limited dynamic turnover of WAPL-1 on chromosomes in the way that the cohesin complexes do. The general shape of the curve is more reminiscent of a freely diffusing molecule without any significant binding and unbinding events (Lippincott-Schwartz et al. 2003).

5.4 Summary of results

This chapter has described the novel application of FRAP to the *C. elegans* germ line in order to assess meiotic cohesin dynamics. It is clear from these experiments that there is some dynamic turnover of cohesin on meiotic prophase chromosomes both visually and quantifiably. There appears to be marked differences in the dynamics of the different cohesin complexes during meiosis. COH-3::mCherry shows significant turnover onto chromosomes and a larger mobile pool with delayed recovery, while REC-8 displays more limited turnover onto chromosomes and has a smaller mobile pool that recovers more quickly. The dynamics of COH-4 are expected to be similar to COH-3 given the close homology and redundancy (Severson et al. 2009). This fundamental difference in dynamics mirrors the clear divergence in sensitivity to WAPL-1 for the different meiotic kleisins, which was described in previous chapters. In support of the finding that whole cohesin complexes are actually turning over on meiotic chromosomes, not just COH-3, FRAP also revealed that SCC-3::GFP shows significant turnover. Unexpectedly, SCC-3 displays some dynamics that are not intermediate between COH-3 and REC-8, as might be expected if it were common to all cohesin complexes. The excess of SCC-3 mobility at late pachytene may arise from the other complexes that are known to exist in *C. elegans* meiosis that will be discussed in chapter 7 (Pasierbek et al. 2001; Mito et al. 2003; Severson et al. 2009).

The FRAP experiments have also uncovered some slight changes in cohesin dynamics at early and late pachytene, suggesting that different events of meiosis may influence cohesin dynamics or visa versa. However, the general difference between the dynamics of the different kleisins is consistent. From the various experiments, it seems that in normal *C. elegans* meiosis the stable association with chromosomes, and therefore cohesive capacity, of COH-3/4 complexes is limited by WAPL-1. However, REC-8 is largely insensitive to WAPL-1, which should facilitate the stable association of REC-8 chromosomes, thus providing robust SCC. Preliminary FRAP experiments in the *wapl-1* mutant background appear to tie up these findings: COH-3::mCherry stability is limited by WAPL-1 while REC-8::GFP is not.

The implication of these findings is that the different dynamics for the different cohesin subunits and likely different complexes could be an important aspect of meiosis and their

functional divergence, given that multiple kleisin subunits are found in meiosis of most organisms except yeast. Turnover of cohesin during prophase could be important for understanding the cohesion exhaustion that occurs in oocytes of older women.

Table 6. Summary of meiotic cohesin FRAP live imaging

Transgene	Early pachytene dynamics	Late pachytene dynamics	Response to loss of WAPL-1
SCC-3::GFP	**23% mobile pool** (compared to 31% for late pachytene controls) **75 s half-life** *slow component* (compared to 97 s for late pachytene controls)	**29% mobile pool** **79 s half-life** *slow component*	-strain not made-
REC-8::GFP	**12% mobile pool** (compared to 17% for late pachytene controls) **33 s half-life** *slow component* (compared to 51 s for late pachytene controls)	**16% mobile pool** **29 s half-life** *slow component*	Increased mobile pool, half-life similar (selection for transgene expression reduced in wapl-1 mutant background)
COH-3:: mCherry	**24% mobile pool** (compared to 33% for late pachytene controls)** **88 s half-life** *slow component* (compared to 214 s for late pachytene controls)**	**26% mobile pool** **148 s half-life** *slow component*	Slightly decreased mobile pool, slightly longer half-life. (Experiment done in *coh-3; coh-4* double mutant background, with already reduced mobility)
GFP::WAPL-1	-similar to LP, not quantified-	**~100% mobile pool** **~1 s half-life** *fast component*	-not possible-

** Late pachytene controls for COH-3::mCherry assessment of early pachytene had few usable repeats. Large error bars and limited reliability of curve shape/,half life.

Figure 42. FRAP live imaging of fluorescently tagged cohesin subunits can quantify dynamics

A. Images demonstrate a typical FRAP experiment to determine a recovery curve, this example is SCC-3::GFP in the *scc-3* (*ku263*) homozygous background at late pachytene. Low resolution settings derived with regular timepoints for curve estimation (timepoints: 10x 3 seconds, 25x 15 seconds). Regions of interest (ROIs) are depicted as drawn in Image J macro to measure mean fluorescence. Yellow ROI = bleached half of nucleus, red ROI = unbleached half of nucleus, green ROI = background inter-nuclear region.

B. Mean raw fluorescence values (Y-axis) of ROIs as measured with Image J over time (seconds) on X-axis. Single nucleus SCC-3::GFP example plotted for 5 minutes (300 seconds).

C. Relative normalized fluorescence of bleached ROI from same example nucleus plotted in Figure 40 B. Background level is subtracted from all mean intensities in bleached and unbleached ROIs. Bleached values are converted as relative to initial pre-bleach and relative to the inverse of the unbleached values, to normalize for acquisition bleaching (Phair et al. 2004). Normalised values are 'triple normalized' by setting initial post-bleach level to zero and scaling all values accordingly for inter-experiment comparison.

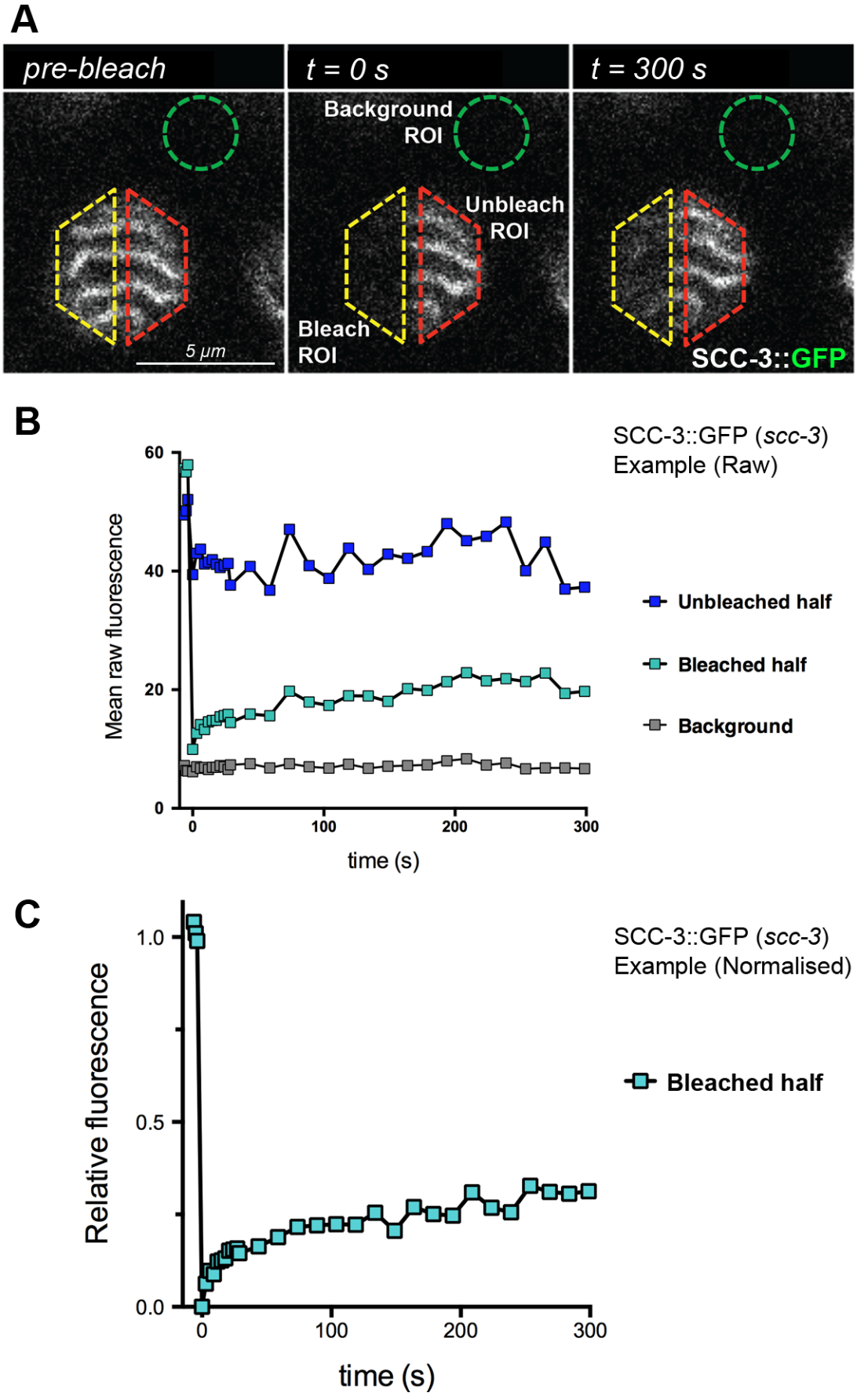
A
pre-bleach
t = 0 s
t = 300 s
Background ROI
Unbleach ROI
Bleach ROI
5 µm
SCC-3::GFP
B
SCC-3::GFP (scc-3)
Example (Raw)
Mean raw fluorescence
60
40
20
0
0
100
200
300
time (s)
Unbleached half
Bleached half
Background
C
SCC-3::GFP (scc-3)
Example (Normalised)
Relative fluorescence
1.0
0.5
0.0
0
100
200
300
time (s)
Bleached half

Figure 43. SCC-3::GFP displays significant mobility and axial reloading

A. FRAP of SCC-3::GFP; *scc-3* strain at late pachytene with high resolution settings to visualize axial recovery. Images = immediately pre-bleach, immediately post bleach (0 s) and 600 s post bleach. Contrast and brightness adjusted equally for three images. Dashed boxes mark bleached area.

B. Mean recovery curve of SCC-3::GFP at late pachytene acquired with low resolution settings and regular timepoints (as in Figure 40 A) and normalized for each experiment (as described in Figure 40 C) before averaging. N = 28. Y-axis is relative normalized mean fluorescence intensity. X-axis = time (seconds). Error bars = SEM. Curve fitted with *Prism 6* (GraphPad), two phase exponential association (see equation below). Plateau = 0.29 (~29% mobile pool of whole nucleus). Half-life of slower component ($\mathbf{k_2}$) = 79 s.

$$y = Ymax_1 \cdot (1 - e^{-k1 \cdot x}) + Ymax_2 \cdot (1 - e^{-k2 \cdot x})$$

C. Mean FRAP recovery curves of SCC-3::GFP from early pachytene and late pachytene nuclei. Analysed and fitted as described in Figure 41 B. Late pachytene (controls) is different dataset to Figure 41 B and acquired concurrently with early pachytene experiments. Timepoints continued till 400 seconds post bleach for improved curve fitting. Error bars = SEM. Early pachytene: n = 9, mobile pool = 23%, slow component half-life = 75 s. Late: n = 10, mobile pool = 31%, slow component half-life = 75 s. Note lower plateau value and faster plateau of early pachytene.

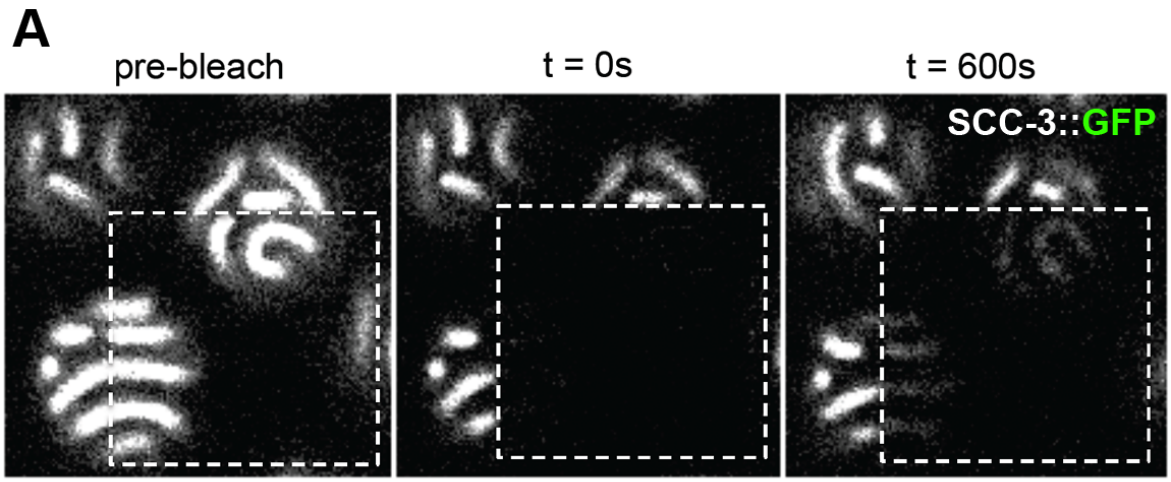
A
pre-bleach
t = 0s
t = 600s
SCC-3::GFP

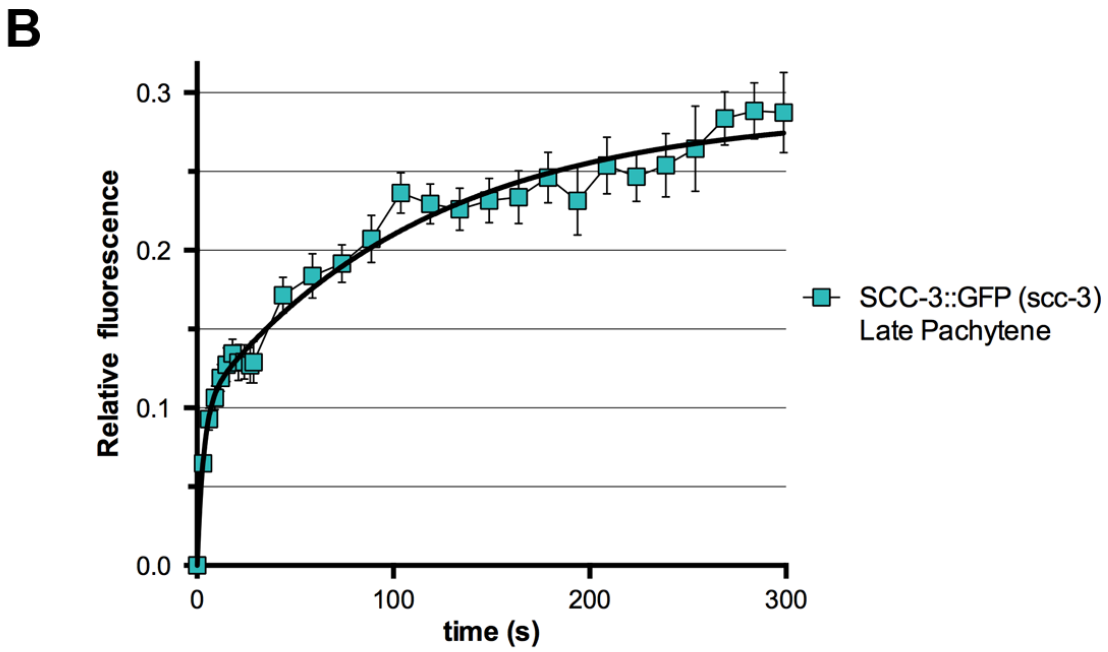
B
Relative fluorescence
0.0
0.1
0.2
0.3
0
100
200
300
time (s)
SCC-3::GFP (scc-3)
Late Pachytene

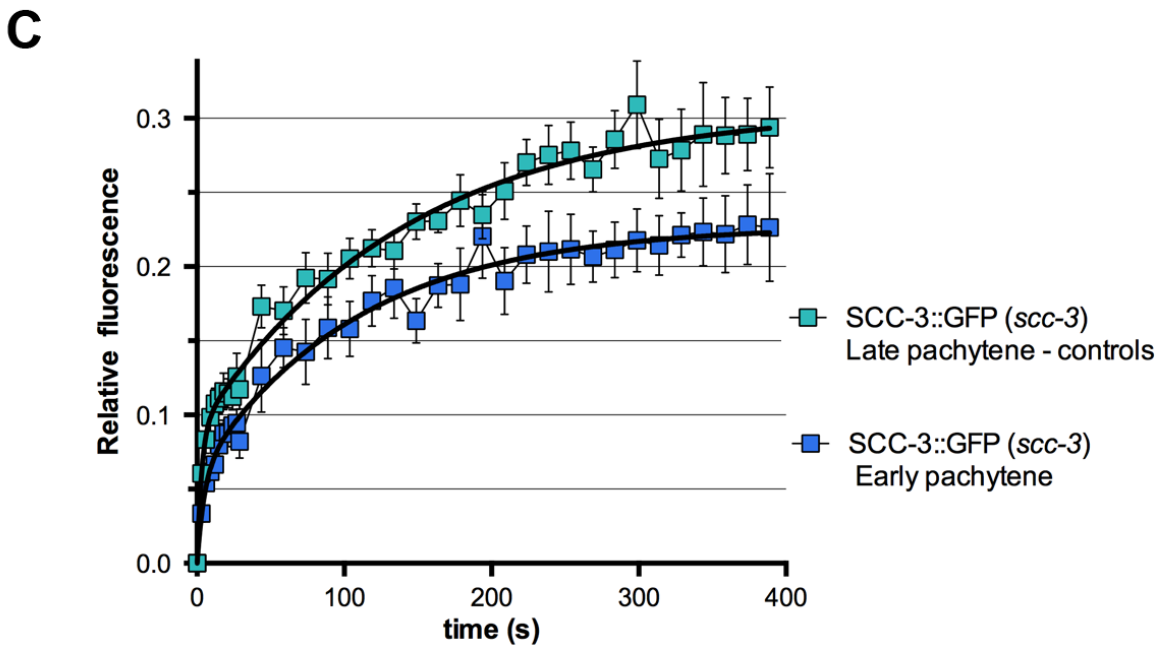
C
Relative fluorescence
0.0
0.1
0.2
0.3
0
100
200
300
400
time (s)
SCC-3::GFP (scc-3)
Late pachytene - controls
SCC-3::GFP (scc-3)
Early pachytene

Figure 44. REC-8::GFP displays small mobile pool and little axial reloading

A. FRAP of REC-8:GFP; *rec-8* strain with high resolution settings to visualize chromosome axis recovery (as described in Figure 41 A). Dashed boxes mark bleached area.

B. Mean recovery curve of REC-8::GFP at late pachytene acquired with low resolution settings (analysis and curve fitting as described in Figure 41, B). n= 31. Y-axis = relative normalized mean fluorescence intensity. X-axis = time (seconds). Error bars = SEM. Plateau = 0.16 (~16% mobile pool of whole nucleus). Half-life of slower component (k_2) = 29 s.

C. Mean FRAP recovery curves of REC-8::GFP comparing early pachytene and late pachytene nuclei (analysed fitted as described in Figure 41 B). Late pachytene (controls) is different dataset to Figure 42 B and acquired concurrently with early pachytene experiments. Extended timepoints for 15 s intervals till 400 seconds post bleach for improved curve fitting. Early pachytene: n = 31, mobile pool = 12%, slow component half-life = 33 s. Late pachytene: n = 6, mobile pool = 17%, slow component half-life = 51 s. Note lower plateau value for early pachytene.

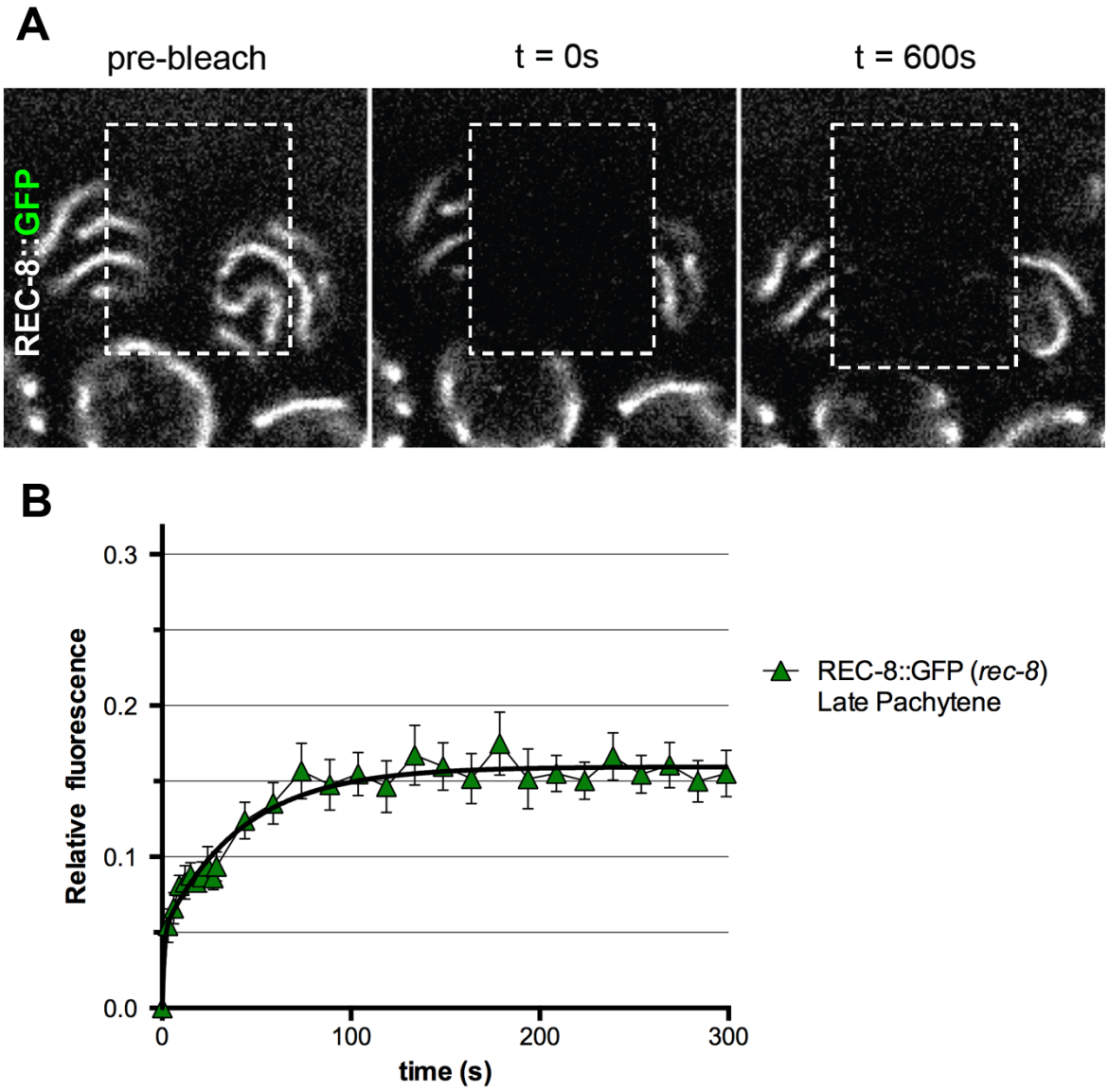
A
pre-bleach
t = 0s
t = 600s
REC-8::GFP
B
Relative fluorescence
0.3
0.2
0.1
0.0
0
100
200
300
time (s)
REC-8::GFP (rec-8)
Late Pachytene
C
Relative fluorescence
0.2
0.1
0.0
0
100
200
300
400
time (s)
REC-8::GFP (rec-8)
Late Pachytene - controls
REC-8::GFP (rec-8)
Early Pachytene

Figure 45. COH-3::mCherry displays significant mobile pool and axial reloading

A. High resolution FRAP of COH-3::mCherry; *coh-3* strain (also containing REC-8::GFP and rec-8 mutation to stabilise expression) to visualize chromosome axis recovery (as described in Figure 41 A). Dashed boxes mark bleached area.

B. Mean recovery curve of COH-3::mCherry at late pachytene acquired with low resolution settings (analysis and curve fitting as described in Figure 41 B). n= 22. Y-axis = relative normalized mean fluorescence intensity. X-axis = time (seconds). Error bars = SEM. Plateau = 0.26 (~26% mobile pool of whole nucleus). Half-life of slower component (k_2) = 148 s.

C. Mean FRAP recovery curves of COH-3::mCherry comparing early pachytene and late pachytene nuclei (analysed and fitted as described in Figure 41 B). Late pachytene (controls) is different dataset to Figure 43, B and acquired concurrently with early pachytene experiments. Early pachytene: n = 20, mobile pool = 24%, slow component half-life = 88 s. Late pachytene: n = 4, mobile pool = 33%, slow component half-life = 214 s. Note similar general shape and final data point values, despite different mobile pool and half-life values.

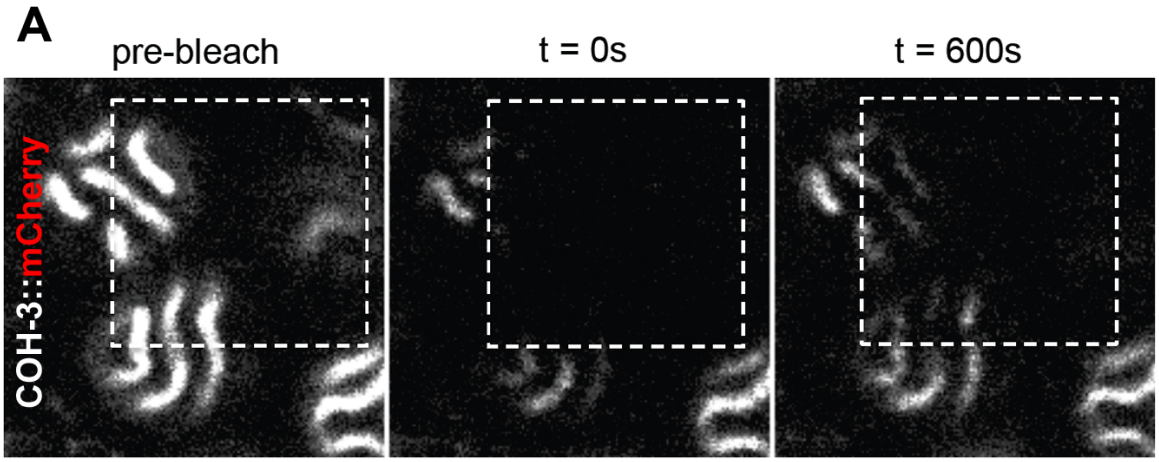
A
pre-bleach
t = 0s
t = 600s
COH-3::mCherry

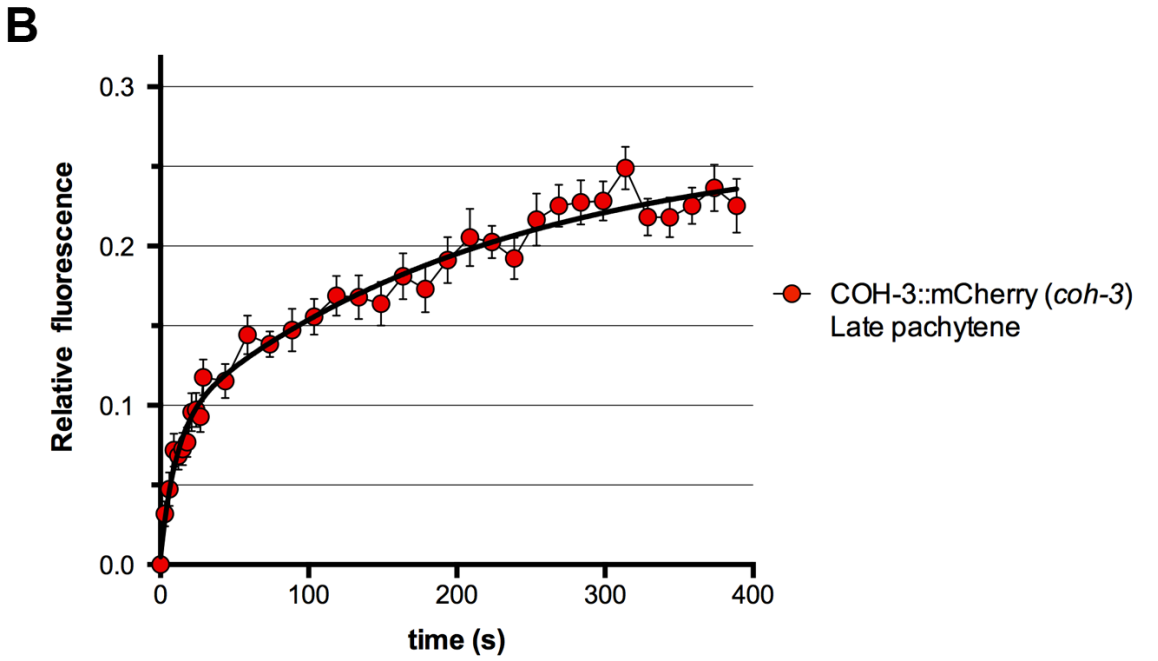
B
Relative fluorescence
0.3
0.2
0.1
0.0
0
100
200
300
400
time (s)
COH-3::mCherry (coh-3)
Late pachytene

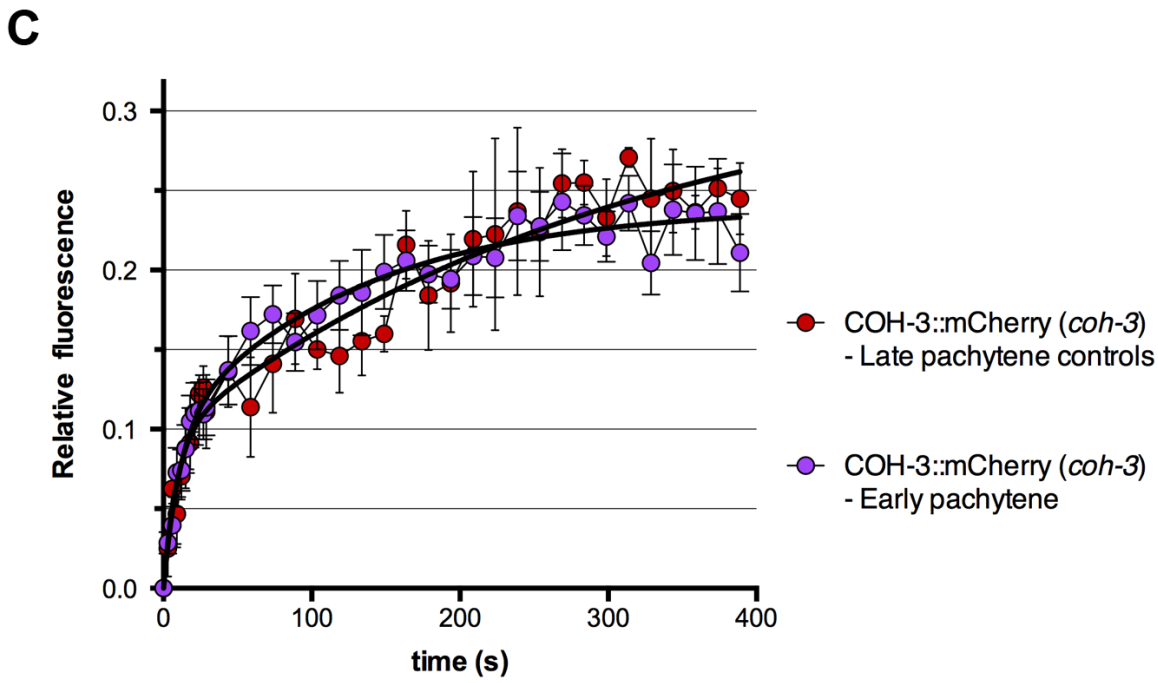
C
Relative fluorescence
0.3
0.2
0.1
0.0
0
100
200
300
400
time (s)
COH-3::mCherry (coh-3)
- Late pachytene controls
COH-3::mCherry (coh-3)
- Early pachytene

Figure 46. FRAP recovery curves comparing late pachytene and early pachytene of SCC-3::GFP, COH-3::mCherry and REC-8::GFP transgenes

A. Late pachytene FRAP curves showing mean normalized fluorescence for SCC-3::GFP, COH-3::mCherry and REC-8::GFP. Same datasets and curves fitted in Figure 41 B, Figure 42 B and Figure 43 B. Note higher plateau (mobile pool) combined with longer time to plateau (half life) for SCC-3 and COH-3 than for REC-8 indicating more dynamic turnover.

B. Early pachytene FRAP curves showing mean normalized fluorescence for SCC-3::GFP, COH-3::mCherry and REC-8::GFP. Same datasets and curves fitted in Figure 41 C, Figure 42 C and Figure 43 C. Note higher plateau (mobile pool) combined with longer time to plateau (half life) for SCC-3 and COH-3 than for REC-8 indicating more dynamic turnover. Also note the more similar curves for SCC-3 and COH-3 at early pachytene compared to late pachytene (Figure 44 A).

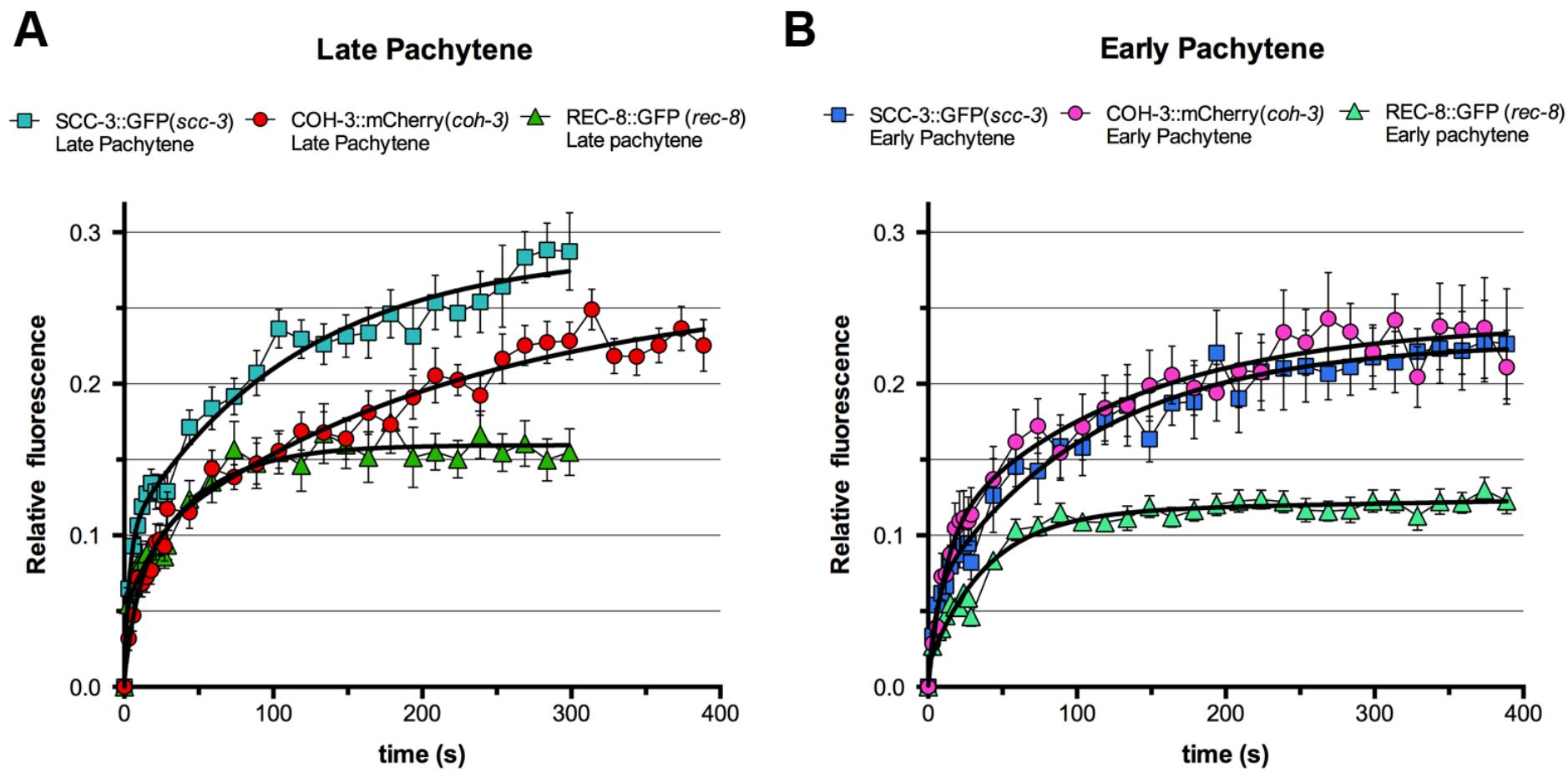
A
Late Pachytene
SCC-3::GFP(scc-3)
Late Pachytene
COH-3::mCherry(coh-3)
Late Pachytene
REC-8::GFP (rec-8)
Late pachytene
Relative fluorescence
0.0
0.1
0.2
0.3
0
100
200
300
400
time (s)
B
Early Pachytene
SCC-3::GFP(scc-3)
Early Pachytene
COH-3::mCherry(coh-3)
Early Pachytene
REC-8::GFP (rec-8)
Early pachytene
Relative fluorescence
0.0
0.1
0.2
0.3
0
100
200
300
400
time (s)

Figure 47. COH-3::mCherry shows reduced mobile pool and reduced axial recovery in *coh-3; coh-4* double mutant

A. FRAP of COH-3:mCherry; *coh-3; coh-4* strain (without REC-8::GFP and rec-8 mutation) with high resolution settings (as described in Figure 41 A). Dashed boxes mark bleached area.

B. Late pachytene mean recovery curve of COH-3::mCherry in *coh-3; coh-4* double mutant background and *coh-3* single mutant background (containing REC-8::GFP) acquired with low resolution settings (analysis and curve fitting as described in Figure 41 B). Single mutant background is same dataset as Figure 43 A. Double mutant background: n= 14, mobile pool = 16%, slow component half-life = 55 s. Single mutant background: n = 22, mobile pool = 26%, slow component half-life = 148 s. Y-axis = relative normalized mean fluorescence intensity. X-axis = time (seconds). Error bars = SEM.

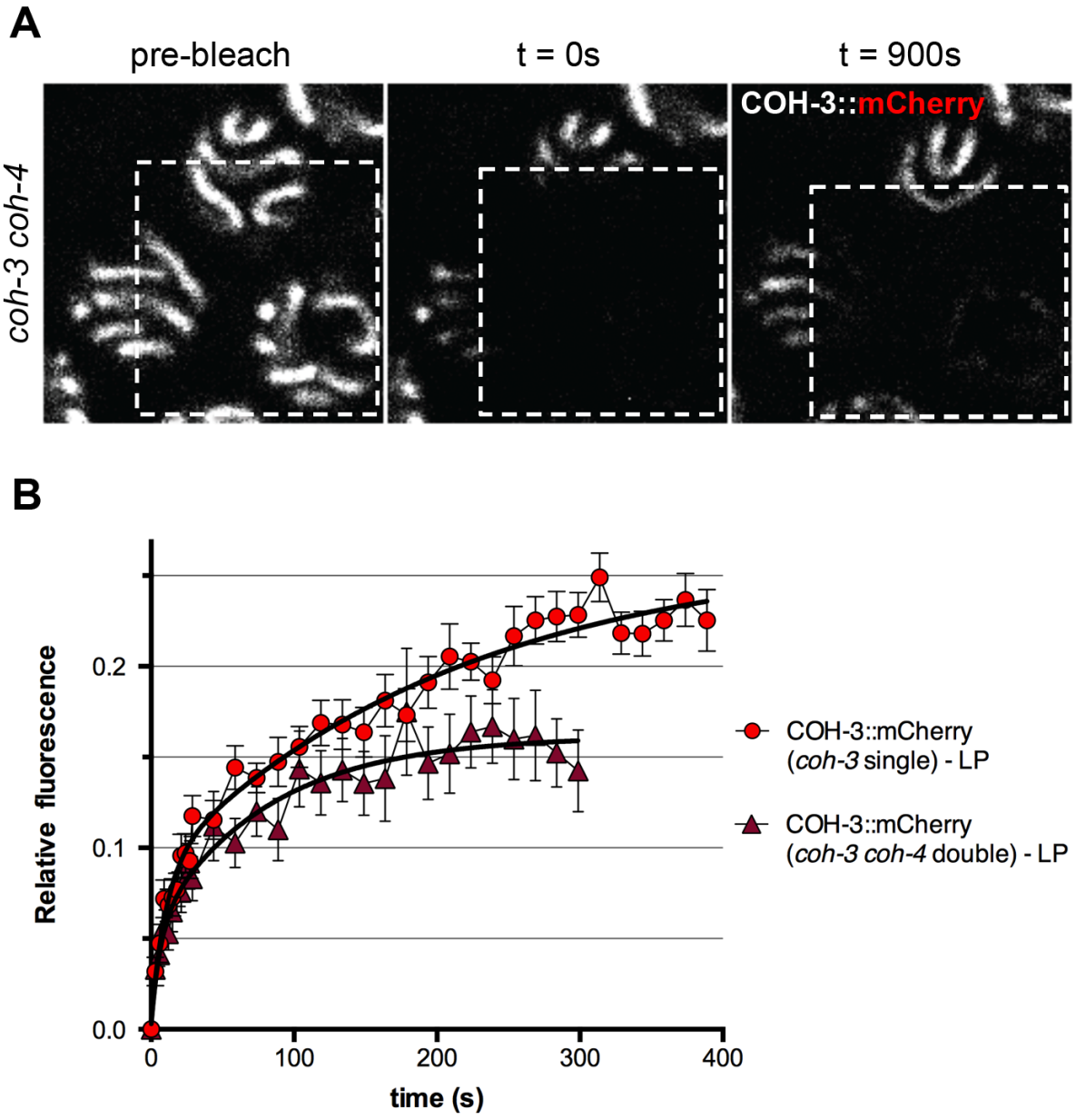
A
pre-bleach
t = 0s
t = 900s
COH-3::mCherry
coh-3 coh-4
B
Relative fluorescence
0.0
0.1
0.2
0
100
200
300
400
time (s)
COH-3::mCherry
(coh-3 single) - LP
COH-3::mCherry
(coh-3 coh-4 double) - LP

Figure 48. COH-3::mCherry and REC-8::GFP FRAP in the *wapl-1* mutant background

A. High resolution FRAP of COH-3::mCherry in *wapl-1* mutant background and control background (double mutant coh-3; coh-4 background used for both to stabilise expression). Images produce as described in Figure 41 A. Dashed boxes mark bleached area.

B. Late pachytene mean recovery curve of COH-3::mCherry in *coh-3; coh-4* background (controls) and *wapl-1*; *coh-3; coh-4* background (mutant) acquired with low resolution settings (analysis and curve fitting as described in Figure 41 B). Controls: n= 12, mobile pool = 18%, half-life = 40 s (one-phase curve). *wapl-1* mutant: n = 12, mobile pool = 14%, half-life = 60 s (one-phase curve). Y-axis = relative normalized mean fluorescence intensity. X-axis = time (seconds). Error bars = SEM. Note lower plateau in *wapl-1* mutant.

C. Late pachytene mean recovery curve of REC-8::GFP in *rec-8* background (controls) and *wapl-1; rec-8* background (mutant) acquired with low resolution settings (analysis and curve fitting as described in Figure 41 B). Controls: n= 8, mobile pool = 17%, slow component half-life = 36. *wapl-1* mutant: n = 16, mobile pool = 26%, slow component half-life = 32 s. Y-axis = relative normalized mean fluorescence intensity. X-axis = time (seconds). Error bars = SEM. Note higher plateau in *wapl-1* mutant.

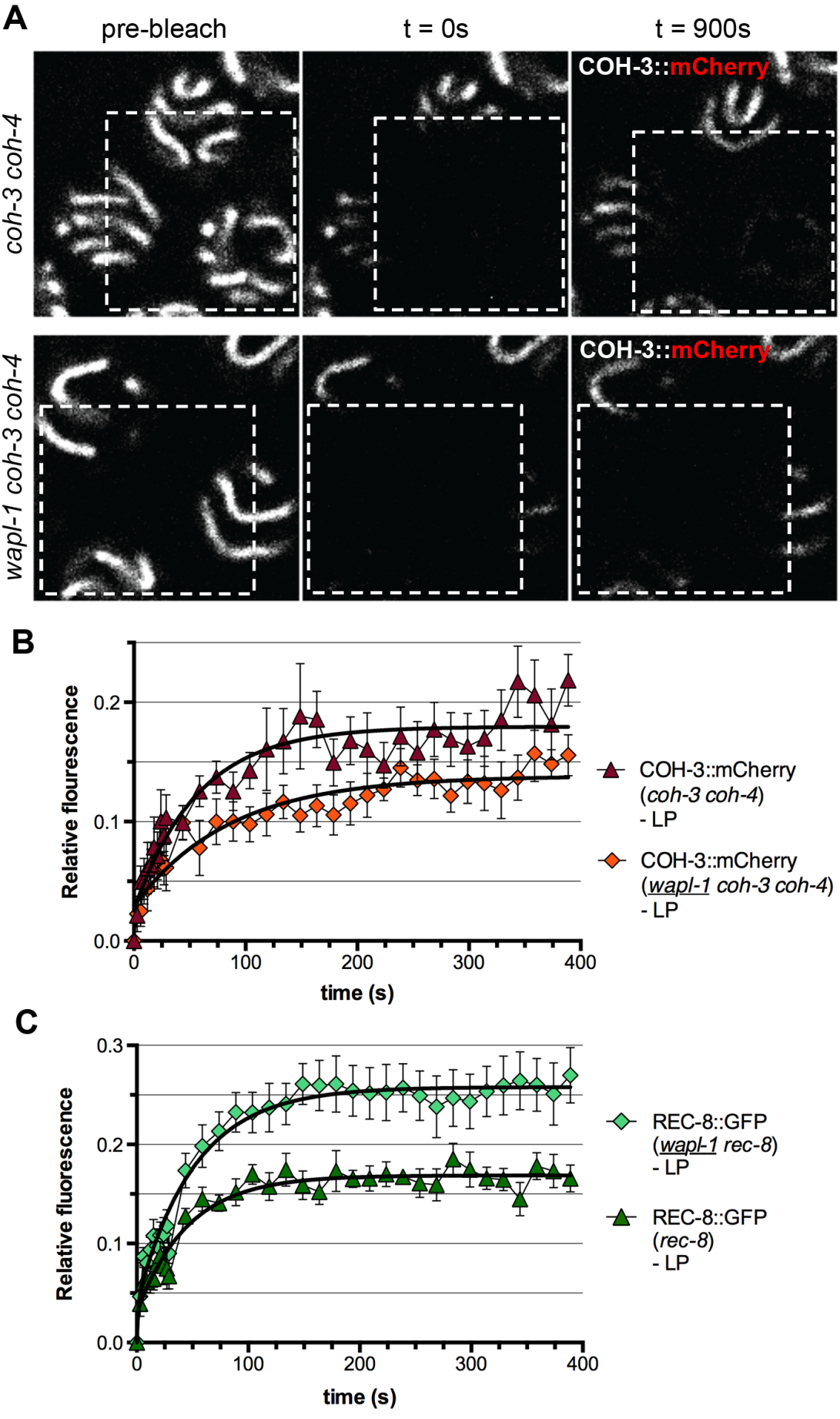
A
pre-bleach
t = 0s
t = 900s
coh-3 coh-4
COH-3::mCherry
wapl-1 coh-3 coh-4
COH-3::mCherry
B
Relative flourescence
0.0
0.1
0.2
0
100
200
300
400
time (s)
COH-3::mCherry
(coh-3 coh-4)
- LP
COH-3::mCherry
(wapl-1 coh-3 coh-4)
- LP
C
Relative fluorescence
0.0
0.1
0.2
0.3
0
100
200
300
400
time (s)
REC-8::GFP
(wapl-1 rec-8)
- LP
REC-8::GFP
(rec-8)
- LP

Figure 49. FRAP of GFP::WAPL-1

A. FRAP of GFP::WAPL-1 in *wapl-1* mutant background at late pachytene. Extra low resolution settings (as used for curve measurement and described for Figure 47 B). Dashed boxes mark bleached area. Note near full recovery to bleached halves of nuclei after t = 4 s.

B. Mean recovery curve of GFP::WAPL-1 at late pachytene acquired with extra low resolution settings and short timepoint intervals, 19x 0.19 s, 14x 4 s (analysis and curve fitting as described in Figure 41 B). . Y-axis = relative normalized mean fluorescence intensity. X-axis = time (seconds). Error bars = SEM. n= 31, mobile pool = 99%, half-life of fast component (majority) = ~1 s.

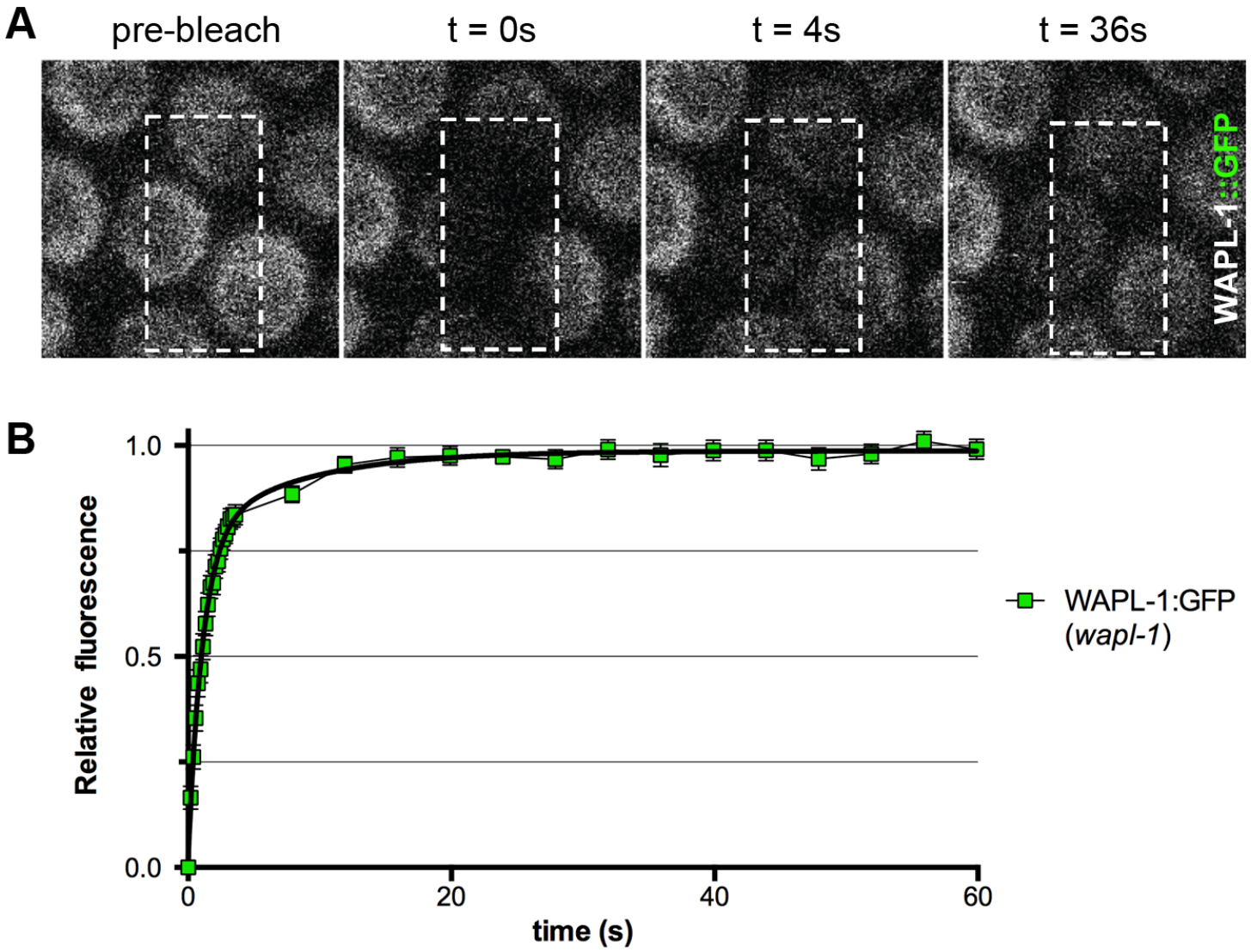
A
pre-bleach
t = 0s
t = 4s
t = 36s
WAPL-1::GFP
B
Relative fluorescence
1.0
0.5
0.0
0
20
40
60
time (s)
WAPL-1:GFP
(wapl-1)

CHAPTER 6: RESULTS

IDENTIFYING COHESIN INTERACTORS AND POST TRANSLATION MODIFICATIONS

6.1 Objectives

Previous chapters have demonstrated that WAPL-1 has an effect on the function and chromosome association of certain cohesin complexes, and studies in mitotic cells have shown direct interactions between WAPL and cohesin complex subunits by IP (Kueng et al. 2006; Gandhi et al. 2008; Shintomi and Hirano 2009; Chatterjee et al. 2013). As a result of this and other studies the current model of WAPL activity is thought to involve a direct destabilizing effect of WAPL on the cohesin complex, thereby transiently opening the SMC-3/kleisin interface, which creates an exit gate for the chromatin fibres (Chan et al. 2012; Eichinger et al. 2013; Ouyang et al. 2013). It is important to determine whether in meiosis WAPL-1 is similarly acting by direct interaction with the meiotic cohesin complexes. The fluorescently tagged transgenes described in chapter 5 provided ideal tools to begin to assess possible interactions between cohesin subunits and WAPL-1, and also to identify novel interactors of meiotic cohesin. This has not been the main focus of this project, but some experiments shown in this chapter tested for such interactions.

Another focus in understanding the precise mechanisms that regulate cohesin function has been to understand how PTMs on cohesin subunits affect different events of the cell cycle. Phosphorylations, acetylations and sumoylations on cohesin subunits at specific residues have all been shown to regulate key processes of mitotic cohesin, and modulate sensitivity to WAPL (Alexandru et al. 2001; Hauf et al. 2005; Rolef Ben-Shahar et al. 2008; Unal et al. 2008; Wu et al. 2012). It is currently unknown whether similar or novel PTMs control the diverse roles that cohesin displays in meiosis. Work described in this chapter has also begun to address this question of meiotic cohesin PTMs.

6.2 Identiffying cohesin interactors by IP

The most traditional method of testing for physical interactions between proteins is to perform IP experiments. Typically a protein of interest is pulled down from a solution containing multiple potential interactors via an immobilized antibody. The co-precipitated proteins with the target protein can be detected by mass spectrometry to assess the whole range of interactors. Instead of the endogenous protein, a transgene expressing the protein of interest fused to tag can be used to improve the specificity of the pull down. Antibodies to the tag should in theory give particularly clean readout of interactors because the tag bait peptide sequence should not be represented in any other endogenous protein. This approach was employed for assessing meiotic cohesin interactions combined with methods developed in our lab that enrich for *C. elegans* meiotic nuclei and extract the nuclear proteins.

6.2.1 REC-8::GFP interactors

It was important to determine the specific interactors of the different meiotic cohesin complexes to understand their specific regulation. The kleisins are most suited for this, as they are meiosis specific, and are themselves the differentiating components of different complexes. The REC-8::GFP transgene, described in chapter 5, shows functional rescue of a *rec-8* mutation and therefore is ideal for testing for interactors. Meiotic nuclei of the REC-8::GFP; *rec-8* strain were enriched for and the nuclear fractions were extracted. In order to determine the maximum interactions both soluble and insoluble fractions were mixed together to make the input for IP. α-GFP antibodies attached to beads (GFP-Trap) were used to pull down REC-8::GFP protein from the input mix, made up from 'soluble' (nucleoplasmic) and 'insoluble' (strongly chromatin bound) fractions. The elution from this IP was analysed by mass spectrometry to identify all the interactors. This sample dataset was compared to a whole nucleus sample similarly analysed by mass spectrometry to act as the input to assess relative IP enrichment. A table in Figure 48 shows some of the top hits from this analysis.

A protein that had a high intensity in the IP relative to the whole dataset but only very weakly or not at all detected in the whole nuclear sample would give a high fold enrichment. The proteins shown in Figure 48 are all in the top 100 hits from this

comparison out of more than 2000 overall listed. All the core cohesin subunits ranked quite highly (highlighted in orange), including REC-8 itself, confirming the success of the IP and that REC-8 does indeed exist within full cohesin complexes during meiosis. It is important to note that the worm homologue of SMC1 is called *him-1*. The value of 7.6 for the Log2 fold enrichment for REC-8 means the normalized relative intensity of REC-8 peptides in the IP sample is ~190 times greater than the normalized relative intensity of REC-8 peptides in the whole nucleus control. Therefore the enrichment of the cohesin subunits in the IP is very strong. As might be expected, WAPL-1 is not enriched in the IP sample at all. This would fit with the finding that REC-8 is not sensitive to WAPL-1. The cohesin loader SCC-2 did give a high relative enrichment in the IP however this protein was filtered out of the final list because only a single unique peptide was identified, below the threshold of 2 set for quality control.

Outside cohesin subunits, all the core axial element proteins that are required for SC formation in *C. elegans* are high in the list: HTP-1, HTP-2, HTP-3 and HIM-3 (highlighted in bright blue). This is in accordance with REC-8 cohesin complexes forming a core component of the axial/lateral element of the SC and showing interdependence for chromosome loading with these other AE components (Ding et al. 2006; Severson et al. 2009). Also of note is TOP-2 (Topoisomerase II); a key protein known to decatenate entanglements of sister chromatids in mitosis and regulate chromosome morphology in budding yeast meiosis (highlighted in pale blue) (Rudolph et al. 1999; Damelin and Bestor 2007; Li et al. 2013). An interaction with cohesin would not be surprising for such a protein. Three components of the anaphase promoting complex (APC) are among the top hits: MAT-1, MAT-2 and MAT-3. Activity of the APC is required for the progression through the cell cycle from metaphase to anaphase by triggering the cleavage of the kleisin subunit of cohesin in both mitosis and meiosis (Uhlmann et al. 1999; Buonomo et al. 2000; Furuta et al. 2000). MAT-1/2/3 were all shown to be required for metaphase to anaphase transition in C. elegans meiosis (Davis et al. 2002). As well as APC members LET-92 is among the hits, the worm homologue of PP2AC, which is the catalytic subunit of protein phosphatase 2. PP2A has been demonstrated in other organisms to prevent REC-8 phosphorylation and protect it from cleavage at the centromeres during meiosis I division and thereby maintain SCC for segregation at meiosis II (Kitajima et al. 2006). Finally, another protein of interest in the top hits is HCP-2 (Holocentric chromosome binding protein). This CENP-F homologue has been shown to play a role in the kinetochore in

mitosis (Moore et al. 1999). The rest of the proteins in the list, which are not highlighted, include various histone variants. These might be expected to interact with cohesin as they form the most core structural components of chromatin, although co-precipitation with cohesin does not seem to be reported in the literature and the predominant mode of interaction with chromatin is thought to be topological (Nasmyth and Haering 2009). Many other proteins showed significant enrichment in the IP, but are not displayed in the Figure 48: only 23 out of the top 62 are shown. Some of these have known or predicted functions but are not overtly related to meiosis or chromosome biology, while many are uncharacterized and show unclear homology by BLAST. More work is required to validate these interactions through further IP or genetic experiments. Especially important would be a mock IP alongside the IP for REC-8.

6.2.2 GFP::WAPL-1 interactors

It was interesting to determine whether WAPL-1 performs its functions through any stable interaction with cohesin, or if WAPL-1 only interacts with cohesin transiently, as suggested by the immunofluorescence and FRAP experiments. The strain with a GFP::WAPL-1 transgene in the *wapl-1* mutant background was used for an IP experiment using GFP-Trap beads, similar to the REC-8::GFP IP. The GFP::WAPL-1 was demonstrated to have correct meiotic function despite some incomplete rescue of the overall fertility of the *wapl-1* (*tm1814*) mutation. Therefore, one would expect any true interactors of WAPL-1 during meiosis to be observed. Figure 49 displays the small list of interactors from this IP. There are several important differences with this experiment from the REC-8::GFP IP. Firstly, a mock IP was performed where the GFP-Trap beads were incubated with nuclear extract from wild-type worms to rule out non-specific interactors with the α-GFP antibody. Secondly the reference sample was an aliquot of the input from a parallel IP experiment rather than a separately obtained whole nucleus sample. Also the type of mass spectrometry analysis was different and should allow for more accurate quantification than for the REC-8::GFP IP. For these datasets the fold enrichment, depicted by the coloured cells in Figure 49, is the raw intensity values over the mean input sample intensity. Rather than comparing the normalized fold enrichment as used for the REC-8::GFP IP. Only a relatively small number of hits show greater enrichment in the IP sample than both the input and the mock. These are shown in Figure 49 after filtering for a threshold Best Protein Score of greater than 70, as well as for a greater enrichment than 4 times from the mock IP.

The top hit in the list is WAPL-1, showing high intensity in the IP and undetected in both the input and the mock. The high number of unique peptides for WAPL1 in the IP sample supports this. 12 unique peptides were detected compared to 5 or less for the rest of the list. This confirms that the primary target of the IP was pulled down. No other cohesin subunits are in the list, including EVL-14/PDS5, which has been shown in several studies to form a dimmer with WAPL and be important for mediating WAPL activity upon cohesin (Shintomi and Hirano 2009; Sutani et al. 2009; Nishiyama et al. 2010; Kulemzina et al. 2012; Ouyang et al. 2013). No SC components or well-described meiotic factors are in the list either. However the second hit, Y48B6A.1, has been indicated as important for maintaining correct germ line proliferation and as a phospho-protein in the mitotic spindle as well as being a ribosome biogenesis factor (Nousiainen et al. 2006; Voutev et al. 2006). Although this lack of direct interaction with cohesin subunits needs to be confirmed by further IP experiments, it would be in line with the general picture of a largely nucleoplasmic protein showing limited stable association with chromosomes.

6.3 Post translational modifications of meiotic cohesin

6.3.1 Mass spectrometry and irradiation

Mass spectrometry provides a very good way of identifying post-translational modifications and determining the precise regulation of different proteins (Olsen and Mann 2013). Cohesin is known to receive PTMs in mitotic cells (Kitagawa et al. 2004; Heidinger-Pauli et al. 2008; Luo et al. 2008) and the IP experiments shown in the preceding sections did identify some peptides with possible modifications. Also a Western blot for α-GFP of the different nuclear fractions from REC-8::GFP; *rec-8* meiotic nuclei showed a shift in size of the band between nuclear 'soluble' and 'insoluble' fractions indicating possible phosphorylation or other modifications in the chromosome-bound REC-8. Phosphorylation is one of the most widely identified PTMs within cells, so we used a method designed to enrich phosphorylated peptides from cell extracts (Thingholm et al. 2006). This was performed on protein extracts from whole nuclei rather than fractionated extracts to capture the full spectrum of phosphorylations and limit the chance for them to be lost. Furthermore, many of the phosphorylation events on cohesin in mitotic cells occur in response to DNA damage. Assuming that external DNA damage will maximize phosphorylation events in cohesin and other proteins, we subjected worms to γ

irradiation before performing the phospho enrichment experiment and also ran a control sample of non-irradiated worms. Mass spec analysis of these samples identified a large number of phosphorylated peptides that were specifically enriched in the irradiated sample. Some that are of particular interest are displayed in Figure 50. As hypothesized there are some phosphorylations on cohesin subunits including SMC-3 S792 and COH-4 S308, which is conserved in COH-3. In addition, this analysis also identified phosphorylation events in cohesin-associated factors such as EVL-14, the worm homologue of PDS-5.

As expected, this experiment also identified phosphorylation events in factors known to be important for responding to DNA damage and cell cycle progression, including MUS-101, HSR-9 (also required for pachytene apoptosis), TOP-1 (topoisomerase I), CDK-1 (master cell cycle kinase) and MCD-1 (an apoptosis factor). Two other phosphorylated proteins are involved in chromosome segregation, which is of interest in relation to cohesin. KNL-2 is a kinetochore component while ICP-1 is a chromosomal passenger protein that localizes to the spindle and stimulates AIR-2 activity. This could be of interest because AIR-2 is known to regulate cohesin at meiotic anaphase (Rogers et al. 2002).

6.4 Summary of results

Understanding the molecular composition of the different cohesin complexes present during meiosis would help us to understand how these complexes affect meiotic chromosome function. In this chapter experiments have been shown that have begun to explore the composition of meiotic cohesin complexes. The IP of a tagged REC-8 transgene and analysis by mass spectrometry has indicated that not only is REC-8 clearly interacting with the other core cohesin subunits, but also with the other key axial element components (Figure 48). These results support findings with REC8 in other organisms and inform us of the structural make up of the SC. Possible interactions of REC-8 with histones, other chromosome factors and important meiotic regulators were also indicated. These interactions require validation, but may provide new lines of investigation within the study of meiotic cohesins. In line with the low sensitivity of REC-8 demonstrated in previous chapters, WAPL-1 was not identified as an interactor of REC-8. COH-3/4 were not enriched in the REC-8::GFP IP, confirming the model that these different kleisin homologues define functionally distinct meiotic cohesin complexes. IP of GFP::WAPL-1

transgene did not show any interaction with REC-8 but also no interaction was identified with any cohesin subunits at all, despite the striking effects shown of WAPL-1 on COH-3/4 complexes. This may reflect the apparent transient nature of WAPL-1 interactions during meiotic prophase (Figure 7 & 47). Further work is needed to determine the validity of this result, especially a reciprocal pull down experiment with COH-3/4.

The precise regulation of cohesin function during meiosis is very likely to involve a myriad of PTMs, as occurs for many processes in the cell. The preliminary results shown here have started to identify some phosphorylations, that are specifically enriched after exogenous DNA damage, demonstrating the validity of the methods used.

Figure 50. Mass spectrometry results from REC-8::GFP IP

List of proteins identified by mass spectrometry that were enriched in anti-GFP IP from the REC-8::GFP; *rec-8* strain compared to a whole nuclear protein sample (control). To order for enrichment the Max Quant intensities for each protein in both datasets were normalized as fold over maximum intensity for the whole dataset (0 to 1, columns 6 & 7, see colour scale). The normalized IP over the normalized whole nucleus (control) gives relative fold enrichment in the IP, by which the list is ordered. The Log2 of this fold enrichment is shown in column 8. Infinite enrichment results from zero detection in the whole nucleus sample. Hits were filtered by criteria of having at least 2 unique peptides as well as a Posterior Error Probability score (PEP) of less than 0.01 (zero = 100% certain of identity). All proteins shown are within top 100 proteins ordered in this way, column 9 shows rank position of the protein within the list. The number of unique peptides for a protein is shown for each sample (columns 4 & 5). Cohesin complex subunits are notable by their high number of peptides in the IP sample. Colours in column 1 and 2 correspond to function or protein family. Orange denotes cohesin complex subunit or auxiliary factors. Bright blue denotes SC components. Pale blue denotes other proteins of functional interest. Histone variants are not highlighted (white). High-ranking proteins not shown here are either uncharacterized or with no overt relevance to meiosis, the cell cycle or chromosome biology.

			Unique peptides		Norm. MQ intensity (Fold over Max)		Log2 Fold (Norm.IP/Norm.Whole nucl.)	
Protein/gene	Function	PEP - score	Whole nucl.	IP	Whole nucl.	IP		List placing
HIL-4	Histone	2.026E-79	0	5			∞	2nd
HIL-3	Histone	1.541E-36	0	3			∞	3rd
HTP-3	SC	1.558E-25	0	5			∞	6th
HTP-2	SC	3.674E-16	0	4			∞	7th
HIL-2	Histone	2.011E-45	0	3			∞	11th
LET-92 (PP2A)	Phosphatase	6.780E-14	0	2			∞	19th
MAT-1	APC	2.145E-116	0	3			∞	21st
HIM-3	SC	4.269E-93	1	11			9.4	33rd
HTP-1	SC	1.182E-85	1	5			8.3	35th
REC-8	Cohesin	1.22E-63	1	10			7.6	36th
HIS-47	Histone	8.260E-126	4	4			7.0	37th
HIL-5	Histone	9.674E-28	1	4			6.9	38th
HIS-24	Histone	1.501E-34	2	6			6.6	40th
HIM-1 (SMC-1)	Cohesin	1.4E-229	4	26			6.3	43rd
HCP-2	Kinetochore	8.759E-12	2	2			5.6	45th
MAT-3	APC	1.307E-15	1	3			5.0	50th
SCC-3	Cohesin	7.569E-54	5	13			4.8	54th
TOP-2	DNA topology	0	21	49			4.8	55th
HIS-46	Histone	1.31E-106	5	7			4.7	56th
HIS-45	Histone	6.29E-18	2	2			4.7	58th
MAT-2	APC	3.72E-56	4	2			4.7	59th
HTZ-1	Histone	4.01E-70	0	3			4.6	61st
SMC-3	Cohesin	0	4	29			4.5	62nd

Normalised MaxQuant MS intensities (fold over max)										
0	0.1	0.2	0.3	0.4	0.5	0.6	0.7	0.8	0.9	1

Figure 51. Mass spectrometry results from GFP::WAPL-1 IP

Table listing relevant proteins identified by mass spectrometry as enriched in anti-GFP IP from the GFP::WAPL-1; *wapl-1* strain compared to the IP input sample and compared to mock IP sample from α-GFP with wildtype (N2) sample. Two technical replicates were run for each sample: (a) and (b). To order the list for IP enrichment, the intensities for each protein in each replicate were calculated as a fold over the mean intensity for the two input replicates. These fold over mean values are represented in columns 7 to 12 by a colour (see scale below). If a protein was detected in the IP and not detected in the input at all, it gave infinite fold enrichment (red). The results were filtered initially for best protein score of greater than 70, for confidence of hits (column 3). The list was also filtered for showing greater than 4 times mean intensity in the IP samples than the mock IP mean. The fold increase in mean IP intensity over the mean input intensity is shown in the final column (all infinite for examples shown). The number of unique peptides identified for any protein in each sample is shown (columns 4, 5 & 6). WAPL-1 is notable by its high number of peptides in the IP sample. Colours in column 1 and 2 correspond to function or protein family. Orange denotes cohesin complex subunit or auxiliary factors. Pale blue denotes other proteins of functional interest. Uncharacterized proteins are not highlighted (white).

			Unique Peptides			Input /mean input		IP /mean input		Mock /mean input		
Protein/gene	**Function**	**Best prot. score**	**Input**	**IP**	**Mock**	**(a)**	**(b)**	**(a)**	**(b)**	**(a)**	**(b)**	**Fold - IP/input**
WAPL-1	Cohesin	120.5	0	12	0							∞
Y48B6A.1	Segregation	835.8	0	4	0							∞
DIM-1	Uncharacterised	97.2	0	1	0							∞
C25H3.7	Uncharacterised	81.9	0	5	0							∞
T23E7.2	Uncharacterised	147.5	0	1	0							∞
Y41D4B.11	Uncharacterised	269.4	0	2	0							∞
ZK484.3	Uncharacterised	334.5	0	2	0							∞

Fold intensity over mean input				
≤ 0.1	≤ 0.5	≤ 1	≤ 4	> 4

Figure 52. Identying phosphorylations after irradiation induced DSBs

List of phosphorylations in response to DSBs from irradiation, identified by mass spectrometry. Phospho-enriched whole nucleus protein sample of wildtype (N2) γ-irradiated worms were compared to equivalent samples from non-irradiated wildtype worms. Phospho-peptide hits shown here are at least 2.5 times more enriched in irradiated samples (on average). Columns 2 to 6 represent Log2 of the fold enrichment over the mean of the normalized values averaged from all samples (see colour scale below). 3 technical replicates were used for both conditions but replicate (a) for the irradiated sample was discarded for technical reasons. Fold change (column 8) shows mean of the normalized irradiated replicates over the mean of the normalized control replicates. p-value is the probability that the increased abundance is false. Residue column = amino acid position of the phosphorylation within the whole protein; S = serine, T = threonine. Colour in Residue column denotes confidence of the identity of that phosphorylation site within peptide, derived from Mascot Delta scores (see colour scale below, pale grey (+) = <10, dark grey (++) = 10-20, purple (+++) = >20). The peptide column gives the actual peptide sequence detected, asterix (*) marks phosphorylated amino acid(s).

		Control replicates			Irradiated replicates		Difference - Irradiated/Control			
Protein/gene	**Function**	**(a)**	**(b)**	**(c)**	**(b)**	**(c)**	**Fold change**	**p -value**	**Residue**	**Phospho-peptide**
MUS-101	DNA damage						39.27	0.0016	S1075	VAEMPVTFS*VSMENR
ICP-1	Segregation						18.98	0.0034	S354	TAPVAQPTVELS*PSRELQR
SMC-3	Cohesin						8.74	0.0046	S792	ELLAQKENFEQEIGSNMSS*QLTSDEEQTVK
KNL-2	Kinetochore						15.29	0.0004	S594	RAS*LEDNRDLNDSIACNRPR
TOP-1	DNA topology						4.64	0.0005	S38	DEPMAS*DSEVPFGELMKR
SYP-4	SC						5.82	0.0006	S448	DILATEQAALS*QEQEPEIVEK
HTP-3	SC						4.01	0.0007	S364 - S368	APAVPITPTEPAS*PVES*PVKEQPQKAPK
EVL-14 (PDS5)	Cohesin						3.43	0.0165	S1429	DNVS*LDNLIISPILDESSGR
COH-4	Cohesin						2.48	0.0065	S308	IAS*EILELDDEVLIPR
MCD-1	Apoptosis						2.32	0.0052	S245	SPS*PMLKEPLFDDNEIR
HSR-9	DNA damage						2.29	0.0057	T51	SLFGNSAVISTPARDST*PDGHIVDSSVITK
CDK-1	Cell cycle kinase						2.53	0.0213	T180	VYT*HEVVTLWYR

Log2 (Fold over mean)										
-5	**-4**	**-3**	**-2**	**-1**	**0**	**1**	**2**	**3**	**4**	**5**

Phosphorylation site confidence		
+	**++**	**+++**

CHAPTER 7: DISCUSSION

7.1 Summary of findings

The overall objective of my PhD was to better understand how cohesin dynamics are regulated during meiotic prophase and how this may impact upon the correct progression of meiotic events. To achieve this, I primarily aimed to determine whether WAPL, an antagonistic factor identified in removing cohesin and limiting SCC in mitotic prophase, has a role in *C. elegans* meiosis. More specifically, I wanted to understand how WAPL-1 it might affect the multiple cohesin complexes that exist in *C. elegans* meiosis, as appear to exist in most organisms except yeast. Experiments with meiotic chromosomes had previously indicated local and genome-wide removal of cohesin may occur during prophase (Suja et al. 1992; Eijpe et al. 2003; Yu and Koshland 2005; Garcia-Cruz et al. ; Hulten 2011). Also, previous findings have suggested that WAPL may be expressed in meiotic nuclei and possibly affects the correct progression of meiosis (Verni et al. 2000; Kuroda et al. 2005; Zhang et al. 2008a). To assess if WAPL-1, the *C. elegans* homologue of WAPL, has any roles in meiosis, I investigated the effects of a null allele of the *wapl-1* gene (*wapl-1*(*tm1814)*). I have shown that *wapl-1* mutants display a dramatic increase in the association of the COH-3/4 kleisins with meiotic prophase chromosomes. In contrast, removal of WAPL-1 had a minimal effect on the levels REC-8 associated with chromosome axis during prophase. SMC-3 showed an intermediate sensitivity of to loss of WAPL-1 implying that both COH-3/4 and REC-8 are likely to operate within the context of full cohesin complexes. The changes in cohesin association in the *wapl-1* mutant are accompanied by diverse defects: reduced fertility, segregation defects during the meiotic divisions, altered chromosome morphology, delays in diplotene chromosome remodeling and persistence of RAD-51 recombination intermediates. These data, together with the expression of a functional GFP::WAPL-1 transgene throughout meiosis, strongly indicate that WAPL-1 is a major regulator of meiotic chromosome function.

Having found that WAPL-1 regulates cohesin association with meiotic prophase chromosomes, it was important to determine whether WAPL-1 affected SCC during meiosis, as this is the most canonical function of cohesin in both mitosis and meiosis (Nasmyth and Haering 2009; McNicoll et al. 2013). In addition, the maintenance of meiotic

SCC has wide reaching impacts on human reproduction (Hassold and Hunt 2001; Jessberger 2012; Nagaoka et al. 2012). To test whether WAPL-1 is antagonizing meiotic SCC, genetic backgrounds were used in which meiotic SCC is compromised at diakinesis. Removing WAPL-1 from such cohesion compromised backgrounds consistently, and often dramatically, improved SCC in diakinesis oocytes. Such cohesion rescue was demonstrated to largely depend on the COH-3/4 kleisins. Therefore, WAPL-1 seems to be limiting the cohesive ability of cohesin complexes containing COH-3/4, while REC-8 complexes are largely unaffected. Furthermore, increased association of COH-3/4 to chromosomes was also shown to accompany the SCC rescue, similar to studies of WAPL in mitosis that demonstrated increased cohesin and SCC (Gandhi et al. 2006; Shintomi and Hirano 2009).

The finding that WAPL-1 regulates the amount of chromosome-associated cohesin during meiotic prophase suggests that there is a dynamic turnover of cohesin complexes at this stage. A parallel aim of my PhD was to definitively demonstrate that meiotic cohesin is actually turning over on chromosomes. Previous experiments in our lab, in which the cohesin loader SCC-2 was knocked down after meiotic S-phase, strongly indicated that some turnover of cohesin might exist during meiotic prophase in *C. elegans*. However, this was inferred from fixed germlines, so to categorically demonstrate this I developed live imaging FRAP methods to monitor the dynamics of cohesin in the *C. elegans* germline. By developing this technique for the first time, I also hoped to understand how live meiotic cohesin dynamics correlate to our findings with WAPL-1. FRAP imaging revealed significant cohesin turnover onto pachytene chromosomes of COH-3::mCherry and SCC-3::GFP, while turnover of REC-8::GFP was lower. My results imply that COH-3 has a much shorter half-life and larger mobile pool than REC-8, both indicating greater dynamic turnover. The increased live dynamics of COH-3 correlate with the greater sensitivities to WAPL-1. The finding that WAPL-1 antagonises cohesin-chromosome association and SCC during meiosis, together with the confirmation that cohesin is turning over during meiotic prophase has considerable implications for the understanding of meiosis and human reproduction. These will be discussed in the following sections, along with questions and uncertainties raised by these findings as well as proposed future investigations. (See Figure 53 for generalized model of findings from this thesis)

7.2 Affect of WAPL-1 on cohesin-chromosome association

Cohesin complexes play central roles in facilitating many key events that happen to chromosomes in the mitotic and meiotic cell division programs. By stably associating with chromatin and topologically entrapping DNA molecules, cohesin provides SCC from S-phase until chromatids segregate at anaphase. In mitosis, where cohesin has been more extensively studied, a large portion of cohesin is removed along the chromosome arms prior to anaphase (Waizenegger et al. 2000; Sumara et al. 2002). As a result, cohesin, and therefore SCC, only significantly remains at the centromeres. The conserved factor called WAPL is responsible for this prophase removal of cohesin and SCC from chromosome arms (Gandhi et al. 2006; Kueng et al. 2006; Shintomi and Hirano 2009). Different populations of the same basic cohesin complex with SCC1 as the kleisin are differentially regulated by PTMs and the presence of other factors to become sensitive, or not, to the antagonizing effect of WAPL (Nishiyama et al. ; Alexandru et al. 2001; Sumara et al. 2002; Hauf et al. 2005; Liu et al. 2013). The actual reason why prophase removal happens is not completely known, though it appears that reduced cohesin facilitates efficient segregation at the moment of anaphase and spares a large pool of SCC1 from cleavage by separase at anaphase. On the other hand, the association of larger amounts of cohesin with chromosomes may be required outside anaphase for DNA repair and gene expression outside its core role in SCC (Klein et al. 1999; Sjogren and Nasmyth 2001; Parelho et al. 2008; Wood et al. 2010). Indeed cohesin is reloaded rapidly at telophase using recycled cohesin removed by WAPL, at a stage when SCC is not even possible since sister chromatids are not present and removing WAPL has a dramatic effect on the organization of chromosomes during G0 (Tedeschi et al. 2013). The prophase pathway appears to solve this paradox, allowing cohesin to perform its different functions through the cell cycle in a very efficient way.

The more complex events of meiosis, such as pairing, synapsis, recombination and two-step release of SCC, place yet further requirements upon cohesin compared to mitosis. This is likely to account for the diversity of meiosis-specific cohesin complexes seen across many taxa (McNicoll et al. 2013). Exactly how these different cohesin complexes are regulated to bring about the coordinated progression of meiosis is only partly understood, especially in comparison to the current knowledge of cohesin functions during mitosis. Despite evidence for some removal of cohesin and local loss of cohesion

prior to meiotic anaphase, it was largely unknown whether WAPL controls the association of cohesin with meiotic chromosomes and thereby might limit meiotic cohesion. To understand if WAPL is active during meiotic prophase could have significant implications for human female reproduction, since cohesion exhaustion in arrested oocytes has been proposed to be an important factor in the dramatic fertility decline in older women (Hassold and Hunt 2001; Lister et al. 2010; Jessberger 2012). The presence of a WAPL-mediated pathway that promotes removal of cohesin during prophase might contribute to such cohesion exhaustion.

The association of cohesin with chromosomes has been shown to correlate with cohesion status in mitosis and meiosis. In mitosis, less cohesin is observed on regions of chromosomes where SCC is lost or relaxed while more cohesin is found where SCC is intact (Waizenegger et al. 2000; Hauf et al. 2005; Shintomi and Hirano 2009). This fits logically with the model proposing that cohesin complexes provide SCC by the topological entrapment of chromatin fibres (Haering et al. 2002; Nasmyth and Haering 2009). Hence, the stable association of cohesin with chromatin is a prerequisite for it to provide SCC. As such, it is a key finding from this project that loss of WAPL-1 causes a significant increase in the amount of cohesin associated with meiotic prophase chromosomes. This effect is striking on the kleisins COH-3/4, but minimal on REC-8. Furthermore, our experiments demonstrating that loss of WAPL-1 can rescue compromised meiotic SCC in background lacking REC-8 further support this idea that COH-3/4 are operating within complete, functional complexes. These data suggest that in normal meiotic nuclei WAPL-1 removes a significant amount of cohesin complexes containing COH-3/4, thereby limiting their stable association with chromatin (Figure 53).

Although the differential effect of WAPL-1 on complexes containing COH-3/4 or REC-8 was not necessarily predicted beforehand, at the same time it is not surprising given the very different meiotic roles shown for these diverged kleisins (Pasierbek et al. 2001; Chan et al. 2003; Severson et al. 2009; Severson and Meyer 2014). In *C. elegans* SCC is largely provided by REC-8 while COH-3/4 is dispensable for SCC, being more important for synapsis, chromosome morphology and DSB repair. Though REC-8 is also, directly, or indirectly, required for DSB repair and normal synapsis. An analogous delegation of meiotic roles for different meiotic cohesin complexes exists in various organisms, including plants and mammals (Bhatt et al. 1999; Xu et al. 2005; Herran et al. 2011;

Ishiguro et al. 2011; Lee and Hirano 2011; Lake and Hawley 2012; Yuan et al. 2012; Ishiguro et al. 2014). This would suggest that the different sensitivity to WAPL-1 of different kleisin subunits could be a fundamental and conserved aspect of their functional divergence. Detailed investigation of WAPL in meiosis of different organisms will reveal whether this is true.

A very recent study published in July of this year has shown that the plant homologues of WAPL play a role in meiosis of *Arabidopsis* (De et al. 2014). Plants lacking WAPL display reduced fertility and a delay in the removal of cohesin complexes containing the REC8 homologue SYN1 from diakinesis chromosomes. The authors also observed chromatin bridges during anaphase, and they conclude that removal of cohesin by WAPL during late prophase is required for efficient chromosome segregation. Whether cohesin staining patterns were altered at earlier meiotic stages such as pachytene was not described, and whether the staining pattern of the other meiotic kleisin SYN3 was affected was also not described. The only other studies that I am aware of that have investigated the possible role of WAPL during meiosis did not assess cohesin binding patterns (Verni et al. 2000; Lopez-Serra et al. 2013).

REC-8, COH-3 and COH-4 are not the only kleisin subunits to be expressed during *C. elegans* meiosis, broadening the potential targets of WAPL-1 activity. It has been shown that the predominantly mitotic kleisin SCC-1 is also expressed in *C. elegans* meiotic prophase (Pasierbek et al. 2001; Mito et al. 2003; Severson and Meyer 2014). In the earliest study they saw peripheral staining at pachytene that they said disappeared at diplotene. The 2003 study found SCC-1 expression strongly peaked at late pachytene and diplotene with large amounts of nucleoplasmic protein, which would correlate with the increase in SMC-3 association. While in the study this year they show weak staining on pachytene chromosomes and again high levels of nucleoplasmic protein from the end of late pachytene onwards. Interestingly, they also demonstrated some residual cohesive function of SCC-1; the already very limited SCC seen in the *rec-8; coh-3; coh-4* triple mutant was even further reduced by loss of SCC-1. Furthermore, in mice RAD21 (SCC1 homologue) has been observed on meiotic chromosomes as well as the meiotic specific kleisins REC8 and RAD21L (Herran et al. 2011; Ishiguro et al. 2011; Llano et al. 2012). Further work is needed to understand the role of SCC-1 in meiosis, but given its known

sensitivity to WAPL in mitotic cells (Stanvitch and Moore 2008), it is possible that increased SCC-1 mediates some of the meiotic effects seen in the *wapl-1* mutant.

Another kleisin called COH-1 was shown to localize to chromosomes at pachytene and diplotene in one study (Pasierbek et al. 2001), though it appears to stain throughout chromatin rather than just at the AE. Its function in meiosis remains uncertain and it is currently viewed as more important for somatic viability, being strongly expressed in somatic nuclei. However, it is possible that COH-1 and associated cohesin complexes are subject to the activity of WAPL-1 during meiosis. Such sensitivity of COH-1, and similarly SCC-1, to WAPL-1 could potentially account for some of the discrepancy in the SMC-3 and COH-3/4 whole nucleus IF quantification at early and late pachytene after loss of WAPL-1. SMC-3 shows a much larger increase at late pachytene than early pachytene in the *wapl-1* mutant compared to wildtype, while COH-3/4 shows a more constant increase at both stages. Alternatively, given that the IF quantification in question is of the whole nucleus it is possible that changes in expression may be more responsible for the discrepancy between SMC-3 and COH-3/4. Further characterization of both SCC-1 and COH-1during meiosis is required, in the context of our findings with WAPL-1.

One could argue it would not be surprising if there is an exaggerated effect on cohesin-chromosome association specifically at late pachytene in the absence of WAPL-1. This is because the expression of the GFP::WAPL-1 transgene is significantly greater towards the end of pachytene and into diplotene. More WAPL-1 protein would be expected to antagonise more cohesin and so the difference in staining between wildtype and *wapl-1* mutant should be greater. Therefore it is slightly unexpected that chromosome association of COH-3/4 was shown to be equally affected by the loss of WAPL-1 at late pachytene and early pachytene. One explanation is that the relatively crude nature of the whole nucleus intensity measurement is unable to detect a greater increase in the chromosome-associated levels of COH-3/4 at late pachytene. Unfortunately, the lineprofile quantification, which gives a more accurate representation of the changes to chromosome association, has so far only been applied to late pachytene. This was simply due to time constraints and will be carried out on ealier meiotic stages in the near future. Another possibility is that COH-3/4 might be so sensitive to the WAPL-1 that the lower levels at earlier stages of meiosis are already sufficient to cause the maximum effect. In support of the former explanation, overexpression of WAPL in mitosis significantly

impacts upon chromosome segregation and can even contribute to tumorigenesis (Oikawa et al. 2004; Gandhi et al. 2006; Kueng et al. 2006; Ohbayashi et al. 2007). Therefore, one would expect that expression levels of WAPL are important for control of cohesin association in meiosis. Further analysis with the lineprofile method or possibly overexpression of WAPL-1 in meiosis may help answer this question.

An interesting finding from the lineprofile analysis, carried out so far, is that it shows a significant increase in the REC-8 immunofluorescence intensity on chromosome axes in the *wapl-1* mutant, despite there being no difference in the whole nucleus quantification for REC-8. Although it is far less pronounced than for COH-3/4 or SMC-3 this discrepancy requires some explanation. It could mean that WAPL-1 limits the association of REC-8 with chromosomes, although to a much lesser extend than the effect on COH-3/4. Or alternatively, increased chromosome/SC compaction in the *wapl-1* mutant may simply concentrate the space that the same amount of loaded protein occupies resulting in higher peak values. If the latter explanation were true then it would imply that the increases seen for COH-3/4 and SMC-3 might actually be an exaggeration. Nevertheless, the effect should apply equally to all subunits subject to the same immunofluorescence method and hence the overall conclusion is valid that COH-3/4 association is far more sensitive to WAPL-1 than REC-8. Experiments taking a more biochemical approach would be ideal to support and clarify these findings. I did attempt to extract the different nuclear protein fractions from the wildtype and *wapl-1* mutant meiotic nuclei to compare the 'soluble' nucleoplasmic and 'insoluble' chromosome associated protein by Western blot. However, unfortunately in all attempts the *wapl-1*mutant showed contamination between the nuclear fractions. An alternative and more comprehensive approach to answer exactly how the different cohesin subunits is affected by WAPL-1 would be to perform ChIP-seq/chip to the different cohesin subunits in the wildtype versus *wapl-1* mutant meiotic nuclei. This would hopefully identify genome-wide changes to binding sites or amount of binding per site (Blat and Kleckner 1999; Ding et al. 2006; Tedeschi et al. 2013).

A final and important point of discussion regarding the cohesin immunofluorescence is that although the anti-COH-3/4 antibody does detect both COH-3 and COH-4, the contribution to this staining from COH-4 is far less. This is not surprising as the antibody was raised to a COH-3 peptide but given the high similarity of the COH-3 and COH-4 sequence there is some degree of cross-reactivity. Unlike with COH-3, we do not have an

antibody deemed reliable for COH-4 specifically, preventing us from concluding a clear picture of COH-4 behaviour. Interestingly, the anti-COH-4 antibody only shows strong tracks in the *coh-3* mutant, otherwise appearing as very discontinuous staining. This hints that there may in fact be an unequal pattern of association when both COH-3 and COH-4 are present. Genetically the two genes are redundant (Severson et al. 2009) and the only study in which staining patterns of these two proteins is shown only used a anti-COH-3/4 antibody that recognises both homologues (Severson and Meyer 2014). As such, conclusions about the individual behaviour of COH-4, at least in the presence of COH-3, cannot be made. Future work with improved anti-COH-4 specific antibodies or a tagged COH-4 transgene will reveal the full picture of its role in meiosis and its regulation by WAPL-1.

Overall the fact that a considerable amount of cohesin is actively removed by WAPL-1 during *C. elegans* meiosis leads to the possibility that a meiotic prophase pathway could be a factor in cohesion exhaustion of arrested oocytes. This notion is further supported by the changes that loss of WAPL-1 causes to various events in meiosis and to the cohesive function of cohesin complexes, as discussed in the following sections.

7.3 Impact of WAPL-1 on meiotic chromosome segregation

The increase in association of cohesin with chromosomes in the *wapl-1* mutant is accompanied by significant effects on a range of meiotic processes, implying that correct regulation of cohesin binding by WAPL-1 is required for correct meiosis. There is a large impact on overall fertility in the *wapl-1* mutant, with significant levels of embryo lethality. This indicated that gametes produced in the mutant might have defects in chromosome segregation. My assessment of oocyte meiotic divisions by live imaging confirmed that WAPL-1 does affect segregation, with abnormal chromosome movements seen in *wapl-1* mutant embryos. From the current understanding of WAPL activity and the increased cohesin levels seen at pachytene one might expect segregation to suffer. Correct alignment on the spindle and coordinated separation of chromosomes at anaphase is highly dependent on SCC, provided by cohesin. Excess cohesin caused by depletion of WAPL in mitosis of human cells and yeast causes delays in segregation and lagging chromosomes (Kueng et al. 2006; Haarhuis et al. 2013; Tedeschi et al. 2013). Interestingly, these two effects were not overtly seen in the *wapl-1* mutant oocyte divisions, but instead the polar bodies invariably display strange behaviours. In mutant

embryos the first polar body undergoes an aberrant division and shows excessive movements. Normally the first polar body remains very compact and shows limited movement (Albertson and Thomson 1993; McNally et al. 2006). Furthermore, the second polar body also moves excessively and has more dispersed chromosomes in the *wapl-1* mutant than in the wild type. Sometimes this second polar body movement even disrupts the mitotic divisions of the embryo. DAPI staining of fixed embryos (data not shown) has found defects in the morphology and location of polar bodies in the *wapl-1* mutant, similar to those seen by the live imaging. Also in agreement, no obvious lagging chromosomes were seen in the fixed embryos nor increase in the number of embryos at the metaphase/anaphase of meiosis I, which would indicate a delay in the segregation. The results from the fixed embryos suggest that the defects seen in live imaging are unlikely to arise from pleiotropic effects of the H2B::mCherry transgene, because the fixed embryos were from standard *wapl-1* mutants. Furthermore, this transgene has been used in previous studies to determine behaviour of chromosomes at meiotic embryo divisions (McNally et al. 2006; Deyter et al. 2010).

Defects in the meiotic divisions could be due to possible errors in spindle attachment and regulation, rather than difficulty in releasing SCC at the anaphase. Cohesin is essential for the appropriate attachment of the spindle to the chromosomes and their correct orientation in meiosis as well as mitosis (Tanaka et al. 2000; Sonoda et al. 2001; Yokobayashi et al. 2003; Salic et al. 2004; Watanabe 2012). It is easily conceivable that incorrect spindle attachment could result from excess cohesin or aberrant distribution of the different complexes within the bivalent structure, in the absence of WAPL-1. Of relevance to this idea, both in my staining experiments and observations by my colleague Sarah Testori, it was noticed that COH-3/4 seems to become restricted mainly to the short arm of the bivalent at diakinesis. The same observation has recently been demonstrated in a study published this year (Severson and Meyer 2014). It could be hypothesized that this distribution of particular cohesin subunits/complexes may influence the attachment of the spindle for the first meiotic division, directly or indirectly. If COH-3/4 are not sufficiently removed from the long arms in the *wapl-1* mutant, one could imagine the erroneous presence of COH-3/4 in the long arms after the first division might cause the spindle to treat the separated homologues as meiosis I-like chromosomes. As such these attachments could trigger a meiosis I type division, hence the attempted division of the first polar body that we see.

Unfortunately the unreliable staining pattern of the anti-COH-3/4 antibody at diakinesis prevented me from making a proper assessment of the COH-3/4 staining in diakinesis oocytes of *wapl-1* mutants. However, preliminary experiments with the COH-3::mCherry transgene suggest that COH-3 may persist on the long arms of the bivalent at diakinesis. Future experiments with a more stable COH-3 or COH-4 tagged transgene will hopefully reveal if WAPL-1 is required for this loss of COH-3/4 from the long arm.

Another experiment to test the hypothesis that WAPL-1 controls appropriate spindle behaviour through COH-3/4 distribution within the bivalent would be to visualise the spindle in the *wapl-1* mutant meiotic divisions. This could be performed either with immunostaining or live imaging of fluorescently tagged spindle components. Interestingly, a recent paper investigating the roles of WAPL in plant meiosis found that spindle assembly and structure showed various abnormalities in male *Wapl* mutant meiotic divisions (De et al. 2014). Although it is hard to draw direct parallels, given that I have looked at female asymmetric divisions with polar bodies, the findings in *Arabidopsis* support the general idea that problems with the spindle may be responsible for the segregation problems we have observed in the *wapl-1* mutant.

The original study that identified WAPL as a gene in *Drosophila* did briefly assess the effect of its loss on meiosis (Verni et al. 2000). They found that it did affect the segregation of achiasmate chromosomes (without COs). Though the predominant findings were that WAPL controls heterochromatin morphology and gene expression in somatic cells. Unlike most subsequent studies they concluded that WAPL is required for the close 'apposition' of sister chromatids rather than antagonizing it. This may arise from a peculiarity of their system or experimental approach. One study of budding yeast Wapl published last year briefly assessed meiosis but after finding no effect on viability of spores in the absence of Wapl concluded that meiotic segregation is not affected by Wapl (Lopez-Serra et al. 2013). The fact that yeast meiosis only has a single cohesin complex containing REC8, unlike most other organisms studied, may partly explain this result. It will be very interesting to see if WAPL is also found to affect chromosome segregation in mammalian meiosis, as this could have important consequences on understanding human fertility.

7.4 Effect of WAPL-1 on meiotic SCC

It was vital in this project to find out whether WAPL-1 is not only controlling the association of cohesin with chromosomes, but also whether meiotic SCC is antagonized by WAPL-1. In mitosis WAPL facilitates the loss of cohesion along chromosome arms while SCC is tightly retained at centromeres. To test if WAPL-1 is limiting the amount of cohesion that meiotic cohesins provide we assessed whether loss of WAPL-1 could rescue SCC defects from cohesion compromised due to lack of REC-8. The addition of the *wapl-1* mutation to all such backgrounds that we looked at resulted in significant and sometimes remarkable rescue of cohesion, which is dependent on COH-3/4 (see chapter 4). Interestingly, removal of WAPL rescued SCC defects in the presence and absence of DSBs, demonstrating that COH-3/4 can provide SCC in the absence of DSBs. It was not possible to test whether cohesive function of REC-8 complexes is limited by WAPL-1, because there is no cohesion-compromised background so far identified in which REC-8 is present. So it still remains theoretically possible that the cohesive function of REC-8 is affected by WAPL-1. However, the simple fact that REC-8 does provide such robust SCC whenever it is present strongly supports the conclusion that WAPL-1 specifically antagonises SCC provided by COH-3/4 complexes. Evidence from the mitotic roles of WAPL is consistent with a model in which WAPL continually modulates cohesin binding throughout the cell cycle (Kueng et al. 2006; Gause et al. 2010; Nishiyama et al. 2010; Chan et al. 2012; Tedeschi et al. 2013). Moreover, recent experiments also show that WAPL antagonises SCC that was established at S-phase during G2 (Chan et al. 2012; Lopez-Serra et al. 2013). These experiments provide support for our conclusion that WAPL-1 is capable of antagonizing SCC during meiotic prophase. Whether WAPL also antagonizes meiotic SCC in other organisms remains to be elucidated.

A key question that follows from my findings is why WAPL-1 preferentially limits the SCC provided by COH-3/4 over REC-8. In mitosis there is a common mechanism by which many cohesin complexes are made insensitive to WAPL: acetylation of the SMC3 subunit by ECO1 acetyltransferase at certain conserved lysine residues (Ivanov et al. 2002; Rolef Ben-Shahar et al. 2008; Unal et al. 2008). This cohesion establishment mechanism normally only occurs at S-phase and its main purpose is to confer resistance to the destabilizing affect of WAPL (Chan et al. 2012). It is interesting therefore that REC-8 loads to chromosomes during pre-meiotic S-phase in *C. elegans* and other organisms (Pasierbek

et al. 2001; Watanabe et al. 2001; Eijpe et al. 2003), while COH-3/4 and a functionally equivalent kleisin in mice, RAD21L, only seem to load after entry to meiosis, following completion of S-phase (Ishiguro et al. 2014; Severson and Meyer 2014). It is possible that SMC-3 loaded at pre-meiotic S-phase, within cohesin complexes containing REC-8, is acetylated by ECO1, making it insensitive to WAPL-1. While SMC-3 within complexes containing COH-3/4 cannot be acetylated because it is loaded to chromosomes after S-phase when ECO-1 is not active.

A study in fission yeast found that Eso1, the *S. pombe* ECO1 homologue, was required to establish centromere cohesion in meiosis (Kagami et al.). Also a study in *Arabidopsis* showed that loss of ECO1 causes segregation and chromosome morphology defects in meiosis (Bolanos-Villegas et al. 2013). However, a study recently published this year has shown that the *Drosophila* homologue of ECO1 is required during meiotic prophase to maintain chiasmata during meiotic prophase (Weng et al. 2014). This suggests that ECO-1 may be active after S-phase in meiosis, though it does not rule out that the timing of loading for different meiotic cohesin complexes may affect their sensitivity to WAPL-1. It is possible that ECO1 may only be active post S-phase for a brief stage or for a very specific subset of cohesin complexes for example. It is also possible that alternative PTMs, coinciding with S-phase, may confer resistance to REC-8 cohesin complexes. This idea is supported by the fact that various other PTMs on cohesin subunits, other than SMC-3 acetylation by ECO1, have already been demonstrated to regulate SCC during mitotic prophase, including phosphorylation of SCC1 and SCC3 and sumoylation of SCC1 (Sumara et al. 2002; Kitajima et al. 2005; Heidinger-Pauli et al. 2008; McAleenan et al. 2012; Wu et al. 2012). An alternative explanation, outside PTMs, for how the timing of loading may control sensitivity to WAPL could be that other factors only present or active during S-phase could affect the way cohesin complexes are loaded to establish SCC. Further characterization of meiotic cohesin PTMs and interactors may help elucidate how different meiotic cohesin complexes establish SCC and respond to WAPL-1.

7.5 Meiotic cohesin reloading

Within the field of meiotic cohesin a contentious question has been whether cohesin reloads to chromosomes during prophase of meiosis. This question has clear relevance to human fertility since mammalian oogenesis includes a long arrest at the end of meiotic prophase that last from before birth until ovulation, two events that can be separated by

up to 50 years (Mira 1998; Zhang and Xia 2012). Therefore, the production of viable eggs in humans requires that oocytes survive this prolonged arrest, during which chiasmata sustained by SCC provide the only connection between homologues. Crucially, loss of cohesin, and hence deterioration of cohesion, during this prolonged arrest is thought to be a major factor in the dramatic decline in female fertility with increasing maternal age (Mark and Zimmering 1977; Hassold and Jacobs 1984; Hassold and Hunt 2001; Jessberger 2012; Nagaoka et al. 2012). Decrease in meiosis-specific cohesins during ageing of arrested oocytes has been confirmed by quantifying IF for different cohesin subunits in both humans and mice (Chiang et al. 2010; Lister et al. 2010; Duncan et al. 2012; Tsutsumi et al. 2014; Yun et al. 2014). Older oocytes have features characteristic of weakened cohesion: larger inter-kinetochore distance, more weakly attached bivalents and lagging chromosomes. Loss of shugoshin (SGO2) form centromeres has also been seen, a factor required to protect cohesion, though it is unclear whether this is causative or symptomatic of cohesin loss.

Knowing that cohesin and cohesion can deteriorate over time, it is important to determine whether cohesin is turning over on chromosomes during meiotic prophase. Not only does this inform how overall cohesin may be lost but also if cohesin is reloaded then it could contribute to maintaining cohesion. Two studies in mice have refuted that functional cohesin turnover (i.e. providing cohesion) occurs during meiotic prophase. One study demonstrated that when all endogenously expressed REC8 is artificially destroyed before metaphase I, REC8 expressed *de novo* during prophase arrest is unable to prevent premature separation of homologues and sister chromatids (Tachibana-Konwalski et al. 2010). This does imply that if there is REC8 reloading it is not sufficient to alone provide SCC within bivalents. However, this experiment does not preclude gradual cohesin turnover contributing to successful maintenance of a chiasma structure within the context of mostly stable bound cohesin. In the second study, they did the reverse experiment by preventing any *de novo* expression of the meiosis specific SMC1-beta subunit in prophase arrested oocytes (Revenkova et al. 2010). This did not result in premature loss of SCC or degradation of chiasmata. However, this does not rule out turnover of recycled cohesin expressed before arrest. Also, the authors did not investigate turnover of multiple different cohesin complexes that exist in mammalian meiosis. Furthermore, even if reloaded cohesin does not provide significant SCC during late prophase arrest, cohesin

turnover at earlier stages of meiotic prophase may affect the various roles of cohesin outside SCC including DNA repair, chromosome morphology and synapsis.

In contrast to the mice studies, a recent study in *Drosophila* suggests that ECO1 is required to maintain chiasmata and for cohesin to remain associated with chromosome axes during meiotic prophase (Weng et al. 2014). ECO1 is the acetyltransferase that acetylates SMC3 and thereby establishes SCC by making cohesin complexes resistant to WAPL removal. The authors specifically knocked down ECO1 after meiotic S-phase, which suggests that newly established cohesion is important for cohesin to resist WAPL activity. This not only supports our finding that WAPL is active during meiotic prophase, but also indicates that there is reloading of cohesin during meiotic prophase. Work in our lab involving knockdown of SCC-2, the cohesin loading factor, has also indicated that cohesin is reloaded to meiotic chromosomes after S-phase and that this is required for the maintenance or formation of chiasmata. However, all this work has been performed on fixed meiotic nuclei and it was important to definitively show whether cohesin is turning over on meiotic chromosomes by studying live meiotic nuclei.

In chapter 5, I demonstrated clearly that cohesin is dynamically turning over on live meiotic prophase chromosomes. FRAP imaging of intact live worms revealed that a significant fraction of COH-3::mCherry is rapidly turning over on pachytene chromosomes, whereas REC-8::GFP turnover occurs at lower levels. Importantly, a similarly significant and rapid turnover was seen for SCC-3::GFP suggesting that the dynamic COH-3 may exist within the context of whole cohesin complexes. This major difference in dynamics of different kleisins correlates with the divergence in their sensitivity to WAPL-1 shown in other experiments. In addition, I showed that loss of WAPL-1 reduces the extent of COH-3::mCherry turnover during pachytene, while it does not reduce the turnover of REC-8::GFP. Together, this evidence suggests that the limited cohesive function of COH-3/4 may directly result from the destabilizing effect of WAPL-1. This is analogous to the mode by which WAPL affects some mitotic cohesin complexes (Kueng et al. 2006; Chan et al. 2012; Tedeschi et al. 2013). The major difference is that in mitosis differently modified populations of the same underlying complex differentially respond to WAPL, all with SCC1 as the kleisin. While in meiosis the varying kleisin subunit of cohesin complexes seems to dictate sensitivity to WAPL. Though it does seem likely that there are subpopulations within the different types of meiotic cohesin complex that

have different dynamics. Further FRAP experiments and better understanding of the regulation of meiotic cohesin by PTMs is required to answer such questions.

The different dynamics of REC-8 and COH-3/4 cohesin complexes may be important for their divergence in roles within meiosis. The greater turnover of COH-3/4 and removal by WAPL-1 may allow its specific role in controlling the structure of the SC and DSB repair. Accordingly, both of these processes are disrupted in the *wapl-1* mutant. While on the other hand, the limited turnover of REC-8 and its limited sensitivity to WAPL-1 may help ensure robust maintenance of SCC until meiotic anaphase as well as being important for the other roles of REC-8. Although these experiments do clearly demonstrate some reloading for the first time, it will be important for the broader context to show that there is cohesin turnover at diplotene/diakinesis where female prophase arrest occurs. It will also be essential to determine if reloaded cohesin can provide any SCC and hence affect the stability of chiasmata.

7.6 Effect of WAPL-1 on meiotic DSBs

The persistence of RAD-51 foci in late pachytene nuclei of *wapl-1* mutants suggests that controlling the levels of chromosome-bound cohesin complexes is important for efficient DNA repair during meiosis. Changes to the levels of cohesin have previously been shown to affect the DNA repair function more readily than SCC (Heidinger-Pauli et al. 2010). It has been hypothesized that reloaded cohesin and reinforced cohesion may stabilize alignment of sisters and appropriate recombination intermediates to allow effective sister repair. I propose a possible model that in meiosis the high turnover of COH-3/4, a process that is facilitated by WAPL-1, mat limit SCC at sites of DSB, thereby facilitating interhomologue repair. Another potential model is that COH-3/4 play a crucial role in the precise structure of the SC, so that increased levels of axis-associated COH-3/4 in the absence of WAPL-1 disrupt SC structure, which in turn affects the efficiency of DSB repair. Evidence for this is in the fact that loss of COH-3/4 almost completely abrogates SC assembly (Severson et al. 2009). Furthermore, disruption of any other major component of the SC has significant consequences on DSB repair (Zetka et al. 1999; MacQueen et al. 2002; Martinez-Perez and Villeneuve 2005; Goodyer et al. 2008). Further evidence for this model comes from our finding that the length of the SC and overall compaction of the chromosome is significantly affected in the *wapl-1* mutants. There is clearly a need for

greater understanding of how cohesin precisely controls and responds to the unique recombination events that occur during meiosis.

A key area for future research is to explore how the dynamic association of cohesin with meiotic chromosomes is regulated by PTMs in different cohesin subunits, as well as by cohesin-interacting proteins. My efforts to map phosphorylation sites in cohesin subunits after irradiation and to identify interactors of meiotic cohesin by immunoprecipitation and mass spectrometry analysis provide a step in that direction.

Figure 53. (over page). Model of regulation of *C. elegans* cohesin dynamics during meiotic prophase and potential impact on human female fertility

A. Depicts a summary model of key findings about cohesin dynamics. WAPL-1 was shown to be active during meiotic prophase and antagonises the stable association of certain cohesin complexes that contain COH-3/4 as their kleisin subunit, during pachytene. This appears to limit their ability to provide SCC through to diakinesis, which was exposed by the absence of other kleisin homologues, namely REC-8. Complexes containing REC-8 kleisin seem to be relatively insensitive to WAPL-1 providing robust SCC whenever present. Mammals also have multiple meiotic specific kleisin subunit orthologues where a similar regulation of meiotic prophase cohesin dynamics by WAPL-1 may occur. (Purple triangular protein marked with letter W represents WAPL-1, circle of three arrows represents turnover)

B. Such meiotic cohesin turnover in prophase arrested oocytes may influence cohesion exhaustion and premature loss of SCC and therefore help explain increased rates of aneuploidy seen in oocytes from older mothers. (Dashed arrow indicates potential causation)

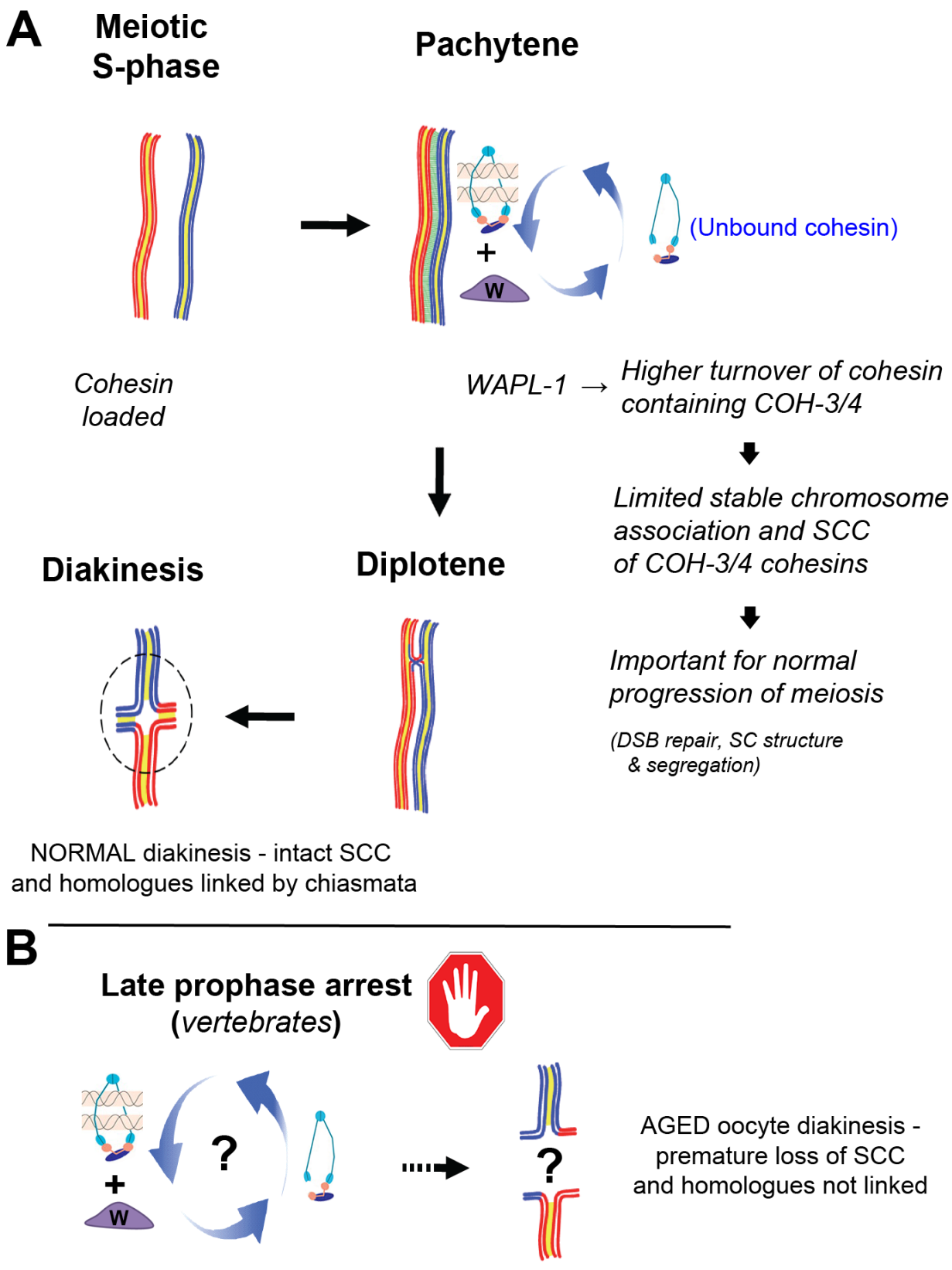
A
Meiotic S-phase
Pachytene
(Unbound cohesin)
W
Cohesin loaded
WAPL-1 → Higher turnover of cohesin containing COH-3/4
Limited stable chromosome association and SCC of COH-3/4 cohesins
Important for normal progression of meiosis
(DSB repair, SC structure & segregation)
Diplotene
Diakinesis
NORMAL diakinesis - intact SCC and homologues linked by chiasmata
B
Late prophase arrest (vertebrates)
?
W
?
AGED oocyte diakinesis - premature loss of SCC and homologues not linked
Turnover of cohesin mediated by WAPL-1 during meiotic prophase could contribute to cohesion exhaustion

CHAPTER 8: APPENDIX

MAPPING AND INITIAL CHARACTERISATION OF *fq9* ALLELE OF *pph-4.1*

8.1 Objectives

At the start of my PhD and continuing from some work begun during my MSc there was a side project that was not overtly related to the main focus of investigating cohesin dynamics. The aim of this project was to map and characterize a crossover deficient mutant that was isolated in a forward genetic screen using EMS mutagenesis. The screen and initial isolation of the mutant was carried out by Sarah Testori, a fellow PhD student. I then mapped and identified the mutation alongside some initial assessment of the meiotic defects, as this chapter will describe. After the molecular identity of the mutation was mapped to *pph-4.1* (worm homologue of protein phosphatase I), we collaborated with a group in Japan, led by Peter Carlton, who had already been working on this gene in meiosis. A collaborative paper with the Carlton lab is currently in press.

8.2 *fq9* mutant shows meiotic defects

Before my arrival in the lab a forward genetic screen for crossover deficient mutants had been carried out by Sarah Testori. The design of this screen was very similar to the one described in studies previously published from our lab (Lightfoot et al. 2011; Labrador et al. 2013). Cytological defects in the germline were identified in F2 progeny by DAPI staining. Of several mutants identified that displayed univalents in diakinesis oocytes, one was initially named '415' and hereafter called *fq9*. My work began with outcrossing this mutant to the wild-type N2 background to isolate the potential causative mutation from any secondary mutations. Homozygous worms carrying the *fq9* mutation were quite sterile and so heterozygous worms were outcrossed to the N2 background, following the mutation by assessment of diakinesis chromosomes in the progeny. The phenotype remained stable after outcrossing for several generations indicating a single mutation locus was likely responsible and therefore suitable for further study.

8.2.1 Univalent phenotype worsens with age

A striking observation of the *fq9* mutant was the apparent variability in the penetrance of the univalent phenotype at diakinesis, even within the same worm. In many adult mutant worms diakinesis oocytes could be seen with mainly univalents, 10 -12 DAPI stained bodies, while immediately next to them are oocytes that only contained bivalents (6 evenly sized DAPI bodies). Intermediate numbers of DAPI bodies (7,8 or 9) in diakinesis oocytes are more rarely seen and the pattern of affected and unaffected oocytes appears to be randomly mosaic with respect to meiotic progression. Typically, adult worms checked by fixation were around 24 hours post L4, as is standard protocol. However, occasionally older worms were assessed due to time constraints (48 hours or more post L4) and it was clear that the balance of affected versus unaffected shifts with the majority of oocytes displaying univalents (Figure 51 A). This age deterioration was quantified by scoring oocytes as having univalents or showing 6 normal looking bivalents in *fq9* homozygous adults of different ages: 24, 48 and 72 hours post L4. A ratio of affected and unaffected oocytes was determined for each worm and this was then averaged to account for variable numbers of appropriate oocytes. The results from this quantification are shown in Figure 51 B. The most significant change occurs between 24 hours post L4 and 48 hours post L4, going from 62% wildtype looking oocytes to 16% respectively. A *t*-test shows this change to be highly significant. There appears to be a further decrease in the number of unaffected oocytes with 6 bivalents but this is not statistically significant from the numbers counted. Other observations suggested that this was not entirely due to maternal rescue and may represent some underlying ageing deterioration, this has since been supported by experiments done in the Carlton lab with whom we have collaborated.

8.2.2 CO formation versus bivalent dissassembly

Given the mosaic phenotype of the diakinesis oocytes it was possible that COs are being formed correctly in the *fq9* mutant but these are unable to be maintained with a possible late loss of cohesion. Immunofluorescence of REC-8 did not show any obvious defects in the axial pattern of cohesin on meiotic chromosomes in *fq9* mutants of any age (data not shown). Staining of other SC components in the mutant did not reveal any major differences to wild type germ lines. This supports the fact that no more than 12 bodies are seen at diakinesis indicating that SCC is not affected in *fq9* mutants. Failure to make COs

appears to be a more likely cause for the univalents at diakinesis rather than disassembly of chiasmata.

In order to consolidate this hypothesis, the *fq9* mutation was crossed to the ZHP-3::GFP transgene and patterns of ZHP-3 foci, which mark CO recombination events (Bhalla et al. 2008), checked by α-GFP staining. In the wild-type germ line ZHP-3 tracks disappear to form 6 foci are seen at late pachytene/diplotene marking the 6 sites of COs. Persistence of ZHP-3 tracks and incorrect number of foci indicate that CO formation *per se* is defective in the *fq9* mutants. Further characterization was not continued after the identity of the mutation was determined because a collaboration was initiated with the Carlton lab, Kyoto University. The age deterioration phenotype in CO formation had not been noticed previously and contributed significantly to their investigation.

8.3 Idenification of the *fq9* mutation

8.3.1 DraI mapping

To begin the mapping of the mutation the quick DraI digest mapping technique was employed to roughly place the mutation to the broad region on one of the six *C. elegans* chromosomes (Davis et al. 2005). This technique makes use of the Hawaiian *C. elegans* strain and its divergent SNP variants from the N2 (wild type) background in which the mutagenesis was performed. The mutant strain was crossed to the Hawaiian strain and homozygous *fq9* mutant were isolated among the progeny and DNA was extracted from these worms. Due the relatively random and sparse distribution of crossovers in relation to the mutation there will be linkage of N2 SNPs in the region around the *fq9* mutation in the worms selected as homozygotes. Other chromosomes and distal regions on the same chromosome should be 50:50 wildtype to Hawaiian SNPs. The position of the mutation is then mapped using a set of SNPs that can be easily identified by performing PCR reactions to amplify the region containing the SNP, followed by digestion with the DraI restriction enzyme, which is produces different banding patterns in the Hawaiian and N2 DNA. From two rounds of this mapping the *fq9* mutation was mapped to the end of the right arm of chromosome III. Knowing the general location of the mutation allowed for it to be balanced with the *qC1* rearrangement, greatly simplifying future experiments.

8.3.2 CGH array mapping

To further map the *fq9* mutation to a smaller region and restrict the number of candidate genes a technique called comparative genomic hybridization (CGH) was used (Kallioniemi et al. 1992; Pease et al. 1994; Mei et al. 2000). This uses a tiling array to measure differences in the ratio of particular variants within a DNA sample. It uses the same logic as the DraI mapping, using the Hawaiian divergent strain to identify a region enriched for N2 sequence around the mutation. The same cross was performed as for the DraI mapping and 100 homozygous *fq9* mutants isolated among the progeny. Due to the larger numbers, some COs are expected to happen quite close to the mutated locus, making the region that is completely enriched for N2 SNPs smaller and reducing the region where the mutation is mapped to. The purified DNA pooled from these recombinants was sent to the Moerman lab in Canada who performed the CGH array, with the recombinant DNA and N2 control DNA used to make the two labeled libraries (Flibotte et al. 2009). The results of this array are depicted in Figure 52 A & B. In accordance with DraI mapping, the CGH array identified a region on the far right arm of chromosome III as the only region where N2 SNPs were greatly enriched. This can be seen by the sudden spike in the mapping signal of the green circles that represent the individual SNPs mapped on chromosome III (Figure 52 A). Closer inspection of chromosome III alone shows the position of the region containing the mutation to centre around 12.5 Mb on the physical map. We were informed that the mutation is expected to lie within ~200Kb either side of this position.

8.3.3 Whole genome sequencing of *fq9* mutants

Although the CGH array significantly reduced the list of candidate genes for the *fq9* mutation, there were still too many to be individually test by complementation and PCR sequencing. Thus, the next step in mapping the *fq9* mutation was to perform whole genome sequencing. Homozygous worms were sequenced using the Illumina TruSeq kit and run by the CSC genomics facility. The sequencing data was assembled by a bioinformatician from our institute, Gopu Dharmalingam, using the standard *C. elegans* N2 reference genome. There were many variants from the reference genome, but focusing on the region mapped by the CGH array one particular mutation appeared to be a very good candidate. It was an 11 bp deletion in exon 2 of a gene called *pph-4.1*, the worm homologue of protein phosphatase 4 (Figure 52 C). The deletion is predicted to cause a frame shift truncation and is homozygous in the mutant. Also, although it is not a well-

known key factor in meiosis, some studies have implicated this gene for having a role in meiosis (Sumiyoshi et al. 2002; Peters et al. 2010).

8.3.4 *fq9* is an allele of *pph-4.1*

PCR sequencing confirmed that the 11 bp deletion is found in the *fq9* mutant and a complementation test showed the *fq9* mutation did not fully complement the *tm1445* deletion allele of *pph-4.1*. This confirmed that *fq9* is a novel allele of *pph-4.1*. We were aware that the role of this gene was being studies already by a group in Kyoto, Japan led by Peter Carlton. Given this, plus the fact that my main project was progressing forward, it was decided that we would collaborate by sending them our balanced allele and sharing our results of the initial characterization to contribute to their study. I then focused solely on the cohesin project. Our findings helped to inform their investigation, culminating in a paper with our combined authorship that is currently in press at PLoS Genetics.

Figure 54. Age effect on univalent phenotype in *fq9* mutant

A. *fq9* mutant shows univalents at diakinesis indicating failure to make or maintain crossovers. 24 hours post L4 adults display heterogeneous mix of oocytes with univalents (more than 6 bodies) and some with 6 normal looking bivalents, both oocyte types are seen side by side (mosaic phenotype). Blue arrow indicates a bivalent, red arrow indicates a univalent. Older *fq9* mutants show greater proportion of diakinesis oocytes with univalents (see row three +48 hours post L4). The -1 and -2 indicates the position of the oocytes relative to the end of the germline.

B. Quantification of the diakinesis phenotype deterioration with age in the fq9 mutant. Oocytes were scored as being 'wildtype' with 6 bodies or instead having univalents with any more than 6 bodies. Most oocytes with univalents show mainly univalents, 10-12. The graph displays the mean percentage of oocytes with 6 bivalents out of the total diakinesis oocytes. The last 4-6 oocytes from both germlines were counted for each worm. At 24 hours post L4 ~62% of oocytes still show 6 bivalents and 38% univalents (germlines = 13, oocytes = 146). The 48 hours post L4 oocytes only have ~16% with 6 bivalents and 84% with univalents (germlines = 11, oocytes = 124). The 72 hours post L4 show 6 bivalents in ~9% of oocytes and univalents in ~91% (germlines = 13, oocytes = 147).

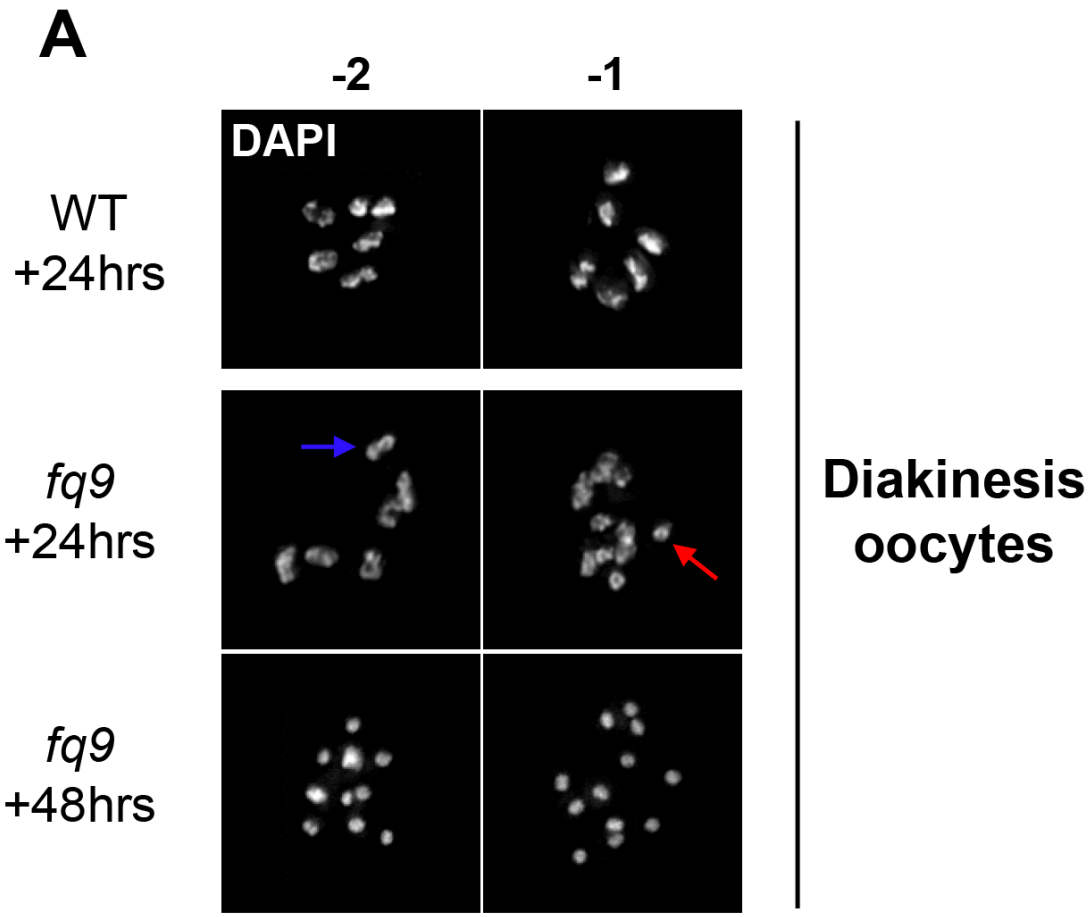
A
-2
-1
DAPI
WT
+24hrs
fq9
+24hrs
fq9
+48hrs
Diakinesis
oocytes

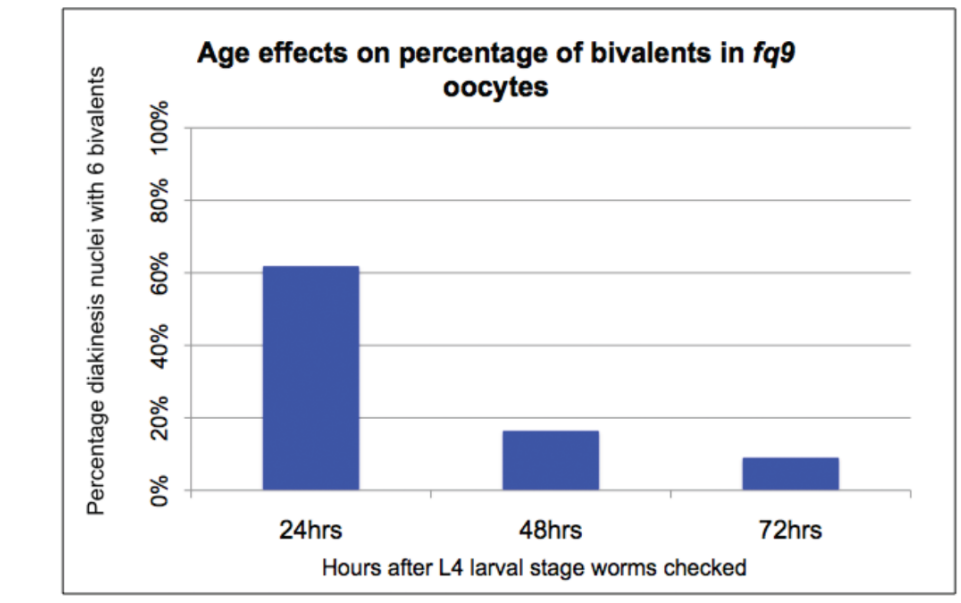
B
Age effects on percentage of bivalents in fq9 oocytes
Percentage diakinesis nuclei with 6 bivalents
0%
20%
40%
60%
80%
100%
24hrs
48hrs
72hrs
Hours after L4 larval stage worms checked

Figure 55. Mapping of *fq9* mutation to *pph-4.1*

A. Rainbow plot showing results across all six *C. elegans* chromosomes of a CGH array to map the *fq9* mutation. The mutation was crossed to the Hawaiian strain and recombinant homozygotes used for mapping. Y-axis is the Log2 of the ratio of signal for the differently labeled libraries: mutant & control. Higher signal indicates greater proportion of the N2 SNP version. X-axis represents the SNP position along a chromosome as an index relative to the whole genome, progressing from 0 at the left of chromosome I through to ~25000 at the right arm of the X chromosome. Circles represent individual SNPs on the array. Colours denote the different chromosomes: I, II, III, IV, V & X.

B. Plot showing chromosome III from the CGH array mapping of the fq9 mutation. Black circles represent individual SNPs from the array. Y-axis is the Log2 of the ratio of signal for N2 over Hawaiian SNP version. X-axis represents physical position on the chromosome in megabases, from the end of the left arm. The red line shows the moving average of the ratio value. The black line marks the predicted position of the mutation from the peak ratios towards the N2 version, at ~12.5Mb.

C. Table showing the identification of the 11pb frameshift deletion in *pph-4.1* with whole genome sequencing of the *fq9* mutation using Illumina TrueSeq. The *pph-4.1* candidate mutation is highlighted in red. Some other nearby variations identified in the *fq9* mutant on the right arm of chromosome III are shown. Columns show characteristics of the identified variation. Nucleotide ref. = corresponding nucleotide(s) in the reference sequence. A dash in the nucleotide change indicates a deletion a letter indicates a substitution. HET or HOM denotes whether the mutation is heterozygous or homozygous. Read depth indicates the number of sequencing reads mapped to that locus.

A

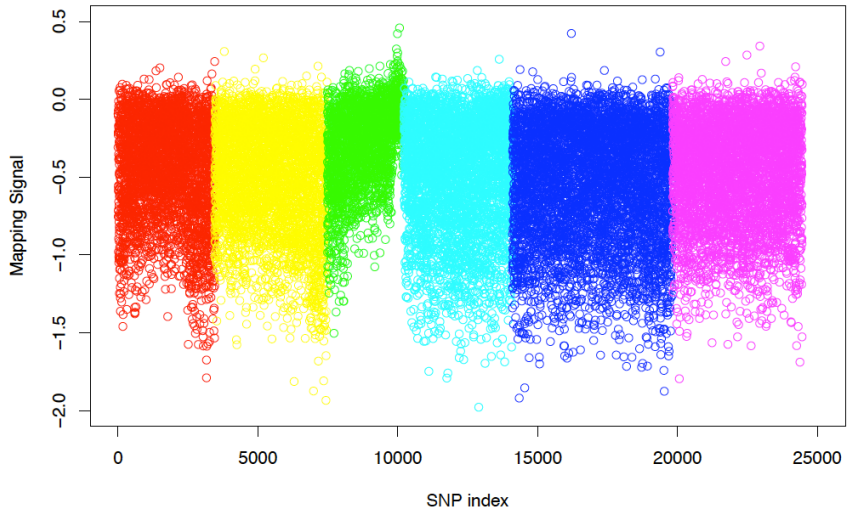

B

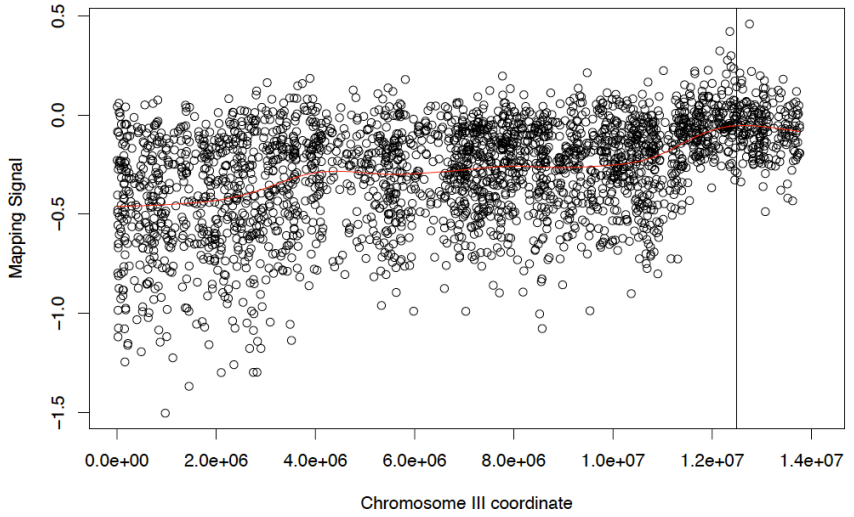

C

Chromosome	Physical position - start	Nucleotide ref.	Nucleotide change	Genotype	Read depth	Exon/intron	Gene name	Mutation type
chrIII	11503421	T	C	HET	104	exonic	Y66D12A.21	nonsynonymous SNV
chrIII	11503442	T	C	HET	100	exonic	Y66D12A.21	nonsynonymous SNV
chrIII	11543274	G	A	HOM	116	exonic	Y66D12A.14	nonsynonymous SNV
chrIII	11576711	C	G	HOM	77	exonic	Y66D12A.8	nonsynonymous SNV
chrIII	**12350969**	**CCGCTAGGATT**	**-**	**HOM**	**31**	**exonic**	**pph-4.1**	**frameshift deletion**
chrIII	12953209	T	G	HOM	72	exonic	ttm-1	nonsynonymous SNV

REFERENCES

Aboussekhra, A., Chanet, R., Adjiri, A., and Fabre, F. 1992. Semidominant suppressors of Srs2 helicase mutations of Saccharomyces cerevisiae map in the RAD51 gene, whose sequence predicts a protein with similarities to procaryotic RecA proteins. *Mol Cell Biol* **12**(7): 3224-3234.

Adames, K.A., Gawne, J., Wicky, C., Muller, F., and Rose, A.M. 1998. Mapping a telomere using the translocation eT1(III;V) in Caenorhabditis elegans. *Genetics* **150**(3): 1059-1066.

Adamo, A., Collis, S.J., Adelman, C.A., Silva, N., Horejsi, Z., Ward, J.D., Martinez-Perez, E., Boulton, S.J., and La Volpe, A. 2010. Preventing nonhomologous end joining suppresses DNA repair defects of Fanconi anemia. *Mol Cell* **39**(1): 25-35.

Agarwal, S. and Roeder, G.S. 2000. Zip3 provides a link between recombination enzymes and synaptonemal complex proteins. *Cell* **102**(2): 245-255.

Alani, E., Padmore, R., and Kleckner, N. 1990. Analysis of wild-type and rad50 mutants of yeast suggests an intimate relationship between meiotic chromosome synapsis and recombination. *Cell* **61**(3): 419-436.

Albertson, D.G. and Thomson, J.N. 1993. Segregation of holocentric chromosomes at meiosis in the nematode, Caenorhabditis elegans. *Chromosome Res* **1**(1): 15-26.

Alexandru, G., Uhlmann, F., Mechtler, K., Poupart, M.A., and Nasmyth, K. 2001. Phosphorylation of the cohesin subunit Scc1 by Polo/Cdc5 kinase regulates sister chromatid separation in yeast. *Cell* **105**(4): 459-472.

Alpi, A., Pasierbek, P., Gartner, A., and Loidl, J. 2003. Genetic and cytological characterization of the recombination protein RAD-51 in Caenorhabditis elegans. *Chromosoma* **112**(1): 6-16.

Anderson, D.E., Losada, A., Erickson, H.P., and Hirano, T. 2002. Condensin and cohesin display different arm conformations with characteristic hinge angles. *J Cell Biol* **156**(3): 419-424.

Angell, R.R., Xian, J., Keith, J., Ledger, W., and Baird, D.T. 1994. First meiotic division abnormalities in human oocytes: mechanism of trisomy formation. *Cytogenet Cell Genet* **65**(3): 194-202.

Aravind, L. and Koonin, E.V. 1998. The HORMA domain: a common structural denominator in mitotic checkpoints, chromosome synapsis and DNA repair. *Trends Biochem Sci* **23**(8): 284-286.

Arumugam, P., Gruber, S., Tanaka, K., Haering, C.H., Mechtler, K., and Nasmyth, K. 2003. ATP hydrolysis is required for cohesin's association with chromosomes. *Curr Biol* **13**(22): 1941-1953.

Atlas of Health in Europe. 2008. Atlas of Health in Europe 2008. In. WHO.

Ault, J.G. and Nicklas, R.B. 1989. Tension, microtubule rearrangements, and the proper distribution of chromosomes in mitosis. *Chromosoma* **98**(1): 33-39.

Austin, J. and Kimble, J. 1987. glp-1 is required in the germ line for regulation of the decision between mitosis and meiosis in C. elegans. *Cell* **51**(4): 589-599.

Bai, X., Peirson, B.N., Dong, F., Xue, C., and Makaroff, C.A. 1999. Isolation and characterization of SYN1, a RAD21-like gene essential for meiosis in Arabidopsis. *Plant Cell* **11**(3): 417-430.

Baltus, A.E., Menke, D.B., Hu, Y.C., Goodheart, M.L., Carpenter, A.E., de Rooij, D.G., and Page, D.C. 2006. In germ cells of mouse embryonic ovaries, the decision to enter meiosis precedes premeiotic DNA replication. *Nat Genet* **38**(12): 1430-1434.

Bannister, L.A., Reinholdt, L.G., Munroe, R.J., and Schimenti, J.C. 2004. Positional cloning and characterization of mouse mei8, a disrupted allelle of the meiotic cohesin Rec8. *Genesis* **40**(3): 184-194.

Barber, L.J., Youds, J.L., Ward, J.D., McIlwraith, M.J., O'Neil, N.J., Petalcorin, M.I., Martin, J.S., Collis, S.J., Cantor, S.B., Auclair, M. et al. 2008a. RTEL1 maintains genomic stability by suppressing homologous recombination. *Cell* **135**(2): 261-271.

Barber, T.D., McManus, K., Yuen, K.W., Reis, M., Parmigiani, G., Shen, D., Barrett, I., Nouhi, Y., Spencer, F., Markowitz, S. et al. 2008b. Chromatid cohesion defects may underlie chromosome instability in human colorectal cancers. *Proc Natl Acad Sci U S A* **105**(9): 3443-3448.

Barnes, T.M., Kohara, Y., Coulson, A., and Hekimi, S. 1995. Meiotic recombination, noncoding DNA and genomic organization in Caenorhabditis elegans. *Genetics* **141**(1): 159-179.

Baudat, F., Buard, J., Grey, C., Fledel-Alon, A., Ober, C., Przeworski, M., Coop, G., and de Massy, B. 2009. PRDM9 is a major determinant of meiotic recombination hotspots in humans and mice. *Science* **327**(5967): 836-840.

Baudat, F., Manova, K., Yuen, J.P., Jasin, M., and Keeney, S. 2000. Chromosome synapsis defects and sexually dimorphic meiotic progression in mice lacking Spo11. *Mol Cell* **6**(5): 989-998.

Baudrimont, A., Penkner, A., Woglar, A., Machacek, T., Wegrostek, C., Gloggnitzer, J., Fridkin, A., Klein, F., Gruenbaum, Y., Pasierbek, P. et al. Leptotene/zygotene chromosome movement via the SUN/KASH protein bridge in Caenorhabditis elegans. *PLoS Genet* **6**(11): e1001219.

Bauerschmidt, C., Woodcock, M., Stevens, D.L., Hill, M.A., Rothkamm, K., and Helleday, T. 2010. Cohesin phosphorylation and mobility of SMC1 at ionizing radiation-induced DNA double-strand breaks in human cells. *Exp Cell Res* **317**(3): 330-337.

Bergerat, A., de Massy, B., Gadelle, D., Varoutas, P.C., Nicolas, A., and Forterre, P. 1997. An atypical topoisomerase II from Archaea with implications for meiotic recombination. *Nature* **386**(6623): 414-417.

Bhalla, N., Wynne, D.J., Jantsch, V., and Dernburg, A.F. 2008. ZHP-3 acts at crossovers to couple meiotic recombination with synaptonemal complex disassembly and bivalent formation in C. elegans. *PLoS Genet* **4**(10): e1000235.

Bhatt, A.M., Lister, C., Page, T., Fransz, P., Findlay, K., Jones, G.H., Dickinson, H.G., and Dean, C. 1999. The DIF1 gene of Arabidopsis is required for meiotic chromosome segregation and belongs to the REC8/RAD21 cohesin gene family. *Plant J* **19**(4): 463-472.

Bishop, D.K. 1994. RecA homologs Dmc1 and Rad51 interact to form multiple nuclear complexes prior to meiotic chromosome synapsis. *Cell* **79**(6): 1081-1092.

Blat, Y. and Kleckner, N. 1999. Cohesins bind to preferential sites along yeast chromosome III, with differential regulation along arms versus the centric region. *Cell* **98**(2): 249-259.

Boateng, K.A., Bellani, M.A., Gregoretti, I.V., Pratto, F., and Camerini-Otero, R.D. 2013. Homologous pairing preceding SPO11-mediated double-strand breaks in mice. *Dev Cell* **24**(2): 196-205.

Bolanos-Villegas, P., Yang, X., Wang, H.J., Juan, C.T., Chuang, M.H., Makaroff, C.A., and Jauh, G.Y. 2013. Arabidopsis CHROMOSOME TRANSMISSION FIDELITY 7 (AtCTF7/ECO1) is required for DNA repair, mitosis and meiosis. *Plant J* **75**(6): 927-940.

Borges, V., Lehane, C., Lopez-Serra, L., Flynn, H., Skehel, M., Rolef Ben-Shahar, T., and Uhlmann, F. 2010. Hos1 deacetylates Smc3 to close the cohesin acetylation cycle. *Mol Cell* **39**(5): 677-688.

Borner, G.V., Kleckner, N., and Hunter, N. 2004. Crossover/noncrossover differentiation, synaptonemal complex formation, and regulatory surveillance at the leptotene/zygotene transition of meiosis. *Cell* **117**(1): 29-45.

Brenner, S. 1974. The genetics of Caenorhabditis elegans. *Genetics* **77**(1): 71-94.

Buheitel, J. and Stemmann, O. 2013. Prophase pathway-dependent removal of cohesin from human chromosomes requires opening of the Smc3-Scc1 gate. *EMBO J* **32**(5): 666-676.

Buhler, C., Shroff, R., and Lichten, M. 2009. Genome-wide mapping of meiotic DNA double-strand breaks in Saccharomyces cerevisiae. *Methods Mol Biol* **557**: 143-164.

Buonomo, S.B., Clyne, R.K., Fuchs, J., Loidl, J., Uhlmann, F., and Nasmyth, K. 2000. Disjunction of homologous chromosomes in meiosis I depends on proteolytic cleavage of the meiotic cohesin Rec8 by separin. *Cell* **103**(3): 387-398.

Caburet, S., Arboleda, V.A., Llano, E., Overbeek, P.A., Barbero, J.L., Oka, K., Harrison, W., Vaiman, D., Ben-Neriah, Z., Garcia-Tunon, I. et al. 2014. Mutant cohesin in premature ovarian failure. *N Engl J Med* **370**(10): 943-949.

Calvente, A., Viera, A., Parra, M.T., de la Fuente, R., Suja, J.A., Page, J., Santos, J.L., de la Vega, C.G., Barbero, J.L., and Rufas, J.S. 2013. Dynamics of cohesin subunits in grasshopper meiotic divisions. *Chromosoma* **122**(1-2): 77-91.

Carballo, J.A., Johnson, A.L., Sedgwick, S.G., and Cha, R.S. 2008. Phosphorylation of the axial element protein Hop1 by Mec1/Tel1 ensures meiotic interhomolog recombination. *Cell* **132**(5): 758-770.

Cha, R.S., Weiner, B.M., Keeney, S., Dekker, J., and Kleckner, N. 2000. Progression of meiotic DNA replication is modulated by interchromosomal interaction proteins, negatively by Spo11p and positively by Rec8p. *Genes Dev* **14**(4): 493-503.

Chan, K.L., Roig, M.B., Hu, B., Beckouet, F., Metson, J., and Nasmyth, K. 2012. Cohesin's DNA exit gate is distinct from its entrance gate and is regulated by acetylation. *Cell* **150**(5): 961-974.

Chan, R.C., Chan, A., Jeon, M., Wu, T.F., Pasqualone, D., Rougvie, A.E., and Meyer, B.J. 2003. Chromosome cohesion is regulated by a clock gene paralogue TIM-1. *Nature* **423**(6943): 1002-1009.

Chatterjee, A., Zakian, S., Hu, X.W., and Singleton, M.R. 2013. Structural insights into the regulation of cohesion establishment by Wpl1. *EMBO J* **32**(5): 677-687.

Chelysheva, L., Diallo, S., Vezon, D., Gendrot, G., Vrielynck, N., Belcram, K., Rocques, N., Marquez-Lema, A., Bhatt, A.M., Horlow, C. et al. 2005. AtREC8 and AtSCC3 are essential to the monopolar orientation of the kinetochores during meiosis. *J Cell Sci* **118**(Pt 20): 4621-4632.

Chen, C., Zhang, W., Timofejeva, L., Gerardin, Y., and Ma, H. 2005. The Arabidopsis ROCK-N-ROLLERS gene encodes a homolog of the yeast ATP-dependent DNA helicase MER3 and is required for normal meiotic crossover formation. *Plant J* **43**(3): 321-334.

Chen, S., Yee, A., Griffiths, M., Larkin, C., Yamashiro, C.T., Behari, R., Paszko-Kolva, C., Rahn, K., and De Grandis, S.A. 1997. The evaluation of a fluorogenic polymerase chain reaction assay for the detection of Salmonella species in food commodities. *Int J Food Microbiol* **35**(3): 239-250.

Chiang, T., Duncan, F.E., Schindler, K., Schultz, R.M., and Lampson, M.A. 2010. Evidence that weakened centromere cohesion is a leading cause of age-related aneuploidy in oocytes. *Curr Biol* **20**(17): 1522-1528.

Choo, K.H. 2001. Domain organization at the centromere and neocentromere. *Dev Cell* **1**(2): 165-177.
Chowdhury, R., Bois, P.R., Feingold, E., Sherman, S.L., and Cheung, V.G. 2009. Genetic analysis of variation in human meiotic recombination. *PLoS Genet* **5**(9): e1000648.
Ciosk, R., Shirayama, M., Shevchenko, A., Tanaka, T., Toth, A., and Nasmyth, K. 2000. Cohesin's binding to chromosomes depends on a separate complex consisting of Scc2 and Scc4 proteins. *Mol Cell* **5**(2): 243-254.
Cohen-Fix, O., Peters, J.M., Kirschner, M.W., and Koshland, D. 1996. Anaphase initiation in Saccharomyces cerevisiae is controlled by the APC-dependent degradation of the anaphase inhibitor Pds1p. *Genes Dev* **10**(24): 3081-3093.
Colaiacovo, M.P., MacQueen, A.J., Martinez-Perez, E., McDonald, K., Adamo, A., La Volpe, A., and Villeneuve, A.M. 2003. Synaptonemal complex assembly in C. elegans is dispensable for loading strand-exchange proteins but critical for proper completion of recombination. *Dev Cell* **5**(3): 463-474.
Collins, I. and Newlon, C.S. 1994. Chromosomal DNA replication initiates at the same origins in meiosis and mitosis. *Mol Cell Biol* **14**(5): 3524-3534.
Copenhaver, G.P., Housworth, E.A., and Stahl, F.W. 2002. Crossover interference in Arabidopsis. *Genetics* **160**(4): 1631-1639.
Couteau, F., Nabeshima, K., Villeneuve, A., and Zetka, M. 2004. A component of C. elegans meiotic chromosome axes at the interface of homolog alignment, synapsis, nuclear reorganization, and recombination. *Curr Biol* **14**(7): 585-592.
Couteau, F. and Zetka, M. 2005. HTP-1 coordinates synaptonemal complex assembly with homolog alignment during meiosis in C. elegans. *Genes Dev* **19**(22): 2744-2756.
Cowan, C.R. and Cande, W.Z. 2002. Meiotic telomere clustering is inhibited by colchicine but does not require cytoplasmic microtubules. *J Cell Sci* **115**(Pt 19): 3747-3756.
Crittenden, S.L., Eckmann, C.R., Wang, L., Bernstein, D.S., Wickens, M., and Kimble, J. 2003. Regulation of the mitosis/meiosis decision in the Caenorhabditis elegans germline. *Philos Trans R Soc Lond B Biol Sci* **358**(1436): 1359-1362.
Crittenden, S.L., Leonhard, K.A., Byrd, D.T., and Kimble, J. 2006. Cellular analyses of the mitotic region in the Caenorhabditis elegans adult germ line. *Mol Biol Cell* **17**(7): 3051-3061.
Crittenden, S.L., Troemel, E.R., Evans, T.C., and Kimble, J. 1994. GLP-1 is localized to the mitotic region of the C. elegans germ line. *Development* **120**(10): 2901-2911.
Cunningham, M.D., Gause, M., Cheng, Y., Noyes, A., Dorsett, D., Kennison, J.A., and Kassis, J.A. 2012. Wapl antagonizes cohesin binding and promotes Polycomb-group silencing in Drosophila. *Development* **139**(22): 4172-4179.
D'Ambrosio, C., Schmidt, C.K., Katou, Y., Kelly, G., Itoh, T., Shirahige, K., and Uhlmann, F. 2008. Identification of cis-acting sites for condensin loading onto budding yeast chromosomes. *Genes Dev* **22**(16): 2215-2227.
Damelin, M. and Bestor, T.H. 2007. The decatenation checkpoint. *Br J Cancer* **96**(2): 201-205.
Daniel, K., Lange, J., Hached, K., Fu, J., Anastassiadis, K., Roig, I., Cooke, H.J., Stewart, A.F., Wassmann, K., Jasin, M. et al. 2011. Meiotic homologue alignment and its quality surveillance are controlled by mouse HORMAD1. *Nat Cell Biol* **13**(5): 599-610.
Davis, E.S., Wille, L., Chestnut, B.A., Sadler, P.L., Shakes, D.C., and Golden, A. 2002. Multiple subunits of the Caenorhabditis elegans anaphase-promoting complex are required for chromosome segregation during meiosis I. *Genetics* **160**(2): 805-813.
Davis, M.W., Hammarlund, M., Harrach, T., Hullett, P., Olsen, S., and Jorgensen, E.M. 2005. Rapid single nucleotide polymorphism mapping in C. elegans. *BMC Genomics* **6**: 118.

de Carvalho, C.E., Zaaijer, S., Smolikov, S., Gu, Y., Schumacher, J.M., and Colaiacovo, M.P. 2008. LAB-1 antagonizes the Aurora B kinase in C. elegans. *Genes Dev* **22**(20): 2869-2885.

De, K., Sterle, L., Krueger, L., Yang, X., and Makaroff, C.A. 2014. Arabidopsis thaliana WAPL is essential for the prophase removal of cohesin during meiosis. *PLoS Genet* **10**(7): e1004497.

de los Santos, T., Hunter, N., Lee, C., Larkin, B., Loidl, J., and Hollingsworth, N.M. 2003. The Mus81/Mms4 endonuclease acts independently of double-Holliday junction resolution to promote a distinct subset of crossovers during meiosis in budding yeast. *Genetics* **164**(1): 81-94.

De Piccoli, G., Torres-Rosell, J., and Aragon, L. 2009. The unnamed complex: what do we know about Smc5-Smc6? *Chromosome Res* **17**(2): 251-263.

de Vries, S.S., Baart, E.B., Dekker, M., Siezen, A., de Rooij, D.G., de Boer, P., and te Riele, H. 1999. Mouse MutS-like protein Msh5 is required for proper chromosome synapsis in male and female meiosis. *Genes Dev* **13**(5): 523-531.

Deardorff, M.A., Kaur, M., Yaeger, D., Rampuria, A., Korolev, S., Pie, J., Gil-Rodriguez, C., Arnedo, M., Loeys, B., Kline, A.D. et al. 2007. Mutations in cohesin complex members SMC3 and SMC1A cause a mild variant of cornelia de Lange syndrome with predominant mental retardation. *Am J Hum Genet* **80**(3): 485-494.

Degner, S.C., Verma-Gaur, J., Wong, T.P., Bossen, C., Iverson, G.M., Torkamani, A., Vettermann, C., Lin, Y.C., Ju, Z., Schulz, D. et al. 2011. CCCTC-binding factor (CTCF) and cohesin influence the genomic architecture of the Igh locus and antisense transcription in pro-B cells. *Proc Natl Acad Sci U S A* **108**(23): 9566-9571.

Dernburg, A.F., McDonald, K., Moulder, G., Barstead, R., Dresser, M., and Villeneuve, A.M. 1998. Meiotic recombination in C. elegans initiates by a conserved mechanism and is dispensable for homologous chromosome synapsis. *Cell* **94**(3): 387-398.

Deyter, G.M., Furuta, T., Kurasawa, Y., and Schumacher, J.M. 2010. Caenorhabditis elegans cyclin B3 is required for multiple mitotic processes including alleviation of a spindle checkpoint-dependent block in anaphase chromosome segregation. *PLoS Genet* **6**(11): e1001218.

Ding, D.Q., Sakurai, N., Katou, Y., Itoh, T., Shirahige, K., Haraguchi, T., and Hiraoka, Y. 2006. Meiotic cohesins modulate chromosome compaction during meiotic prophase in fission yeast. *J Cell Biol* **174**(4): 499-508.

Ding, D.Q., Yamamoto, A., Haraguchi, T., and Hiraoka, Y. 2004. Dynamics of homologous chromosome pairing during meiotic prophase in fission yeast. *Dev Cell* **6**(3): 329-341.

Dong, H. and Roeder, G.S. 2000. Organization of the yeast Zip1 protein within the central region of the synaptonemal complex. *J Cell Biol* **148**(3): 417-426.

Drouaud, J., Khademian, H., Giraut, L., Zanni, V., Bellalou, S., Henderson, I.R., Falque, M., and Mezard, C. 2013. Contrasted patterns of crossover and non-crossover at Arabidopsis thaliana meiotic recombination hotspots. *PLoS Genet* **9**(11): e1003922.

Duncan, F.E., Hornick, J.E., Lampson, M.A., Schultz, R.M., Shea, L.D., and Woodruff, T.K. 2012. Chromosome cohesion decreases in human eggs with advanced maternal age. *Aging Cell* **11**(6): 1121-1124.

Eichinger, C.S., Kurze, A., Oliveira, R.A., and Nasmyth, K. 2013. Disengaging the Smc3/kleisin interface releases cohesin from Drosophila chromosomes during interphase and mitosis. *EMBO J* **32**(5): 656-665.

Eijpe, M., Offenberg, H., Jessberger, R., Revenkova, E., and Heyting, C. 2003. Meiotic cohesin REC8 marks the axial elements of rat synaptonemal complexes before cohesins SMC1beta and SMC3. *J Cell Biol* **160**(5): 657-670.

Fernius, J., Nerusheva, O.O., Galander, S., Alves Fde, L., Rappsilber, J., and Marston, A.L. 2013. Cohesin-dependent association of scc2/4 with the centromere initiates pericentromeric cohesion establishment. *Curr Biol* **23**(7): 599-606.

Flibotte, S., Edgley, M.L., Maydan, J., Taylor, J., Zapf, R., Waterston, R., and Moerman, D.G. 2009. Rapid high resolution single nucleotide polymorphism-comparative genome hybridization mapping in Caenorhabditis elegans. *Genetics* **181**(1): 33-37.

Fox, P.M., Vought, V.E., Hanazawa, M., Lee, M.H., Maine, E.M., and Schedl, T. 2011. Cyclin E and CDK-2 regulate proliferative cell fate and cell cycle progression in the C. elegans germline. *Development* **138**(11): 2223-2234.

Franasiak, J.M., Forman, E.J., Hong, K.H., Werner, M.D., Upham, K.M., Treff, N.R., and Scott, R.T., Jr. 2014. The nature of aneuploidy with increasing age of the female partner: a review of 15,169 consecutive trophectoderm biopsies evaluated with comprehensive chromosomal screening. *Fertil Steril* **101**(3): 656-663 e651.

Fraune, J., Schramm, S., Alsheimer, M., and Benavente, R. 2012. The mammalian synaptonemal complex: protein components, assembly and role in meiotic recombination. *Exp Cell Res* **318**(12): 1340-1346.

Fung, J.C., Rockmill, B., Odell, M., and Roeder, G.S. 2004. Imposition of crossover interference through the nonrandom distribution of synapsis initiation complexes. *Cell* **116**(6): 795-802.

Furuta, T., Tuck, S., Kirchner, J., Koch, B., Auty, R., Kitagawa, R., Rose, A.M., and Greenstein, D. 2000. EMB-30: an APC4 homologue required for metaphase-to-anaphase transitions during meiosis and mitosis in Caenorhabditis elegans. *Mol Biol Cell* **11**(4): 1401-1419.

Gandhi, N.S., Young, K., Warmington, J.R., and Mancera, R.L. 2008. Characterization of sequence and structural features of the Candida krusei enolase. *In Silico Biol* **8**(5-6): 449-460.

Gandhi, R., Gillespie, P.J., and Hirano, T. 2006. Human Wapl is a cohesin-binding protein that promotes sister-chromatid resolution in mitotic prophase. *Curr Biol* **16**(24): 2406-2417.

Garcia, S.A. and Nagai, M.A. 2011. Transcriptional regulation of bidirectional gene pairs by 17-beta-estradiol in MCF-7 breast cancer cells. *Braz J Med Biol Res* **44**(2): 112-122.

Garcia-Cruz, R., Brieno, M.A., Roig, I., Grossmann, M., Velilla, E., Pujol, A., Cabero, L., Pessarrodona, A., Barbero, J.L., and Garcia Caldes, M. 2010. Dynamics of cohesin proteins REC8, STAG3, SMC1 beta and SMC3 are consistent with a role in sister chromatid cohesion during meiosis in human oocytes. *Hum Reprod* **25**(9): 2316-2327.

Gasior, S.L., Wong, A.K., Kora, Y., Shinohara, A., and Bishop, D.K. 1998. Rad52 associates with RPA and functions with rad55 and rad57 to assemble meiotic recombination complexes. *Genes Dev* **12**(14): 2208-2221.

Gause, M., Misulovin, Z., Bilyeu, A., and Dorsett, D. 2010. Dosage-sensitive regulation of cohesin chromosome binding and dynamics by Nipped-B, Pds5, and Wapl. *Mol Cell Biol* **30**(20): 4940-4951.

Gerlich, D., Koch, B., Dupeux, F., Peters, J.M., and Ellenberg, J. 2006. Live-cell imaging reveals a stable cohesin-chromatin interaction after but not before DNA replication. *Curr Biol* **16**(15): 1571-1578.

Gerton, J.L., DeRisi, J., Shroff, R., Lichten, M., Brown, P.O., and Petes, T.D. 2000. Global mapping of meiotic recombination hotspots and coldspots in the yeast Saccharomyces cerevisiae. *Proc Natl Acad Sci U S A* **97**(21): 11383-11390.

Gheorghisan-Galateanu, A.A., Hinescu, M.E., and Enciu, A.M. 2014. Ovarian adult stem cells: hope or pitfall? *J Ovarian Res* **7**: 71.

Giroux, C.N., Dresser, M.E., and Tiano, H.F. 1989. Genetic control of chromosome synapsis in yeast meiosis. *Genome* **31**(1): 88-94.
Goodyer, W., Kaitna, S., Couteau, F., Ward, J.D., Boulton, S.J., and Zetka, M. 2008. HTP-3 links DSB formation with homolog pairing and crossing over during C. elegans meiosis. *Dev Cell* **14**(2): 263-274.
Gruber, S., Arumugam, P., Katou, Y., Kuglitsch, D., Helmhart, W., Shirahige, K., and Nasmyth, K. 2006. Evidence that loading of cohesin onto chromosomes involves opening of its SMC hinge. *Cell* **127**(3): 523-537.
Gruber, S., Haering, C.H., and Nasmyth, K. 2003. Chromosomal cohesin forms a ring. *Cell* **112**(6): 765-777.
Guiraldelli, M.F., Eyster, C., Wilkerson, J.L., Dresser, M.E., and Pezza, R.J. 2013. Mouse HFM1/Mer3 is required for crossover formation and complete synapsis of homologous chromosomes during meiosis. *PLoS Genet* **9**(3): e1003383.
Gutierrez-Caballero, C., Herran, Y., Sanchez-Martin, M., Suja, J.A., Barbero, J.L., Llano, E., and Pendas, A.M. 2011. Identification and molecular characterization of the mammalian alpha-kleisin RAD21L. *Cell Cycle* **10**(9): 1477-1487.
Haarhuis, J.H., Elbatsh, A.M., van den Broek, B., Camps, D., Erkan, H., Jalink, K., Medema, R.H., and Rowland, B.D. 2013. WAPL-mediated removal of cohesin protects against segregation errors and aneuploidy. *Curr Biol* **23**(20): 2071-2077.
Hadjur, S., Williams, L.M., Ryan, N.K., Cobb, B.S., Sexton, T., Fraser, P., Fisher, A.G., and Merkenschlager, M. 2009. Cohesins form chromosomal cis-interactions at the developmentally regulated IFNG locus. *Nature* **460**(7253): 410-413.
Haenni, S., Ji, Z., Hoque, M., Rust, N., Sharpe, H., Eberhard, R., Browne, C., Hengartner, M.O., Mellor, J., Tian, B. et al. 2012. Analysis of C. elegans intestinal gene expression and polyadenylation by fluorescence-activated nuclei sorting and 3'-end-seq. *Nucleic Acids Res* **40**(13): 6304-6318.
Haering, C.H., Lowe, J., Hochwagen, A., and Nasmyth, K. 2002. Molecular architecture of SMC proteins and the yeast cohesin complex. *Mol Cell* **9**(4): 773-788.
Haering, C.H., Schoffnegger, D., Nishino, T., Helmhart, W., Nasmyth, K., and Lowe, J. 2004. Structure and stability of cohesin's Smc1-kleisin interaction. *Mol Cell* **15**(6): 951-964.
Handyside, A.H., Montag, M., Magli, M.C., Repping, S., Harper, J., Schmutzler, A., Vesela, K., Gianaroli, L., and Geraedts, J. 2012. Multiple meiotic errors caused by predivision of chromatids in women of advanced maternal age undergoing in vitro fertilisation. *Eur J Hum Genet* **20**(7): 742-747.
Hartman, T., Stead, K., Koshland, D., and Guacci, V. 2000. Pds5p is an essential chromosomal protein required for both sister chromatid cohesion and condensation in Saccharomyces cerevisiae. *J Cell Biol* **151**(3): 613-626.
Hassold, T. and Hunt, P. 2001. To err (meiotically) is human: the genesis of human aneuploidy. *Nat Rev Genet* **2**(4): 280-291.
Hassold, T.J. 1998. Nondisjunction in the human male. *Curr Top Dev Biol* **37**: 383-406.
Hassold, T.J. and Jacobs, P.A. 1984. Trisomy in man. *Annu Rev Genet* **18**: 69-97.
Hauf, S., Roitinger, E., Koch, B., Dittrich, C.M., Mechtler, K., and Peters, J.M. 2005. Dissociation of cohesin from chromosome arms and loss of arm cohesion during early mitosis depends on phosphorylation of SA2. *PLoS Biol* **3**(3): e69.
Heidinger-Pauli, J.M., Mert, O., Davenport, C., Guacci, V., and Koshland, D. 2010. Systematic reduction of cohesin differentially affects chromosome segregation, condensation, and DNA repair. *Curr Biol* **20**(10): 957-963.
Heidinger-Pauli, J.M., Unal, E., Guacci, V., and Koshland, D. 2008. The kleisin subunit of cohesin dictates damage-induced cohesion. *Mol Cell* **31**(1): 47-56.

Heidinger-Pauli, J.M., Unal, E., and Koshland, D. 2009. Distinct targets of the Eco1 acetyltransferase modulate cohesion in S phase and in response to DNA damage. *Mol Cell* **34**(3): 311-321.

Herran, Y., Gutierrez-Caballero, C., Sanchez-Martin, M., Hernandez, T., Viera, A., Barbero, J.L., de Alava, E., de Rooij, D.G., Suja, J.A., Llano, E. et al. 2011. The cohesin subunit RAD21L functions in meiotic synapsis and exhibits sexual dimorphism in fertility. *EMBO J* **30**(15): 3091-3105.

Higgins, J.D., Armstrong, S.J., Franklin, F.C., and Jones, G.H. 2004. The Arabidopsis MutS homolog AtMSH4 functions at an early step in recombination: evidence for two classes of recombination in Arabidopsis. *Genes Dev* **18**(20): 2557-2570.

Hillers, K.J. and Villeneuve, A.M. 2003. Chromosome-wide control of meiotic crossing over in C. elegans. *Curr Biol* **13**(18): 1641-1647.

Hillier, L.W., Marth, G.T., Quinlan, A.R., Dooling, D., Fewell, G., Barnett, D., Fox, P., Glasscock, J.I., Hickenbotham, M., Huang, W. et al. 2008. Whole-genome sequencing and variant discovery in C. elegans. *Nat Methods* **5**(2): 183-188.

Hirano, T. 2005. SMC proteins and chromosome mechanics: from bacteria to humans. *Philos Trans R Soc Lond B Biol Sci* **360**(1455): 507-514.

Hodges, C.A., LeMaire-Adkins, R., and Hunt, P.A. 2001. Coordinating the segregation of sister chromatids during the first meiotic division: evidence for sexual dimorphism. *J Cell Sci* **114**(Pt 13): 2417-2426.

Hodges, C.A., Revenkova, E., Jessberger, R., Hassold, T.J., and Hunt, P.A. 2005. SMC1beta-deficient female mice provide evidence that cohesins are a missing link in age-related nondisjunction. *Nat Genet* **37**(12): 1351-1355.

Hodgkin, J., Horvitz, H.R., and Brenner, S. 1979. Nondisjunction Mutants of the Nematode CAENORHABDITIS ELEGANS. *Genetics* **91**(1): 67-94.

Hollingsworth, N.M. and Brill, S.J. 2004. The Mus81 solution to resolution: generating meiotic crossovers without Holliday junctions. *Genes Dev* **18**(2): 117-125.

Hollingsworth, N.M., Goetsch, L., and Byers, B. 1990. The HOP1 gene encodes a meiosis-specific component of yeast chromosomes. *Cell* **61**(1): 73-84.

Hollingsworth, N.M., Ponte, L., and Halsey, C. 1995. MSH5, a novel MutS homolog, facilitates meiotic reciprocal recombination between homologs in Saccharomyces cerevisiae but not mismatch repair. *Genes Dev* **9**(14): 1728-1739.

Hollingsworth, R.E., Jr. and Sclafani, R.A. 1993. Yeast pre-meiotic DNA replication utilizes mitotic origin ARS1 independently of CDC7 function. *Chromosoma* **102**(6): 415-420.

Hopkins, J., Hwang, G., Jacob, J., Sapp, N., Bedigian, R., Oka, K., Overbeek, P., Murray, S., and Jordan, P.W. 2014. Meiosis-specific cohesin component, Stag3 is essential for maintaining centromere chromatid cohesion, and required for DNA repair and synapsis between homologous chromosomes. *PLoS Genet* **10**(7): e1004413.

Hou, F. and Zou, H. 2005. Two human orthologues of Eco1/Ctf7 acetyltransferases are both required for proper sister-chromatid cohesion. *Mol Biol Cell* **16**(8): 3908-3918.

Howard-Till, R.A., Lukaszewicz, A., Novatchkova, M., and Loidl, J. 2013. A single cohesin complex performs mitotic and meiotic functions in the protist tetrahymena. *PLoS Genet* **9**(3): e1003418.

Hu, B., Itoh, T., Mishra, A., Katoh, Y., Chan, K.L., Upcher, W., Godlee, C., Roig, M.B., Shirahige, K., and Nasmyth, K. 2011. ATP hydrolysis is required for relocating cohesin from sites occupied by its Scc2/4 loading complex. *Curr Biol* **21**(1): 12-24.

Huis in 't Veld, P.J., Herzog, F., Ladurner, R., Davidson, I.F., Piric, S., Kreidl, E., Bhaskara, V., Aebersold, R., and Peters, J.M. 2014. Characterization of a DNA exit gate in the human cohesin ring. *Science* **346**(6212): 968-972.

Hulten, M.A. 2011. On the origin of crossover interference: A chromosome oscillatory movement (COM) model. *Mol Cytogenet* **4**: 10.

Hunter, N. and Borts, R.H. 1997. Mlh1 is unique among mismatch repair proteins in its ability to promote crossing-over during meiosis. *Genes Dev* **11**(12): 1573-1582.

Hunter, N. and Kleckner, N. 2001. The single-end invasion: an asymmetric intermediate at the double-strand break to double-holliday junction transition of meiotic recombination. *Cell* **106**(1): 59-70.

Ishiguro, K., Kim, J., Fujiyama-Nakamura, S., Kato, S., and Watanabe, Y. 2011. A new meiosis-specific cohesin complex implicated in the cohesin code for homologous pairing. *EMBO Rep* **12**(3): 267-275.

Ishiguro, K., Kim, J., Shibuya, H., Hernandez-Hernandez, A., Suzuki, A., Fukagawa, T., Shioi, G., Kiyonari, H., Li, X.C., Schimenti, J. et al. 2014. Meiosis-specific cohesin mediates homolog recognition in mouse spermatocytes. *Genes Dev* **28**(6): 594-607.

Ishiguro, T., Tanaka, K., Sakuno, T., and Watanabe, Y. 2010. Shugoshin-PP2A counteracts casein-kinase-1-dependent cleavage of Rec8 by separase. *Nat Cell Biol* **12**(5): 500-506.

Ivanov, D., Schleiffer, A., Eisenhaber, F., Mechtler, K., Haering, C.H., and Nasmyth, K. 2002. Eco1 is a novel acetyltransferase that can acetylate proteins involved in cohesion. *Curr Biol* **12**(4): 323-328.

Jacobs, P.A. 1992. The chromosome complement of human gametes. *Oxf Rev Reprod Biol* **14**: 47-72.

Jagiello, G. and Fang, J.S. 1979. Analyses of diplotene chiasma frequencies in mouse oocytes and spermatocytes in relation to ageing and sexual dimorphism. *Cytogenet Cell Genet* **23**(1-2): 53-60.

James, R.D., Schmiesing, J.A., Peters, A.H., Yokomori, K., and Disteche, C.M. 2002. Differential association of SMC1alpha and SMC3 proteins with meiotic chromosomes in wild-type and SPO11-deficient male mice. *Chromosome Res* **10**(7): 549-560.

Jamieson, M.E., Coutts, J.R., and Connor, J.M. 1994. The chromosome constitution of human preimplantation embryos fertilized in vitro. *Hum Reprod* **9**(4): 709-715.

Jan, S.Z., Hamer, G., Repping, S., de Rooij, D.G., van Pelt, A.M., and Vormer, T.L. 2012. Molecular control of rodent spermatogenesis. *Biochim Biophys Acta* **1822**(12): 1838-1850.

Jantsch, V., Pasierbek, P., Mueller, M.M., Schweizer, D., Jantsch, M., and Loidl, J. 2004. Targeted gene knockout reveals a role in meiotic recombination for ZHP-3, a Zip3-related protein in Caenorhabditis elegans. *Mol Cell Biol* **24**(18): 7998-8006.

Jaramillo-Lambert, A., Ellefson, M., Villeneuve, A.M., and Engebrecht, J. 2007. Differential timing of S phases, X chromosome replication, and meiotic prophase in the C. elegans germ line. *Dev Biol* **308**(1): 206-221.

Jefferies, J. 2008. Fertility assumptions for the 2006-based national population projections. *Popul Trends*(131): 19-27.

Jessberger, R. 2012. Age-related aneuploidy through cohesion exhaustion. *EMBO Rep* **13**(6): 539-546.

Jimenez, R. 2009. Ovarian organogenesis in mammals: mice cannot tell us everything. *Sex Dev* **3**(6): 291-301.

Jin, H., Guacci, V., and Yu, H.G. 2009. Pds5 is required for homologue pairing and inhibits synapsis of sister chromatids during yeast meiosis. *J Cell Biol* **186**(5): 713-725.

Kagami, A., Sakuno, T., Yamagishi, Y., Ishiguro, T., Tsukahara, T., Shirahige, K., Tanaka, K., and Watanabe, Y. Acetylation regulates monopolar attachment at multiple levels during meiosis I in fission yeast. *EMBO Rep* **12**(11): 1189-1195.

Kallioniemi, A., Kallioniemi, O.P., Sudar, D., Rutovitz, D., Gray, J.W., Waldman, F., and Pinkel, D. 1992. Comparative genomic hybridization for molecular cytogenetic analysis of solid tumors. *Science* **258**(5083): 818-821.

Kassir, Y., Granot, D., and Simchen, G. 1988. IME1, a positive regulator gene of meiosis in S. cerevisiae. *Cell* **52**(6): 853-862.

Katis, V.L., Lipp, J.J., Imre, R., Bogdanova, A., Okaz, E., Habermann, B., Mechtler, K., Nasmyth, K., and Zachariae, W. 2010. Rec8 phosphorylation by casein kinase 1 and Cdc7-Dbf4 kinase regulates cohesin cleavage by separase during meiosis. *Dev Cell* **18**(3): 397-409.

Keeney, S., Giroux, C.N., and Kleckner, N. 1997. Meiosis-specific DNA double-strand breaks are catalyzed by Spo11, a member of a widely conserved protein family. *Cell* **88**(3): 375-384.

Kelly, K.O., Dernburg, A.F., Stanfield, G.M., and Villeneuve, A.M. 2000. Caenorhabditis elegans msh-5 is required for both normal and radiation-induced meiotic crossing over but not for completion of meiosis. *Genetics* **156**(2): 617-630.

Kim, K.P., Weiner, B.M., Zhang, L., Jordan, A., Dekker, J., and Kleckner, N. 2010. Sister cohesion and structural axis components mediate homolog bias of meiotic recombination. *Cell* **143**(6): 924-937.

Kimble, J.E. and White, J.G. 1981. On the control of germ cell development in Caenorhabditis elegans. *Dev Biol* **81**(2): 208-219.

Kitagawa, R., Bakkenist, C.J., McKinnon, P.J., and Kastan, M.B. 2004. Phosphorylation of SMC1 is a critical downstream event in the ATM-NBS1-BRCA1 pathway. *Genes Dev* **18**(12): 1423-1438.

Kitajima, T.S., Hauf, S., Ohsugi, M., Yamamoto, T., and Watanabe, Y. 2005. Human Bub1 defines the persistent cohesion site along the mitotic chromosome by affecting Shugoshin localization. *Curr Biol* **15**(4): 353-359.

Kitajima, T.S., Miyazaki, Y., Yamamoto, M., and Watanabe, Y. 2003. Rec8 cleavage by separase is required for meiotic nuclear divisions in fission yeast. *EMBO J* **22**(20): 5643-5653.

Kitajima, T.S., Sakuno, T., Ishiguro, K., Iemura, S., Natsume, T., Kawashima, S.A., and Watanabe, Y. 2006. Shugoshin collaborates with protein phosphatase 2A to protect cohesin. *Nature* **441**(7089): 46-52.

Kleckner, N. 2006. Chiasma formation: chromatin/axis interplay and the role(s) of the synaptonemal complex. *Chromosoma* **115**(3): 175-194.

Kleckner, N., Zickler, D., Jones, G.H., Dekker, J., Padmore, R., Henle, J., and Hutchinson, J. 2004. A mechanical basis for chromosome function. *Proc Natl Acad Sci U S A* **101**(34): 12592-12597.

Klein, F., Mahr, P., Galova, M., Buonomo, S.B., Michaelis, C., Nairz, K., and Nasmyth, K. 1999. A central role for cohesins in sister chromatid cohesion, formation of axial elements, and recombination during yeast meiosis. *Cell* **98**(1): 91-103.

Kogo, H., Tsutsumi, M., Inagaki, H., Ohye, T., Kiyonari, H., and Kurahashi, H. 2012. HORMAD2 is essential for synapsis surveillance during meiotic prophase via the recruitment of ATR activity. *Genes Cells* **17**(11): 897-912.

Kogut, I., Wang, J., Guacci, V., Mistry, R.K., and Megee, P.C. 2009. The Scc2/Scc4 cohesin loader determines the distribution of cohesin on budding yeast chromosomes. *Genes Dev* **23**(19): 2345-2357.

Koszul, R., Kim, K.P., Prentiss, M., Kleckner, N., and Kameoka, S. 2008. Meiotic chromosomes move by linkage to dynamic actin cables with transduction of force through the nuclear envelope. *Cell* **133**(7): 1188-1201.

Kouznetsova, A., Novak, I., Jessberger, R., and Hoog, C. 2005. SYCP2 and SYCP3 are required for cohesin core integrity at diplotene but not for centromere cohesion at the first meiotic division. *J Cell Sci* **118**(Pt 10): 2271-2278.

Kueng, S., Hegemann, B., Peters, B.H., Lipp, J.J., Schleiffer, A., Mechtler, K., and Peters, J.M. 2006. Wapl controls the dynamic association of cohesin with chromatin. *Cell* **127**(5): 955-967.

Kulemzina, I., Schumacher, M.R., Verma, V., Reiter, J., Metzler, J., Failla, A.V., Lanz, C., Sreedharan, V.T., Ratsch, G., and Ivanov, D. 2012. Cohesin rings devoid of Scc3 and Pds5 maintain their stable association with the DNA. *PLoS Genet* **8**(8): e1002856.

Kuroda, M., Oikawa, K., Ohbayashi, T., Yoshida, K., Yamada, K., Mimura, J., Matsuda, Y., Fujii-Kuriyama, Y., and Mukai, K. 2005. A dioxin sensitive gene, mammalian WAPL, is implicated in spermatogenesis. *FEBS Lett* **579**(1): 167-172.

Kurze, A., Michie, K.A., Dixon, S.E., Mishra, A., Itoh, T., Khalid, S., Strmecki, L., Shirahige, K., Haering, C.H., Lowe, J. et al. A positively charged channel within the Smc1/Smc3 hinge required for sister chromatid cohesion. *EMBO J* **30**(2): 364-378.

Labrador, L., Barroso, C., Lightfoot, J., Muller-Reichert, T., Flibotte, S., Taylor, J., Moerman, D.G., Villeneuve, A.M., and Martinez-Perez, E. 2013. Chromosome movements promoted by the mitochondrial protein SPD-3 are required for homology search during Caenorhabditis elegans meiosis. *PLoS Genet* **9**(5): e1003497.

Lake, C.M. and Hawley, R.S. 2012. The molecular control of meiotic chromosomal behavior: events in early meiotic prophase in Drosophila oocytes. *Annu Rev Physiol* **74**: 425-451.

Lammens, A., Schele, A., and Hopfner, K.P. 2004. Structural biochemistry of ATP-driven dimerization and DNA-stimulated activation of SMC ATPases. *Curr Biol* **14**(19): 1778-1782.

Lamont, L.B., Crittenden, S.L., Bernstein, D., Wickens, M., and Kimble, J. 2004. FBF-1 and FBF-2 regulate the size of the mitotic region in the C. elegans germline. *Dev Cell* **7**(5): 697-707.

Larsen, M.R., Thingholm, T.E., Jensen, O.N., Roepstorff, P., and Jorgensen, T.J. 2005. Highly selective enrichment of phosphorylated peptides from peptide mixtures using titanium dioxide microcolumns. *Mol Cell Proteomics* **4**(7): 873-886.

Latypov, V., Rothenberg, M., Lorenz, A., Octobre, G., Csutak, O., Lehmann, E., Loidl, J., and Kohli, J. 2010. Roles of Hop1 and Mek1 in meiotic chromosome pairing and recombination partner choice in Schizosaccharomyces pombe. *Mol Cell Biol* **30**(7): 1570-1581.

Lee, J. and Hirano, T. 2011. RAD21L, a novel cohesin subunit implicated in linking homologous chromosomes in mammalian meiosis. *J Cell Biol* **192**(2): 263-276.

Lengronne, A., Katou, Y., Mori, S., Yokobayashi, S., Kelly, G.P., Itoh, T., Watanabe, Y., Shirahige, K., and Uhlmann, F. 2004. Cohesin relocation from sites of chromosomal loading to places of convergent transcription. *Nature* **430**(6999): 573-578.

Li, X.M., Yu, C., Wang, Z.W., Zhang, Y.L., Liu, X.M., Zhou, D., Sun, Q.Y., and Fan, H.Y. 2013. DNA topoisomerase II is dispensable for oocyte meiotic resumption but is essential for meiotic chromosome condensation and separation in mice. *Biol Reprod* **89**(5): 118.

Lightfoot, J., Testori, S., Barroso, C., and Martinez-Perez, E. 2011. Loading of meiotic cohesin by SCC-2 is required for early processing of DSBs and for the DNA damage checkpoint. *Curr Biol* **21**(17): 1421-1430.

Lim, J.G., Stine, R.R., and Yanowitz, J.L. 2008. Domain-specific regulation of recombination in Caenorhabditis elegans in response to temperature, age and sex. *Genetics* **180**(2): 715-726.
Lin, W., Jin, H., Liu, X., Hampton, K., and Yu, H.G. 2011. Scc2 regulates gene expression by recruiting cohesin to the chromosome as a transcriptional activator during yeast meiosis. *Mol Biol Cell* **22**(12): 1985-1996.
Lippincott-Schwartz, J., Altan-Bonnet, N., and Patterson, G.H. 2003. Photobleaching and photoactivation: following protein dynamics in living cells. *Nat Cell Biol* **Suppl**: S7-14.
Lister, L.M., Kouznetsova, A., Hyslop, L.A., Kalleas, D., Pace, S.L., Barel, J.C., Nathan, A., Floros, V., Adelfalk, C., Watanabe, Y. et al. 2010. Age-related meiotic segregation errors in mammalian oocytes are preceded by depletion of cohesin and Sgo2. *Curr Biol* **20**(17): 1511-1521.
Liu, H., Jang, J.K., Kato, N., and McKim, K.S. 2002. mei-P22 encodes a chromosome-associated protein required for the initiation of meiotic recombination in Drosophila melanogaster. *Genetics* **162**(1): 245-258.
Liu, H., Rankin, S., and Yu, H. 2013. Phosphorylation-enabled binding of SGO1-PP2A to cohesin protects sororin and centromeric cohesion during mitosis. *Nat Cell Biol* **15**(1): 40-49.
Livak, K.J., Flood, S.J., Marmaro, J., Giusti, W., and Deetz, K. 1995. Oligonucleotides with fluorescent dyes at opposite ends provide a quenched probe system useful for detecting PCR product and nucleic acid hybridization. *PCR Methods Appl* **4**(6): 357-362.
Llano, E., Gomez, H.L., Garcia-Tunon, I., Sanchez-Martin, M., Caburet, S., Barbero, J.L., Schimenti, J.C., Veitia, R.A., and Pendas, A.M. 2014. STAG3 is a strong candidate gene for male infertility. *Hum Mol Genet* **23**(13): 3421-3431.
Llano, E., Herran, Y., Garcia-Tunon, I., Gutierrez-Caballero, C., de Alava, E., Barbero, J.L., Schimenti, J., de Rooij, D.G., Sanchez-Martin, M., and Pendas, A.M. 2012. Meiotic cohesin complexes are essential for the formation of the axial element in mice. *J Cell Biol* **197**(7): 877-885.
Loidl, J., Klein, F., and Scherthan, H. 1994. Homologous pairing is reduced but not abolished in asynaptic mutants of yeast. *J Cell Biol* **125**(6): 1191-1200.
Lopez-Schier, H. and St Johnston, D. 2001. Delta signaling from the germ line controls the proliferation and differentiation of the somatic follicle cells during Drosophila oogenesis. *Genes Dev* **15**(11): 1393-1405.
Lopez-Serra, L., Lengronne, A., Borges, V., Kelly, G., and Uhlmann, F. 2013. Budding yeast Wapl controls sister chromatid cohesion maintenance and chromosome condensation. *Curr Biol* **23**(1): 64-69.
Losada, A., Hirano, M., and Hirano, T. 1998. Identification of Xenopus SMC protein complexes required for sister chromatid cohesion. *Genes Dev* **12**(13): 1986-1997.
Losada, A., Yokochi, T., and Hirano, T. 2005. Functional contribution of Pds5 to cohesin-mediated cohesion in human cells and Xenopus egg extracts. *J Cell Sci* **118**(Pt 10): 2133-2141.
Losada, A., Yokochi, T., Kobayashi, R., and Hirano, T. 2000. Identification and characterization of SA/Scc3p subunits in the Xenopus and human cohesin complexes. *J Cell Biol* **150**(3): 405-416.
Lowe, J., Cordell, S.C., and van den Ent, F. 2001. Crystal structure of the SMC head domain: an ABC ATPase with 900 residues antiparallel coiled-coil inserted. *J Mol Biol* **306**(1): 25-35.

Lui, D.Y. and Colaiacovo, M.P. 2013. Meiotic development in Caenorhabditis elegans. *Adv Exp Med Biol* **757**: 133-170.
Luo, H., Li, Y., Mu, J.J., Zhang, J., Tonaka, T., Hamamori, Y., Jung, S.Y., Wang, Y., and Qin, J. 2008. Regulation of intra-S phase checkpoint by ionizing radiation (IR)-dependent and IR-independent phosphorylation of SMC3. *J Biol Chem* **283**(28): 19176-19183.
Lynn, A., Soucek, R., and Borner, G.V. 2007. ZMM proteins during meiosis: crossover artists at work. *Chromosome Res* **15**(5): 591-605.
MacQueen, A.J., Colaiacovo, M.P., McDonald, K., and Villeneuve, A.M. 2002. Synapsis-dependent and -independent mechanisms stabilize homolog pairing during meiotic prophase in C. elegans. *Genes Dev* **16**(18): 2428-2442.
MacQueen, A.J., Phillips, C.M., Bhalla, N., Weiser, P., Villeneuve, A.M., and Dernburg, A.F. 2005. Chromosome sites play dual roles to establish homologous synapsis during meiosis in C. elegans. *Cell* **123**(6): 1037-1050.
MacQueen, A.J. and Villeneuve, A.M. 2001. Nuclear reorganization and homologous chromosome pairing during meiotic prophase require C. elegans chk-2. *Genes Dev* **15**(13): 1674-1687.
Maddox, A.S. and Maddox, P.S. 2012. High-resolution imaging of cellular processes in Caenorhabditis elegans. *Methods Cell Biol* **107**: 1-34.
Mancera, E., Bourgon, R., Brozzi, A., Huber, W., and Steinmetz, L.M. 2008. High-resolution mapping of meiotic crossovers and non-crossovers in yeast. *Nature* **454**(7203): 479-485.
Mark, H.F. and Zimmering, S. 1977. Centromeric effect on the degree of nonrandom disjunction in the female Drosophila melanogaster. *Genetics* **86**(1): 121-132.
Martin, J.S., Winkelmann, N., Petalcorin, M.I., McIlwraith, M.J., and Boulton, S.J. 2005. RAD-51-dependent and -independent roles of a Caenorhabditis elegans BRCA2-related protein during DNA double-strand break repair. *Mol Cell Biol* **25**(8): 3127-3139.
Martinez-Perez, E., Schvarzstein, M., Barroso, C., Lightfoot, J., Dernburg, A.F., and Villeneuve, A.M. 2008. Crossovers trigger a remodeling of meiotic chromosome axis composition that is linked to two-step loss of sister chromatid cohesion. *Genes Dev* **22**(20): 2886-2901.
Martinez-Perez, E. and Villeneuve, A.M. 2005. HTP-1-dependent constraints coordinate homolog pairing and synapsis and promote chiasma formation during C. elegans meiosis. *Genes Dev* **19**(22): 2727-2743.
Martini, E., Diaz, R.L., Hunter, N., and Keeney, S. 2006. Crossover homeostasis in yeast meiosis. *Cell* **126**(2): 285-295.
Maruyama, R., Velarde, N.V., Klancer, R., Gordon, S., Kadandale, P., Parry, J.M., Hang, J.S., Rubin, J., Stewart-Michaelis, A., Schweinsberg, P. et al. 2007. EGG-3 regulates cell-surface and cortex rearrangements during egg activation in Caenorhabditis elegans. *Curr Biol* **17**(18): 1555-1560.
Mazin, A.V., Bornarth, C.J., Solinger, J.A., Heyer, W.D., and Kowalczykowski, S.C. 2000. Rad54 protein is targeted to pairing loci by the Rad51 nucleoprotein filament. *Mol Cell* **6**(3): 583-592.
Mazina, O.M., Mazin, A.V., Nakagawa, T., Kolodner, R.D., and Kowalczykowski, S.C. 2004. Saccharomyces cerevisiae Mer3 helicase stimulates 3'-5' heteroduplex extension by Rad51; implications for crossover control in meiotic recombination. *Cell* **117**(1): 47-56.
McAleenan, A., Clemente-Blanco, A., Cordon-Preciado, V., Sen, N., Esteras, M., Jarmuz, A., and Aragon, L. 2013. Post-replicative repair involves separase-dependent removal of the kleisin subunit of cohesin. *Nature* **493**(7431): 250-254.

McAleenan, A., Cordon-Preciado, V., Clemente-Blanco, A., Liu, I.C., Sen, N., Leonard, J., Jarmuz, A., and Aragon, L. 2012. SUMOylation of the alpha-kleisin subunit of cohesin is required for DNA damage-induced cohesion. *Curr Biol* **22**(17): 1564-1575.

McGuinness, B.E., Hirota, T., Kudo, N.R., Peters, J.M., and Nasmyth, K. 2005. Shugoshin prevents dissociation of cohesin from centromeres during mitosis in vertebrate cells. *PLoS Biol* **3**(3): e86.

McKee, A.H. and Kleckner, N. 1997. Mutations in Saccharomyces cerevisiae that block meiotic prophase chromosome metabolism and confer cell cycle arrest at pachytene identify two new meiosis-specific genes SAE1 and SAE3. *Genetics* **146**(3): 817-834.

McKim, K.S., Green-Marroquin, B.L., Sekelsky, J.J., Chin, G., Steinberg, C., Khodosh, R., and Hawley, R.S. 1998. Meiotic synapsis in the absence of recombination. *Science* **279**(5352): 876-878.

McNally, K., Audhya, A., Oegema, K., and McNally, F.J. 2006. Katanin controls mitotic and meiotic spindle length. *J Cell Biol* **175**(6): 881-891.

McNally, K.L. and McNally, F.J. 2005. Fertilization initiates the transition from anaphase I to metaphase II during female meiosis in C. elegans. *Dev Biol* **282**(1): 218-230.

McNicoll, F., Stevense, M., and Jessberger, R. 2013. Cohesin in gametogenesis. *Curr Top Dev Biol* **102**: 1-34.

Mehta, G.D., Kumar, R., Srivastava, S., and Ghosh, S.K. 2013. Cohesin: functions beyond sister chromatid cohesion. *FEBS Lett* **587**(15): 2299-2312.

Mei, R., Galipeau, P.C., Prass, C., Berno, A., Ghandour, G., Patil, N., Wolff, R.K., Chee, M.S., Reid, B.J., and Lockhart, D.J. 2000. Genome-wide detection of allelic imbalance using human SNPs and high-density DNA arrays. *Genome Res* **10**(8): 1126-1137.

Mets, D.G. and Meyer, B.J. 2009. Condensins regulate meiotic DNA break distribution, thus crossover frequency, by controlling chromosome structure. *Cell* **139**(1): 73-86.

Michaelis, C., Ciosk, R., and Nasmyth, K. 1997. Cohesins: chromosomal proteins that prevent premature separation of sister chromatids. *Cell* **91**(1): 35-45.

Minn, I.L., Rolls, M.M., Hanna-Rose, W., and Malone, C.J. 2009. SUN-1 and ZYG-12, mediators of centrosome-nucleus attachment, are a functional SUN/KASH pair in Caenorhabditis elegans. *Mol Biol Cell* **20**(21): 4586-4595.

Mira, A. 1998. Why is meiosis arrested? *J Theor Biol* **194**(2): 275-287.

Mito, Y., Sugimoto, A., and Yamamoto, M. 2003. Distinct developmental function of two Caenorhabditis elegans homologs of the cohesin subunit Scc1/Rad21. *Mol Biol Cell* **14**(6): 2399-2409.

Miyazaki, W.Y. and Orr-Weaver, T.L. 1994. Sister-chromatid cohesion in mitosis and meiosis. *Annu Rev Genet* **28**: 167-187.

Molk, J.N., Schuyler, S.C., Liu, J.Y., Evans, J.G., Salmon, E.D., Pellman, D., and Bloom, K. 2004. The differential roles of budding yeast Tem1p, Cdc15p, and Bub2p protein dynamics in mitotic exit. *Mol Biol Cell* **15**(4): 1519-1532.

Moore, L.L., Morrison, M., and Roth, M.B. 1999. HCP-1, a protein involved in chromosome segregation, is localized to the centromere of mitotic chromosomes in Caenorhabditis elegans. *J Cell Biol* **147**(3): 471-480.

Muller, H.J. 1916. The mechanism of crossing over. *Am Nat* **50**(592): 193–221.

Munz, P. 1994. An analysis of interference in the fission yeast Schizosaccharomyces pombe. *Genetics* **137**(3): 701-707.

Myers, S., Bottolo, L., Freeman, C., McVean, G., and Donnelly, P. 2005. A fine-scale map of recombination rates and hotspots across the human genome. *Science* **310**(5746): 321-324.

Nabeshima, K., Villeneuve, A.M., and Colaiacovo, M.P. 2005. Crossing over is coupled to late meiotic prophase bivalent differentiation through asymmetric disassembly of the SC. *J Cell Biol* **168**(5): 683-689.
Nagaoka, S.I., Hassold, T.J., and Hunt, P.A. 2012. Human aneuploidy: mechanisms and new insights into an age-old problem. *Nat Rev Genet* **13**(7): 493-504.
Nasmyth, K. 2011. Cohesin: a catenase with separate entry and exit gates? *Nat Cell Biol* **13**(10): 1170-1177.
Nasmyth, K. and Haering, C.H. 2005. The structure and function of SMC and kleisin complexes. *Annu Rev Biochem* **74**: 595-648.
-. 2009. Cohesin: its roles and mechanisms. *Annu Rev Genet* **43**: 525-558.
Neale, M.J., Pan, J., and Keeney, S. 2005. Endonucleolytic processing of covalent protein-linked DNA double-strand breaks. *Nature* **436**(7053): 1053-1057.
Nicklas, R.B. 1974. Chromosome segregation mechanisms. *Genetics* **78**(1): 205-213.
Nishiyama, T., Ladurner, R., Schmitz, J., Kreidl, E., Schleiffer, A., Bhaskara, V., Bando, M., Shirahige, K., Hyman, A.A., Mechtler, K. et al. Sororin mediates sister chromatid cohesion by antagonizing Wapl. *Cell* **143**(5): 737-749.
-. 2010. Sororin mediates sister chromatid cohesion by antagonizing Wapl. *Cell* **143**(5): 737-749.
Niu, H., Wan, L., Baumgartner, B., Schaefer, D., Loidl, J., and Hollingsworth, N.M. 2005. Partner choice during meiosis is regulated by Hop1-promoted dimerization of Mek1. *Mol Biol Cell* **16**(12): 5804-5818.
Nousiainen, M., Sillje, H.H., Sauer, G., Nigg, E.A., and Korner, R. 2006. Phosphoproteome analysis of the human mitotic spindle. *Proc Natl Acad Sci U S A* **103**(14): 5391-5396.
Novak, I., Wang, H., Revenkova, E., Jessberger, R., Scherthan, H., and Hoog, C. 2008. Cohesin Smc1beta determines meiotic chromatin axis loop organization. *J Cell Biol* **180**(1): 83-90.
Nybo Andersen, A.M., Wohlfahrt, J., Christens, P., Olsen, J., and Melbye, M. 2000. Maternal age and fetal loss: population based register linkage study. *BMJ* **320**(7251): 1708-1712.
Odenthal-Hesse, L., Berg, I.L., Veselis, A., Jeffreys, A.J., and May, C.A. 2014. Transmission distortion affecting human noncrossover but not crossover recombination: a hidden source of meiotic drive. *PLoS Genet* **10**(2): e1004106.
Offenberg, H.H., Schalk, J.A., Meuwissen, R.L., van Aalderen, M., Kester, H.A., Dietrich, A.J., and Heyting, C. 1998. SCP2: a major protein component of the axial elements of synaptonemal complexes of the rat. *Nucleic Acids Res* **26**(11): 2572-2579.
Ohbayashi, T., Oikawa, K., Yamada, K., Nishida-Umehara, C., Matsuda, Y., Satoh, H., Mukai, H., Mukai, K., and Kuroda, M. 2007. Unscheduled overexpression of human WAPL promotes chromosomal instability. *Biochem Biophys Res Commun* **356**(3): 699-704.
Oikawa, K., Ohbayashi, T., Kiyono, T., Nishi, H., Isaka, K., Umezawa, A., Kuroda, M., and Mukai, K. 2004. Expression of a novel human gene, human wings apart-like (hWAPL), is associated with cervical carcinogenesis and tumor progression. *Cancer Res* **64**(10): 3545-3549.
Olsen, J.V. and Mann, M. 2013. Status of large-scale analysis of post-translational modifications by mass spectrometry. *Mol Cell Proteomics* **12**(12): 3444-3452.
Otter, M., Schrander-Stumpel, C.T., and Curfs, L.M. 2010. Triple X syndrome: a review of the literature. *Eur J Hum Genet* **18**(3): 265-271.
Ouyang, Z., Zheng, G., Song, J., Borek, D.M., Otwinowski, Z., Brautigam, C.A., Tomchick, D.R., Rankin, S., and Yu, H. 2013. Structure of the human cohesin inhibitor Wapl. *Proc Natl Acad Sci U S A* **110**(28): 11355-11360.

Page, S.L. and Hawley, R.S. 2004. The genetics and molecular biology of the synaptonemal complex. *Annu Rev Cell Dev Biol* **20**: 525-558.

Pan, J., Sasaki, M., Kniewel, R., Murakami, H., Blitzblau, H.G., Tischfield, S.E., Zhu, X., Neale, M.J., Jasin, M., Socci, N.D. et al. 2011. A hierarchical combination of factors shapes the genome-wide topography of yeast meiotic recombination initiation. *Cell* **144**(5): 719-731.

Panizza, S., Tanaka, T., Hochwagen, A., Eisenhaber, F., and Nasmyth, K. 2000. Pds5 cooperates with cohesin in maintaining sister chromatid cohesion. *Curr Biol* **10**(24): 1557-1564.

Parelho, V., Hadjur, S., Spivakov, M., Leleu, M., Sauer, S., Gregson, H.C., Jarmuz, A., Canzonetta, C., Webster, Z., Nesterova, T. et al. 2008. Cohesins functionally associate with CTCF on mammalian chromosome arms. *Cell* **132**(3): 422-433.

Pasierbek, P., Fodermayr, M., Jantsch, V., Jantsch, M., Schweizer, D., and Loidl, J. 2003. The Caenorhabditis elegans SCC-3 homologue is required for meiotic synapsis and for proper chromosome disjunction in mitosis and meiosis. *Exp Cell Res* **289**(2): 245-255.

Pasierbek, P., Jantsch, M., Melcher, M., Schleiffer, A., Schweizer, D., and Loidl, J. 2001. A Caenorhabditis elegans cohesion protein with functions in meiotic chromosome pairing and disjunction. *Genes Dev* **15**(11): 1349-1360.

Pauli, A., Althoff, F., Oliveira, R.A., Heidmann, S., Schuldiner, O., Lehner, C.F., Dickson, B.J., and Nasmyth, K. 2008. Cell-type-specific TEV protease cleavage reveals cohesin functions in Drosophila neurons. *Dev Cell* **14**(2): 239-251.

Pauli, A., van Bemmel, J.G., Oliveira, R.A., Itoh, T., Shirahige, K., van Steensel, B., and Nasmyth, K. 2010. A direct role for cohesin in gene regulation and ecdysone response in Drosophila salivary glands. *Curr Biol* **20**(20): 1787-1798.

Pease, A.C., Solas, D., Sullivan, E.J., Cronin, M.T., Holmes, C.P., and Fodor, S.P. 1994. Light-generated oligonucleotide arrays for rapid DNA sequence analysis. *Proc Natl Acad Sci U S A* **91**(11): 5022-5026.

Penkner, A.M., Fridkin, A., Gloggnitzer, J., Baudrimont, A., Machacek, T., Woglar, A., Csaszar, E., Pasierbek, P., Ammerer, G., Gruenbaum, Y. et al. 2009. Meiotic chromosome homology search involves modifications of the nuclear envelope protein Matefin/SUN-1. *Cell* **139**(5): 920-933.

Peoples, T.L., Dean, E., Gonzalez, O., Lambourne, L., and Burgess, S.M. 2002. Close, stable homolog juxtaposition during meiosis in budding yeast is dependent on meiotic recombination, occurs independently of synapsis, and is distinct from DSB-independent pairing contacts. *Genes Dev* **16**(13): 1682-1695.

Peoples-Holst, T.L. and Burgess, S.M. 2005. Multiple branches of the meiotic recombination pathway contribute independently to homolog pairing and stable juxtaposition during meiosis in budding yeast. *Genes Dev* **19**(7): 863-874.

Peters, N., Perez, D.E., Song, M.H., Liu, Y., Muller-Reichert, T., Caron, C., Kemphues, K.J., and O'Connell, K.F. 2010. Control of mitotic and meiotic centriole duplication by the Plk4-related kinase ZYG-1. *J Cell Sci* **123**(Pt 5): 795-805.

Petronczki, M., Siomos, M.F., and Nasmyth, K. 2003. Un menage a quatre: the molecular biology of chromosome segregation in meiosis. *Cell* **112**(4): 423-440.

Phair, R.D. and Misteli, T. 2001. Kinetic modelling approaches to in vivo imaging. *Nat Rev Mol Cell Biol* **2**(12): 898-907.

Phair, R.D., Scaffidi, P., Elbi, C., Vecerova, J., Dey, A., Ozato, K., Brown, D.T., Hager, G., Bustin, M., and Misteli, T. 2004. Global nature of dynamic protein-chromatin interactions in vivo: three-dimensional genome scanning and dynamic interaction networks of chromatin proteins. *Mol Cell Biol* **24**(14): 6393-6402.

Phillips, C.M. and Dernburg, A.F. 2006. A family of zinc-finger proteins is required for chromosome-specific pairing and synapsis during meiosis in C. elegans. *Dev Cell* **11**(6): 817-829.

Prieto, I., Pezzi, N., Buesa, J.M., Kremer, L., Barthelemy, I., Carreiro, C., Roncal, F., Martinez, A., Gomez, L., Fernandez, R. et al. 2002. STAG2 and Rad21 mammalian mitotic cohesins are implicated in meiosis. *EMBO Rep* **3**(6): 543-550.

Prieto, I., Suja, J.A., Pezzi, N., Kremer, L., Martinez, A.C., Rufas, J.S., and Barbero, J.L. 2001. Mammalian STAG3 is a cohesin specific to sister chromatid arms in meiosis I. *Nat Cell Biol* **3**(8): 761-766.

Qiao, H., Chen, J.K., Reynolds, A., Hoog, C., Paddy, M., and Hunter, N. 2012. Interplay between synaptonemal complex, homologous recombination, and centromeres during mammalian meiosis. *PLoS Genet* **8**(6): e1002790.

Rankin, S., Ayad, N.G., and Kirschner, M.W. 2005. Sororin, a substrate of the anaphase-promoting complex, is required for sister chromatid cohesion in vertebrates. *Mol Cell* **18**(2): 185-200.

Ren, Q., Yang, H., Rosinski, M., Conrad, M.N., Dresser, M.E., Guacci, V., and Zhang, Z. 2005. Mutation of the cohesin related gene PDS5 causes cell death with predominant apoptotic features in Saccharomyces cerevisiae during early meiosis. *Mutat Res* **570**(2): 163-173.

Revenkova, E., Eijpe, M., Heyting, C., Hodges, C.A., Hunt, P.A., Liebe, B., Scherthan, H., and Jessberger, R. 2004. Cohesin SMC1 beta is required for meiotic chromosome dynamics, sister chromatid cohesion and DNA recombination. *Nat Cell Biol* **6**(6): 555-562.

Revenkova, E., Herrmann, K., Adelfalk, C., and Jessberger, R. 2010. Oocyte cohesin expression restricted to predictyate stages provides full fertility and prevents aneuploidy. *Curr Biol* **20**(17): 1529-1533.

Rockman, M.V. and Kruglyak, L. 2009. Recombinational landscape and population genomics of Caenorhabditis elegans. *PLoS Genet* **5**(3): e1000419.

Rockmill, B. and Roeder, G.S. 1990. Meiosis in asynaptic yeast. *Genetics* **126**(3): 563-574.

Rogers, E., Bishop, J.D., Waddle, J.A., Schumacher, J.M., and Lin, R. 2002. The aurora kinase AIR-2 functions in the release of chromosome cohesion in Caenorhabditis elegans meiosis. *J Cell Biol* **157**(2): 219-229.

Rolef Ben-Shahar, T., Heeger, S., Lehane, C., East, P., Flynn, H., Skehel, M., and Uhlmann, F. 2008. Eco1-dependent cohesin acetylation during establishment of sister chromatid cohesion. *Science* **321**(5888): 563-566.

Rollins, R.A., Korom, M., Aulner, N., Martens, A., and Dorsett, D. 2004. Drosophila nipped-B protein supports sister chromatid cohesion and opposes the stromalin/Scc3 cohesion factor to facilitate long-range activation of the cut gene. *Mol Cell Biol* **24**(8): 3100-3111.

Rollins, R.A., Morcillo, P., and Dorsett, D. 1999. Nipped-B, a Drosophila homologue of chromosomal adherins, participates in activation by remote enhancers in the cut and Ultrabithorax genes. *Genetics* **152**(2): 577-593.

Rowland, B.D., Roig, M.B., Nishino, T., Kurze, A., Uluocak, P., Mishra, A., Beckouet, F., Underwood, P., Metson, J., Imre, R. et al. 2009. Building sister chromatid cohesion: smc3 acetylation counteracts an antiestablishment activity. *Mol Cell* **33**(6): 763-774.

Royen, M.E.v., Farla, P., Mattern, K.A., Geverts, B., Trapman, J., and Houtsmuller, A.B. 2008. Fluorescence Recovery After Photobleaching
(FRAP) to Study Nuclear Protein Dynamics
in Living Cells. in *The Nulceus*, pp. pp 363-385.

Rudolph, C., Kunz, C., Parisi, S., Lehmann, E., Hartsuiker, E., Fartmann, B., Kramer, W., Kohli, J., and Fleck, O. 1999. The msh2 gene of Schizosaccharomyces pombe is involved in mismatch repair, mating-type switching, and meiotic chromosome organization. *Mol Cell Biol* **19**(1): 241-250.
Salic, A., Waters, J.C., and Mitchison, T.J. 2004. Vertebrate shugoshin links sister centromere cohesion and kinetochore microtubule stability in mitosis. *Cell* **118**(5): 567-578.
Santaguida, S. and Musacchio, A. 2009. The life and miracles of kinetochores. *EMBO J* **28**(17): 2511-2531.
Sarin, S., Prabhu, S., O'Meara, M.M., Pe'er, I., and Hobert, O. 2008. Caenorhabditis elegans mutant allele identification by whole-genome sequencing. *Nat Methods* **5**(10): 865-867.
Sato, A., Isaac, B., Phillips, C.M., Rillo, R., Carlton, P.M., Wynne, D.J., Kasad, R.A., and Dernburg, A.F. 2009. Cytoskeletal forces span the nuclear envelope to coordinate meiotic chromosome pairing and synapsis. *Cell* **139**(5): 907-919.
Schlecht, H.B., Lichten, M., and Goldman, A.S. 2004. Compartmentalization of the yeast meiotic nucleus revealed by analysis of ectopic recombination. *Genetics* **168**(3): 1189-1203.
Schmitz, J., Watrin, E., Lenart, P., Mechtler, K., and Peters, J.M. 2007. Sororin is required for stable binding of cohesin to chromatin and for sister chromatid cohesion in interphase. *Curr Biol* **17**(7): 630-636.
Schvarzstein, M., Wignall, S.M., and Villeneuve, A.M. 2010. Coordinating cohesion, co-orientation, and congression during meiosis: lessons from holocentric chromosomes. *Genes Dev* **24**(3): 219-228.
Seitan, V.C., Krangel, M.S., and Merkenschlager, M. 2012. Cohesin, CTCF and lymphocyte antigen receptor locus rearrangement. *Trends Immunol* **33**(4): 153-159.
Severson, A.F., Ling, L., van Zuylen, V., and Meyer, B.J. 2009. The axial element protein HTP-3 promotes cohesin loading and meiotic axis assembly in C. elegans to implement the meiotic program of chromosome segregation. *Genes Dev* **23**(15): 1763-1778.
Severson, A.F. and Meyer, B.J. 2014. Divergent kleisin subunits of cohesin specify mechanisms to tether and release meiotic chromosomes. *Elife*: e03467.
Shelton, C.A. and Bowerman, B. 1996. Time-dependent responses to glp-1-mediated inductions in early C. elegans embryos. *Development* **122**(7): 2043-2050.
Shin, Y.H., Choi, Y., Erdin, S.U., Yatsenko, S.A., Kloc, M., Yang, F., Wang, P.J., Meistrich, M.L., and Rajkovic, A. 2012. Hormad1 mutation disrupts synaptonemal complex formation, recombination, and chromosome segregation in mammalian meiosis. *PLoS Genet* **6**(11): e1001190.
Shinohara, A., Ogawa, H., and Ogawa, T. 1992. Rad51 protein involved in repair and recombination in S. cerevisiae is a RecA-like protein. *Cell* **69**(3): 457-470.
Shintomi, K. and Hirano, T. 2009. Releasing cohesin from chromosome arms in early mitosis: opposing actions of Wapl-Pds5 and Sgo1. *Genes Dev* **23**(18): 2224-2236.
Sjogren, C. and Nasmyth, K. 2001. Sister chromatid cohesion is required for postreplicative double-strand break repair in Saccharomyces cerevisiae. *Curr Biol* **11**(12): 991-995.
Smith, A.V. and Roeder, G.S. 1997. The yeast Red1 protein localizes to the cores of meiotic chromosomes. *J Cell Biol* **136**(5): 957-967.
Smolikov, S., Eizinger, A., Hurlburt, A., Rogers, E., Villeneuve, A.M., and Colaiacovo, M.P. 2007. Synapsis-defective mutants reveal a correlation between chromosome

conformation and the mode of double-strand break repair during Caenorhabditis elegans meiosis. *Genetics* **176**(4): 2027-2033.
Smolikov, S., Schild-Prufert, K., and Colaiacovo, M.P. 2009. A yeast two-hybrid screen for SYP-3 interactors identifies SYP-4, a component required for synaptonemal complex assembly and chiasma formation in Caenorhabditis elegans meiosis. *PLoS Genet* **5**(10): e1000669.
Snowden, T., Acharya, S., Butz, C., Berardini, M., and Fishel, R. 2004. hMSH4-hMSH5 recognizes Holliday Junctions and forms a meiosis-specific sliding clamp that embraces homologous chromosomes. *Mol Cell* **15**(3): 437-451.
Sonoda, E., Matsusaka, T., Morrison, C., Vagnarelli, P., Hoshi, O., Ushiki, T., Nojima, K., Fukagawa, T., Waizenegger, I.C., Peters, J.M. et al. 2001. Scc1/Rad21/Mcd1 is required for sister chromatid cohesion and kinetochore function in vertebrate cells. *Dev Cell* **1**(6): 759-770.
Spiller, C.M., Feng, C.W., Jackson, A., Gillis, A.J., Rolland, A.D., Looijenga, L.H., Koopman, P., and Bowles, J. 2012. Endogenous Nodal signaling regulates germ cell potency during mammalian testis development. *Development* **139**(22): 4123-4132.
Stanvitch, G. and Moore, L.L. 2008. cin-4, a gene with homology to topoisomerase II, is required for centromere resolution by cohesin removal from sister kinetochores during mitosis. *Genetics* **178**(1): 83-97.
Starr, D.A. and Fridolfsson, H.N. 2010. Interactions between nuclei and the cytoskeleton are mediated by SUN-KASH nuclear-envelope bridges. *Annu Rev Cell Dev Biol* **26**: 421-444.
Stenoien, D.L., Patel, K., Mancini, M.G., Dutertre, M., Smith, C.L., O'Malley, B.W., and Mancini, M.A. 2001. FRAP reveals that mobility of oestrogen receptor-alpha is ligand- and proteasome-dependent. *Nat Cell Biol* **3**(1): 15-23.
Storlazzi, A., Tesse, S., Gargano, S., James, F., Kleckner, N., and Zickler, D. 2003. Meiotic double-strand breaks at the interface of chromosome movement, chromosome remodeling, and reductional division. *Genes Dev* **17**(21): 2675-2687.
Strachan, T. 2005. Cornelia de Lange Syndrome and the link between chromosomal function, DNA repair and developmental gene regulation. *Curr Opin Genet Dev* **15**(3): 258-264.
Strom, L., Lindroos, H.B., Shirahige, K., and Sjogren, C. 2004. Postreplicative recruitment of cohesin to double-strand breaks is required for DNA repair. *Mol Cell* **16**(6): 1003-1015.
Strom, L. and Sjogren, C. 2005. DNA damage-induced cohesion. *Cell Cycle* **4**(4): 536-539.
Sturtevant, A.H. 1915. Castle and Wright on Crossing over in Rats. *Science* **42**(1080): 342.
Suja, J.A., Antonio, C., and Rufas, J.S. 1992. Involvement of chromatid cohesiveness at the centromere and chromosome arms in meiotic chromosome segregation: a cytological approach. *Chromosoma* **101**(8): 493-501.
Sumara, I., Vorlaufer, E., Gieffers, C., Peters, B.H., and Peters, J.M. 2000. Characterization of vertebrate cohesin complexes and their regulation in prophase. *J Cell Biol* **151**(4): 749-762.
Sumara, I., Vorlaufer, E., Stukenberg, P.T., Kelm, O., Redemann, N., Nigg, E.A., and Peters, J.M. 2002. The dissociation of cohesin from chromosomes in prophase is regulated by Polo-like kinase. *Mol Cell* **9**(3): 515-525.
Sumiyoshi, E., Sugimoto, A., and Yamamoto, M. 2002. Protein phosphatase 4 is required for centrosome maturation in mitosis and sperm meiosis in C. elegans. *J Cell Sci* **115**(Pt 7): 1403-1410.

Sun, H., Treco, D., and Szostak, J.W. 1991. Extensive 3'-overhanging, single-stranded DNA associated with the meiosis-specific double-strand breaks at the ARG4 recombination initiation site. *Cell* **64**(6): 1155-1161.
Sutani, T., Kawaguchi, T., Kanno, R., Itoh, T., and Shirahige, K. 2009. Budding yeast Wpl1(Rad61)-Pds5 complex counteracts sister chromatid cohesion-establishing reaction. *Curr Biol* **19**(6): 492-497.
Szostak, J.W., Orr-Weaver, T.L., Rothstein, R.J., and Stahl, F.W. 1983. The double-strand-break repair model for recombination. *Cell* **33**(1): 25-35.
Tachibana-Konwalski, K., Godwin, J., van der Weyden, L., Champion, L., Kudo, N.R., Adams, D.J., and Nasmyth, K. 2010. Rec8-containing cohesin maintains bivalents without turnover during the growing phase of mouse oocytes. *Genes Dev* **24**(22): 2505-2516.
Tanaka, K., Hao, Z., Kai, M., and Okayama, H. 2001. Establishment and maintenance of sister chromatid cohesion in fission yeast by a unique mechanism. *EMBO J* **20**(20): 5779-5790.
Tanaka, T., Cosma, M.P., Wirth, K., and Nasmyth, K. 1999. Identification of cohesin association sites at centromeres and along chromosome arms. *Cell* **98**(6): 847-858.
Tanaka, T., Fuchs, J., Loidl, J., and Nasmyth, K. 2000. Cohesin ensures bipolar attachment of microtubules to sister centromeres and resists their precocious separation. *Nat Cell Biol* **2**(8): 492-499.
Tedeschi, A., Wutz, G., Huet, S., Jaritz, M., Wuensche, A., Schirghuber, E., Davidson, I.F., Tang, W., Cisneros, D.A., Bhaskara, V. et al. 2013. Wapl is an essential regulator of chromatin structure and chromosome segregation. *Nature* **501**(7468): 564-568.
Thingholm, T.E., Jorgensen, T.J., Jensen, O.N., and Larsen, M.R. 2006. Highly selective enrichment of phosphorylated peptides using titanium dioxide. *Nat Protoc* **1**(4): 1929-1935.
Toth, A., Ciosk, R., Uhlmann, F., Galova, M., Schleiffer, A., and Nasmyth, K. 1999. Yeast cohesin complex requires a conserved protein, Eco1p(Ctf7), to establish cohesion between sister chromatids during DNA replication. *Genes Dev* **13**(3): 320-333.
Trelles-Sticken, E., Adelfalk, C., Loidl, J., and Scherthan, H. 2005. Meiotic telomere clustering requires actin for its formation and cohesin for its resolution. *J Cell Biol* **170**(2): 213-223.
Tsubouchi, H. and Ogawa, H. 1998. A novel mre11 mutation impairs processing of double-strand breaks of DNA during both mitosis and meiosis. *Mol Cell Biol* **18**(1): 260-268.
Tsutsumi, M., Fujiwara, R., Nishizawa, H., Ito, M., Kogo, H., Inagaki, H., Ohye, T., Kato, T., Fujii, T., and Kurahashi, H. 2014. Age-related decrease of meiotic cohesins in human oocytes. *PLoS One* **9**(5): e96710.
Uhlmann, F., Lottspeich, F., and Nasmyth, K. 1999. Sister-chromatid separation at anaphase onset is promoted by cleavage of the cohesin subunit Scc1. *Nature* **400**(6739): 37-42.
Uhlmann, F. and Nasmyth, K. 1998. Cohesion between sister chromatids must be established during DNA replication. *Curr Biol* **8**(20): 1095-1101.
Unal, E., Arbel-Eden, A., Sattler, U., Shroff, R., Lichten, M., Haber, J.E., and Koshland, D. 2004. DNA damage response pathway uses histone modification to assemble a double-strand break-specific cohesin domain. *Mol Cell* **16**(6): 991-1002.
Unal, E., Heidinger-Pauli, J.M., Kim, W., Guacci, V., Onn, I., Gygi, S.P., and Koshland, D.E. 2008. A molecular determinant for the establishment of sister chromatid cohesion. *Science* **321**(5888): 566-569.

Unal, E., Heidinger-Pauli, J.M., and Koshland, D. 2007. DNA double-strand breaks trigger genome-wide sister-chromatid cohesion through Eco1 (Ctf7). *Science* **317**(5835): 245-248.
van Heemst, D., James, F., Poggeler, S., Berteaux-Lecellier, V., and Zickler, D. 1999. Spo76p is a conserved chromosome morphogenesis protein that links the mitotic and meiotic programs. *Cell* **98**(2): 261-271.
van Heemst, D., Kafer, E., John, T., Heyting, C., van Aalderen, M., and Zickler, D. 2001. BimD/SPO76 is at the interface of cell cycle progression, chromosome morphogenesis, and recombination. *Proc Natl Acad Sci U S A* **98**(11): 6267-6272.
Vaur, S., Feytout, A., Vazquez, S., and Javerzat, J.P. 2012. Pds5 promotes cohesin acetylation and stable cohesin-chromosome interaction. *EMBO Rep* **13**(7): 645-652.
Verni, F., Gandhi, R., Goldberg, M.L., and Gatti, M. 2000. Genetic and molecular analysis of wings apart-like (wapl), a gene controlling heterochromatin organization in Drosophila melanogaster. *Genetics* **154**(4): 1693-1710.
Villeneuve, A.M. 1994. A cis-acting locus that promotes crossing over between X chromosomes in Caenorhabditis elegans. *Genetics* **136**(3): 887-902.
Visootsak, J. and Graham, J.M., Jr. 2009. Social function in multiple X and Y chromosome disorders: XXY, XYY, XXYY, XXXY. *Dev Disabil Res Rev* **15**(4): 328-332.
Voutev, R., Killian, D.J., Ahn, J.H., and Hubbard, E.J. 2006. Alterations in ribosome biogenesis cause specific defects in C. elegans hermaphrodite gonadogenesis. *Dev Biol* **298**(1): 45-58.
Wagner, C.R., Kuervers, L., Baillie, D.L., and Yanowitz, J.L. 2010. xnd-1 regulates the global recombination landscape in Caenorhabditis elegans. *Nature* **467**(7317): 839-843.
Waizenegger, I.C., Hauf, S., Meinke, A., and Peters, J.M. 2000. Two distinct pathways remove mammalian cohesin from chromosome arms in prophase and from centromeres in anaphase. *Cell* **103**(3): 399-410.
Wang, F., Yoder, J., Antoshechkin, I., and Han, M. 2003. Caenorhabditis elegans EVL-14/PDS-5 and SCC-3 are essential for sister chromatid cohesion in meiosis and mitosis. *Mol Cell Biol* **23**(21): 7698-7707.
Wang, S.W., Read, R.L., and Norbury, C.J. 2002. Fission yeast Pds5 is required for accurate chromosome segregation and for survival after DNA damage or metaphase arrest. *J Cell Sci* **115**(Pt 3): 587-598.
Wang, T.F. and Kung, W.M. 2002. Supercomplex formation between Mlh1-Mlh3 and Sgs1-Top3 heterocomplexes in meiotic yeast cells. *Biochem Biophys Res Commun* **296**(4): 949-953.
Watanabe, Y. 2012. Geometry and force behind kinetochore orientation: lessons from meiosis. *Nat Rev Mol Cell Biol* **13**(6): 370-382.
Watanabe, Y. and Nurse, P. 1999. Cohesin Rec8 is required for reductional chromosome segregation at meiosis. *Nature* **400**(6743): 461-464.
Watanabe, Y., Yokobayashi, S., Yamamoto, M., and Nurse, P. 2001. Pre-meiotic S phase is linked to reductional chromosome segregation and recombination. *Nature* **409**(6818): 359-363.
Welz-Voegele, C. and Jinks-Robertson, S. 2008. Sequence divergence impedes crossover more than noncrossover events during mitotic gap repair in yeast. *Genetics* **179**(3): 1251-1262.
Weng, K.A., Jeffreys, C.A., and Bickel, S.E. 2014. Rejuvenation of meiotic cohesion in oocytes during prophase I is required for chiasma maintenance and accurate chromosome segregation. *PLoS Genet* **10**(9): e1004607.
Westergaard, M. and von Wettstein, D. 1972. The synaptinemal complex. *Annu Rev Genet* **6**: 71-110.

Wicky, C., Alpi, A., Passannante, M., Rose, A., Gartner, A., and Muller, F. 2004. Multiple genetic pathways involving the Caenorhabditis elegans Bloom's syndrome genes him-6, rad-51, and top-3 are needed to maintain genome stability in the germ line. *Mol Cell Biol* **24**(11): 5016-5027.
Williamson, D.H., Johnston, L.H., Fennell, D.J., and Simchen, G. 1983. The timing of the S phase and other nuclear events in yeast meiosis. *Exp Cell Res* **145**(1): 209-217.
Wilson, T.E., Grawunder, U., and Lieber, M.R. 1997. Yeast DNA ligase IV mediates non-homologous DNA end joining. *Nature* **388**(6641): 495-498.
Winters, T., McNicoll, F., and Jessberger, R. 2014. Meiotic cohesin STAG3 is required for chromosome axis formation and sister chromatid cohesion. *EMBO J* **33**(11): 1256-1270.
Wojtasz, L., Cloutier, J.M., Baumann, M., Daniel, K., Varga, J., Fu, J., Anastassiadis, K., Stewart, A.F., Remenyi, A., Turner, J.M. et al. 2012. Meiotic DNA double-strand breaks and chromosome asynapsis in mice are monitored by distinct HORMAD2-independent and -dependent mechanisms. *Genes Dev* **26**(9): 958-973.
Wojtasz, L., Daniel, K., Roig, I., Bolcun-Filas, E., Xu, H., Boonsanay, V., Eckmann, C.R., Cooke, H.J., Jasin, M., Keeney, S. et al. 2009. Mouse HORMAD1 and HORMAD2, two conserved meiotic chromosomal proteins, are depleted from synapsed chromosome axes with the help of TRIP13 AAA-ATPase. *PLoS Genet* **5**(10): e1000702.
Wood, A.J., Severson, A.F., and Meyer, B.J. 2010. Condensin and cohesin complexity: the expanding repertoire of functions. *Nat Rev Genet* **11**(6): 391-404.
Woods, D.C. and Tilly, J.L. 2013. Isolation, characterization and propagation of mitotically active germ cells from adult mouse and human ovaries. *Nat Protoc* **8**(5): 966-988.
Wu, N., Kong, X., Ji, Z., Zeng, W., Potts, P.R., Yokomori, K., and Yu, H. 2012. Scc1 sumoylation by Mms21 promotes sister chromatid recombination through counteracting Wapl. *Genes Dev* **26**(13): 1473-1485.
Xu, H., Beasley, M., Verschoor, S., Inselman, A., Handel, M.A., and McKay, M.J. 2004. A new role for the mitotic RAD21/SCC1 cohesin in meiotic chromosome cohesion and segregation in the mouse. *EMBO Rep* **5**(4): 378-384.
Xu, H., Beasley, M.D., Warren, W.D., van der Horst, G.T., and McKay, M.J. 2005. Absence of mouse REC8 cohesin promotes synapsis of sister chromatids in meiosis. *Dev Cell* **8**(6): 949-961.
Xu, Z., Cetin, B., Anger, M., Cho, U.S., Helmhart, W., Nasmyth, K., and Xu, W. 2009. Structure and function of the PP2A-shugoshin interaction. *Mol Cell* **35**(4): 426-441.
Yokobayashi, S., Yamamoto, M., and Watanabe, Y. 2003. Cohesins determine the attachment manner of kinetochores to spindle microtubules at meiosis I in fission yeast. *Mol Cell Biol* **23**(11): 3965-3973.
Youds, J.L., Mets, D.G., McIlwraith, M.J., Martin, J.S., Ward, J.D., NJ, O.N., Rose, A.M., West, S.C., Meyer, B.J., and Boulton, S.J. 2010. RTEL-1 enforces meiotic crossover interference and homeostasis. *Science* **327**(5970): 1254-1258.
Yu, H. 2013. Chromosome biology: Wapl spreads its wings. *Curr Biol* **23**(20): R923-925.
Yu, H.G. and Koshland, D. 2005. Chromosome morphogenesis: condensin-dependent cohesin removal during meiosis. *Cell* **123**(3): 397-407.
Yuan, L., Liu, J.G., Zhao, J., Brundell, E., Daneholt, B., and Hoog, C. 2000. The murine SCP3 gene is required for synaptonemal complex assembly, chromosome synapsis, and male fertility. *Mol Cell* **5**(1): 73-83.
Yuan, L., Yang, X., Ellis, J.L., Fisher, N.M., and Makaroff, C.A. 2012. The Arabidopsis SYN3 cohesin protein is important for early meiotic events. *Plant J* **71**(1): 147-160.

Yuan, L., Yang, X., and Makaroff, C.A. 2011. Plant cohesins, common themes and unique roles. *Curr Protein Pept Sci* **12**(2): 93-104.
Yun, Y., Lane, S.I., and Jones, K.T. 2014. Premature dyad separation in meiosis II is the major segregation error with maternal age in mouse oocytes. *Development* **141**(1): 199-208.
Zakharyevich, K., Ma, Y., Tang, S., Hwang, P.Y., Boiteux, S., and Hunter, N. 2010. Temporally and biochemically distinct activities of Exo1 during meiosis: double-strand break resection and resolution of double Holliday junctions. *Mol Cell* **40**(6): 1001-1015.
Zakharyevich, K., Tang, S., Ma, Y., and Hunter, N. 2012. Delineation of joint molecule resolution pathways in meiosis identifies a crossover-specific resolvase. *Cell* **149**(2): 334-347.
Zalevsky, J., MacQueen, A.J., Duffy, J.B., Kemphues, K.J., and Villeneuve, A.M. 1999. Crossing over during Caenorhabditis elegans meiosis requires a conserved MutS-based pathway that is partially dispensable in budding yeast. *Genetics* **153**(3): 1271-1283.
Zetka, M.C., Kawasaki, I., Strome, S., and Muller, F. 1999. Synapsis and chiasma formation in Caenorhabditis elegans require HIM-3, a meiotic chromosome core component that functions in chromosome segregation. *Genes Dev* **13**(17): 2258-2270.
Zhang, B., Chang, J., Fu, M., Huang, J., Kashyap, R., Salavaggione, E., Jain, S., Kulkarni, S., Deardorff, M.A., Uzielli, M.L. et al. 2009. Dosage effects of cohesin regulatory factor PDS5 on mammalian development: implications for cohesinopathies. *PLoS One* **4**(5): e5232.
Zhang, J., Hakansson, H., Kuroda, M., and Yuan, L. 2008a. Wapl localization on the synaptonemal complex, a meiosis-specific proteinaceous structure that binds homologous chromosomes, in the female mouse. *Reprod Domest Anim* **43**(1): 124-126.
Zhang, J., Shi, X., Li, Y., Kim, B.J., Jia, J., Huang, Z., Yang, T., Fu, X., Jung, S.Y., Wang, Y. et al. 2008b. Acetylation of Smc3 by Eco1 is required for S phase sister chromatid cohesion in both human and yeast. *Mol Cell* **31**(1): 143-151.
Zhang, L., Wang, S., Yin, S., Hong, S., Kim, K.P., and Kleckner, N. 2014. Topoisomerase II mediates meiotic crossover interference. *Nature* **511**(7511): 551-556.
Zhang, M. and Xia, G. 2012. Hormonal control of mammalian oocyte meiosis at diplotene stage. *Cell Mol Life Sci* **69**(8): 1279-1288.
Zhang, Z., Ren, Q., Yang, H., Conrad, M.N., Guacci, V., Kateneva, A., and Dresser, M.E. 2005. Budding yeast PDS5 plays an important role in meiosis and is required for sister chromatid cohesion. *Mol Microbiol* **56**(3): 670-680.
Zickler, D. and Kleckner, N. 1998. The leptotene-zygotene transition of meiosis. *Annu Rev Genet* **32**: 619-697.
Zierhut, C., Berlinger, M., Rupp, C., Shinohara, A., and Klein, F. 2004. Mnd1 is required for meiotic interhomolog repair. *Curr Biol* **14**(9): 752-762.